The Effects of Solution Conditions on the Kinetics of Microbial Ferrous-Iron Oxidation by *Leptospirillum Ferriphilum* in Continuous Culture

Tunde Victor OJUMU

Thesis presented for the Degree of
Doctor of Philosophy
In the Department of Chemical Engineering
UNIVERSITY OF CAPE TOWN

February 2008

Abstract

The Effects of Solution Conditions on the Kinetics of Microbial Ferrous-Iron Oxidation by *Leptospirillum Ferriphilum* in Continuous Culture

Tunde Victor Ojumu
Department of Chemical Engineering, University of Cape Town, Private Bag Rondebosch 7700, South Africa

The objective of this work was to investigate the effects of a wide range of solution conditions, namely: temperature, pH, dissolved Al and Mg, and the effect of total iron concentration on the kinetics of microbial ferrous-iron oxidation by *Leptospirillum ferriphilum*, with a view to developing a comprehensive rate equation. This objective was pursued by carrying out microbial ferrous-iron oxidation experiment in continuous stirred tank reactors under the following range of conditions: temperature: 18 – 45°C; pH: 0.80 – 2.00; Al concentration: 1.30 – 16.00 g L^{-1}; Mg concentration: 1.30 – 16.00 g L^{-1} and iron concentration: 2 – 12 g L^{-1}. The experiments were monitored by the measurement of the changes in oxygen and carbon dioxide concentration in the off-gas streams, and the redox potential measurement. These were used to determine the ferrous-iron utilisation rate via both, degree-of-reduction and material balances.

For all experiments conducted, the rate of microbial ferrous-iron oxidation by *Leptospirillum ferriphilum* culture increased with a decrease in redox potential. The rates were described using a Monod-type equation, modified to account for the various effects investigated. Increasing temperature from 18 to 42 °C resulted to an increase in maximum specific ferrous-iron utilisation rate, which can be accurately described over this temperature range by an Arrhenius equation. The effect of a wide range of solution pH on the maximum specific rates was such that $q_{Fe^{2+}}^{\max}$ increased to a maximum value at pH 1.3 and then declined as pH increases.

The microbial activity was impaired as solution ionic strength is increased by added Al and Mg sulphates. Although moderate individual concentrations of Mg tend to promote biomass growth, Al appeared to be inhibitory at all concentrations. Higher total iron concentrations tend to increase biomass concentration and the rate of ferrous-iron oxidation. However, the $q_{Fe^{2+}}^{\max}$ decreased with increasing ferric-iron concentrations, indicating that the energy requirement/demand per cell decreases. The yield expression for all the experiments indicated that maintenance coefficients are negligible. The biomass yield was a weak function of temprature and pH, but significantly dependent on solution ionic strength.

The derived model in each investigation was able to describe microbial ferrous-iron oxidation kinetics over the range of solution conditions studied. A comprehensive model development was attempted, which incorporated all the factors investigated to describe the iron oxidation kinetics by *L. ferriphilum* in a continuous culture. This study provided an understanding of how heap bioleach operation can be effectively managed with respect to the factors investigated.

Summary

Microbial ferrous-iron oxidation has been established as a critical sub-process in bioleaching of sulphide minerals and this has led to continued development of a fundamental understanding of the mechanism of the process. A literature survey showed that most studies on microbial ferrous-iron oxidation were carried out in laboratory agitated aerated reactors and published kinetic studies have been carried out over a relatively narrow range of conditions in terms of temperatures, pH and dissolved ion concentrations. In bioleach heaps, these are conditions that vary widely throughout the heap and during the time of operation. In addition, the level of iron concentration in the heap is small (< 5 g L^{-1}) compared to industrial tank reactors (10 – 20 g L^{-1}). Hence, existing studies do not reflect the ferrous-iron oxidation kinetics relevant to microbes in typical bioleach heap. The aim of this work was to investigate the effects of wide range of solution conditions, namely: temperature, pH, dissolved Al and Mg, and the effect of total iron concentration on the kinetics of microbial ferrous-iron with a view to developing a comprehensive rate equation to describe the kinetics under these conditions.

A review of literature has shown that *Leptospirillum ferriphilum* is one of the iron-oxidising bacteria; a mesophile known to be a dominant iron-oxidiser in many tank and heap bioleach operations. The kinetics of microbial ferrous-iron oxidation has been investigated over a narrow range of conditions, which fall into the range of optimum conditions of most bacteria. Thus previous studies are relevant only to stirred tank operation where these conditions can be controlled for optimal bacterial performance. However, heap conditions are not optimal, often exhibiting extreme conditions in terms of temperature, pH, and O_2 and CO_2 availability.

The mechanism of microbial ferrous-iron oxidation is well described with respect to *Acidithiobacillus ferrooxidans* and it is believed that the same holds for other mesophilc bacteria and archaea (although not actually proven). The rate of microbial growth and ferrous-iron oxidation were found to be dependent on ferrous and ferric iron concentration, which is consistent with the chemiosmotic mechanism proposed for energy assimilation. The rate of this process is also dependent on other factors such as temperature, pH, and O_2 and CO_2 availability, which are known to vary significantly in the heap. High concentrations of

cations resulting from dissolution of gangue minerals in bioleach heaps are also known as a potential factor which could inhibit microbial growth and the oxidation process.

A number of rate equations have been developed over the years by several authors to describe mesophilic microbial ferrous-iron oxidation. These are Monod-type equations which had their roots in the Michealis-Menten expression for enzyme-substrate interaction kinetics, and they describe the two macroscopic reactions of oxidation reactions and microbial growth. These models are expressed as either rate or specific rate of microbial ferrous-iron oxidation, coupled to the microbial growth rate via the Pirt equation, involving the maximum biomass yield and cell maintenance.

A review of these equations showed that they were obtained from studies using a variety of experimental methods. These include continuous stirred tank reactors, batch, shake flask experiments, oxygen uptake experiment and controlled potential experiment. A direct comparison of some of the more prominent models relative to a set of data for *At. ferrooxidans* showed that most of the models can be made to fit the same set of data fairly closely and that the rate inhibition by ferric-iron may not be as significant as previously assumed. None of the models reviewed appear to describe oxidation kinetics well at high ferric to ferrous iron ratios. The effect of other parameters such as pH, temperature, concentration of oxygen and other ions on microbial ferrous iron oxidation kinetics have been studied to some degree, but usually within fairly limited ranges. No model allows incorporation of all of these parameters simultaneously.

The microbial ferrous-iron oxidation by mesophilic bacteria was studied in a well-aerated and pH controlled culture at dilution rates ranging from 0.009 to 0.130 h^{-1} in a continuous stirred tank bioreactor. The microbial culture used in these studies was predominantly *L. ferriphilum*. Several experiments were carried out in continuous stirred tank bioreactors maintained at 400 rpm stirring speed and aeration rates between 250 to 400 ml min^{-1} under the following conditions:

- Temperature ranging from 18 to 45 °C, at pH 1.3 and at feed concentration of 12 g L^{-1} ferrous-iron concentration
- Solution pH ranging from 0.8 to 2.0, at 42 °C and at feed concentration of 12 g L^{-1} ferrous-iron concentration
- Ionic strength ranging from 0.12 to 1.3 M (achieved by dissolving Al^{3+} and/or Mg^{2+} as sulphates) at 42 °C, pH 1.3 at feed concentration of 5 g L^{-1} ferrous-iron concentration

- Feed iron concentrations ranging from 2 to 12 g L^{-1} at 42 °C and solution pH of 1.3

The microbial growth and oxidation kinetics were monitored by the analysis of the off-gas measurement for oxygen and carbon dioxide concentrations and the rate of ferrous-iron oxidation was calculated from the oxygen and carbon dioxide utilisation, using the degree-of-reduction balance. The values calculated showed good agreement when compared with those determined from substrate mass balance in all experiments. The comparison was used to confirm the validity of the methodology used for all experiments performed.

The kinetics of the oxidation reaction were modelled using the simplified ferric-iron inhibition rate equation, describing the microbial specific rate of ferrous-iron utilisation rate in terms of ferric-to-ferrous iron ratio, which is coupled to the microbial growth rate via Pirt expression invoving the maximum biomass yield and cell maintenance:

$$q_{Fe^{2+}} = \frac{q^{\max}_{Fe^{2+}}}{1 + K'_{Fe^{2+}} \frac{[Fe^{3+}]}{[Fe^{2+}]}} \qquad 3.15$$

$$q_{Fe^{2+}} = \frac{-r_{Fe^{2+}}}{C_X} = \frac{\mu}{Y^{\max}_{Fe^{2+}X}} + m_{Fe^{2+}} \qquad 2.13c$$

However, further analysis of results suggested that the kinetics are better described by an expanded type of rate equation similar to the Jone and Kelly (1983) equation, which uses two parameters to distinguish between ferrous and ferric iron effects:

$$q_{Fe^{2+}} = \frac{q^{\max}_{Fe^{2+}}}{1 + \frac{K_1}{[Fe^{2+}]} + K_2 \frac{[Fe^{3+}]}{[Fe^{2+}]}} \qquad 8.9$$

The effects of various factors studied were separately described by simple functions of the kinetic parameters in Equation 8.9 for each experimental data set. While $q^{\max}_{Fe^{2+}}$ increased exponentially with temperature, as described by an Arrhenius function, its relationship with solution pH is described by a quadriatic function. $q^{\max}_{Fe^{2+}}$ decreased linearly with increasing ionic strength due to added Al and Mg sulphates while the effect of a decrease in total iron concentration *increased* $q^{\max}_{Fe^{2+}}$ in an exponential-like form.

Although the maintenance coefficient can also be expressed as a function of all these effects, its magnitude relative to $q^{\max}_{Fe^{2+}}$ is so small that it can be neglected. The maximum biomass yield, $Y^{\max}_{Fe^{2+}X}$ is a weak function of temperature and pH but decreased significantly as the ionic

strength increased. The $Y^{max}_{Fe^{2+}X}$ is also shown to decrease linearly with decrease in total iron concentration. $q^{max}_{Fe^{2+}}$, K_1 and K_2 in Equation 8.9 could be replaced by their corresponding functions of the individual factors investigated as shown in Equations 8.11, 8.12, 8.13 and 8.16 for the effects of temperature, pH, ionic strength and total iron concentration respectively.

$$q_{Fe^{2+}} = \frac{4.67\times10^{7}\exp\left(-\frac{38.10}{RT}\right)}{1+\frac{0.01014}{[Fe^{2+}]}+(5.53\times10^{-5}T-0.015897)\frac{[Fe^{3+}]}{[Fe^{2+}]}} \quad 8.11$$

$$q_{Fe^{2+}} = \frac{33.63\,pH-11.54(pH)^{2}-9.49}{1+\frac{0.0286\,pH+0.0706}{[Fe^{2+}]}+4\times10^{-5}e^{2.22\,pH}\frac{[Fe^{3+}]}{[Fe^{2+}]}} \quad 8.12$$

$$q_{Fe^{2+}} = \frac{24.88-7.02I}{1+\frac{0.0494e^{-2.94I}}{[Fe^{2+}]}+(1.03-0.458)\times10^{-3}I\frac{[Fe^{3+}]}{[Fe^{2+}]}} \quad 8.13$$

$$q_{Fe^{2+}} = \frac{16.15+49.43\exp\left(-0.025[Fe^{3+}]\right)}{1+\frac{0.0177}{[Fe^{2+}]}+0.0016\frac{[Fe^{3+}]}{[Fe^{2+}]}} \quad 8.14$$

where T is in Kelvin, $[Fe^{2+}]$, $[Fe^{3+}]$ and I (ionic strength) are expressed in M ($mol.L^{-1}$). A rate equation of the form of Equation 8.15 was proposed qualitatively, showing the functionality of the various kinetic parameters on the individual factors studied.

$$q_{Fe^{2+}} = \frac{q^{max}_{Fe^{2+}}(T,pH,[Fe^{3+}],I)}{1+\frac{K_1(pH,I)}{[Fe^{2+}]}+K_2(T,pH,I)\frac{[Fe^{3+}]}{[Fe^{2+}]}} \quad 8.15$$

This study provided an understanding of how heap bioleach operation can be effectively managed with respect to the parameters investigated in order to enhance microbial ferrous-iron oxidation for improvement of metal recovery.

Declaration

I declare that this thesis is my own work. It is being submitted for the degree of Doctor of Philosophy (PhD) in the University of Cape Town. This thesis has not been submitted before for any degree or examination in any other university.

……
Ojumu, TV

……day of ……..2008

Dedication

To the memory of my father, Frederick Abimbola Ojumu and my mother Caroline Adubi Ojumu, who sacrified so much and gave so much love, that I could have the foundation necessary to attain this height.

Acknowledgements

I wish to sincerely thank both my supervisors. Dr. Jochen Petersen, for allowing me to explore this field of research. I am grateful for his constructive criticism and guidance throughout this work, and his words of encouragement, when I seemed to be confused at the early stage. Prof. Geoffrey Hansford for his friendly advice, enthusiasm and for criticising this research in a constructive manner. I wish to thank Deutscher Akademischer Austausch Dienst (DAAD) and the University of Cape Town for providing the financial support in the form of scholarships.

My dear wife, Adefolake Mayokun Ojumu, thank you for supporting me, and thus being alone, when I decided to come down to Cape Town in order to realise my vision. I really appreciate all these sacrifices made for me over the past three years, and I thank you for taking good care of our children during this time, when I was hardly there with you to assist in carrying my part of the burden. I love you, dear. I wish to thank Victor and Favour for having to do without their dad at this crucial time of their development, for your prayers and for believing in my ideals. I love you, and I look forward to seeing you as grown ups, so that I can also read your theses.

I would like to thank Prof. Sue Harrison, Dr. Rob van Hille and Kamunga Kazadi: for questions, comments and remarks during our usual seminars. They contributed tremendously to the success of this research. I wish to thank the entire staff of Chemical Engineering Department for the smiling faces and the ready-to-help attitude. A grateful thank you to the Nigerian community at Chemeng and my other friends for making my stay at Chemeng more interesting, and thank you for your support when I was bereaved.

There is more to life than being purely an academic: I thank Pastor Sola Oduwole and Dr. Laja Osoniyi for their encouragement and prayers, and for supervising my spiritual life often through disappointments and setbacks. I bless the name of the Lord Almighty, for making it possible for me to attain this height. I thank God for making this a reality, for it is not by my power nor by my strength, but by the Spirit of the most high God.

All glory, all honour, all power belongs to God.

Tunde, Nov. 2007

List of Publications and Presentations

1. Ojumu TV, Petersen J, Searby GE, Hansford GS (2005) A review of rate equations proposed for microbial ferrous-iron oxidation with a view to application to heap bioleaching. Presented at 16th International Biohydrometallurgy Symposium (IBS 2005), 25–29 September 2005
2. Ojumu TV, Petersen J, and Hansford GS (2006) Effects of solution conditions of heap bioleach systems on microbial ferrous-iron oxidation kinetics of *Leptospirillum ferriphilum*. Presented at Mineral Processing Conference 2006 (MinProc 2006) Cape Town 3 – 4 August 2006
3. Ojumu TV, Petersen J, and Hansford GS (2006) The effects of total iron concentration on the microbial ferrous-iron oxidation kinetics of *Leptospirillium ferriphilum*. Presented at the 6th European Symposium on Biochemical Engineering Science (ESBES 6), 27 – 30 August 2006 in Salzburg/Austria
4. Ojumu TV, Petersen J, Searby GE, Hansford GS (2006) A review of rate equations proposed for microbial ferrous-iron oxidation with a view to application to heap bioleaching. *Hydrometallurgy* **83** (1-4): 21 – 28.
5. Ojumu TV, Petersen J and Hansford GS (2007) The effect of aluminium and magnesium sulphate on the rate of ferrous iron oxidation by *Leptospirillum ferriphilum* in continuous culture. *Advanced Materials Research* **20-21**: 447-451
6. Petersen J and Ojumu TV (2007) The effect of total iron concentration and iron speciation on the rate of ferrous iron oxidation kinetics of *Leptospirillum ferriphilum* in continuous tank systems. *Advanced Materials Research* **20-21**:156-159
7. Ojumu TV, Petersen J and Hansford GS (2008) The effect of dissolved cations on microbial ferrous-iron oxidation by *Leptospirillum ferriphilum* in a continuous culture. *Hydrometallurgy* (Accepted)
8. T.V. Ojumu, S.T.L. Harrison, G.S. Hansford and J. Petersen (2008) Biooxidation kinetics of *Leptospirillum ferriphilum* under heap bioleach conditions. To be presented at Hydrometallurgy 2008 - 6th International Symposium - Honoring Robert Shoemaker, by SME - Society for Mining, Metallurgy, and Exploration. Aug. 17 – 20, Phoenix, Arizona.

Table of Contents

List of Figures

List of Tables

Nomenclature

Symbol	Description	Unit
a_i	activity of species *i*	Mol L^{-1}
b	Constant in Ratkowsky equation 2.36	$h^{-0.5}$ $K^{-0.5}$
c	Constant in Ratkowsky equation 2.37	K^{-1}
C_X	Bacteria concentration	mmol C L^{-1}
D	Dilution rate	h^{-1}
d_i	the effective ionic diameter	nm
E	Redox potential of the solution (Pt-Ag/AgCl)	mV
E_a	Activation energy	kJ mol^{-1}
F	Faraday's constant	C mol^{-1}
[Fe T]	Total iron concentration	g L^{-1} (mmol Fe.L^{-1})
$[Fe^{2+}]$	Ferrous-iron concentration	mmol Fe L^{-1}
$[Fe^{2+}]_{in}$	Influent ferrous-iron concentration	mmol Fe^{2+} L^{-1}
$[Fe^{2+}]_{out}$	Effluent ferrous-iron concentration	mmol $Fe^{2+}L^{-1}$
$[Fe^{2+}]_{threshold}$	Threshold ferrous-iron concentration	mmol $Fe^{2+}L^{-1}$
$[Fe^{3+}]$	Ferric-iron concentration	mmol Fe^{3+} L^{-1}
K_0	Frequency factor of activation energy	mmol Fe^{2+} h^{-1}
Ks	Monod substrate affinity constant	mmol Fe^{2+} L^{-1}
K_m	Michaelis-Menten constant	mmol Fe^{2+} L^{-1}
$K'_{Fe^{2+}}$	Apparent affinity constant in Equation 3.15	Dimensionless
$K_{Fe^{2+}}$ (K_1)	Ferrous-iron based affinity constant	mmol Fe^{2+} L^{-1}
$K_{Fe^{3+}}$	Ferric-iron based inhibitory constant	mmol Fe^{3+} L^{-1}
$K_2 = \frac{K_{Fe^{2+}}}{K_{Fe^{3+}}}$	Constant in Equation 8.1	Dimensionless
k_d	Death rate constant	
I	Ionic strength	mmol L^{-1}
m_s	Maintenance coefficients based on substrate (ferrous-iron)	mol Fe^{2+} (mol C)h^{-1}
$m_{Fe^{2+}}$	Maintenance coefficients based on ferrous-iron	mol Fe^{2+} (mol C)h^{-1}
m_{O_2}	Maintenance coefficients based on oxygen	mol Fe^{2+} (mol O_2)h^{-1}
$q_{Fe^{2+}}$	Microbial specific ferrous-iron utilisation rate	mol Fe^{2+} (mol C)h^{-1}
$q^{max}_{Fe^{2+}}$	Maximum microbial specific ferrous-iron utilisation rate	mol Fe^{2+} (mol C)h^{-1}
q_{O_2}	Microbial specific oxygen utilisation rate	mol Fe^{2+} (mol O_2)h^{-1}
$q^{max}_{O_2}$	Maximum microbial specific oxygen utilisation rate	mol Fe^{2+} (mol O_2)h^{-1}
$r_{Fe^{2+}}$	Ferrous-iron utilisation rate	mmol Fe^{2+} h^{-1}
$r^{max}_{Fe^{2+}}$	Maximum ferrous-iron utilisation rate	mmol Fe^{2+} h^{-1}
$-r_{O_2}$	Oxygen utilisation rate	mmol O_2 h^{-1}
$-r_{CO_2}$	Carbon dioxide utilisation rate	mmol CO_2 h^{-1}
r_X	Biomass production rate	mmol C h^{-1}
R	Universal gas constant	kJ mol^{-1} K^{-1}
R^2	Regression coefficient	Dimensionless
[S]	Substrate concentration	mmol
SSE	Sum of the squared error	Dimensionless
T	Absolute temperature	K
T_{opt}	Optimum temperature	K

Symbol	Description	Unit
T_{min}	Minimum temperature	K
T_{max}	Maximum temperature	K
V	Reactor volume	m^3
Y_{SX}	Microbial yield on substrate, *S*	mol C $(mol\ Fe^{2+})^{-1}$
$Y^{max}_{Fe^{2+}X}$	Maximu microbial yield on ferrous-iron	mol C $(mol\ Fe^{2+})^{-1}$
$Y^{max}_{O_2X}$	Maximu microbial yield on oxygen	mol C $(mol\ O_2)^{-1}$
z_i	represents the ionic charge	Coloumb

Greek Symbols

τ	Residence time	h
μ	Specific growth rate	h^{-1}
μ_{max}	Maximum specific growth rate	h^{-1}
Φ	Volumetric gas flow rate	L h^{-1}
γ_i	Activity coefficient	Dimensionless

Chapter 1

Introduction

1.1 Background

Bioleaching of sulphide minerals has been described by many authors as a process which involves oxidation and dissolution of metal-bearing minerals (such as copper sulphide ore), which is mediated by microorganisms (mainly bacteria and archea). Bioleaching is used industrially as a pre-treatment method for refractory gold ores prior to cyanidation and for extraction of copper from secondary copper sulphide ores. It is currently under development for extraction of metals such as cobalt, nickel, and zinc from their respective ores. Various bioleaching techniques have been developed for mineral extraction depending on the ore grades. These range from stirred tank bioleaching used for finely milled flotation concentrates, to heap bioleaching for low grade ore and concentrates; to irrigated dump leaching, usually for marginal grade of run-of-mine ores (Brierley and Brierley, 2001; Rawlings, 2002; Rossi, 1990).

The microbial ferrous-iron oxidation is the main driving force of bioleaching. Ferric-iron is the critical reagent for the oxidation of many sulphide minerals of industrial relevance. The bioleaching process involves a chemical leach of the sulphide mineral by acid and ferric-iron, producing ferrous-iron and releasing the desired metal into solution, as well as producing a variety of reduced sulphur compounds. The key role of microorganisms is to facilitate oxidation of ferrous-iron to the ferric form, and the reduced sulphur compounds to sulphur and or sulphate (Boon, 1996; Sand *et al.*, 1995; Schippers and Sand, 1999), thereby sustaining the leaching process. Therefore microbial ferrous-iron oxidation is critical to bioleaching, and it has been shown that microbial ferrous-iron oxidation can be

2×10^5 to 10^6 times faster than the abiotic oxidation under the same conditions (Lacey and Lawson, 1970).

A large amount of research effort has been directed towards the study of microbial growth and ferrous-iron oxidation kinetics over the past three decades in order to efficiently exploit microbial potential for metal recovery from ore bodies (Blight and Ralph, 2004; Boon, 1996; Boon *et al.*, 1995a; Crundwell, 1997; Garcia and Silva, 1991; Gomez and Cantero, 1998; Hansford, 1997; Jones and Kelly, 1983; Lacey and Lawson, 1970; Lizama and Suzuki, 1989; MacDonald and Clark, 1970; Meruane *et al.*, 2002). Various kinetic studies have been carried out, including the initial rate experiment in batch cultures, continuous culture experiments and studies using iso-potential devices. Some of the rate equations presented in these studies were defined as specific microbial growth rate using a Monod-type form for ferrous substrate limitation, with further terms added to account for ferric product inhibition, ferrous substrate limitation and inhibition (Crundwell, 1997; Gomez *et al.*, 1996; Harvey and Crundwell, 1997; Jones and Kelly, 1983; Kelly and Jones, 1978; MacDonald and Clark, 1970; Norris *et al.*, 1988).

A few of the published rate Equations were described as rates and specific rates of substrate utilization and were derived from Michaelis–Menten Equation for enzyme kinetics (Boon, 1996; Breed *et al.*, 1999; Breed and Hansford, 1999a; Breed and Hansford, 1999b; Huberts, 1994; Nemati and Webb, 1997; Searby and Hansford, 2003) and include the maximum yield constant and cell maintenance via the Pirt Equation. Other rate Equations are derived from the chemiosmotic theory or electrochemical analogies (Crundwell, 1997; Meruane *et al.*, 2002). These studies have used essentially *Acidithiobacillus ferrooxidans*[1] cultures with few studies on *Leptospirillum ferrooxidans* or *Leptospirillum*-like bacteria, and recently the results of some thermophilic cultures have been published (Franzmann *et al.*, 2005; Searby and Hansford, 2003).

However, it has been shown that most of the proposed rate equations could be made to fit the same set of experimental data, and that some of the underlying assumptions need to be re-examined as it appeared that ferric inhibition might not be as significant a factor compared to ferrous availability as previously assumed (Ojumu *et al.*, 2006; Searby,

[1] *Acidithiobacillus ferrooxidans* was formerly called *Thiobacillus ferrooxidans* but was renamed by Kelly and Wood (2000) to reflect its acidophilic nature.

2006). It is also noted that while some rate equations include terms to account for the effects of temperature, pH and inhibition due to arsenic, most studies have been carried out within a narrow range of operating conditions, limited to conditions near the optimum of microbial activity. In addition, most studies were carried out at one fixed total iron concentration, usually in excess of 10 g L^{-1}.

Thus previous studies are largely relevant only to tank bioleaching operations, where the operating parameters (e.g. temperature, pH) can be controlled for optimum microbial performance in order to achieve maximum productivity. Consequently, a lot of progress has been made in tank bioleaching with metal recovery of 95 to 98% achievable after 5 days (Brierley, 2005). On the other hand, due to depleting high grade ores, and the associated huge cost required to concentrate abundant low grade ores for tank bioleach operations, bioleaching is applied on a large scale in heaps and dumps for low-grade ores (especially those of copper sulphide minerals). It is likely that the existing studies on microbial ferrous-iron oxidation kinetics do not reflect the ferrous-iron oxidation kinetics that are relevant to microorganisms attached to ore particles in bioleach heaps.

In heap bioleach systems, parameters such as solution pH and temperature vary widely and are difficult if not impossible to control. This is expected as the design and complexities in heap do not allow for mixing/homogeneity of ore bodies, leach solution and aerated gas. Plug flow and diffusion within the stagnant zones remain the only mode of transport by which these phases come in contact with one another for chemical reactions to occur. The reported temperature profiles of a typical bioleach heap treating copper sulphide ores showed the wide variation of this parameter from bottom up and top down (Casas *et al.*, 1998; Dixon, 2000; Petersen and Dixon, 2007b; Sidborn *et al.*, 2003). In addition, the total iron concentration is usually less than 5 g L^{-1} and it is characterised with high content of gangue minerals which could result in a build-up of high concentrations of dissolved salts in the recycled pregnant leach solution (PLS). These factors could create potentially adverse conditions for the microbial population and interfere with the microbial ferrous-iron oxidation, which is critical to bioleach efficiency. Although the principal mechanisms and dynamics of bioleaching are well understood, these conditions might be some of the reasons why rate and extent of metal recovery in heap bioleach operation remains much below what could be achieved in theory.

Therefore, it is important to study the microbial ferrous-iron oxidation kinetics with respect to changes in solution pH, total iron concentrations, dissolved salts and operating temperature within the range relevant to bioleach heaps. This will provide the understanding of how solution conditions and some operating factors relevant to bioleach heaps (*i.e.* away from optimum) affect microbial population and the microbial ferrous-iron oxidation. This study will provide a useful contribution towards the development of an efficient modelling tool, which can be used to improve the design of bioleach heaps and serve as a diagnostic tool for existing heap operations.

1.2 The research objectives

In order to effectively model and understand the bioleach process, fundamental study on microbial ferrous-iron oxidation is important. In general, the objective of this work is to investigate the microbial ferrous-iron oxidation kinetics under the conditions (such as solution pH, temperature, iron concentration and dissolved cations) that are relevant to bioleach heaps by simulating these conditions in a chemostat. In more specific terms, this work investigates the microbial ferrous-iron oxidation kinetics of *Leptospirillum ferriphilum* with the following objectives:

1. Determination of effects of wide changes in temperature and solution pH on the microbial growth and kinetics of the oxidation process. It important to understand the effect of extreme temperature and pH beyond the respective optimum for typical mesophiles like *L. ferriphilum.*

2. The investigation of the effects of total iron concentration on the microbial population and the oxidation kinetics since heap operations are characterised with very low iron concentration compared to tank leaching.

3. Investigation of the effects of dissolved magnesium and aluminium cations arising from gangue materials during leaching on the microbial growth and the oxidation kinetics.

4. Development of a kinetic model for bacterial ferrous oxidation in a typical heap bioleach environment.

This investigation will provide the understanding for the following questions:

1. What are the effects of the non-optimal condition on the kinetics?
2. What are the effects of total dissolved salts and the resulting ionic strength on microbial growth and ferrous-iron oxidation?

1.3 The scope and limitation of the thesis

This research investigated the effects of solution conditions on microbial ferrous-iron oxidation in a continuous stirred tank reactor using a mesophilic culture containing predominantly *Leptospirillum ferriphilum*. Although a chemostat does not mimic real life situations in the heap, the focus is on fundamental studies based on the assumption that the oxidation process can be studied independently of other competing reactions (e.g. ferric leaching of sulphide minerals) and other important factors (e.g mass transfer limitation) in bioleach heaps. These effects (pH, temperature, dissolved salts and total iron concentration) were studied separately and their interactions were not considered in this study. The results might not be directly translated to real heap bioleach case situations, but will provide some understanding of how wide changes in solution and operating conditions found in bioleach heap operation influence microbial growth and ferrous-iron oxidation.

1.4 Thesis outline

This thesis is divided into nine chapters. Following the introductory chapter, it starts with a review of the relevant literature on bioleaching and microbial ferrous-iron oxidation. This will be introduced by a brief historical background of bioleaching, from its origin to current applications and its present status *vis-à-vis* current process under development. The accepted mechanism and the characteristics of microorganisms involved in bioleaching will be discussed with emphasis on the importance of microbial ferrous-iron oxidation. The kinetics of microbial ferrous-iron oxidation will be discussed followed by a brief historical development in modelling microbial ferrous-iron oxidation kinetics. The factors affecting microbial ferrous-iron oxidation will be discussed with reference to

effects of pH, temperature and dissolved cations followed by an overview of solution chemistry of iron in the biohydrometallurgy context and bioleach heaps kinetics.

Detailed experimental methods and materials used in this work will be discussed in Chapter 3. This will include the description of how off-gas analysis can be used to monitor microbial ferrous-iron oxidation kinetics. The theoretical calculation involved in microbial growth and substrate utilisation will be described in detail.

The experimental results are presented and discussed in Chapters 4, 5, 6 and 7. The effect of changes in temperature is studied in Chapter 4, the effect of changes in solution pH in Chapter 5, the effect of dissolved cations and total iorn concentration are discussed in Chapter 6 and 7 respectively. The experimental data were fitted to an appropriate rate equation from previous studies following from the analysis of rate Equations reviewed in Chapter 2 and the associated constants are presented and discussed in Chapters 4, 5 and 6. The study in Chapter 7 formed the basis for the development/modification of existing rate equation. The proposed equation was discussed in the conctext of these experiments in Chapter 8 where the significance of the equation parameters were discussed. The understanding gained from these studies was discussed in Chapter 9 with recommendation for future work to complement the understanding gleaned from this research.

Chapter 2

Literature Review

In this chapter, the historical background, the microorganisms involved and the generally acceptable mechanisms of bioleaching are discussed. Microbial ferrous-iron oxidation was reviewed extensively in the context of bioleaching with emphasis on conditions relevant to heap bioleaching in order to understand the current trend and development in microbial ferrous-iron oxidation in the contect of heap bioleaching and identify the gaps in the literature, thereby justifying the need for this study.

2.1 Historical background on bioleaching

Bioleaching has been in existence since ancient times, but the awareness of the involvement of microorganisms in mineral leaching was unknown until fairly recently (Colmer and Hinkle, 1947 ; Rossi, 1990). In the eighteenth century, large scale leaching of copper was used in Spain at Tharsis and Rio Tinto mines. This was considered to be a natural phenomenon as the miners were not aware of the involvement of microbes (Brandl, 2001; Rawlings, 2002). Rio Tinto (the "dark coloured" river) obtained its name from the redish brown colour imparted to the water by the high concentration of ferric-iron. Although this dissolved ferric-iron (and the less easily seen dissolved copper) is due to natural microbial activity (Rawlings, 2002), it was believed that the Rio Tinto ore or the Spanish climate had some obscure and mysterious quality. For many years, and that this technique appeared to work at Rio Tinto and no where else. During the same period, the leaching of low grade copper ore was attempted in south-western states of the USA, but without any success (Rossi, 1990).

The role of microorganisms in the bioleaching process became apparent in 1947 when certain bacteria belonging to the genus *Acidithiobacillus* (formerly *Thiobacillus*) were found in mine water and subsequently in the 1950's *At. ferrooxidans* and *At. thiooxidans* were identified as the microbes responsible for the metal dissolution (for review, see Acevedo, 2002; Olson *et al.*, 2003; Rawlings, 2002; Rossi, 1990). It was after Bryner *et al.* (1954) and Bryner and Anderson (1957) provided evidence of the ability of *At. ferrooxidans* to oxidise other metal sulphides that intensive research on the potential of microorganisms to oxidise other metals begun. Consequently, Duncan *et al.* (1967) published a list of nineteen metal sufides the solubilisation of which had been shown to be enhanced by *At. ferrooxidans*. Since then, the microorganism has been isolated from all the acid drainage waters flowing from ore-bodies, mines and dumps of low grade ore, as well as in all the old heaps at Rio-Tinto, Fenice Capanne (in Italy), and Szomolnok in Romania, where leaching had been performed as a result of microbial mediation for centuries. This led to establishment of correlation between the presence of the bacterium and the dissolution of metals in copper leaching operations (Brierley, 1982; Rossi, 1990).

Copper was the first metal to be extracted in 1950 from run-of-mine materials with commercial application of biohydrometallurgy, which made use of dump leaching technique (Acevedo, 2000; Brierley and Brierley, 2001; Olson *et al.*, 2003). The design of dump leaching does not promote microbial growth and activity due to poor aeration, thus commercial heap leaching became operational in the 1960s (Rossi, 1990). Heaps were designed so as to provide for good aeration thus facilitating the activity of the microbes and ensure better metal recovery (for review, see Olson *et al.*, 2003; Rawlings *et al.*, 2003). Extraction of other metals such as uranium, gold, etc by biohydrometallurgy operation followed in 1980 when the first commercial plant for asenopyrite gold pretreatment was commissioned in late 1980 (Olson *et al.*, 2003). Goldfield's BIOX process at the Fairview Mine in South Africa has the longest history in operating bio-oxidation plants: it treats refractory arsenopyrite/pyrite gold-bearing concentrate in large aerated stirred tank continuous flow reactors (Marais, 1990).

In the mid 1980s, there was also a breakthrough in heap bioleaching practice when the first copper mine, Lo Aguirre in Chile commenced industrial scale copper heap bioleach from an ore containing 1 to 2 % copper with a production of 14,000 tonnes of fine copper

per year. Since the 1980s bioleaching has been increasingly used (Acevedo, 2002; Akcil, 2004; Brierley and Brierley, 2001; Montealegre *et al.*, 1993). Today, dump, heap and tank reactors are well established processes, applied on large scale bioleaching operations for copper and refractory gold concentrates around the world (Rawlings *et al.*, 2003). Substantial progress has been recorded in the commercial application of bioleaching for metal recovery especially for copper extraction and in the treatment of arsenopyrite gold-bearing concentrate (Brierley and Brierley, 2001).

The use of bioleaching for other metals has also been demonstrated on a pilot-scale or at least at the laboratory scale. For example, the first commercial plant for bioleaching and recovery of cobalt was commissioned in Uganda for treating cobaltiferous pyrite concentrate, grading 1.38 % cobalt with 92 % cobalt recovery. In all cases, huge success has been recorded with tank reactors: metal recovery of 95 to 98 % is achievable within 5 days (Brierley, 2005). On the other hand, heap bioleaching, though suitable for metal recovery from low-grade sulphide whole ores, is still a developing technology. Industrially it is practised in two main applications, the dissolution of pyrite and arsenopyrite in refractory gold ores to liberate cyanide leachable gold, and the dissolution of copper from sulphide minerals. Biological dissolution of copper sulphide minerals occurs also in dumps but is limited due to poor aeration. Acid rock drainage (ARD) can in a sense be seen as a natural dump bioleaching process (Petersen and Dixon, 2007c). In fact early work on bioleaching addressed it as acid mine drainage (AMD) problems (Lacey and Lawson, 1970; Rossi, 1990).

More recently, a lot of research is geared toward the understanding of principles, mechanisms and dynamics of heap bioleaching (Casas *et al.*, 1998; Petersen and Dixon, 2004; Petersen and Dixon, 2006; Petersen and Dixon, 2007b; Petersen and Dixon, 2007c; Sidborn *et al.*, 2003) so as to make the operation more productive.

2.2 The mechanism of bioleaching

The mechanism of bioleaching of sulphide minerals was first proposed by Silverman and Ehrlich (1964) and this has been a subject of much debate in the last decade (Boon, 2001; Hansford, 1997; Pogliani and Donati, 1999; Sand *et al.*, 1995; Sand *et al.*, 2001; Tributsch, 2001). As described previously in the introduction, it is now generally accepted

that mineral bioleaching is a combined chemical/microbial process in which ferric-iron and protons form part of the reactant of the leaching reaction. The key role of the microorganisms is to generate/regenerate the leaching agents and to facilitate the reaction by creating a reaction space in which the leaching takes place. It has been reported that microorganisms form an exopolysaccharide (EPS) layer when they attach to the mineral (Gehrke *et al.*, 1998; Rohwerder *et al.*, 2003; Sand *et al.*, 2001) but not when growing as planktonic (free) cells (Devasia *et al.*, 1993). Bioleaching reactions take place most rapidly and efficiently within this EPS layer and therefore the EPS serves as the reaction space (Rohwerder *et al.*, 2003; Sand *et al.*, 2001; Tributsch, 2001).

Mechanistically, bioleaching of sulphide mineral proceeds via three main sub-processes (Boon, 1996; Boon *et al.*, 1995a; Clark and Norris, 1996; Hansford and Vargas, 2001) as shown in Figure 2.1: (1) chemical attack of the sulphide mineral by ferric-iron and/or protons, releasing the metal into solution (as in the case of copper) or exposing metal of interest for cyanidation (the case of occluded gold), ferric-iron is reduced to ferrous-iron in the process and sulphur species are formed. Here, the ferric-iron is the oxidizing agent; it oxidizes the metal sulphide via two pathways depending on the mineral type: the thiosulphate and polysufide mechanisms (Schippers and Sand, 1999). (2) Microbial oxidation of reduced ferrous-iron to ferric-iron, (3) Microbial oxidation of sulphur moiety to elemental sulphr and/or sulphate ion respectively.

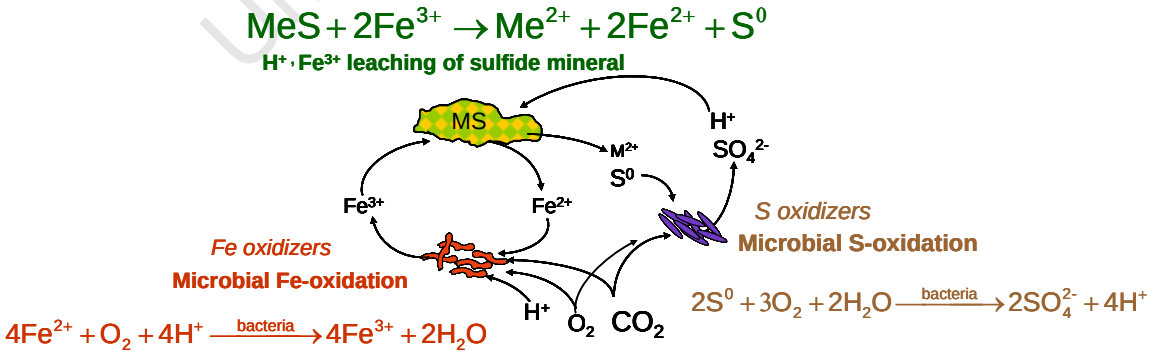

Figure 2.1. The schematic representation of bioleaching mechanism
Source: modified after Breed (1999b) and Hansford and Vargas (2001)

A thiosulphate mechanism was proposed for the oxidation of acid insoluble metal sulphides such as pyrite (FeS_2) and molybdenite (MoS_2), and a polysulphide mechanism for acid soluble metal sulphides such as sphalerite (ZnS), chalcopyrite ($CuFeS_2$) or galena (PbS). In the thiosulphate pathway (Figure 2.2a), solubilisation is through ferric iron attack on the acid-insoluble metal sulphides with thiosufate being the main intermediate and sulphate the end product. In the polysulphide pathway (Figure 2.2b), solubilisation of the acid-soluble metal sulphide is through a combined attack by ferric iron and protons with elemental sulphur as the main intermediate.

This elemental sulphur is relatively stable but may be oxidized to sulphate by sulphur-oxidizing microbes such as *Acidithiobacillus thiooxidans* or *Acidithiobacillus caldus* (for review, see Rawlings, 2007). The important reactions in bioleaching of sulphide minerals as shown in Figure 2.1 are represented in Equations 2.1 to 2.3

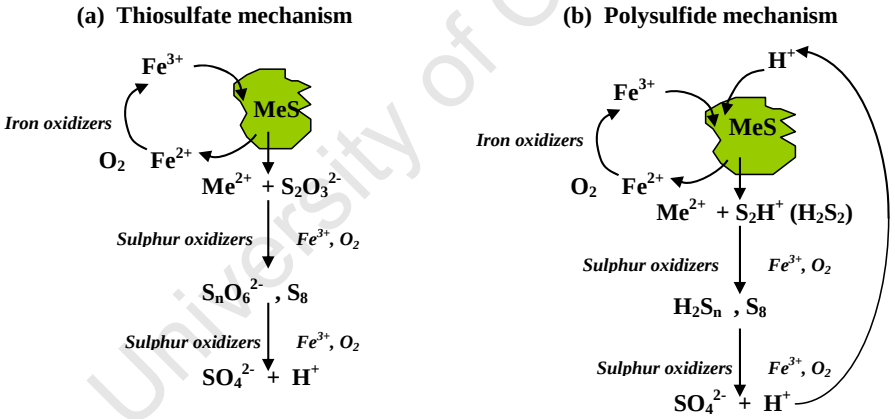

Figure 2.2 Schematic representation of bioleaching mechanism showing the sulphur pathways (a) the thiosulphate pathway, and (b) the polysulphide pathways as proposed by Schippers and Sand (1999) for bioleaching of sulphide mineral of the type MeS.
Source: Adapted from Rohwerder and Sand (2007)

$$2Fe^{3+} + MeS \rightarrow 2Fe^{2+} + Me^{2+} + S^0 \downarrow \qquad 2.1$$

$$2Fe^{2+} + \tfrac{1}{2}O_2 + 2H^+ \xrightarrow{microorganisms} 2Fe^{3+} + H_2O \qquad 2.2$$

$$S + \tfrac{3}{2}O_2 + H_2O \xrightarrow{microorganisms} H_2SO_4 \qquad 2.3$$

The ferrous iron produced in Equation 2.1 is re-oxidized back to ferric iron as shown in Equation 2.2 by iron-oxidizing microorganisms so that the leaching reaction in Equation 2.1 can continue in a cyclic manner. The sulphur species are oxidized to sulphuric acid by sulphur oxidizing microbes. The role of the microorganisms in the solubilisation of metal sulphides is not only to provide sulphuric acid for a proton attack, but to keep the iron in the oxidized ferric state for an oxidative attack on the mineral. From the later, it can be seen that the microbial ferrous-iron oxidation to ferric-iron is a critical sub-process in bioleaching of sulphide minerals.

2.3 The microorganisms involved in bioleaching

A variety of microorganisms is found in heap and tank bioleaching, and is classified into three types: iron-oxidizers, sulphur oxidizers and the heterotrophs. Conditions in bioleach heaps are more varied than in stirred tanks due to the presence of many potential ecological niches. Regions with very different temperatures, solution pH, aeration, mineral type, nutrient availability, biofilm formation, etc. exist within a heap and therefore the diversity of microorganisms are much greater (for review, see Rawlings, 2007). Although the microorganisms found in both processes are generally similar, the proportion and type of microbes present depends entirely on the conditions under which the heaps or tanks are operated. Most of the research conducted in bioleaching has extensively used bacteria belonging to the geni *Acidithiobacillus*, *Leptospirillum* and *Acidiphilum*, classified as mesophiles, and *Sulfobacillus*, *Ferroplasma*, *Solfolobus*, *Metallosphaera* and *Acidianus*, classified as thermophiles and extreme thermophiles, as shown in Table 2.1 (for review, see Kinnunen, 2004; Rawlings, 2002).

Acidiphilum species are exceptionally different. They are acid-tolerant, gram-negative heterotrophs rather than iron- or sulphur-oxidizing autotrophs. They are not directly involved in bioleaching, but have been found to be growing closely with *At. ferrooxidans* where they feed on organic products produced by iron and sulphur oxidisers (Goebel and Stackebrandt, 1994; Hallberg and Johnson, 2001). This ability to feed on organic carbon forms the basic principle for the development of a double-layer plate technique, whereby freshly grown acidophilic heterotrophic are mixed into an inorganic pour plate medium (Johnson, 1995; Johnson and McGinness, 1991), thus

alleviating the tedium in the cultivation of iron and sulphur oxidisers on the plate (for details, see Rawlings, 2002).

Table 2.1 Microbial characteristics of the most studied microbes used in bioleaching.

Microbes	Classification	Oxidation	Temperature (°C)	pH
Acidothiobacillus ferrooxidans	M	Iron, sulphur	15 – 35 31*	1.4 – 6.0 1.8 – 2.0
Acidothiobacillus thiooxidans	M	sulphur	10 – 37 28 – 30*	0.5 – 6.0 2.0 – 3.5*
Leptospirillum ferrooxidans	M	Iron	<10 – 45 30 – 37*	1.1 – 4.0 1.6 – 2.0*
Leptospirillum ferriphilum	M	Iron	<45 30 – 37*	1.4 – 1.8*
Acidothiobacillus caldus	MT	Sulphur	<52 45*	
Acidmicrobium ferrooxidans	MT	Iron	45 – 50*	2*
Leptospirillum thermoferrooxidans	MT	Iron	30 – 55 45 – 50*	>1.3 1.7 – 1.9*
Sulfobacillus acidophilus	MT	Iron, sulphur	30 – 55 45 – 50*	2*
Sulfobacillus thermosulfidooxidans	MT	Iron, sulphur	30 – 60 45 – 48*	1.5 – 5.5 2*
Ferroplasma acidiphilum	M	Iron	15 – 45 35*	1.3 – 2.2 1.7*
Sulfolobus metallicus	T	Iron, sulphur	50 – 75 65*	1 – 4.5 1.3 – 1.7*
Metallosphaera sedula	T	Iron, sulphur	50 – 80 75*	1.0 – 4.5 2 – 3*
Acidianus brierleyi	T	Iron, sulphur	45 – 75 70*	1 – 6 1.5 – 2.0*
Acidianus infernus	ET	Sulphur	65 – 96 90*	1 – 5.5 2.0*

M (mesophiles), MT (moderate thermophiles), T (thermophiles), ET(extreme thermophiles),
* (optimum parameters). **Source**: adapted from Rawlings (2002) and Kinnunen (2004)

The commercial importance of bioleaching bacteria is based on their ability to use the energy generated from the oxidation of ferrous iron, inorganic reduced sulphur compounds and other elements in their reduced states as their source of energy, thus catalyzing the natural mineral ores dissolution/oxidative processes (Rawlings, 2005; Rawlings *et al.*, 1999; Rossi, 1990).

2.3.1 Mesophilic bacteria

These are the most common iron-oxidizing microorganisms found in commercial bioleaching systems at moderate temperatures (below 40°C) and are believed to be a consortium of Gram-negative bacteria. These include the iron- and sulphur-oxidizing *Acidithiobacillus ferrooxidans*, the sulphur oxidizing *At. thiooxidans*, *At. caldus* and the iron-oxidizing *Leptospirillum ferrooxidans* and *L. ferriphilum* (Coram and Rawlings, 2002; Rawlings *et al.*, 1999; Watling, 2006). The Acidithiobacilli are obligate autotrophic Gram-negative bacteria, capable of growing at pH below 1.5. *At. ferrooxidans* being preferentially aerobic use oxygen as electron acceptor and either ferrous-iron or reduced sulphur as electron donor. Under anaerobic condition, they use ferric-iron as electron acceptor, oxidising reduced sulphur compounds as the electron donor. The flexibility of their potential substrate makes them an important bacteria in acid mine drainage (Johnson, 2006).

Mesophilic bacteria have been found to predominate in commercial stirred tank bioleaching reactors (Rawlings, 1997). Studies have shown that in tank processes operating under this condition, the steady state ferric iron concentration is usually high, and *At. ferrooxidans* appears to be less important than a combination of *Leptospirillum* and *At. thiooxidans* or *At. caldus* (Rawlings *et al.*, 1999). A recent study has proved that the dominant *Leptospirillum* in a commercial operation was *L. ferriphilum* rather than *Leptospirillum ferrooxidans* previously reported (Coram and Rawlings, 2002). This was also confirmed by the work of Kinnunen and Puhakka (2004). A fluidized bed operated at 37°C and pH 1.4 was dominated by *L. ferriphilum* with a small proportion of *Ferroplasma*-like archaea (Rawlings, 2005). Some iron oxidising mesophilic archaea, *Ferroplasma acidophilus*, *Ferroplasma acidarmanus* and *Ferroplasma cupricumulans* have also been isolated recently. They are pleomorphic microorganisms lacking cell walls and can tolerate extremely low pH (Dopson *et al.*, 2004; Edwards *et al.*, 2000; Golyshina *et al.*, 2000; Hawkes *et al.*, 2006).

2.3.2 Moderate thermophilic (MT), thermophiles and extreme thermophilic (ET) microbes

These are microorganisms that thrive at temperatures between 45 – 60 °C (MT), 60 – 80 °C (T) and temperatures greater than 80 °C (ET). As temperature increases between 45 and 60 °C, mesophiles are succeeded by moderate thermophiles. The genera *Sulfobacillus* is the most studied group of thermophiles. *Sulfobacillus* species are Gram-positive and endospore-forming bacteria, and have been isolated from bioleaching operations at 50 °C with *At. caldus* being the dominant species (Norris *et al.*, 2000). *Sulfobacillus* and *Acidimicrobium* were reported to dominate another bioleaching consortia at temperatures of 50 °C and with some members of the archaeal genus, *Ferroplasma* (Golyshina *et al.*, 2000; Pizarro *et al.*, 1996). The types of microorganisms found in heap-leaching processes are similar to those found in stirred-tank processes with *At. ferrooxidans*, *At. Thiooxidans* and *L. ferrooxidans* being most frequently detected (Franzmann *et al.*, 2005; Golyshina *et al.*, 2000; Pizarro *et al.*, 1996). However, the proportions of these bacteria can vary in population depending on the conditions of various regions in the heap.

Biomining consortia are dominated by archaea rather than bacteria at temperatures of about 70 ^{o}C, with species of *Sulfolobus* and *Metallosphaera* being most prominent. An archaeon similar to *Sulfolobus metallicus* has been found to dominate at 70 °C but excluded at higher temperatures with other *Metalosphaera*-like and *Sulfolobus*-like archaea dominating at 80°C. Archaea belong to the genus *Acidianus*, such as *Ad. ambivalensi* or *Ad. Infernos*, are also capable of growing at high temperature (90°C for *Ad. infernus*) on reduced sulphur and at low pH (for review, see Rawlings, 2002; Rawlings, 2007). Some novel isolates have also been reported to grow on pyrite and chalcopyrite at 88 °C (Norris and Owen, 1993) and 90 °C (Plumb *et al.*, 2000) and in both cases maximum copper extraction was observed at 85 °C (Norris, 2007).

The main difference between archaea and bacteria cells is in their cell structure. The bacterial cells are made up of a rigid cell wall consisting of peptidoglycan and a cell membrane consisting of phospholipids and sterols. This is to protect the cell from its environment. On the other hand, the archaeal cells wall is made up of one or two layers of proteins or glycoproteins which are closely associated with the cell membrane (Konig, 1988). The lack of structural rigidity allows the cells to adapt the fluidity of their cell membrane to cope with elevated temperature and extreme acidity (DeRosa *et al.*, 1991).

These also make them to be more prone to damage by mechanical shear stress, so limiting the maximum loading the system can withstand in the tank reactor (Clark and Norris, 1996; Raja, 2005).

2.4 The microbial characteristics

Most of the microbes involved in the bioleaching of sulphide of minerals are those that are responsible for producing the ferric iron and sulphuric acid required for the leaching reactions. These are the iron- and sulphur-oxidizing chemolithrophic bacteria and archaea. Although these microbes have different temperatures for optimum performance and are employed in different types of processes, they have a number of features in common that make them especially suitable for their role in mineral solubilisation:

- they grow autotrophically by fixing carbon dioxide from the atmosphere
- they obtain their energy by using either ferrous iron or reduced inorganic sulphur compounds (some use both) as an electron donor, and generally use oxygen as the electron acceptor;
- they are acidophiles, which means they grow in low pH environments (pH 1.4 to 1.6 is typical), and
- they are tolerant of a wide range of metal ions concentration. This characteristic varies within and between species (Rawlings, 2002; Rossi, 1990).

2.5 The applications of bioleaching techniques

At the industrial scale, bioleaching is applied in two main types of processes: Stirred tank-type and Irrigated-Dump and Heap processes. Stirred tank bioleaching allows for good control of pertinent operating parameters. It is can be operated under conditions necessary for optimum microbial activity, resulting in a better performance and high productivity. Tank bioleaching requires relatively long residence times. The mineral feed needs to be in the form of a finely milled concentrate – similar to smelting and roasting. This precludes the technique from use with low-grade ores and thus is mostly used in biooxidation of ore concentrates. Tank bioleaching has the highest operating cost, hence is used for leaching of high value ore/concentrate. The setup is such that the bioreactors are arranged in series

and/or parallel. The tanks are well aerated and operated in a continuously stirred mode (Figure 2.3a). The feed is added to the first tank and the overflow stream is connected from tank to tank until biooxidation of the mineral concentrate is sufficiently complete (Brandl, 2001; Schnell, 1997). The relatively homogeneous nature of the slurry in tank bioleaching allows for good control of process parameters over the other techniques. However, limitations in reactor volume restrict its application to the treatment of mineral concentrates or when moderate volumes of ore are to be processed. For instance, over 11,000 tons of gold concentrates are bio-oxidized in reactors every year (Acevedo, 2000; Brierley and Brierley, 2001; van Aswegen *et al.*, 2007). Past and present commercial applications of tank bioleaching are shown in Table 2.2

Heap and dump bioleaching are examples of the irrigated type. Heap bioleaching has become widely practised for copper extraction from low grade deposits. Unlike dump leaching, heap bioleaching involves the use of size reduction equipment. Crushed ores are preconditioned and agglomerated through tumbling with sulphuric acid and/or irrigated solution to prevent segregation of particles of different sizes prior to stacking on prepared pads in layers for leaching (Brierley and Brierley, 2001).

The fundamental departure from dump to heap is the case of fairly uniform particle sizes and the introduction of aeration from underneath (as shown in Figure 2.3b). This ensures an aerobic environment in which microbes can thrive, generating ferric-iron and acid (Brandl, 2001; Montealegre *et al.*, 1993; Rawlings *et al.*, 2003), thus increasing the proportion of copper recovery that is associated with sulphide minerals. The heap is irrigated (continuously or intermittently) from the top and the solution is left to seep through the ore bed where it can react with the target minerals. Dissolved metals are then transported with the flowing solution to the bottom of the heap from where they are removed via the drainage system into collection ponds as pregnant leach solution (PLS). The target metal is removed from the PLS through a suitable technology (by solvent extraction, cementation or adsorption) and the barren solution returned to the top surface of the heap for re use (Petersen and Dixon, 2007b; Petersen and Dixon, 2007c). This technique is mostly applied to bioleaching of copper and refractory gold-bearing ores (Rawlings, 2002; Rawlings *et al.*, 2003).

Although it presents a number of advantages such as low operating costs and simplicity of operation, the heap bioleach operation suffers from severe limitations. The construction and heterogeneous nature of the system make some of the operating conditions uncontrollable, and extreme conditions such as hot spots, high concentration of total dissolved solids (TDS), poor solution distribution, low rate of oxygen and carbon dioxide transfer and high pH may occur (Petersen and Dixon, 2004). These contribute to extended periods of operation to achieve sufficient conversion.

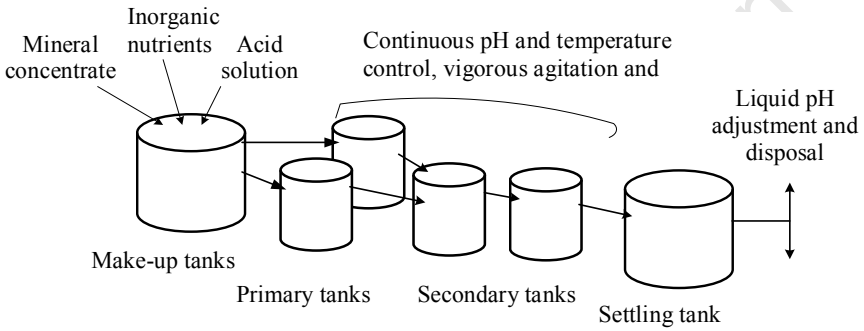

a. Tank bioleaching

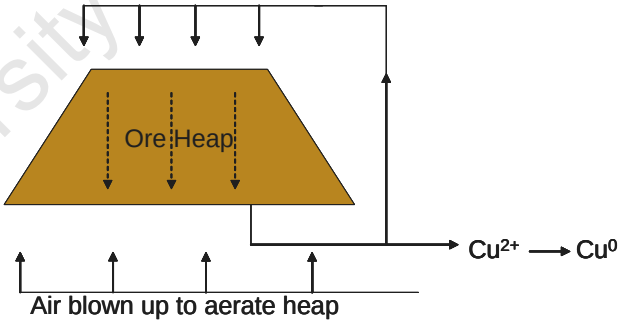

b. Heap bioleaching

Figure 2.3 Schematic diagramme of tank-type and irrigated-type bioleaching processes
Source: modified after Rawlings (2002)

In-situ bioleaching involves leaching of the ore in place, using drill hole solution systems without actual removal from the ore body probably due to inaccessibility of the site. It is used for low-grade ore and in cases where it is not economical to pre-treat the ore by the conventional mining methods (Brandl, 2001; Murr and Brierley, 1978; Schnell, 1997). Commercial application of in-situ, dump and heap leaching to bioleaching and recovery of

copper are widely reported (Brierley and Brierley, 2001; Domic, 2007; du Plessis *et al.*, 2007; Kinnunen, 2004). Although current application of tank leaching is on the pretreatment of gold from recalcitrant arsenopyrite, its application to nickel, zinc and other metal in the near future is promising (Olson *et al.*, 2003; Rawlings *et al.*, 2003). Table 2.2 also shows locations where heap bioleaching is being practised on a large scale.

Table 2.2 Examples of commercial application of stirred tank-type and irrigated-type bioleaching plants

Metal	Leaching method	Country practised	Plant	Size (tons. Ore per day	Years in operation	Reference
Au	Tank (BIOX®)	Brazil	SaÕ Bento	150	1992-present	1,2,3,5
Au	Tank (BIOX®)	Australia	Harbour Lights	40	1992-1999	1,2,3,5
Au	Tank (BIOX®)	Australia	Wiluna	158	1993-present	1,2,3,5,6
Au	Tank (BIOX®)	South Africa	Fair view	62	1986, 1991-present	1,2,3,5,6
Au	Tank (BIOX®)	Ghana	Ashanti-Sansu	960	1994-present	1,2,3,5
Au	Tank (BIOX®)	Peru	Tamboraque	60	1998-2002	1,2,5
Au	Tank (BIOX®)	Australia	Fosterville	211	2005-present	6
Au	Tank (BIOX®)	Kazakhstan	Suzdal	196	2005-present	6
Au	Tank (BacTech)	Australia	Youanmi	120	1994-1998	1,2,3,5
Au	Tank (BacTech)	Australia	Beaconsfield	68	2000-present	3,5
Au	Tank (Mintek-Bac-Tech)	China	Laizhou	100	2001-present	3,5
Co	Tank (BRGM)	Uganda	Kasese Cobalt	240	1999-present	1,4,5
Au	Heap	Nevada, US	Newmont		1999-present	7
Cu	Heap	Chile	Lo Aquire	16000	1980-1996	2,3
Cu	Heap	Australia	Mt. Leyshon	1370	1992-1997	2,3
Cu	Heap	Arizona	Phelps Dodge Morenci	-	2001 - present	8
Cu	Heap	Chile	Cerro Colorado	16000	1993-present	1,2,3
Cu	Heap	Australia	Girilambone	2000	1993-2005	1,2,3
Cu	Heap	Chile	Ivan-Zar	1500	1994-present	2,3
Cu	Heap	Chile	Quebrada Blanca	17300	1994-present	1,2,3
Cu	Heap	Chile	Andacollo	10000	1996-present	1,2,3
Cu	Heap	Chile	Dos Amigos	3000	1996-present	1,2,3
Cu	Heap	Peru	Cerro Verde	32000	1996-present	2,3
Cu	Heap	Chile	Zaldivar	20000	1998-present	1,2,3
Cu	Heap	Myanmar	S&K Copper	18000	1998-present	3
Cu	Heap	USA	Equitorial Tonopah	24500	2000-2001	1,2,3
others	Heap	Finland	Talvivaara	33000 Ni, 60000 Zn, 10000 Cu, 1200 Co	2004[a], 2008[b]	9

For detail review, see (1) Brandl(2001), (2) Brierley and Brierley (2001), (3) Olson *et al.* (2003), (4) Rawlings (2002), (5) Rawlings *et al.* (2003). (7) Plumb *et al.* (2007a), (8) (Phelps Dodge Mining Company, 2003), (9). (Talvivaara, 2008)
Source: modified after Kinnunen (2004)

2.6 Kinetics of copper sulphide

As discussed in Section 2.2, it is abundantly clear that microbial oxidation of minerals proceeds indirectly by ferric leaching. Therefore, it is reasonable to analyse mineral leaching kinetics, even in a bioleach context, by the fundamentals of oxidative leaching of sulfide minerals by ferric ions. Abiotic leach kinetics of minerals in ferric-iron media (i.e. ferric sulphate) have widely investigated and models are readily available for most common sulfides. In most of the models, minerals reaction kinetics are proportional to the ratio of ferric-to-ferrous ion concentrations in solution approximately to the one-half power as shown in Equation 2.4. This equation describes the kinetics of pyrite leaching as mixed control oxidative leaching (Holmes and Crundwell, 2000; Nicol, 1993; Petersen and Dixon, 2007a).

$$r_{me} = g_{me}\frac{dX_{me}}{dt} = g_{me}k_{me}\frac{[Fe^{3+}]}{[Fe^{2+}]}f(X_{me}) \qquad 2.4$$

where g_{me} is the pyrite mineral grade, X is the conversion, k_{me} is the rate constant, and $f(X_{me})$ is a topological term that accounts for the decline of rate in proportion to the decline in surface area available to leaching, which is in turn a function of the mineral conversion. Most commonly used are the shrinking sphere and shrinking core type models. Chalcocite kinectics follows a mixed control rate expression similar to that of pyrite though its leaching proceeds in two distinct stages (for review, see Petersen and Dixon, 2007a). However, unlike the other sulfide minerals, chalcopyrite leach kinetics is govern by complex surface phenomena which is currently under much debate, the leaching reaches a maximum at relatively low ferric to ferrous ratios, but slows down at more elevated the ferric-to-ferrous ratio in solution. Petersen and Dixon (2006) proposed equation 2.5 which is a sum of two parallel reactions with mixed control kinetics similar to 2.4, which replace each other around some critical ferric to ferrous ratio R_{crit}. This is consistent with the meachnism proposed by Hiroyoshi *et al.* (2004).

$$r_{cpy} = g_{cpy}k_{cpy}Rf(X_{cpy})\left(A\exp\frac{R}{R_{crit}} + B(1-\exp\frac{R}{R_{crit}})\right) \qquad 2.5$$

where $R = [Fe^{3+}]/[Fe^{2+}]$ and A and B are Arrhenius function to account for effect of temperature (for review, see Petersen and Dixon, 2007a) .

2.7 The microbial ferrous-iron oxidation

Oxidation of ferrous to ferric-iron forms an important part of the respiratory mechanisms of iron oxidizing bacteria and their effectiveness in bioleaching operations depends on the rate of the oxidation process. The mechanism was first proposed by Mitchell (1966), a chemiosmotic mechanism which involves coupling of the transfer of electrons across an energy-transducing membrane to the production of energy-rich molecules. This mechanisms was further applied by Ingledew (1982) to describe the bioenergetics of the growth of *At. ferrooxidans* on ferrous-iron, and it is assumed that the same holds for other iron-oxidizing bacteria and archaea. Although this assumption has not been verified in the literature, it is important to note that archaea and bacteria have different cell structure which could probably differentiate their metabolism.

The microorganisms obtain their energy from the ferrous oxidation using oxygen as the oxidizing agent. According to Ingledew (1982), the acidophilic life style of of *At. ferrooxidans* imposes a challenge of maintaining the internal pH of the cell close to neutrality, the author reported the pH of the cell cytoplasm to be between pH 6.5 to 7.0. *At. ferrooxidans* grows on Fe^{2+} at this acidic condition with electron-transport chain mediating between the two half cell reactions:

$$2Fe^{2+} \rightarrow 2Fe^{3+} + 2e^{-} \qquad E_h^o = +770mV$$

$$2e^{-} + \tfrac{1}{2}O_2 + 2H^{+} \rightarrow H_2O \qquad E_h^o = -1120mV$$

$$\text{overall reaction}: \; 2Fe^{2+} + \tfrac{1}{2}O_2 + 2H^{+} \rightarrow 2Fe^{3+} + H_2O + \text{Energy} \qquad E_h^o = -350mV$$

The overall reaction consumes Fe^{2+}, O_2, and H^+ to give H_2O, Fe^{3+} and energy for CO_2 fixation and cell growth (Ingledew, 1982). This oxidation takes place in the periplasmic space and is facilitated by the enzyme complex constituting the electron transport chain (namely: rusticyanin, cytochrome c and cytochrome a) (Cavazza *et al.*, 1995). The electron transferred across the cell membrane promotes the reduction of oxygen. This reduction of oxygen requires a proton, which must be brought from outside of the cell membrane as shown in Figure 2.4. This proton electrochemical gradient (due to difference between the cytoplasmic pH and the bulk solution) catalyzes the conversion of ADP to ATP, which is the energy carrier in the cell, which is then picked up for the

oxygen reduction to form water (for review see Ingledew, 1982; Rossi, 1990). Therefore, it is clear that ferrous oxidation is an energy generation process of the bacteria and thus forms the basis for their survival

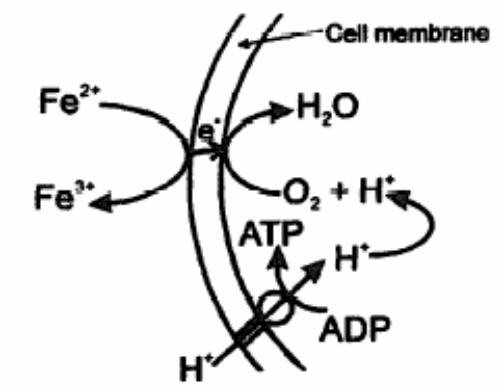

Figure 2.4 Schematic representation of proton circuit and ferrous oxidation by *At. ferrooxidans*
Source: Crundwell (1997)

The proton electrochemical gradient is controlled by the available proton channels associated with ATPase on the cell membrane. The membrane is impermeable to protons and proton transfer occurs only through these channels. According to Rawlings (2005), the outer cell membrane of *At. ferrooxidans* cell wall has been shown to contain high molecular weight c-type cytochrome (Cyc2) which acts as the primary electron acceptor (see Figure 2.5), the electron is then passed to the second cytochrome (Cyc1) in the periplasm possibly via rusticyanin, and then on to c cytochrome oxidase (Rawlings, 2005; Yarzabal *et al.*, 2002).

Although Maciag and Lundgren (1964) reported that the energy released in the ferrous oxidation process is used in the fixation of dissolved CO_2 through the Calvin reductive pentose phosphate cycle, studies have shown from thermodynamic consideration that at least 2 moles of Fe^{2+} must be oxidized to give enough redox potential energy (ΔG calculated to be -8.1 kcal mol^{-1}) needed for the phosphorylation of ADP to ATP (ΔG estimated to be -8.9 to 16 kcal mol^{-1}) (Ingledew, 1982; Tuovinen and Kelly, 1972).

Ferrous-iron oxidation is also needed to produced reduced $NAD(P)^+$ for CO_2 fixation and other anabolic processes by transfer of electrons from Fe^{2+}.

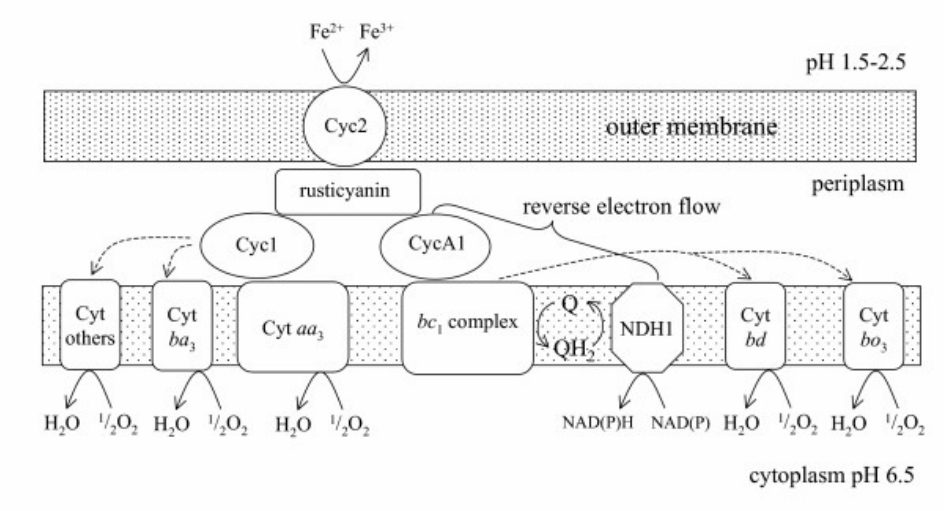

Figure 2.5 A model of the iron oxidation electron transport pathway of *At. ferrooxidans* showing electron transfer generating proton gradient and reverse electron transport for NADH formation
Source: Rawlings (2005)

The free energy for this process (ΔG = + 25kcal) can be calculated given the following redox potential values:

$NAD(P)^+/NAD(P)H \quad E_h^o = -305$ mV

$Fe^{2+}/Fe^{3+} \quad E_h^o = -770$mV

The fixation of 1 mole of CO_2 by Calvin cycle requires 3 mole ATP and 2 moles NAD(P)H. Thus it can be shown as reported in Ingledew (1982) that 22.4 moles of Fe^{2+} are needed for fixing 1 mole of CO_2 from thermodynamic consideration. These values would give a maximum theoretical yield on ferrous-iron of 0.53 g carbon/mole Fe^{2+} (i.e 1 mol carbon/22.4 mol Fe^{2+}). However, the measured values reported by Tuovinen and Kelley (1972) and Beck (1960) are much less than half of the theoretical value. This is expected as 100% conversion of energy from metabolic processes to cell mass is not possible, other anabolic processes in the cell that requiring energy were not considered in the theoretical estimation (for details, see Cavazza *et al.*, 1996; Cavazza *et al.*, 1995;

Ingledew, 1982; Nunzi *et al.*, 1993). Bacteria use the energy first for cell maintenance to ensure proper functioning and the remainder for cell synthesis.

2.8 The kinetics of microbial ferrous-iron oxidation

Equations 2.1 to 2.3 in section 2.2 represent the typical general reaction equation involved in bioleaching. It is the microbial ferrous-iron (Eq. 2.1) that drives/sustains bioleaching of sulphide minerals.

Generally, the microbial growth kinetics equation proposed by Monod in 1942 (as reported in Rossi, 1990) had its roots in the Michaelis–Menten model for enzyme-substrate interaction kinetics (Lehninger, 1975). According to the model, the enzyme E combines with the substrate to form enzyme-substrate complex, ES, which subsequently decomposes to form product, P and free enzyme, E. The basic assumption behind Michaelis-Menten enzyme kinetics is that the formation of an enzyme-substrate complex is reversible, while formation of product and free enzyme is irreversible. These chemical reactions for complex and product formation are represented by Equation 2.6

$$E + S \underset{K_2}{\overset{K_1}{\rightleftharpoons}} ES \xrightarrow{K_3} P + E \qquad 2.6$$

where: K_1 = rate constant for complex formation

K_2 = rate constant for reverse complex formation, and

K_3 = rate constant for product formation

Furthermore, by assuming an equilibrium state for the enzyme adsorption and de-sorption of the substrate and setting the rate of formation of the enzyme-substrate complex to zero ($d(ES)/dt = 0$) at equilibrium, it can be shown that the rate Equation for a single substrate enzymatic reaction is expressed as in Equation 2.7

$$v = \frac{d[P]}{dt} = \frac{K_2[E_T][S]}{K_m + [S]} \qquad 2.7$$

where $K_m = \frac{K_2 + K_3}{K_1}$ and $[E_T] = [E_0] + [ES]$

The maximum value of v is V_{max}, which occurs at very high [S] when 100% of the enzyme is in the "*busy*" state, K_m is sufficiently small at under this condition and the reaction rate follows a zero order course and the exponential phase occurs. If the limiting substrate concentration [S] is sufficiently small, its contribution to the denominator can be neglected. The kinetics become first order with respect to limiting substrate concentration, and K_m is the value of the limiting substrate concentration at which the specific reaction rate is half the maximum value.

Hence $V_{max} = K_2[E]_T$; V_{max} can replace $K_2[E]_T$ in the Equation above to give the common form of the Michaelis-Menten Equation:

$$v = \frac{V_{max}[S]}{K_m + [S]} \qquad 2.8$$

On the basis of experimental data Monod reported that the growth rate of *Escherichia coli* is directly proportional to its population X as shown in Equation 2.9:

$$r_X = \frac{dX}{dt} = \mu X \qquad 2.9$$

The proportionality constant, μ is called the specific growth rate. Monod ascertained that μ is a hyperbolic function of limiting substrate concentration and proposed the expression of this function in the form of Equation 2.10

$$\mu = \frac{\mu_{max}[S]}{K_m + [S]} \qquad 2.10$$

where μ_{max} is the maximum specific growth rate. The Monod kinetics expression is similar to and based upon Michaelis-Menten kinetics for enzymes. Monod kinetics assumed that bacteria cells may be regarded as a collection of enzymes to which Michaelis-Menten kinetics can be applied. One can think of Monod kinetics as

describing a chain of enzymatically mediated reactions with a limiting step described by Michaelis-Menten kinetics. However, if microbial growth is considered to be the result of enzymatic reactions in which one reaction is slower than the other, then the Michaelis-Menten Equation may be considered as the biochemical explanation of the usually good fit that Monod's Equation exhibits in growth modelling (Roels and Kossen, 1978). Monod proposed a microbial yield term (yield coefficient), defined as the ratio of the biomass growth rate to the substrate consumption rate.

$$Y = \frac{\frac{dX}{dt}}{-\frac{d[S]}{dt}} \qquad 2.11$$

A convenient method to determine the kinetic parameters for a microbial culture is to run a one-stage continuous stirred tank bioreactor at steady state with different dilution rates (Doran, 1995). If the bioreactor is fed with sterile feed, at steady-state condition, cell death and accumulation of biomass are negligible, it can be shown that specific microbial growth rate is equal to the dilution rate. Therefore, by varying the feed flow rate, the reactor performance at any specific growth rate can be determined for different feed substrate concentrations.

In order to model the mass balance for a steady-state chemostat with respect to biomass and substrate, the expressions for specific microbial growth rate and biomass yield from the substrate are required. The growth of a culture can be classified as substrate-limited and substrate-sufficient according to the availability of the actual substrate under consideration in relation to other essential substrates (Zeng and Deckwer, 1995). However, the specific growth rate is determined by the limiting substrate at a certain residual concentration, or vice versa. With respect to microbial ferrous-iron oxidation, the formulation of the kinetics is basically derived from the Monod Equation which relates microbial specific growth rate to the concentration of the limiting substrate, ferrous-iron (Monod, 1949) according to Equation 2.12

$$\mu = \frac{\mu_{max}[Fe^{2+}]}{K_{Fe^{2+}} + [Fe^{2+}]} \qquad 2.12$$

where μ and μ_{max} have been defined previously but with unit; mmolC(mmolFe.h)$^{-1}$, $[Fe^{2+}]$ is the concentration of the limiting substrate (mmol.L^{-1}) and $K_{Fe^{2+}}$ is called the saturation or affinity constant (mmol.L^{-1}). A low value of $K_{Fe^{2+}}$ is an indication that the microorganism has strong affinity towards the limiting substrate, and vice versa. It is also called the Michaelis-Menten constant. The rate of microbial growth, r_X (mmolC.L^{-1}.h^{-1}) is directly proportional to its population (concentration, C_x) as shown in Equation 2.13, this has been defined previously (Equation 2.9):

$$r_X = \frac{dC_X}{dt} = \mu C_X \qquad 2.13$$

where μ is the proportionality constant, it represents the growth rate per cell with the unit mmolC L^{-1}(mmolC L^{-1})$^{-1}$h^{-1}. The yield of microbes based on substrate consumed, biomass yield Y_{SX} is defined as the mole of biomass produced C_x, per mole of substrate consumed/oxidized $[Fe^{2+}]$, thus biomass yield on ferrous-iron can be obtained from the ratio of the rate of biomass growth to the rate of ferrous-iron utilization (oxidation) $r_{Fe^{2+}}$. Similar Equation can be written for biomass yield on oxygen consumed (see Equation 2.14).

$$-r_{Fe^{2+}} = \frac{1}{Y_{Fe^{2+}X}} r_X \ , \ -r_{O_2} = -\frac{1}{Y_{O_2X}} r_X \qquad 2.14$$

where r_{O_2} is the rate of oxygen consumption and Y_{O_2X} is the biomass yield on oxygen. Equation 2.14 has been found to be inadequate to explain observed trends in microbial growth and has been modified to include terms to account for endogenous respiration (Herbert *et al.*, 1956) or energy used by existing cells (Pirt, 1965). According to Pirt (1965), the energy derived during substrate utilization is channelled into two main courses: firstly for maintenance processes within the microbe, these are non-growth associated processes such as turnover of cell material, cell motility, adjustment of cell membrane potential, and internal pH and other endogenous metabolism and secondly for microbial growth. Therefore Equation (2.14) is modified by Pirt to incorporate the maintenance term as shown in Equations 2.15. This concept was first applied to microbial ferrous-iron oxidation by Boon (1995a). Pirt's Equation is the most used

expression for biomass yield from a substrate; Pirt proposed that the rate of microbial growth under substrate-limited conditions and balanced growth has an effect on the observed biomass yield (Equation 2.15b):

$$r_{Fe^{2+}} = \frac{1}{Y_{Fe^{2+}X}} r_X + m_{Fe^{2+}} C_X \qquad 2.15a$$

$$\frac{1}{Y_{Fe^{2+}X}} = \frac{1}{Y^{\max}_{Fe^{2+}X}} + \frac{m_{Fe^{2+}}}{\mu} \qquad 2.15b$$

$$q_{Fe^{2+}} = -\frac{r_{Fe^{2+}}}{C_X} = \frac{\mu}{Y^{\max}_{Fe^{2+}X}} + m_{Fe^{2+}} \qquad 2.15c$$

where, $Y_{Fe^{2+}X}$ is the observed biomass yield (e.g. g biomass · g substrate consumed^{-1});

$Y^{\max}_{Fe^{2+}X}$ is the maximum microbial yield in the absence of competing reactions consuming ATP (e.g. g biomass ·g substrate consumed^{-1}), μ is the specific microbial growth rate (h^{-1}), $q_{Fe^{2+}}$ is the specific rate of substrate utilisation. It measures the amount of substrate utilised per biomass (e.g. mol of substrate consumed per mol of biomass, per hour), and $m_{Fe^{2+}}$ is the maintenance coefficient, which is the specific substrate uptake rate for maintenance activities (e.g. g substrate consumed (g biomass)$^{-1}$ hours^{-1}). $Y^{\max}_{Fe^{2+}X}$ is usually considered as an imaginary value which relates to the observed yield (Doran, 1995) that can never be observed since the maximal observable biomass yield appears at the critical dilution rate.

However, for a continuous culture at steady state, Equations 2.15 are useful because μ = D (dilution rate) and therefore need not be determined, this is derived in Section 2.9. Therefore, the parameters, μ_{max}, $K_{Fe^{2+}}$, $Y^{\max}_{Fe^{2+}X}$ and $m_{Fe^{2+}}$ characterized the steady-state conditions of microbial ferrous-iron oxidation under a continuous mode at various dilution rates.

These values can be calculated if the steady state substrate, Fe^{2+} and biomass, C_X concentrations are known for different dilution rates. The kinetic parameters

(μ_{max}, $K_{Fe^{2+}}$) can be determined graphically by linearising the appropriate governing Equation. For example using the Monod type equation (Equation 2.12), Lineweaver-Burk, Eadie-Hofstee, and Langmuir plots can be plotted, to obtain the required constants. These plotting procedures give different degrees of distortion in the experimental data which amplifies the errors in the determination at low substrate concentration. The mathematical descriptions of the plots are explained below:

The Linearisation technique using Lineweaver-Burk method (Lineweaver and Burk, 1934) evaluates the reciprocal of Equation 2.12 as shown in Equation 2.16

$$\frac{1}{D} = \frac{K_{Fe^{2+}}}{\mu_{max}}\left(\frac{1}{[Fe^{2+}]}\right) + \frac{1}{\mu_{max}} \qquad 2.16$$

By plotting $1/D$ versus $1/[Fe^{2+}]$, μ_{max} can be obtained from the intercept on the ordinate, and $K_{Fe^{2+}}$ from the slope of the resulting straight line. The Linearised Monod Equation by Eadie-Hofstee method (Hofstee *et al.*, 1959) is given by Equation 2.17

$$\frac{D}{[Fe^{2+}]} = \frac{\mu_{max}}{K_{Fe^{2+}}} - \frac{D}{K_{Fe^{2+}}} \qquad 2.17$$

The plot of $D/[Fe^{2+}]$ versus D gives a straight line with the slope of $-1/K_{Fe^{2+}}$ and intercept of $\mu_{max}/K_{Fe^{2+}}$. Using the Langmuir method (Verger and DeHaas, 1976), the Linearised Monod gives Equation 2.18:

$$\frac{[Fe^{2+}]}{D} = \frac{K_{Fe^{2+}}}{\mu_{max}} + \frac{[Fe^{2+}]}{\mu_{max}} \qquad 2.18$$

By plotting $[Fe^{2+}]/D$ versus $[Fe^{2+}]$ a straight line with the slope $1/\mu_{max}$ and intercept $K_{Fe^{2+}}/\mu_{max}$ is obtained. These linearised plots are shown in Figure 2.6

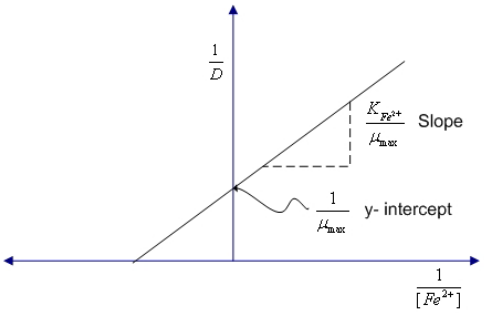

(a) Lineweaver-Burk plot

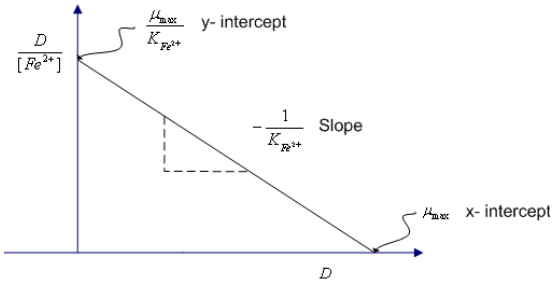

(b) Eadie-Hofstee

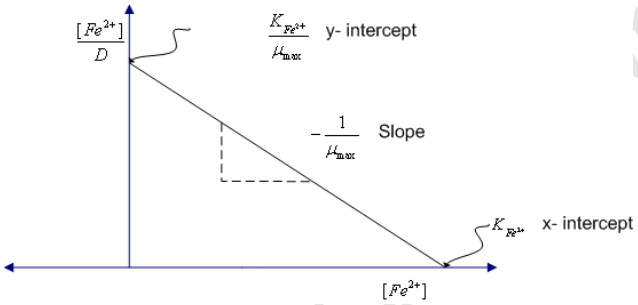

(b) Langmuir plot

Figure 2.6 The plots of linearised Monod Equations using (a) Lineweaver-Burk, (b) Eadie-Hofstee and (c) Langmuir methods.

2.8.1 Biomass yield and Maintenance

Following Pirt's concept that the substrate utilisation rate is coupled with the microbial growth and cell maintenance as shown in Equations 2.15

$$q_{Fe^{2+}} = -\frac{r_{Fe^{2+}}}{C_X} = \frac{\mu}{Y^{\max}_{Fe^{2+}X}} + m_{Fe^{2+}} \qquad 2.15$$

Some researchers have challenged this concept, reporting varying biomass yield and maintenance at different conditions (Neijssel and Tempest, 1976), thus a modified equation was proposed to account for the observed increase in maintenance energy requirement at low biomass growth rates.

$$q_{Fe^{2+}} = \frac{\mu}{Y^{\max}_{Fe^{2+}X}} + m_{Fe^{2+}} + c\mu\, m_{Fe^{2+}} \qquad 2.19$$

where c represent a constant to account for the growth rate dependence of maintenance energy. Pirt also modified his model to include the growth rate dependence of

maintenance by assuming that as biomass growth rate approached maximum, the growth rate dependent portion of the maintenance energy reduces to zero as shown in Equation 2.20. This is described in detail in Dempers(2001) and Dempers (2003)

$$q_{Fe^{2+}} = \frac{\mu}{Y^{\max}_{Fe^{2+}X}} + m_{Fe^{2+}} + m^{v}_{Fe^{2+}}(1 - k\mu) \qquad 2.20$$

where $m^{v}_{Fe^{2+}}$ represent the growth rate dependent coefficient and $k = 1/\mu^{\max}$ an empirical constant.

Different values of biomass yield have also been found on substrate-limited and substrate-sufficient cultures. This was attributed to the fact that biomass growth and substrate utilisation and dissipation of energy of non-growth processes can be uncoupled. Some work has been done to account for non-growth energy consumption (Kelly and Jones, 1978; Liu *et al.*, 1988; MacDonald and Clark, 1970). However, Kelly and Jones (1978) have reported that microbial growth and substrate utilisation can be uncoupled in batch systems, and the *At. ferrooxidans* has the potential to dissipate energy generated in the absence of growth.

Some researchers have estimated maintenance requirements using the constant maintenance Pirt Equation (Boon, 1996; Breed *et al.*, 1999; Breed and Hansford, 1999a; Jones and Kelly, 1983). Boon was only able to use this Equation to model continuous culture, while Jones and Kelly (1983) obtained different result, when it was used to model cultures under competitive and non-competitive ferric-iron inhibition. The equation did not reflect the effects of varying pH and temperature on a continuous culture, due to the scattering of the data (Breed *et al.*, 1999; Breed and Hansford, 1999a).

However, a theoretical maximum yield for a system can be determined based on the dissipation of available Gibbs free energy. This was developed by Heijnen and van Dijken (1992) using a black box approach. This requires setting up a macrochemical balance from the simultaneous solution of individual charge and elemental balances. The macrochemical balance is used to determine the Gibbs free energy of the reaction, which is equal to the Gibbs free energy dissipated. This energy is made up of two components: growth related and maintenance related as shown in Equation 2.21

$$\frac{D_S^{01}}{r_x} = \left(\frac{D_S^{01}}{r_x}\right)_{growth} + \frac{m_E}{\mu} \qquad 2.21$$

where D_s^{01}/r_x represent the dissipation of Gibbs energy needed to produce 1 Carbon mole of biomass from a given carbon source in kJ.molC^{-1}. m_E is the specific rate of consumption of maintenance energy in kJ.(molC.h)$^{-1}$. It has been shown that for autotrophic growth involving reverse electron transfer, D_s^{01}/r_x = 3500 kJ.molC^{-1}, and that the maintenance requirement can be determined from the correlation in Equation 2.22 (Heijnen and van Dijken, 1992; Tijhuis *et al.*, 1993)

$$m_E = 5.7 \exp\left[\frac{-6.94 \times 104}{R}\left(\frac{1}{T} - \frac{1}{298}\right)\right] \qquad 2.22$$

The aforementioned shows that extensive work has been carried out on microbial ferrous oxidation, and various experimental methods have been used in these studies especially with *At. ferrooxidans* and *Leptospirillum* species. However, the reported model parameters vary from one author to another. The theoretical details involved in the determination of a useful equation to predict the trend of some parameters in microbial ferrous-iron oxidation kinetics will be discussed in Section 2.8.

2.9 A theoretical formulation of microbial oxidation of ferrous – Iron

The kinetic and yield parameters for a Fe^{2+} oxidizing culture can be determined by performing a mass balance for biomass- and substrate over the bioreactor concerned at different residence times (Boon *et al.*, 1995a; Sundkvist *et al.*, 2007). The following general assumptions apply:

1. The reaction is carried out in a well-mixed reactor with uniform temperature and concentration
2. There is no accumulation of biomass in the reactor by attachment to the walls.
3. There is no formation of iron precipitate such as jarosite;
4. The feed and discharge flow rates are equal and the reactor volume is constant
5. The culture is substrate-limited with respect to Fe^{2+}

6. The Feed solution is sterile and no growth inhibition factors are present (or are constant).

The overall biomass balance for active cells in the reactor over time will be given by the following Equation:

$$V\frac{dC_X}{dt} = FC_{X0} - FC_X + \mu C_X V - k_d C_X V \qquad 2.23$$

where $\boldsymbol{V}$ is the reactor volume; F , the flow rate; C_X biomass concentration; μ specific growth rate; k_d specific death rate. Assuming that the feed is sterile ($C_X = 0$) and that the bioreactor is operated at relatively short residence times, then the death rate is negligible ($k_d = 0$). It can be shown as in Equation 2.23 that for a bioreactor operated at steady state, the specific growth rate, μ is equal to the dilution rate *D*:

$$\mu = \frac{F}{V} = D = \frac{1}{\tau} \qquad 2.24$$

where $\boldsymbol{\tau}$ is the residence time.

However, for the overall substrate balance, the amount of Fe^{2+} in the bioreactor at a given time can be written as given in Equation 2.

$$V\frac{d[Fe^{2+}]}{dt} = F[Fe^{2+}]_0 - F[Fe^{2+}] - \frac{\mu C_X}{Y_{FeX}^{\max}}V - m_{Fe^{2+}}C_X V \qquad 2.25$$

where

$\frac{\mu C_X}{Y_{FeX}^{\max}}$ is the fraction rate used for growth

$m_{Fe^{2+}}C_X$ is the fraction rate used for cell maintenance

It can be shown that steady state biomass concentration and the ferric-to-ferrous ratio can be predicted at any given dilution rate if the parameters, $\mu_{\max}$, $K_{Fe^{2+}}$, $Y_{Fe^{2+}X}^{\max}$ and $m_{Fe^{2+}}$ are known as shown in Equations 2.26 and 2.27.

$$C_X = \left([Fe^{2+}]_0 - \frac{D.K_{Fe^{2+}}}{\mu_{\max} - D}\right) \Big/ \frac{1}{Y_{FeX}^{\max}} - \frac{m_{Fe^{2+}}}{D} \qquad 2.26$$

$$\ln\frac{[Fe^{3+}]}{[Fe^{2+}]} = \ln\left(\frac{[Fe^{2+}]_0}{\frac{D.K_{Fe^{2+}}}{\mu_{max} - D}} - 1\right) \qquad 2.27$$

The detail derivation of Equations 2.26 and 2.27 is shown in Appendix A1.1. Figure 2.7 shows the variation of biomass concentration with dilution rate for a chemostat as predicted by Equation 2.26, given a reasonable guess of μ_{max}, $K_{Fe^{2+}}$, $Y^{max}_{Fe^{2+}X}$ and $m_{Fe^{2+}}$. This plot is based on the assumption that the Monod Equation 2.10 is applicable. The biomass was fairly constant and only declines sharply as the system approaches the washout region.

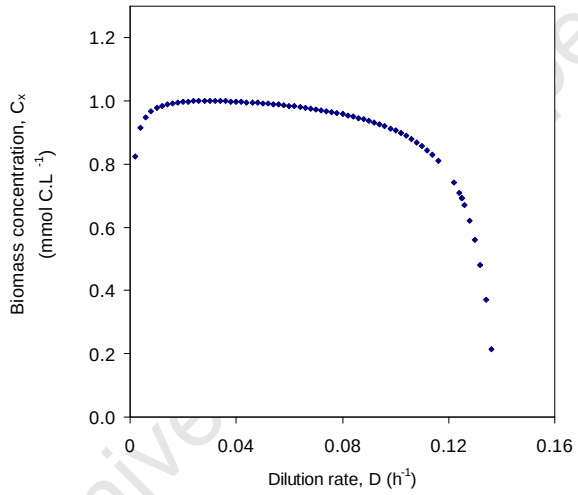

Figure 2.7 Predicted trend of biomass concentration with dilution rate based on the Monod Equation 2.8

2.10 The development of kinetic equations for microbial ferrous-iron oxidation

The rate equations for microbial ferrous-iron oxidation have been reviewed and some of the published rate equations are shown in Table 2.3. Lacey and Lawson (1970) applied the Monod kinetic equation in the study of microbial ferrous iron oxidation in batch culture and observed that the bacterial specific growth rate decreases with increasing concentration of ferrous iron, an optimum specific growth rate was also reported at

31°C. This work was further extended to include the effects of ferric-iron inhibition on microbial growth by Kelly and Jones (1978). The kinetic constants in their kinetic model were found to vary with initial ferrous iron concentration. This was attributed to ferrous and ferric iron inhibition in both the batch and continuous systems investigated. However, the authors reported evidence of competitive and non-competitive ferric-iron inhibition in their subsequent article and came up with models (Equation 2.28 and 2.29) describing bacterial ferrous oxidation in continuous mode (Jones and Kelly, 1983).

$$\mu = \frac{\mu_{max}}{1 + \frac{K_1}{[Fe^{2+}]} + \frac{K_1}{K_2}\frac{[Fe^{3+}]}{[Fe^{2+}]}} \qquad 2.28$$

$$\mu = \frac{\mu_{max}[Fe^{2+}]}{(K_1 + [Fe^{2+}])\left(1 + \frac{[Fe^{3+}]}{K_2}\right)} \qquad 2.29$$

where K_1 = the substrate affinity coefficient in mmol $Fe^{2+}.L^{-1}$
and K_2 = the ferric inhibition constant in mmol $Fe^{3+}.L^{-1}$

These inhibition equations are special cases derived from linear mixed inhibition model as described by Cortes *et al.* (2001), in which the rate depends on the concentrations *s* of substrate and *i* of product according to Equation 2.30

$$f_R = \frac{V.s}{K_s\left(1 + \frac{i}{K_C}\right) + s.\left(1 + \frac{i}{K_U}\right)} \qquad 2.30$$

Where *V* is the maximum,
K_s is the Michaelis-Menten constant,
K_C is the competitive inhibition constant and
K_U is the uncompetitive inhibition constant.

In competitive inhibition i/K_U is negligible leading to Jones and Kelly's Equation 2.28 and the two inhibition constants are equal in pure non-competitive inhibition resulting to Equation 2.29. This is reviewed further in Section 8.1.

Other researchers have confirmed that product (ferric-iron) inhibition kinetic models are applicable to microbial growth and ferrous-iron oxidation by *At. ferrooxidans* and *L. ferrooxidans* using batch and continuous culture, and respiration experiments (Liu *et al.*, 1988; Norris *et al.*, 1988). Braddock *et al.* (1984) has further extended this approach to

include threshold ferrous-iron concentration, which account for the value of ferrous-iron concentration (a low value) below which no microbial growth will occur.

$$\mu = \frac{\mu_{max}[Fe^{2+}]}{1 + \frac{K_{Fe^{2+}}}{[Fe^{2+}] - [Fe^{2+}]_t}} \qquad 2.31$$

where $[Fe^{2+}]_t$ = threshold ferrous-iron concentration in mmol $Fe^{2+} L^{-1}$

Table 2.3 Selected published kinetic models for ferrous-iron oxidation with *At. Ferrooxidans*

Author	Model	Conditions
Lacey & Lawson 1970	$\mu = \frac{\mu_{max}[Fe^{2+}]}{Y_{sx}K_m + [Fe^{2+}]}$	Batch STR T= 25-30 °C, pH = 2-2.3 Fe_T = 6g.l^{-1}
MacDonald & Clark 1970	$\mu = \frac{\mu_{max}[Fe^{2+}]}{K_m + [Fe^{2+}]}$	Continuous T= 28°C, pH =2. 2
Kelly & Jones 1978	$\mu = \frac{\mu_{max}[Fe^{2+}]}{K_S\left(1 + \frac{[Fe^{3+}]}{K_P}\right) + [Fe^{2+}]\left(1 + \frac{[Fe^{3+}]}{K_c}\right)}$	Shake Flask T= 30°C, pH =1.6
Braddock *et al* 1984	$\mu = \frac{\mu_{max}([Fe^{2+}] - [Fe^{2+}]_t)}{K_m + ([Fe^{2+}] - [Fe^{2+}]_t)}$	Continuous T= 22°C, Fe_T = 9 -22 mM Isolate AK1
Liu *et al* 1988	$\mu = \frac{\mu_{max}[Fe^{2+}]}{[Fe^{2+}] + K_s(1 + K_i[Fe^{3+}])}$	Continuous T= 35°C, pH = 1.8 Fe_T = 0.52-3.29 gFe^{2+}.L^{-1}
Lizama & Suzuki 1989	$-r_{O_2} = \frac{k'_3[X][Fe^{2+}]}{[Fe^{2+}] + K_m\left[1 + \frac{[X]}{K'_i} + \frac{[Fe^{3+}]}{K_{if}} + \frac{[X][Fe^{3+}]}{\alpha K'_i K_{if}}\right]}$	Initial Rate T = 29 °C, pH = 1.8-2.0 Fe_T = 0.25-26 mM
Nikolov & Karamanev 1992	$\mu = \frac{\mu_{max}[Fe^{2+}]}{[Fe^{2+}] + K_s + [Fe^{3+}]\frac{K_s}{K_i} + \frac{([Fe^{2+}])^2}{K_{si}}}$	Continuous T= 29°C, pH = 1.8-2.0 Fe_T = 2-70.8 g.L^{-1}
Huberts 1994	$-r_{Fe^{2+}} = a_1\left(\frac{P_{O_2}}{k_B + P_{O_2}}\right)\left(\frac{[Fe^{2+}]}{[Fe^{2+}] + K_{Fe^{2+}}\left(1 + \frac{[Fe^{3+}]}{K'}\right)}\right)$	Continuous T= 30°C, pH = 2.0
Crundwell 1997	$-r_{Fe^{2+}} = k\left(\frac{[Fe^{2+}]/[H^+]}{K_{Fe^{2+}} + [Fe^{2+}]/[H^+] + K_i[Fe^{3+}]}\right)^{0.5}\left(\frac{p_{O_2}}{k_B + p_{O_2}}\right)^{0.5}$	theoretical, fitted to data from Huberts, 1994
Hansford 1997, [3]	$q_{Fe^{2+}} = \frac{q^{max}_{Fe^{2+}}}{1 + K_{Fe^{2+}}\frac{[Fe^{3+}]}{[Fe^{2+}]}}$	only fitted to *Leptospirillum* data
Webb & Nemati 1998	$\frac{d[Fe^{2+}]}{dt} = \frac{K_0 e^{\frac{Ea}{RT}}[X][Fe^{2+}]}{\left(1 + \frac{[Fe^{3+}]}{K_i}\right)(K_m + [Fe^{2+}])}$	Initial Rate T = 30 °C, pH = 2.0 Fe_T =0.45-31.5 kg.m^{-3}
Boon *et al* 1999	$q_{O_2} = \frac{q^{max}_{O_2}}{1 + \frac{K_s}{[Fe^{2+}] - [Fe^{2+}]_t} + \frac{K_s}{K_i}\cdot\frac{[Fe^{3+}]}{[Fe^{2+}] - [Fe^{2+}]_t}}$	Continuous T= 30°C pH = 1.8-1.9 Fe_T = 0.05-0.36M
Meruane *et al* 2002	$q_{Fe^{2+}} = \frac{K^*_1 \exp\left[\frac{nF}{2RT}\left(E^m - E^0_h\right)\right]\left\{1 - \exp\left[\frac{nF}{RT}\left(E^m - E\right)\right]\right\}}{1 + \frac{K^*_2}{[Fe^{2+}]} + K^*_3 \exp\left[\frac{nF}{RT}\left(E_h - E^0_h\right)\right]}$	Electrochemical cell T= 30°C, pH = 1.8 Fe_T = 0.05-1 g.L^{-1}

Source: Adapted from Searby (2006) and Ojumu *et al.* (2006)

Most of the proposed kinetic equations were formulated in terms of specific microbial growth rate (μ). However, Boon and co-workers have described the kinetics in terms of specific ferrous-iron utilization rate using a competitive ferric inhibition model derived from the Michaelis-Menten expression. This was found to be more useful in terms of experimental measurement as well as engineering application (Boon, 1996; Boon *et al.*, 1999b; Hansford, 1997; van Scherpenzeel *et al.*, 1998). The authors have further simplified the inhibition proposed by Lacey and Lawson (1970), and Jones and Kelly (1983) to include dependence on the ferric-ferrous iron ratio.

They showed that the redox potential (ferric to ferrous iron concentration ratio) is the dominant factor in the kinetic equation governing the microbial ferrous-iron oxidation. It was shown however, that the oxidation rate is stoichiometrically related to oxygen consumption rate under all circumstances (Boon *et al.*, 1995a; Boon *et al.*, 1995b; Boon *et al.*, 1999b). The authors combined the Braddock's threshold theory with the competitive product (ferric iron) inhibition kinetics (Equation 2.28) and used the correlation between ferrous oxidation rate, microbial growth and maintenance via Pirt's Equation. Therefore, by measuring CO_2, O_2 consumption rates and ferric to ferrous ratio, the microbial growth and ferrous-iron oxidation kinetics have been described with specific microbial ferrous-iron utilization model (q model) in both batch and continuous systems. (Boon *et al.*, 1999a; 1999b):

$$q_{Fe^{2+}} = \frac{r_{Fe^{2+}}}{C_x} = \frac{q_{Fe^{2+}}^{\max}}{1 + \frac{K_1}{[Fe^{2+}] - [Fe^{2+}]_t} + \frac{K_1}{K_2} \cdot \frac{[Fe^{3+}]}{[Fe^{2+}] - [Fe^{2+}]_t}} \qquad 2.32$$

A simplified version of the ferric inhibited growth model of Equation 2.32 above was presented by Hansford (1997) (Equation 2.33). The author reported that the contribution of the second term to the denominator is insignificant: this was demonstrated in a batch experiment. This has been proved to be useful in describing microbial ferrous oxidation under mesophilic conditions (Breed *et al.*, 1999; Breed and Hansford, 1999a; 1999b; Hansford and Vargas, 2001), and recently under extreme thermophilic condition (Searby, 2006; Searby and Hansford, 2003) .

$$q_{Fe^{2+}} = \frac{q_{Fe^{2+}}^{max}}{1 + \frac{K_1}{K_2}\frac{[Fe^{3+}]}{[Fe^{2+}]}} \quad 2.33$$

Crundwell (1997) formulated a model based on the fundamental chemiosmotic theory proposed by Ingledew (1982) for the electron/proton transport mechanism of *At. ferrooxidans*. The author modelled microbial ferrous-iron oxidation rate as being analogous to an electrochemical cell or battery by making use of the fact that this mechanism serves as the energy generator for the entire cell's metabolic activity. The proposed kinetic model (Equation 2.34) is similar to Monod but raises it to the power of half and is able to account for the effects of ferric and ferrous ions, hydrogen ions and oxygen concentration.

$$\mu = K\left(\frac{[Fe^{2+}]/[H^+]}{K_{Fe^{2+}} + [Fe^{2+}]/[H^+] + K_i[Fe^{3+}]}\right)^{0.5} \cdot \left(\frac{O_2}{K_{O_2} + O_2}\right)^{0.5} \quad 2.34$$

The kinetic Equation derived by Meruane et al (2002) was formulated by combining electrochemical theory with the Michaelis–Menten dynamics for the ferrous–ferric oxidation reaction:

$$\mu = \frac{\mu_{max} - K_1\frac{[Fe^{3+}]}{[Fe^{2+}]}}{1 + K_2 \cdot \frac{1}{[Fe^{2+}]} + K_3\frac{[Fe^{3+}]}{[Fe^{2+}]}} \quad 2.35$$

The rate Equation (Equation. 2.35) is almost identical to the ferric inhibition model (Equation 2.28) except for the additional term in the numerator. It was determined from the assumption that the electron transfer step in the cell membrane is fully reversible, i.e. there exists a ferric/ferrous iron ratio at which the rates of electron transfer from and to ferrous-iron adsorbed onto the membrane are equal and no net oxidation occurs.

2.11 Comparison of the fundamental kinetic models

The fundamental rate models presented above have emerged over three decades of research and in each case the models were calibrated against a set of experimental data generated by the individual authors using different experimental techniques, as indicated

in Table 2.3. It is worth comparing some of these models, if all are calibrated against the same set of experimental data. This has been done for a set of data points presented by Boon (1999b), and is presented in Figure 2.8. The models compared were those given in Equation 2.12, 2.28, 2.32 – 2.35. The relevant parameters of each model were obtained through the Excel Solver routine by minimizing the sum of square errors between measured and predicted values. The μ-based models were directly compared to the q- or rate base models by assuming that the maintenance coefficient in the Pirt Equation (Equation 2.15) is small and can be neglected.

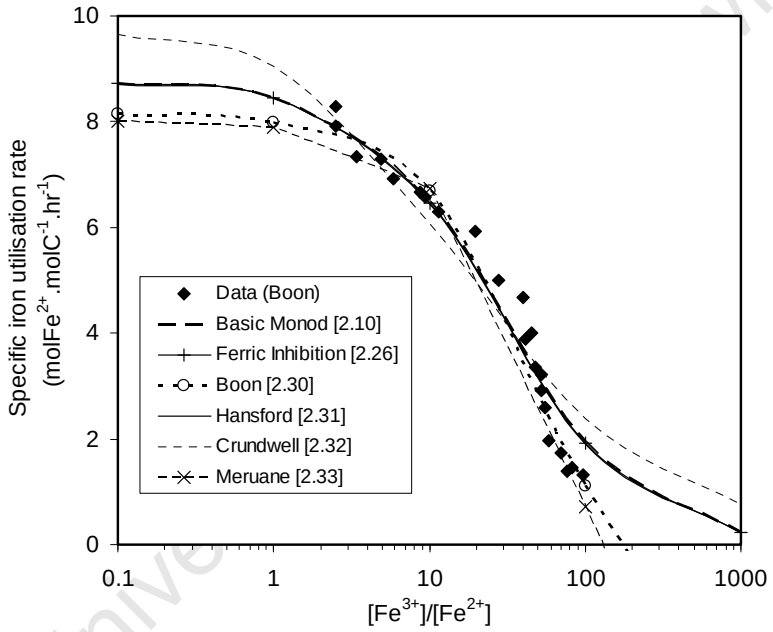

Figure 2.8 Comparison of various rate Equations calibrated to the same set of data for *Acidithiobacillus ferroxidans* by Boon (1999). The numbers in square brackets refer to the relevant Equations in the text.
Source: Modified after Ojumu *et al.*(2006)

The results indicate that in the case of *At. ferrooxidans* the differences between the models, based on substrate utilisation and ferric inhibition (Equations 2.12, 2.32 and 2.33), are effectively negligible, and that none fits the data particularly well beyond a ferric to ferrous ratio of about 100. Crundwell's model (2.34) gives a significantly worse fit, but it also follows the same trends as the previous models. Therefore, it is postulated here, that the effects of ferric inhibition on microbial growth and utilization rates are negligible and

that it is in fact the limitation of ferrous substrate that effectively drives microbial ferrous oxidation kinetics.

On the other hand, the models by Boon and Meruane (Equations (2.32) and (2.35) respectively), fit the data reasonably well over the entire range. Both of these models allow for a subtractive term – a threshold ferrous concentration in Boon's model and a term accounting for the reversibility of electron transfer in the cell membrane in Meruane's model. In this latter case it could be either relative lack of ferrous iron or relative abundance of ferric iron that reduces the overall rate of ferrous iron utilization. Both of these two would predict negative ferrous iron oxidation rates at a ferric to ferrous ratio above about 150 – 200, which appears contradictory. In Boon's model this could be seen as a cut-off point, beyond which the model is no longer valid. By contrast, Meruane's model, which is based on an assumption of reversibility, should remain valid with the cell reducing ferric – a scenario that remains unproven.

In the absence of data measured at ferric to ferrous ratios higher than 100, however, any model extrapolation must be treated with caution. In reality, it is likely that microbial growth does indeed cease below a certain minimum concentration of ferrous iron, while ferrous utilization for cell maintenance may still continue. As indicated above, maintenance was considered negligible for the purpose of this evaluation. A meaningful description of maintenance ferrous utilization would require more data at substantially higher ferrous to ferric ratios.

2.12 Kinetic models compensated for factors affecting microbial ferrous-iron oxidation

Most of the studies on microbial ferrous-iron oxidation have been dedicated to the effects of ferrous-iron and ferric-iron concentrations on the kinetics, while other factors, relevant to bioleach heaps, that may have a significant effect on microbial growth and the oxidation process, have been much less studied. The following subsection gives a brief overview.

2.12.1 Effect of solution pH

Changes in pH have been found not to have a significant effect on microbial growth and ferrous-iron oxidation by iron oxidizing microbes in their normal operating window. The

study conducted by Breed and Hansford (1999a) revealed that no significant effect of pH was shown on the maximum specific ferrous iron and oxygen utilization rates within the range studied (pH 1.10-1.70). However, the authors reported that the apparent affinity constant K ($=K_1/K_2$) in Equation (2.33) increases linearly with increasing pH.

$$q_{Fe^{2+}} = \frac{q_{Fe^{2+}}^{max}}{1 + (0.0048\,pH - 0.0043)\dfrac{[Fe^{3+}]}{[Fe^{2+}]}} \qquad 2.36$$

According to Pesic (1993), *At. ferrooxidans* is significantly inhibited at pH below 1.5 and above 3.5 (for details, see Nemati *et al.*, 1998). However, Coram (2002) reported that the optimum pH for *L. ferriphilum* lies between 1.4 and 1.8 while Plumb *et al.* (2007b) reported that it exhibited a broad optimum pH with a peak at pH 2.0. The authors used microbial activity as a proxy measure of microbial growth. Recent reports have shown that microbial growth on ferrous-iron are negatively affected at pH greater than 2.0 (du Plessis *et al.*, 2007; van Aswegen *et al.*, 2007). Although there seems to be no definite optimum pH, the resistance of iron oxidizing microbes to low pH was attributed to the composition of their cell wall. At very low pH the cell might require more energy to maintain the proton gradient, since the cell cytoplasm must be maintained at or near neutral values, thus the maintenance will be at the expense of cell growth.

Inhibition at high pH, on the other hand, could be explained since protons are required as a substrate in the oxidation reaction (Equation 2.2), they are also important to prevent the formation of Fe^{3+} precipitate, which has negative effect on bioleaching application (Meruane *et al.*, 2002). The proton gradient is the driving force for the synthesis of ATP as described by Ingledew (1982). Crundwell's model incorporates the effect of pH in terms of proton concentration in his model (Equation 2.34), postulating that pH affects the speciation of the ferrous ion, and that in fact it is the $Fe(OH)^+$ complex that adsorbs to the microbe, the predominance of which is strongly pH dependent (Crundwell, 1997). However recent studies have shown that microbial ferrous-iron oxidation can be sustained at pH 0.9 (Kinnunen and Puhakka, 2005; Özkaya *et al.*, 2007b), the increased tolerance at lower pH might have been due to adaptation of the microbial species.

Ferric-iron precipitation

At higher pHs, ferric-iron is sparingly soluble and readily precipitates as hydroxides, oxyhydroxides and hydroxylsulphate (jarosite) compounds (MacDonald and Clark, 1970). It hydrolyses in water, forming insoluble hydroxyl compounds,

$$Fe^{3+} + 3H_2O \leftrightarrow Fe(OH)_3 + 3H^+$$

and in the presence of a suitable mono-valent cation, such as K^+, Na^+, NH_4^+ and H_3O^+, and excess sulphate, forms a competing precipitation reaction – ferric hydroxysulphate

$$3Fe^{3+} + M^+ + H_2SO_4^- + 6H_2O \leftrightarrow MFe_3(SO4)_2(OH)_6 + 8H^+$$

$$8Fe^{3+} + SO_4^- + 14H_2O \leftrightarrow Fe_8O_8(OH)_6(SO4)_2 + 22H^+$$

The nature of the precipitate depends on the type of cation M. If present, it forms a crystalline compound, jarosite, and when absent, an amorphous compound results. Its nature also depends on pH and temperature. Eneroth and Koch (2004) reported that ammonium jarosite was predominant at pH 1.6 in ferrous-iron oxidation by *At. ferrooxidans* and at pH 3.2 schwertmannite was observed. Another recent study by Kupka *et al.* (2007) has shown that schwertmannite is dominant at low temperature oxidation of ferrous-iron by *At. ferrooxidans*. Ferric-iron precipitate has been reported to hinder oxidation by forming a diffusion barrier (Nemati *et al.*, 1998) and reducing free ferric-iron available for leaching.

2.12.2 Effect of operating temperature

Microorganisms are classified in terms of the temperature range at which they survive, with optimum temperatures in the 30°C range for mesophiles, 50°C range for moderate thermophiles, and above 65°C for extreme thermophiles. At temperatures below the optimum the microbes become inactive and they are no longer viable at temperatures above it, as shown in Figure 2.9. The effect of temperature maximum specific rates is mostly expressed using the Arrhenius function, Equation 2.37 (Breed *et al.*, 1999; Franzmann *et al.*, 2005; Lacey and Lawson, 1970; MacDonald and Clark, 1970; Nemati

and Webb, 1997; Özkaya *et al.*, 2007a). This function describes effect of temperature below the optimum temperature as shown in Figure 2.9.

$$\mu_{\max} = K_o e^{-\frac{E_a}{RT}} \qquad 2.37$$

where E_a is the activation energy in ($J.mol^{-1}$)

K_o is the frequency factor (h^{-1})

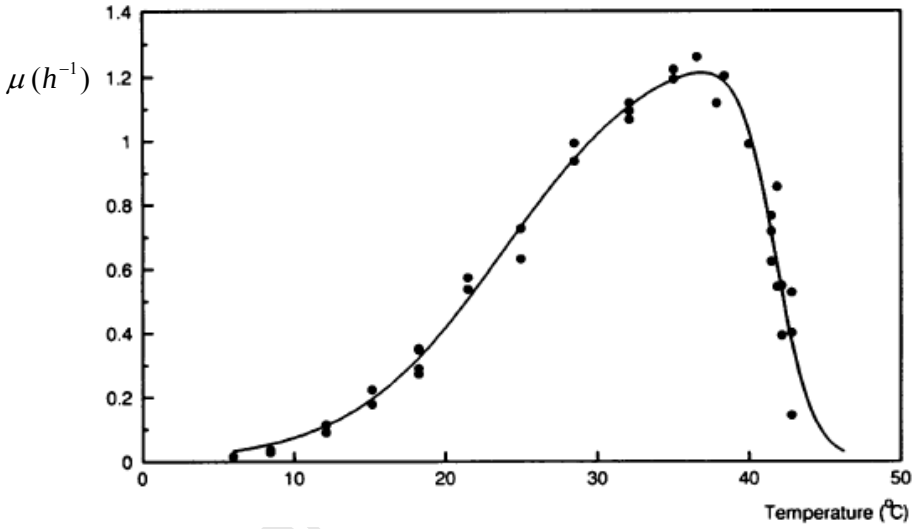

Figure 2.9 Example of showing the effect of temperature on specific growth rate.
Source: Taken from Zwietering (1991).

The activation energy E_a can be determined from the linear plot of $\ln(\mu_{\max})$ versus (T^{-1}). E_a essentially represents the activation energy of the process rather that for a particular reaction, since microbial growth also involves a number of complicated biochemical reactions within the cell. However, it is reasonable to expect that for the ferrous-iron system, the activation energy for the microbial oxidation should be lower than the abiotic oxidation. Table 2.4 shows the list of activation energies of microbial ferrous-iron oxidation obtained from the literature and the temperature range of study.

The temperature-growth dependence is also described using the Ratkowsky model (Equation 2.38) (Ratkowsky *et al.*, 1982)

$$\sqrt{\mu_{\max}} = b(T - T_o) \qquad 2.38$$

where T_o is a conceptual temperature of no metabolic significance (i.e. no significant growth)

Table 2.4 Activation energies describing temperature effects on some selected biolaching microorganism

	Optimum Temperature	Activation Energy E_a ($kJ.mol^{-1}$)	Temperature range studied °C	References
A. brierleyi	71.5	NR	45 – 95	
S. thermosulfidooxidans	51.2	51	27 – 65	
"F. cyprexacervatum"	55.2	65	35 – 65	
Am. Ferrooxidans	48.8	62	10 – 59	(Franzmann
F. acidiphilum	39.6	79	12.7-47.2	*et al.*, 2005)
L. ferriphilum	38.6	89	15 – 58	
L. ferrooxidans	36.7	80, 35.63[f]	8 – 55 (30 – 40)[f]	
At. ferrooxidans	29.6	32, 33.9[a], 68.4[b], 51.2[c], 47.2[d], 80[e]	10 – 55	

[f] Breed (1999), [a] Lacey (1970), [b] Nemati (1997), [c] MacDonald (1970), [d] Ahonen (1989), [a] Okereke (1991); **Source**: Adapted from Franzmann (2005) and Searby (2006)

Equation 2.38 was further extended to cover the entire temperature range, accounting for decreasing rates above and below the optimum temperature for microbial growth and activity (Ratkowsky *et al.*, 1983). The optimum and maximum growth temperatures are usually close, as was shown by Gomez and Cantero (1998) and recently by Franzmann *et al.* (2005) for some commonly found microbes in bioleach heaps. This confirms the rapid deactivation of the microbes, when subjected to conditions beyond the optimum temperature.

$$\sqrt{\mu_{\max}} = b(T - T_{\min})\left(1 - e^{c(T - T_{\max})}\right) \quad 2.39$$

where T_{min} and T_{max} are the minimum and maximum growth temperatures respectively, at which the rate of growth is zero. The parameter b is the regression coefficient of the square root of growth rate constant versus degrees Kelvin for temperatures below the optimal temperature, and c is a constant obtained by data fitting.

Recently Ratkowsky *et al* (2005) reported that the reaction of globular proteins to temperature is similar to how bacteria react to temperature and proposed a mechanistic function (Equation 2.40) by employing a kinetic model incorporating thermodynamic parameters for temperature-induced enzyme denaturation.

$$r = \frac{cT\exp[-(\Delta H_A / RT)]}{1 + \exp\{-n(\Delta H^* - T\Delta S^* + \Delta C_p[(T - T_H^*) - T\ln(T / T_S^*)])/RT\}} \quad 2.40$$

where r is the reaction rate, ΔH_A is the enthalpy of activation, ΔH^* is the enthalpy change at T_H^*, the convergence temperature for enthalpy, ΔS^* is the entropy change at T_S^*, the convergence temperature for entropy, and ΔC_p is the heat capacity change between the native and denatured states of the enzyme systems, n is the number of amino acid residues in the protein.

Published studies on temperature dependence of specific rates have used either of Equation 2.38 and 2.39. The model proposed by Hinshelwood (1946) is an Arrhenius type based on the assumption of complete irreversibility of denaturation reaction. Both the enzyme reaction and the high-temperature denaturation show an Arrhenius type of temperature dependency and are of zero order as shown in Equation 2.41.

Hinshelwood model: $$\mu_{\max} = A_1 e^{-\frac{E_a}{RT}} - A_2 e^{-\frac{E_b}{RT}} \quad 2.41$$

where A_1, and A_2 are frequency factors (h^{-1}) and E_a and E_b are the activation energies (J mol^{-1}) of the enzyme reaction and the high-temperature denaturation, respectively.

Schoolfield et al (1981) proposed another function which is based on the fact that cell deactivation also occurs at low temperatures in addition to the high temperatures. The

model (Equation 2.42) is a modified form of a previously published equation to reduce correlation between parameters

$$\mu_{\max} = \frac{\mu_{25}\frac{T}{298}e^{-\frac{H_a}{R}\left(\frac{1}{298}-\frac{1}{T}\right)}}{1+e^{\frac{H_l}{R}\left(\frac{1}{T_c}-\frac{1}{T}\right)}+e^{\frac{H_h}{R}\left(\frac{1}{T_h}-\frac{1}{T}\right)}} \qquad 2.42$$

where μ_{25} is the specific growth rate at 25°C, (h^{-1}), T_c, is the temperature (K) at which the enzyme is 50% inactivated due to low temperature, H is the enthalpy of activation (J mol^{-1}), and T_h is the temperature (K) at which the enzyme is 50% inactivated due to high temperature.

Zwietering (1991) has shown that the Ratkowsky model gave a better prediction if modified such that extrapolation above and below the maximum, T_{max} and minimum, T_{min} growth temperature predicts positive values of the specific rates as shown in Equation 2.43

$$\mu_{\max} = b^2(T - T_{\min})^2\left(1 - e^{c(T-T_{\max})}\right) \qquad 2.43$$

Recently, Petersen (2007) combined Arrhenius and Ratkowsky models to obtain a new 4 parameter model shown in Equation 2.44

$$f(T) = \alpha \cdot \exp\left(\frac{E_a}{R(T+273)}\right)\cdot\left(1-\exp(\beta(T-T_{\max}))\right)^2 \qquad 2.44$$

with T in °C. The primary advantage of the approach is that it involves real physical/biological phenomena rather than being purely empirical.

The above review has shown that a number of models have been proposed for temperature dependence of specific rates, many of which contain more than two parameters. Most of these parameters cannot be directly measured, but can only be determined from regression of observed data. Therefore, the accuracy of parameters depends on the number of available data points.

Most of the studies on the effect of temperature on mesophiles have shown the effects on maximum rates (Breed *et al.*, 1999; Nemati and Webb, 1997), however, other parameters like affinity constants, yield and cell maintenance are also affected. Breed *et al.* (1999)

have also shown the linear dependence of the apparent affinity constant with temperature, but that this dependency was not as significant as the effect of solution pH (Breed and Hansford, 1999a). Searby (2006) has also shown a linear dependence of the apparent affinity constant with temperature in thermophilic microbial ferrous-iron oxidation. Low temperature studies have also revealed that microbial growth and ferrous-iron oxidation are slow but not ceased, and that loss of ferric-iron due to precipitation is reduced thus increasing availability of ferric-iron for mineral leaching (Dopson *et al.*, 2007; Kupka *et al.*, 2007). Studies on optimum temperature have shown that it is pH dependent (MacDonald and Clark, 1970), decreasing with decreasing pH (Nemati *et al.*, 1998). This is expected as both temperature and pH affect the cell membrane permeability.

2.12.3 Effect of dissolved metal ions

Inhibitory concentrations of dissolved metals, such as arsenic, copper, mercury, nickel, uranium, etc., on microbial growth and ferrous oxidation have been reported by many authors (Cabrera *et al.*, 2005a; Cabrera *et al.*, 2005b; Garcia and Silva, 1991; Nies, 1999; Tuovinen *et al.*, 1971; Wang *et al.*, 2004). However, there is a limited number of publications where an inhibition term is incorporated into a rate equation. Noteworthy is the study on the effects of arsenic (Harvey and Crundwell, 1997). It is also of interest that while the catalytic effect of Ag^{+} in chalcopyrite bioleaching was reported (Wang *et al.*, 2004), this ion is also highly inhibitory at concentration greater than 1 μM (Garcia and Silva, 1991). It has also been reported that aluminium concentrations exceeding 10 g L^{-1} adversely affected the growth of an unspecified ferrous iron oxidizer (Tuovinen *et al.*, 1971).

The fact that dissolved metals have different inhibitory concentration means they have different effects on the physiology of the microbes. This can in part be explained in terms of Ingledew's chemiosmotic model (Ingledew, 1982); these metals/salts exert different osmotic pressures on the microbial cell thus resulting in different tolerance levels. Also, the observed effects can be due to direct inhibition of the cells' metabolism by these ions. Blight and Ralph (2004) report that increased ionic strength significantly reduces bacterial doubling time and microbial ferrous oxidation rate.

The inhibitory effect of metal cations, depending on their concentration, is such that the bacteria, if not completely poisoned, will have a prolonged lag phase until they develop a

resistance to this condition. Nies (1999) reported three mechanism of metal resistance by microorganisms. The accumulation of any metal in the cytoplasm can be decreased by effluxing, this is an active extrusion of the heavy-metal ion from the cell (Nies and Silver, 1995). Another mode is to segregate the metals into complex compounds by complexing with thiol-containing molecules, this mechanism only applies to "sulphur loving" metals. Metal ions may be reduced to a less toxic oxidation state. However, for most of the metals, the microbial resistance mechanism may involve the combination of two or all of these basic mechanisms.

2.12.4 The effect of oxygen and carbon dioxide concentrations

Oxygen is the electron acceptor in bacterial ferrous oxidation (Equation 2.1). The reduction of oxygen takes place within the cytoplasmic membrane, and oxygen needs to be transported from the solution across the cell membrane to participate in the reaction. To this end it interacts in an enzyme-substrate interaction mechanism very similar to that for ferrous iron and can thus be modelled by Michaelis-Menten kinetics. A simple Monod term accounting for oxygen concentration would hence look as follows:

$$\mu = \mu_{max} \frac{[Fe^{2+}]}{K_{Fe^{2+}} + [Fe^{2+}]} \cdot \frac{[O_2]}{K_{O_2} + [O_2]} \qquad 2.45$$

This formulation of the oxygen term has been used by Huberts (1994), except that oxygen concentration has been replaced by the partial pressure of oxygen in the gas phase, which is assumed proportional to the dissolved concentration, but more easily measured. Crundwell (1997) also incorporates a Monod type oxygen term into his model, but raised to the half power, as shown in Equation (2.34). In this case the oxygen term occurs as a consequence of evaluating the entire electron-proton circuit as a fuel cell, with oxygen reduction as the cathodic half reaction. The use of oxygen partial pressure as measure of dissolved oxygen concentration is tenuous. Dissolved oxygen concentrations in solution are always low due to its low solubility in water. In a rapidly operating bio-oxidation system, the adsorption of oxygen may be gas-liquid mass transfer limited and thus govern the overall rate rather than microbial oxidation kinetics.

2.12.5 Synergistic effects

The combined/synergistic effects of all the factors mentioned above on microbial ferrous-iron oxidation kinetics have not been adequately studied. Combination of rate terms accounting for all three substrates of the ferrous oxidation process – ferrous ions, oxygen and acid – has been proposed only in Crundwell's model (Equation 2.34). Other rate equations rarely combine terms for more than two effects at the same time. The microbial optimum temperature was reported to be pH dependent (Nemati *et al.*, 1998), and so were the various kinetic constants, for example as shown by Breed *et al.* (1999a)

It has been suggested by Rossi (1990) that the microbial specific growth rate should be the product of the Monod terms of all essential substrates of the microbe. Likewise, it could be argued, should limiting terms be multiplied into a given rate equation. From a purely mathematical point of view, this would appear illogical as the overall contribution of all the terms to specific growth rate diminishes. What would be logical is that the substrate that is most growth-limiting at a particular point in time (or the factor most inhibiting) should govern the rate Equation at that moment. However, some systematic study into such synergistic effects and how to model them need to be carried out.

2.13 Solution chemistry of iron in biohydrometallurgy

Iron is the second most abundant metal (after aluminium) and the fourth most abundant element of the earth's crust. Its solution chemistry is both colourful and complex; it exhibits three different oxidation states and forms a variety of strong complexes that provide unique properties and impact on its hydrometallurgical characteristics. In the iron sulphate system found in the bioleach heap environment, large proportions of the free ferric-iron are in form of complexes. In acidified sulphate solutions, ferrous and ferric ions form complexes with sulphate and hydrogen ions such as $FeSO_4$, $FeHSO_4^+$ $FeSO_4^+$, $FeOH^{2+}$, $Fe_2(OH)_2^{4+}$, $Fe(OH)_2^+$ etc. but all the iron ions will be in free (uncomplexed) form when the solution is infinitely diluted. Huberts (1994) reported that the percentage of free ferrous and ferric iron in a solution containing 9 g L^{-1} total iron concentration was estimated to be 50 % and 1 % respectively, while the rest was in complexed form. These proportions vary depending on sulphate concentration, the solution pH, ionic strength and solution temperature. The

stability of the iron species in solution depends on their corresponding equilibrium constant.

Bioleach liquor is characterised by a high concentration of dissolved salts (see Petersen and Dixon, 2004). Due to the high concentration of dissolved ions, ionic interactions become very significant. Table 2.5 shows the concentrations of dissolved solids greater than 10 ppm for a particular heap bioleach liquor with extreme concentrations of aluminium and magnesium. At the conditions of a bioleach plant, chemical species exist as charged ions with high possibility of ion pairing. This means that during bio-oxidation of ferrous iron in bioleaching operation, the substrate (ferrous iron) and product (ferric iron) not only exist as hexa-hydrated complexes but also as a series of complex ions, paired with various existing anions, which is mainly sulphate (SO_4^{2-}), which needs to be taken into account.

Table 2.5 Analysed composition of PLS from a Chilean chalcocite based heap bioleach operation

Element	Concentration [mg L^{-1}]	Element	Concentration [mg L^{-1}]
Al	12 200	Na	1 670
Ca	467	Zn	376
Co	16.2	Cl^-	1 300
Cu	2 000	F^-	80.1
Fe	2 460	NO_2^-	28.1
Mg	10 100	NO_3^-	106
Mn	669	o-PO_4	532
P	221	SO_4^{2-}	116 880
K	29.0		

Operating condition: T (°C) = 18 – 22
Feed pH = 1.24
PLS pH = 2.20
Eh $_{(mV\ vs.\ SHE)}$ = 640
(Source: Petersen and Dixon, 2004)

The form in which ferrous-iron is oxidized at the bacterial cell surface seems to be controversial, it was reported in Huberts (1994) that the growth of *At. ferrooxidans* is dependent on sulphate species and postulated that ferrous-iron need to be complexed with sulphate in the bulk solution before taking part in electron transport. It was also proved from a chemical point of view, that the presence of sulphate affected ferric-iron

reduction at UO_2 surface (Nicol *et al.*, 1975); the electron transfer to ions in solution was maximum when ferric-iron to sulphate ratio was one. The $FeSO_4^+$ – complex was suggested to be the most electro-reactive species in solution, as decrease in electron transfer was observed at higher concentration of sulphate due to the presence of the $Fe(SO_4)_2^-$ complex.

Predicting iron species in bioleach solution remains a challenge; some authors have published equilibrium data for several pertinent species as a function of temperature (Dry, 1984; Zemaitis *et al.*, 1986) and prediction of speciation at elevated temperatures is hampered due to limited availability of thermodynamic data. The Gibbs-Helmholtz expression is useful in calculating the effect of temperature on equilibrium constant (Sandler, 1999) for example for a given reaction (Equation 2.46)

$$a.A + b.B \leftrightarrow c.C + d.D \qquad 2.46$$

$$K = \frac{[a_C]^c}{[a_A]^a[a_B]^b} = \exp\left(\frac{-\Delta G(T)}{RT}\right) \qquad 2.47$$

where K = equilibrium constant for a reaction
R = Universal gas constant
a_i = activity of species i
a, b and c are the stoichiometric coefficient of Equation 2.46

Thermodynamic properties are related to temperature using the heat capacities or mean heat capacities (Atkins and Paula, 2002)

$$\Delta G^o(T) = \Delta H^o(T) - T\Delta S^o(T)$$

$$\Delta H^o(T) = \Delta H^o(T^o) + \int_{T^o}^{T} \Delta \overline{C}_P^o(T)dT \qquad 2.48$$

$$\Delta S^o(T) = \Delta S^o(T^o) + \int_{T^o}^{T} \Delta \overline{C}_P^o(T)dT$$

$$\Delta G^o_{rxn}(T) = \Delta G^o_{rxn}(T^o) - (T - T^o)\Delta S^o_{rxn}(T^o) + (T - T^o)\Delta \overline{C}_P^o(T) - T\left(\ln\frac{T}{T^o}\right)\Delta \overline{C}_P^o(T) \qquad 2.49$$

However, the use of the Criss-Cobble correlation to predict heat capacity data for ionic species allows the estimation of Gibbs free energy data at elevated temperature (for details, see Archer, 1997). The correlation relies on the 'correspondence principle' as follows:

A standard state can be chosen at every temperature such that the partial molar entropies of one class of ions at that temperature are linearly related to the corresponding entropies at some reference temperature (Bryson and Nicol, 1996; Criss and Cobble, 1964b).
The mean heat capacity is given as;

$$\overline{C}_P^o(T) = \frac{a(T)}{\ln\left(T/T^o\right)} - \frac{(1-b(T))}{\ln\left(T/T^o\right)} S_a^o(T^o) \qquad 2.50$$

where $\overline{C}_P^o$ is the substance mean heat capacity ($J.mol^{-1}.K^{-1}$)
$a(T)$ and $b(T)$ are Criss-Cobble constant at temperature T ($J.mol^{-1}$)
T^o reference temperature (298 K).

The Criss-Cobble data, $a(T)$ and $b(T)$, can be obtained from Criss and Cobble (1964b) & (1964a). Therefore, the equilibrium constant for reactions with ionic species at various temperatures can be estimated from Equation 2.47.

2.13.1 Redox potential and Nernst Equation

Redox measurements frequently taken in the industrial bioleach operations relate to the electrochemical potential of the solution of interest. The Nernst Equation can be interpreted to estimate the ratio of the activities or concentrations of the redox couples (e.g. ferric to ferrous irons). This ratio refers to the activities of the free components (Atkins and Paula, 2002). Thus it is important to understand the iron speciation in the bioleach solution.

$$E = E_0 + \frac{RT}{nF}.\ln\left(\frac{\prod_i a_i}{\prod_j a_j}\right) \qquad 2.51$$

$$E_0 = \frac{\Delta G^0}{nF}$$

Where
- E is the solution redox potential (mV)
- E_0 solution potential at standard state
- n number of electron transferred
- F Faraday's constant (96500 J/V.mol)
- R Universal Gas constant
- ΔG Gibbs free energy
- a activity of specie
- i and j oxidized (Fe^{3+}) and reduced (Fe^{2+}) species respectively.

Activities of chemical species: The ionic concentrations (activities) of chemical species in bioleach liquor are not really equal to their respective analytical concentration. The ionic interactions are so strong that the approximation of replacing activities by molalities is only valid in very dilute solutions (less than 10^{-3} mol.kg^{-1} in total concentration) and for accurate estimation it is important to use activity of chemical species (Atkins and Paula, 2002; Bockris and Reddy, 1970). The ionic activity is related to the analytical concentration according to Equation 2.52. The detail derivation is common in many chemistry texts (see Atkins and Paula, 2002):

$$a = \gamma_i C_i \qquad 2.52$$

where γ_i represents the activity coefficient of ionic species *i*, it measures the interaction of the ionic species with oppositely charged ions and molecules present in the solution; and C_i, concentration of the species *i*. The calculation of activity coefficients of ionic species is based on the assumption that dissolved electrolyte in water completely dissociates into ions (Atkins and Paula, 2002; Zemaitis *et al.*, 1986).

An activity coefficient of less than unity is as a result of ionic interactions and unity is assumed in an infinitely dilute solution. The degree of ionic interaction and ionic strength depends on ionic concentrations as well as their charges. Some models have been developed for determining the activity-coefficient of ions in solution, such as the Debye-Huckel model and the Davis model. These were derived based on the consideration that interaction between the ions solution are purely electrostatic which explains the attraction between oppositely charged ions, and the complete dissociation of dissolved solute in water. The above consideration resulted in and formed the basis of the development of commercially available software packages (e.g. MinteQ, VisualMinteq, HSC Chemistry) for predicting the chemistry of reacting species in solution which has found application in hydrometallurgical processes.

The Debye-Huckel model takes into account the columbic interactions existing between ionic species in the estimation of activity coefficient. Thus the effect of ionic charges can be investigated (for review, see Atkins and Paula, 2002; Bockris and Reddy, 1970;

Stumm and Morgan, 1996). The activity coefficient γ_i is expressed as given in Equation 2.53:

$$-\log_{10}\gamma_i = \frac{Az_i^2\sqrt{I}}{1+d_iB\sqrt{I}} \qquad 2.53$$

where A and B represent the Debye-Huckel constants at specified temperature and pressure, $\boldsymbol{z_i}$ represents the ionic charge of the specie, d_i the effective ionic diameter and I is the ionic strength of the electrolyte solution (mol/l). The ionic strength is given by

$$I = \tfrac{1}{2}\sum m_i z_i^2$$
$$I \approx \tfrac{1}{2}\sum C_i z_i^2 \qquad 2.54$$

where m_i = molality of species i
C_i = concentration of specie i

The Debye-Huckel Equation is theoretically valid for dilute solution with ionic strength of less than 0.1 molal due to simplications and assumptions made in considering the ionic atmosphere (Zemaitis *et al.*, 1986). Although the model was derived for dilute solution (Ionic strength less than 0.1), some success has been reported in applying it at higher concentration, particularly when ion-pair equilibria are taken into consideration (Dry and Bryson, 1988). Refer to Appendix A1.2 for the details of model parameters used in this study.

2.13.2 Effect of ionic strength on reaction rate

The influence of ionic strength on rate of reaction is important in biohydrometallurgical processes especially its effect on ferrous-iron oxidation in the presence of gangue materials. This has been described in may chemistry text (Atkins and Paula, 2002; Laidler and Meiser, 1982). For a given reaction of the form (Equation 2.55):

$$A + B \longrightarrow C \qquad 2.55$$

The dependence of the rate constant k can be obtained by expressing the rate equation in term of the concentration of the activated complex with the basis that the overall rate of reaction is proportional to the concentration of the activated complex, [X*] as shown in Equation 2.56

$$Rate = k'[X^*] = k[A][B] = k_o[A][B]\frac{\gamma_A\gamma_B}{\gamma^*} \quad 2.56$$

Where k_o is given as

$$k_o = k'\frac{[X^*]}{[A][B]}\frac{\gamma^*}{\gamma_A\gamma_B} = k'K^* \quad 2.57$$

It follows from Equation 2.56 that

$$\log_{10} k = \log_{10} k_o + \log_{10}\frac{\gamma_A\gamma_B}{\gamma^*} \quad 2.58$$

And by applying the limiting Debye-Huckel law, Equation 2.53 becomes

$$\log_{10}\gamma = -Az^2\sqrt{I} \quad 2.59$$

By substituting Equation 2.59 into 2.58, it can be shown that the rate constant is a linear function of ionic strength as shown in Equation 2.60. Therefore, for reaction involving ions of the same charge, increase in ionic strength would result in increase in the rate constant. While a decrease in rate constant would be obtained for ions of opposite charges. However, the for netral species, the rate constant is expected to be independent of ionic strength since z_Az_B is zero; this has been observed in the base catalyzed hydrolysis of ethyl acetate (Laidler and Meiser, 1982).

$$\log_{10} k = \log_{10} k_o + 2Az_Az_B\sqrt{I} \quad 2.60$$

2.13.3 Speciation of a typical iron solution: a theoretical approach

This section reviews the application of the commercially available softwares (Visual Minteq and HSC Chemistry) to estimate the ionic species and composition in a simulated simple iron and typical bioleach solutions, and also the theoretical details involved. The importance of this computational exercise is to show the distribution of iron species in a typical iron rich solution. Consider a solution containing 12 g L^{-1} of total iron with ferric to ferrous iron ratio of 50 at pH 1.3. The iron speciation and corresponding concentrations are shown in Table 1.5. The table corroborates the fact that various kinds of species can be found in a typical iron solution. It is evident from the table that at pH 1.3, iron exists in solution mostly as complex species. While about one-third of ferrous-iron exists as free ferrous-iron, almost all the ferric-iron is present in complex form, and associated with sulphate ions, with only about 2% ferric-iron existing

as free ions. (see Table 2.7). The theoretical details are as follows: According to Barrett *et al.* (1993) for ferric iron and sulphate solution system, the complexes, $[FeSO_4]^+$, $[FeHSO_4]^{2+}$ and $[Fe(SO_4)_2]^-$ contribute to the ferric-iron speciation in addition to the hydrolysis products of Fe^{3+}. The SO_4^{2-} speciation is associated with these ions. The equilibria reactions involved are shown in Equation 2.61 to 2.69

Table 2.6 The iron-ion speciation of solution of 12 g.L^{-1} total Fe at ferric-to-ferrous ratio of 50 and pH 1.3, and their corresponding concentrations.

Specie	Concentration	Activity	Log activity
$Fe(OH)_{2\ (aq)}$	2.5×10^{-21}	2.8×10^{-21}	-20.6
$Fe(OH)^{2+}$	5.4×10^{-8}	3.9×10^{-8}	-7.4
$Fe(OH)^{3-}$	2.8×10^{-30}	2.0×10^{-30}	-29.7
$Fe(OH)_{3\ (aq)}$	9.2×10^{-16}	9.9×10^{-16}	-15.0
$Fe(OH)^{4-}$	3.1×10^{-21}	2.2×10^{-21}	-20.7
$Fe(SO4)^{2-}$	6.1×10^{-3}	4.4×10^{-3}	-2.4
Fe^{2+}	5.8×10^{-4}	1.6×10^{-4}	-3.8
Fe^{3+}	4.4×10^{-4}	2.4×10^{-5}	-4.6
$Fe_2(OH)_2^{4+}$	1.8×10^{-7}	1.0×10^{-9}	-9.0
$Fe_2(OH)_4^{5+}$	1.5×10^{-11}	4.8×10^{-15}	-14.3
$FeOH^+$	6.0×10^{-12}	4.3×10^{-12}	-11.4
$FeOH^{2+}$	2.9×10^{-5}	8.0×10^{-6}	-5.1
$FeSO_4$ (aq)	9.7×10^{-4}	1.0×10^{-3}	-3.0
$FeSO_4^+$	2.3×10^{-2}	1.7×10^{-2}	-1.8
H^+	6.9×10^{-2}	5.0×10^{-2}	-1.3
HSO_4^-	2.4×10^{-1}	1.8×10^{-1}	-0.8
OH^-	9.3×10^{-13}	6.8×10^{-13}	-12.2
SO_4^{2-}	8.1×10^{-2}	2.2×10^{-2}	-1.7

$$HSO_4^- \Leftrightarrow H^+ + SO_4^{2-} \quad 2.61$$

$$Fe(1,0) + SO_4^{2-} \Leftrightarrow [FeSO_4]^+ \quad 2.62$$

$$Fe(1,0) + HSO_4^- \Leftrightarrow [FeHSO_4]^{2+} \quad 2.63$$

$$[FeSO_4]^+ + SO_4^{2-} \Leftrightarrow [Fe(SO_4)_2]^{2-} \quad 2.64$$

$$[Fe(H_2O)_6]^{3+} \Leftrightarrow H^+ + [Fe(H_2O)_5OH]^{2+} \quad 2.65$$

$$[Fe(H_2O)_5OH]^{2+} \Leftrightarrow H^+ + [Fe(H_2O)_4(OH)_2]^{+} \quad 2.66$$

$$[Fe(H_2O)_4(OH)_2]^{+} \Leftrightarrow H^+ + [Fe(H_2O)_3(OH)_3] \quad 2.67$$

$$2[Fe(H_2O)_5OH]^{2+} \Leftrightarrow H_2O + [(H_2O)_5FeOFe(H_2O)_5]^{4+} \quad 2.68$$

$$[Fe(H_2O)_3(OH)_3] \Leftrightarrow H^+ + [Fe(H_2O)_2(OH)_4]^{-} \quad 2.69$$

Table 2.7 Ionic distributions of species of ferric-to-ferrous ratio of 50 containing 12 g.L^{-1} total Fe

Component	% of total component concentration	Species name
SO_4^{2-}	22.38	SO_4^{2-}
	6.32	$FeSO_4^{+}$
	3.35	$Fe(SO_4)^{2-}$
	67.68	HSO_4^{-}
	0.27	$FeSO_{4\ (aq)}$
Fe^{2+}	37.62	Fe^{2+}
	62.38	$FeSO_{4\ (aq)}$
Fe^{3+}	1.51	Fe^{3+}
	77.78	$FeSO_4^{+}$
	20.62	$Fe(SO4)^{2-}$
	0.10	$FeOH^{2+}$

Writing the expression of equilibrium constants of the above species will involve some complex algebra, these are simplified by using the following notations:

Fe(x,y), where x represent the number of Fe^{3+}centres and y, the number of OH groups.

Fe(1,S), Fe(1,HS) and Fe(1,2S) represent the complexes, $[FeSO_4]^{+}$, $[FeHSO_4]^{2+}$ and $[Fe(SO_4)_2]^{-}$ respectively(Barrett *et al.*, 1993). The equilibrium constants of the above Equations can be respectively written as shown in Equations 2.70 to 2.78

$$K_{S2} = [H^+][SO_4^{2-}]/[HSO_4^-] \quad 2.70$$

$$K_{1S} = [Fe(1,S)]/[Fe(1,0)][SO_4^{2-}] \quad 2.71$$

$$K_{HS} = [Fe(1,HS)]/[Fe(1,0)][HSO_4^-] \quad 2.72$$

$$K_{2S} = [Fe(1,2S)]/[Fe(1,S)][SO_4^{2-}] \quad 2.73$$

$$K_1 = [Fe(1,1)][H^+]/[Fe(1,0)] \quad 2.74$$

$$K_2 = [Fe(1,2)][H^+]/[Fe(1,1)] \quad 2.75$$

$$K_3 = [Fe(1,3)][H^+]/[Fe(1,2)] \quad 2.76$$

$$K_{22} = [Fe(1,2)]/[Fe(1,1)]^2] \quad 2.77$$

$$K_4 = [Fe(1,4)][H^+]/[Fe(1,3)] \quad 2.78$$

The total concentrations of Fe^{3+}, T(Fe) and sulphate ions T(S) are defined as

$$T(Fe) = [Fe(1,0)] + [Fe(1,1)] + [Fe(1,2)] + [Fe(1,3)] + [Fe(1,4)] + 2[Fe(2,2)] + [Fe(1,S)] + [Fe(1,HS)] + [Fe(1,2S)] \quad 2.79$$

$$T(S) = [S] + [HS] + [Fe(1,S)] + [Fe(1,HS)] + [Fe(1,2S)] \quad 2.80$$

where K_{S2} is the second dissociation constant of sulphuric acid, S and HS represent the sulphate and hydrogen sulphate ions respectively. Equation 2.70 to 2.80 contains 11 Equation in 12 unknowns. By combining Equations 2.71 to 2.73 and 2.74 to 2.78, Equation 2.79 can be expressed as:

$$T(Fe) = F + K_1F/[H^+] + \beta_2F/[H^+]^2 + \beta_3F/[H^+]^3 + \beta_4F/[H^+]^4 + 2K_{22}\left(K_1F/[H^+]\right)^2 + K_{1S}F[S] + K_{HS}F[H^+][S]/K_{S2} + K_{1S}K_{2S}F[S]^2 \quad 2.81$$

where β_i represents an overall formation constants; $\beta_2 = K_1K_2$, $\beta_3 = K_1K_2K_3$ and $\beta_3 = K_1K_2K_3K_4$. F represents [Fe(1,0)]. And also by combining Equation 2.70 to 2.73, Equation 2.80 can be expressed as a quadratic in terms of sulphate ion, [S]:

$$2K_{1S}K_{2S}F[S]^2 + \left\{1 + [H^+]/K_{S2} + K_{HS}F[H^+]/K_{S2} + K_{1S}F\right\}[S] - T(S) = 0 \quad 2.82$$

By expressing Equation 2.80 for [S] in terms of F and T(S), Equation 2.81 can written such that F is the only unknown given that $[H^+]$, T(S) and T(Fe) can be specified. This Equation can be solved iteratively to give F (i.e. Fe(1,0)) from which the speciation fractions can be calculated. The speciation fraction are given by Equations 2.83

$$\alpha_{10} = F/T(Fe) \qquad \alpha_{11} = \alpha_{10}K_1/[H^+]$$

$$\alpha_{12} = \alpha_{10}\beta_2/[H^+]^2 \qquad \alpha_{13} = \alpha_{10}\beta_3/[H^+]^3$$

$$\alpha_{22} = 2(\alpha_{10}K_1)^2 K_{22}T(Fe)/[H^+]^2 \qquad \alpha_{14} = \alpha_{10}\beta_4/[H^+]4 \qquad 2.83$$

$$\alpha_{1S} = \alpha_{10}K_{1S}[S] \qquad \alpha_{HS} = \alpha_{10}K_{HS}[H^+][S]/K_{S2}$$

$$\alpha_{2S} = \alpha_{10}K_{1S}K_{2S}[S]^2$$

where α values refer to the fractions of the complexes, Fe(1,0), Fe(1,1), Fe(1,2), Fe(1,3), Fe(2,2), Fe(1,4), Fe(1,S), Fe(1,HS) and Fe(1,2S) respectively. The plots of α values for major Fe^{3+} components are shown in Figure 2.10 for a typical ferric-iron and sulphate system occurring in microbial ferrous-iron oxidation containing 0.3M and 0.45M respectively.

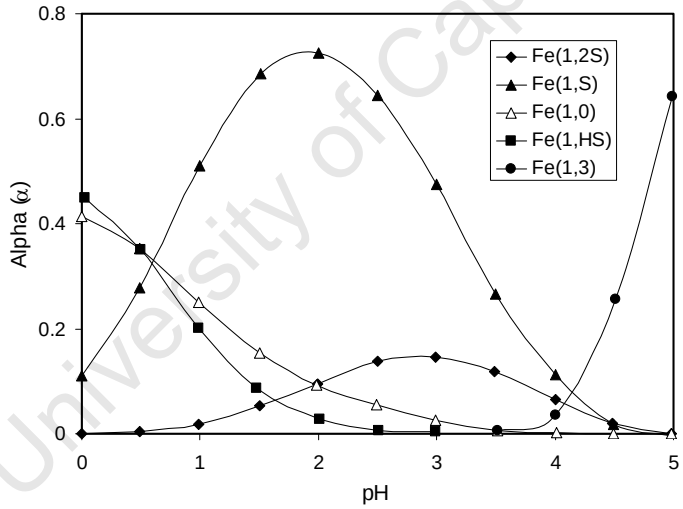

Figure 2.10 Speciation of major ferric-iron components in a solution of 0.3 M ferric and 0.45 M sulphate system.
Source: Source: (Barrett *et al.*, 1993)

2.14 Bioleaching kinetics in heaps

Although the concept of heap bioleaching appears to be a very simple process, the sub-processes taking place within the heap, as solution drips through the ore bed are rather complex, and their interactions not yet fully understood. Dixon and Petersen (2003) have

distinguished between the processes ranging from the macro- to the grain-scale, as is illustrated in Figure 2.11. At the macro scale, the entire heap leaching kinetics is governed primarily by transport of mass and energy into, through, and out of the heap structure. This involves the solution, heat and gas flows across the heap.

Level	Sub-processes	Illustration
Heap Scale	Solution flow through packed bed Gas advection Water vapour transport Heat balance	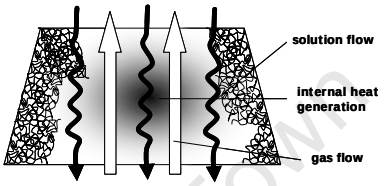
Aggregate Scale	Gas adsorption Particle diffusion Microbial growth Microbial attachment Microbial oxidation	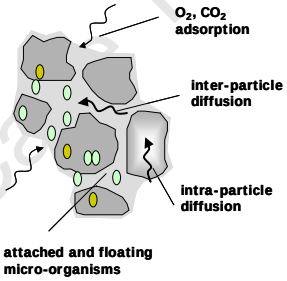
Particle Scale	Topological effects Intra-particle diffusion Particle and grain size distribution	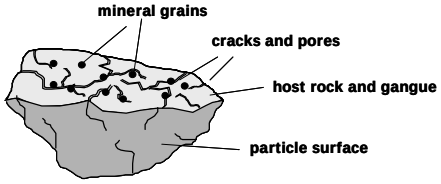
Grain Scale	Ferric/ferrous reduction Mineral oxidation Sulphur oxidation Surface processes	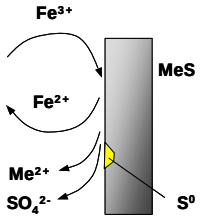

Figure 2.11 Schematic representation of sub-processes in heap bioleaching (Source: adapted from Dixon and Petersen, 2003)

At the aggregate scale, gas uptake into liquid phase, intra- and inter-particle diffusion within the stagnant zones, and bacterial growth and oxidation are all contributing to the

leaching kinetics. This is also called aggregate scale. The bacterial growth and activity includes the growth behaviour of different microbial strain as a function of temperature and concentration of dissolved constituents (e.g. ferrous and ferric iron, O_2, CO_2 and acid), any synergies between these and the concomitant iron and sulphur oxidation reactions.

At the particle scale, leaching is governed by the way in which mineral grains are distributed on a single particle. This is referred to as the topological effect. Mineral grains may be present as anything from free grains to highly localised spots at the particle surface. Their distribution and accessibility within particles directly determine the leachability of the target mineral. Furthermore, in low grade ores the mineralogy of the gangue matrix is also of some significance, as it can interfere with mineral leaching and biological phenomena.

Finally, at the grain scale, the chemical and electrochemical interactions at the grain surface determine the leaching kinetics. The oxidation kinetics of the sulphide minerals is a function of ferric-to-ferrous ratio in solution and temperature (as characterised by the reaction activation energy). The reaction may be further complicated due to interaction between different minerals (galvanic interaction), as is the case with pyrite being present in many base metal sulphide ores. Also the direct microbial interaction with exposed mineral surfaces (contact leaching mechanism) as reported by Sand *et al.*(2001) is may also be significant at this level. Recent studies have shown that this may be important in heap bioleaching as bacterial attachment is a function of available substrate surfaces (Harneit and Sand, 2007; Mafanya *et al.*, 2007)

2.15 Summary and Problem Statements

The simplicity, absence of gaseous emissions, low operating cost and applicability to low grade ore have made bioleaching attractive to the metallurgical industries compared to pyrometallurgical techniques. These have resulted in diverse research interest in the attempt to understand the mechanisms of reactions involved in this process and formulate models important for the design of these operations.

Industrial application of bioleaching falls into two categories, tank and heap bioleaching. Almost all of the rate equations have been developed in the context of tank bioleaching.

This is not surprising considering that these are engineered processes operated under controlled conditions at which the overall rate of bioleaching is near optimal. This implies that parameters such as temperature and pH are maintained close to optimum values, whereas the ferric to ferrous ratio prevailing in the system is governed primarily by the interplay between micro-organisms, mineral concentrate and tank residence times.

On the other hand, it can be inferred from Section 2.14 that heap bioleach processes offer no control over the prevailing operating conditions. Moreover, parameters such as temperature and pH can vary widely over time and location within the heap. While pyrite heaps are known to reach considerable temperatures, often into the thermophile range, heaps of copper sulphide minerals remain largely cold, often at temperatures well below those commonly studied in the laboratory. It is also important to note that there are relatively large quantities of gangue materials compared to desirable minerals within a typical heap. Continuous recycle of the solution inventory, and the protracted times of exposure can result in the release of considerable concentrations of cations into the heap leach solution, to the point where they exceed limits commonly considered toxic to microbial population and as a result negatively affect microbial growth and ferrous-iron oxidation. The analysis of a typical pregnant leach solution (PLS) from a Chilean chalcocite based heap operation is shown in Table 2.5. The table indicates that the solution contains numerous cations, and at very high concentrations especially of Al and Mg (12.2 and 10.1 g/L respectively). The solution conditions are far from what would be considered optimal in a typical tank bioleach operation. The analysis also indicates that the dissolved cations are mostly present as sulphates, resulting in a solution of very high ionic strength.

Modelling of heap bioleaching is complex and challenging due to a large number of phenomena involved. Processes such as solution transport, gas and heat transport, mineral kinetics, mineral interactions, bacterial kinetics, diffusion effects, etc. all needed to be considered (Dixon and Petersen, 2003). Petersen and Dixon (2004) have shown however, that the microbial ferrous-iron oxidation step can be the rate controlling step in heap bioleaching if the microbial populations are under adverse conditions as outlined in Table 2.5. Modelling of these effects remains strictly empirical, and this is important, as

none of the existing rate equations have neither been confirmed to be valid nor been calibrated under these extreme conditions.

The studies on microbial ferrous-iron oxidation in relation to operating parameters, such as total iron concentration, solution pH, and temperatures has been carried out mostly in batch and continuous systems. These studies were carried out within a narrow range of these parameters; total iron concentration effects were in excess of 10 g L^{-1} and studies on the effects solution pH were mostly at 1.5, though there have been recent studies at 0.9; temperature studies were within the optimum range for the microbial activity. However, the situation in heaps is different in terms of wide variation of these operating conditions; the total iron content of ore treated with using bioleach technique is less than 5 g L^{-1}, a concentration of about 2 g L^{-1} is often reported.

The effects of dissolved cations from gangue minerals, and contribution of the resulting ionic interaction to ferrous bio-oxidation has not been effectively studied. Available studies on microbial ferrous-iron oxidation were carried out independently of the mineral ores and dissolved cations. This is understandable, as the *in-situ* reduction of the available ferric-iron makes it technically impossible to study the kinetic under this condition. The understanding of the interaction between microorganisms and dissolved cations is important in the kinetic studies of ferrous iron oxidation. Though their inhibitory effects have been reported in some literature (Tuovinen *et al.*, 1971), emphasis was not on kinetic studies, and where kinetic studies were considered, it was limited to the effect of arsenic, heavy metal ions and sodium sulphate, all with respect to *At. ferrooxidans*. Increase in ionic strength due to dissolved ions in the bioleach liquor imposes an energy load on the bacteria as a result of osmotic gradient between inner and outer part of the cell. Although the Pirt's model accounts for a maintenance term – energy required in order to keep the microbes alive without replication – there is no existing correlation in the literature between maintenance, total dissolved solids and/or the ionic strength of bioleach liquor.

The knowledge of how all these conditions (total iron concentration, solution pH, temperature and dissolved cations) affect the microbial biomass would provide an understanding of how the microbial ferrous-iron oxidation kinetics should be modelled in the context of heap bioleach operation. This could be used to complement the tools

available for diagnosis of bioleach heaps such as computer models. This knowledge would require carefully designed sets of fundamental studies to investigate microbial growth and ferrous-iron oxidation under these aforementioned conditions.

Chapter 3

Materials and Methods

This chapter is concerned with detailed description of the materials used for the experiments, the experimental procedures followed and the analytical techniques. The theoretical aspects of the analysis of the data generated are also discussed.

3.1 Materials

3.1.1 Experimental rig

A diagrammatic representation of the experimental rig is shown in Figure 3.1. It consist of a single 2 L jacketed Z61104CT04 Applikon® autoclavable stirred tank bioreactor, which is made of borosilicate glass. The bioreactor has a height-to-diameter ratio, H/D ≈1.32 and a working volume of 1Litre. Attached to the bioreactor is a Grant Y6 constant temperature water bath which maintains desired temperature within the bioreactor by circulating water through the bioreactor jacket. The feed was pumped into the bioreactor by Masterflex® model 7521-57 L/S™ variable-speed drives fitted with L/S™ 7013-20 standard pump heads and L/S™ 13 Norprene® food tubing. A chemostat tube was used to maintain a constant volume within the bioreactor. The liquid was removed from the bioreactor by means of a L/S™ 7014-20 standard pump head and L/S™ 14 Norprene® food tubing fitted on a Masterflex® model 7521-57 L/S™ fixed-speed drive.

Mixing and gas dispersion was achieved by a pitched (45°) four-blade turbine impeller located 2 cm from the base of the bioreactor which rotates via a flexible coupling linked to an Applikon P100 motor and an Applikon 1012 stand-alone speed controller. Inlet gas was supplied by a Peak Scientific OAG2000DA oilless air compressor, the gas flow rate to the bioreactors was controlled using a Brooks model 5850S mass flow controller and a Brooks model 0154 microprocessor control and read-out unit. A reflux condenser using an ethylene/glycol mixture from a Grant LTD6G low-temperature bath was attached to the bioreactor to dry off-gas to 6°C prior to entering the gas analyzers. Also attached is a Metrohm® redox electrodes (Pt-Ag/AgCl) for measurement of the solution potential of liquid in the bioreactor.

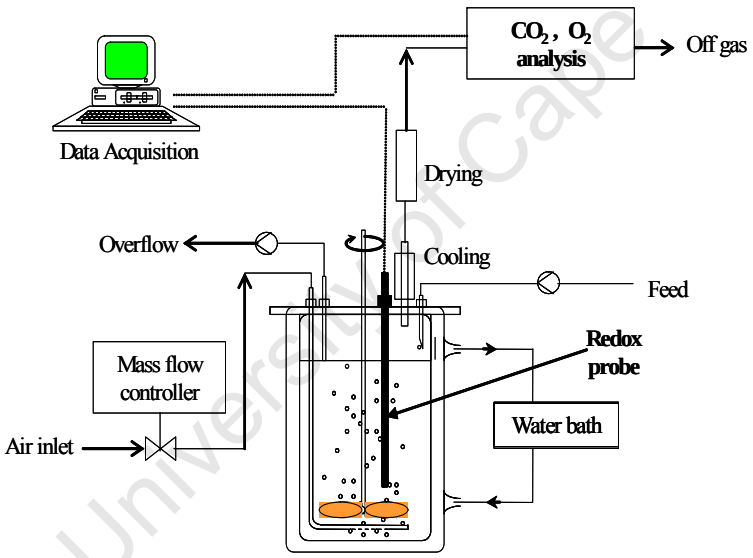

Figure 3.1 Diagrammatic representation of experimental rig.
Source: Modified after Breed (1999)

The off-gas from the bioreactor was passed through a cloth filter and a Hartmann & Braun CGEK sample gas conditioner fitted with a CGKA 1 automatic condensate outlet. The gas analyzer is made up of a Hartmann & Braun Uras 4 NDIR (nondispersive infrared) industrial photometer for measurement of CO_2 concentration and a Hartmann & Braun Magnos 6 G oxygen analyzer. The CO_2 and O_2 concentrations for each bioreactor and the inlet air were alternately logged by computer. The solution potential is also logged by the attached computer

3.1.2 Growth medium

Analytical-grade reagents were used for all the experiments. The ferrous-iron media consisted of the desired quantity (in g L^{-1}) of Fe^{2+} (added as $FeSO_4$. $7H_2O$), 1.11 K_2SO_4, 0.53 $(NH_4)_2HPO_4$, 1.83 $(NH_4)_2SO_4$ and 10 mL of Vishniac solution, a trace element solution (Vishniac and Santer, 1957), adjusted to the desired pH ($0.7 \leq pH \leq 1.30$) using concentrated H_2SO_4 . No attempt was made to maintain sterile conditions. In order to prepare the Vishniac solution, 15 g L^{-1} EDTA ($C_{10}H_{12}FeN_2NaO_8$.$3H_2O$, M = 421.10 g/mol) is dissolved in demineralized water. Next 1 g L^{-1} $ZnSO_4$. $2H_2O$ is added and the pH is set to 6.0. Then successively 1.0 g L^{-1} $CoCl_2.6H_2O$, 1.0 g L^{-1} $MnCl_2.4H_2O$, 0.5 g L^{-1} $CuSO_4.5H_2O$, 5.0 g L^{-1} $FeSO_4.7H_2O$, 0.5 g L^{-1} $Na_2MoO_4.2H_2O$, and 0.5 g L^{-1} $CaCl_2.2H_2O$ were added. Each component needs to be completely dissolved before addition of the next. When all components are dissolved the pH is set to 4.0 with 1 M H_2SO_4 solution.

3.1.3 Bacterial Culture

The inoculum was originally obtained from a vat-type two-stage (2 × 20L) continuous bioleaching mini-plant treating a pyrite-arsenopyrite concentrate, in Gamsberg, South Africa. After isolation of the ferrous-iron oxidising species, *Leptospirillum ferriphilum* sp. nov. was recently found to be the only ferrous-iron oxidising species (Coram and Rawlings, 2002), contrary to the earlier finding that, it was dominated by the species *Leptospirillum ferrooxidans* and *Acidithiobacillus thiooxidans* (Rawlings, 1995). The stock culture was maintained in a continuous stirrer tank bioreactor at residence time of 72 hours on ferrous-iron feed containing 12 g L^{-1} total iron. The results reported in this thesis were obtained between November 2004 and March 2007.

3.2 Methods

3.2.1 Microbial ferrous-iron oxidation under continuous operation

Continuous culture experiments with *L. ferriphilum* were carried out in the stirred tank double walled bioreactor with a working volume of 1 Litre. The bioreactor was maintained at desired temperature by means of a water bath. The cell suspension was agitated by the lip seal stirrer at 400 rpm. The culture was aerated with dry air at

between 225 to 350 mL min^{-1}. The stirring speed and aeration rate were chosen to provide sufficient oxygen and carbon dioxide transfer on the one hand, and accurate O_2 and CO_2 off-gas analyses on the other (Boon 1996; Boon *et al.* 1998). The dried off-gas from the bioreactor and the reference air were analyzed for oxygen and carbon dioxide concentrations using a gas analyzer, and were monitored on-line using a data-acquisition program. This enabled the oxygen utilization rate, r_{O_2}, carbon dioxide utilization rate, r_{CO_2}, and biomass concentration, C_X, to be determined (Boon, 1996; Boon *et al.*, 1995b). This program also controlled the valves that led the gas flow to the gas analyzer (four bioreactors were attached to only one O_2 and CO_2 analyzing unit). During the continuous culture experiments the ferrous-iron medium was fed to, and removed from, the bioreactors by means of variable-speed pumps as described in Section 3.1.1

The pH of the solution in the bioreactors was not controlled directly. However, it was maintained at the required pH by manipulating the pH of the feed to the bioreactors using concentrated solution of sulphuric acid. The actual pH of the solution depended on both the desired solution pH and the prevailing dilution rate. The ferrous-iron oxidation kinetics was investigated for at least five different dilution rates ranging from 0.015 to 0.130 h^{-1} (calculated from weight decrease of the feed vessel, see Appendix B1.1). The bioreactor was operated at each dilution rate for at least three residence times before steady-state was assumed. Steady-state was assumed only once the oxygen and carbon dioxide concentrations in the off-gas and the redox potential in the culture liquor were constant. The steady state was maintained for at least one residence time in order to allow for the determination of ferrous and total iron concentration in the influent and effluent samples before changing the parameter for subsequent experiments.

New reactors were usually restarted by mixing 50% of stock with fresh ferrous-iron feed, and the solution potential of the resulting solution was allowed to attain 600 mV (on Ag/AgCl electrode) before switching the system into continuous mode to start the experiments. The ferrous and total iron determinations were performed regularly on the feed samples to correct for errors incurred during sample the preparation. Wall growth was minimized by shutting down the bioreactor at regular intervals and scrubbing the

walls of the bioreactors and all available surfaces with a bottle brush and metal scourers. The intervals of cleaning depend on the experimental conditions, but were usually between 3 to 7days.

3.2.2 Experimental study on the effects operating temperature

The continuous culture experiments were carried out in air-sparged, stirred bioreactors of the configuration described above (working volume of 1 L). The bioreactors' liquor pH was carefully controlled at pH 1.30 ± 0.05 by adjusting the feed pH. The feed solution was the growth medium (see section 3.1.2 above) containing 12±0.5 g L^{-1} of Fe^{2+} added as $FeSO_4.7H_2O$ while aeration of the bioreactors was maintained between 225 to 350 mL min^{-1}. The temperature of the bioreactors were maintained at 15, 20, 25, 30, 36, 42, 45 ºC with deviation of ± 0.05 ºC by circulating water from controlled temperature baths through the bioreactor jackets. The microbial ferrous-iron oxidation kinetics were investigated in the bioreactor at some selected dilution rates ranging between 0.0085 and 0.10 h^{-1}. The steady state measurements (Fe^{2+}, total iron, and solution potential) were taken and the respective O_2 and CO_2 steady state data were downloaded from a data logger for analysis. Regular bioreactor maintenance was observed as prescribed above.

3.2.3 Experimental study on the effects of solution pH

The experimental procedure for studies on the effects of solution pH was similar to the above. The bioreactor temperature was maintained at 42 ºC, the growth medium contained 12 ± 0.5 g L^{-1} of Fe^{2+} added as $FeSO_4.7H_2O$ and aeration was maintained between 225 to 350 mL min^{-1}. Series of microbial ferrous-iron oxidation kinetics investigations were conducted at bioreactor solution pHs of 0.80, 1.00, 1.30, 1.50, 1.70 and 2.00 with deviation of ± 0.05, which was controlled by adjusting the feed pH. The kinetic studies were carried out at dilution rates ranging between 0.01 and 0.10 h^{-1}.

3.2.4 Experimental study on the effects of total iron concentrations

The continuous culture experiments were carried out in air-sparged, stirred bioreactors of configuration described Section 3.1.1, at the same condition; temperature (42 ºC) and

pH (pH 1.3) as above. However to investigate the effect of total iron concentration, series of experiments were carried out in a similar manner, by changing the total iron concentration in the growth medium (added as 2, 3, 5, 8, 12 g L^{-1} of Fe^{2+}). The kinetic studies were repeated at dilution rates ranging between 0.015 and 0.17 h^{-1} for each of the investigations. The steady state measurements and data were obtained as described in Section 3.2.1 for analysis.

3.2.5 Experimental study on the effects of dissolved Mg^{2+} and Al^{3+}

The kinetic studies to investigate the effects of dissolved cations were carried out in the continuous stirred tank bioreactor with a 1 litre working volume. The temperature of the bioreactor was maintained at 42 ºC and the culture pH was controlled at 1.30 ± 0.05. Aeration of the bioreactors was maintained at between 225 to 350 mL.min^{-1}. However, the feed solution (growth medium) was made to contain 5.0 ± 0.05 g L^{-1} of Fe^{2+} added as $FeSO_4.7H_2O$. Mg^{2+} and/or Al^{3+} were added to the growth medium as prescribed in Table 3.1 in order to investigate their effects on the oxidation kinetics.

The kinetics were investigated at dilution rates ranging between 0.04 and 0.130 h^{-1}. The steady state measurements (Fe^{2+}, total iron, Mg^{2+}, $Al^{3+}$and solution potential) and respective O_2 and CO_2 steady state data were downloaded for analysis. Regular bioreactor cleaning was observed as described in Section 3.2.1.

Table 3.1 The media composition for study on the effects of dissolved Al^{3+} and Mg^{2+} on microbial ferrous-iron oxidation kinetics*.

	Run 1	Run 2	Run 3	Run 4	Run 5	Run 6	Run 7	Run 8	Run 9	Run 10
Fe^{2+} (added as $FeSO_4.7H_2O$)	5.00	5.00	5.00	5.00	5.00	5.00	5.00	5.00	5.00	5.00
Al^{3+} (added as $Al_2(SO_4)_3.16H_2O$)	2.25	-	1.30	10.00	-	5.00	10.00	12.00	14.00	16.00
Mg^{2+} (added as $MgSO_4.7H_2O$)	-	3.05	1.30	-	10.00	5.00	10.00	12.00	14.00	16.00

* All measurement is in gL^{-1}. The media composition for Run 1 to 3 are such that the theoretical total SO_4 concentration was the same as plain growth medium with 12 gL^{-1} Fe^{2+} concentration

3.3 Analytical procedure

3.3.1 Iron analysis and measurement of Al^{3+} and Mg^{2+} concentration

The solution potential of the bioreactor liquor and the feed were measured periodically using a redox electrode (Pt-Ag/AgCl). The redox probe was calibrated regularly under the same condition prior to use as described below – this allows determination of the ferric-to-ferrous iron ratio in the bioreactor and feed solution. The total iron concentration in both feed and bioreactor solutions were determined by titration with potassium dichromate using the BDS indicator (Vogel, 1987). This allows determination of ferrous and ferric-iron concentrations. The ferrous iron concentrations in both solutions were also determined by titration with potassium dichromate (Vogel, 1987). Thus the ferrous-iron utilization rate, $r_{Fe^{2+}}$ can be calculated.

Al^{3+} and Mg^{2+} concentrations were determined by Atomic Absorption Spectroscopy (AAS). Samples (feed and effluent) were prepared by dissolution in concentrated HCl solution.

3.3.2 Redox probe calibration

The redox electrode (Ag/AgCl//$LiCl_3$/Pt cell) was calibrated against the half reaction of ferrous to ferric oxidation: $Fe^{2+} \rightarrow Fe^{3+} + e$ which is the only redox couple existing in the bioreactors. The calibration curve was plotted using the Nernst Equation shown in Equation 3.1. This enables the determination of ferric-to-ferrous iron in the bioreactors.

$$Eh = Eh' + \frac{RT}{nF} \ln \frac{[Fe^{3+}]}{[Fe^{2+}]} \qquad 3.1$$

Where Eh' is defined as the solution potential measured at equal total ferric and ferrous-iron concentration which accounts for activity coefficient, formation of complexes, electrode type and fouling of the electrode. The theoretical aspect of the calibration using Nernst Equation is discussed in detailed in Appendix B1.2

3.3.3 Cell concentration in terms of cell number

In addition to the use of off gas data for determination of cell concentration, C_X (in mmolC L^{-1}), discussed in Section 3.4.5, cell concentration was also determined using

direct microscopic counting using a Thoma counting chamber with well dimension of 0.02 mm in depth and a 1/400 mm^2 area and phase constrast optics at a magnification of 1000 x. Although the inherent error of this method is high (Konishi *et al.*, 1995), the reproducibility of the method has been found to be acceptable (Raja, 2005). A 10 ul of a diluted sample was ejected into the well of the counting chamber under a coverslip (note that samples were diluted depending total iron concentration, the sample taken fron 2 g L^{-1} total iron culture was used directly with dilution). Direct counts were made at 1000 x magnification using phase contrast microscopy. The concentration of cells (in cells ml^{-1}) in the diluted sample was determined using Equation B1.14

3.4 Analysis of kinetic data

3.4.1 Degree of reduction balance

The general stoichiometric formula for representing bacteria is approximately $CH_{1.8}O_{0.5}N_{0.2}$ (Jones and Kelly, 1983; Roels and Kossen, 1978). If the sources of carbon and nitrogen are limited to CO_2 and NH_4^+, the Equation for representing bacterial growth on ferrous-iron can be stoichiometrically derived from the elemental balances on carbon, hydrogen, oxygen, nitrogen and iron, and the charge balance (Jones and Kelly, 1983; Roels and Kossen, 1978). This has been shown to be:

$$CO_2 + 0.2NH_4^+ + \frac{1-4.2Y_{Fe^{2+}X}}{4Y_{Fe^{2+}X}}O_2 + \frac{1}{Y_{Fe^{2+}X}}Fe^{2+} + \left(\frac{1}{Y_{Fe^{2+}X}} - 0.2\right)H^+ \rightarrow CH_{1.8}O_{0.5}N_{0.2} + \frac{1}{Y_{Fe^{2+}X}}Fe^{3+} + \left(\frac{1}{2Y_{Fe^{2+}X}} - 0.6\right)H_2O \quad 3.2$$

The theoretical formulation is described in more detail in Appendix B1.3 This stoichiometric equation provides the following relationships between production and consumption rates of the compounds. The rate of ferrous-iron oxidation is equal to the rate of production of ferric-iron as shown in Equation 3.3

$$-r_{Fe^{2+}} = r_{Fe^{3+}} \quad 3.3$$

The above equation shows that the rate of biomass production can be determined directly from the carbon dioxide consumption rate, and the total amount of biomass produced can be determined directly from the total amount of carbon dioxide consumed.

$$r_X = -r_{CO_2} \tag{3.4}$$

Note that in these equations production rates are positive while consumption rates are negative. By using the degree of reduction balance, a relationship can be established between the rate of microbial ferrous-iron oxidation and the oxygen and carbon dioxide consumption rates. This relationship is shown in Equation 3.5. The theoretical details are discussed in Appendix B1.3

$$-r_{Fe^{2+}} = -4r_{O_2} - 4.2r_{CO_2} \tag{3.5}$$

This equation shows the effect of using an integrated stoichiometric equation for microbial ferrous-iron oxidation and biomass growth compared with using a separate stoichiometric equation for the oxidation of ferrous-iron which would result to $-r_{Fe^{2+}} = -4r_{O_2}$. The term $-4.2r_{CO_2}$ has only a minor effect on Equation 3.5 with regards to oxygen consumption, however, ignoring this term for the case of ferrous-iron oxidation will cause an error of less than 5% in the mass balance.

3.4.2 The biomass yield

The $Y_{Fe^{2+}X}$ in Equation 3.2 is defined as the amount of biomass, as carbon moles produced per mole of ferrous-iron oxidized which can be rewritten from Equation 2.14 as:

$$Y_{Fe^{2+}X} = \frac{r_X}{-r_{Fe^{2+}}} \tag{3.6}$$

Similarly for yield on oxygen, Y_{O_2X}

$$Y_{O_2X} = \frac{r_X}{-r_{O_2}} \tag{3.7}$$

Assuming that Pirt's relationship (Pirt, 1965) is applicable to describe the relationship between ferrous-iron oxidized for biomass growth and maintenance. Equation 2.15 can also be written in terms of biomass yield on oxygen:

$$\frac{1}{Y_{O_2X}} = \frac{1}{Y^{\max}_{O_2X}} + \frac{m_{O_2}}{D} \qquad 3.8$$

Similar equation can be written for biomass of ferrous-iron.

$$\frac{1}{Y_{Fe^{2+}X}} = \frac{1}{Y^{\max}_{Fe^{2+}X}} + \frac{m_{Fe^{2+}}}{D} \qquad 3.9$$

By means of the degree-of-reduction balance, the energetic parameters on oxygen ($Y^{\max}_{O_2X}$ and m_{O_2}) and ferrous-iron ($Y^{\max}_{Fe^{2+}X}$ and $m_{Fe^{2+}}$) which can be obtained from the plot of $1/Y_{O_2X}$ or $1/Y_{Fe^{2+}X}$ versus $1/D$, can be related as shown below:

$$\frac{1}{Y^{\max}_{O_2X}} = \frac{1 - 4.2Y^{\max}_{Fe^{2+}X}}{4Y^{\max}_{Fe^{2+}X}}$$
$$m_{O_2} = \frac{m_{Fe^{2+}}}{4} \qquad 3.10$$

Equation 3.10 is important, as it is useful for checking the validity and consistency of these parameters. For a reasonable consistency, the parity plot of Equations 3.10 should follow equation of the type $y = x$, where x and y are determined separately.

3.4.3 The specific ferrous-iron utilisation (oxidation) rate

The microbial specific ferrous-iron oxidation rate, $q_{Fe^{2+}}$, is defined as the rate of ferrous-iron oxidation per mole of biomass (i.e per carbon mole): $q_{Fe^{2+}} = \frac{-r_{Fe^{2+}}}{C_X}$. By dividing Equation 2.15a by biomass concentration, C_X, and assuming that the Monod equation for chemostat applies. The Pirt's Equation can be re-written as previously in Equation 2.15c:

$$q_{Fe^{2+}} = -\frac{r_{Fe^{2+}}}{C_X} = \frac{D}{Y^{\max}_{Fe^{2+}X}} + m_{Fe^{2+}} \quad 3.11$$

Similarly, Equation 3.11 can be written in terms of microbial specific oxygen utilisation rate, q_{O_2}

$$q_{O_2} = -\frac{r_{O_2}}{C_X} = \frac{D}{Y^{\max}_{O_2X}} + m_{O_2} \quad 3.12$$

Alternatively, the energetic parameters $Y^{\max}_{O_2X}$ and m_{O_2}, and $Y^{\max}_{Fe^{2+}X}$ and $m_{Fe^{2+}}$ can be calculated from the corresponding plot of q_{O_2} or $q_{Fe^{2+}}$ versus D.

3.4.4 The maximum specific microbial growth rate

Given that the energetic parameter can be determined, the maximum specific microbial growth rate $\mu^{\max}$ can determined by rewriting Equations 3.11 and 3.12 in terms of $q^{\max}_{O_2X}$ and $q^{\max}_{Fe^{2+}X}$

$$q^{\max}_{Fe^{2+}} = \frac{\mu^{\max}}{Y^{\max}_{Fe^{2+}X}} + m_{Fe^{2+}} \quad 3.13$$

$$q^{\max}_{O_2} = \frac{\mu^{\max}}{Y^{\max}_{O_2X}} + m_{O_2} \quad 3.14$$

However, $q^{\max}_{O_2X}$ and $q^{\max}_{Fe^{2+}X}$ can be obtained using a kinetic equation similar to Monod's, which relates the kinetics of specific microbial ferrous-iron oxidation rate with ferric-to-ferrous iron ratio measurable in the bioreactor. For example, using the simplified form suggested by Hansford (1997)

$$q_{Fe^{2+}} = \frac{q^{\max}_{Fe^{2+}}}{1 + K'_{Fe^{2+}} \dfrac{[Fe^{3+}]}{[Fe^{2+}]}} \quad 3.15$$

and similarly for oxygen based kinetics:

$$q_{O_2} = \frac{q_{O_2}^{\max}}{1 + K'_{O_2}\dfrac{[Fe^{3+}]}{[Fe^{2+}]}} \qquad 3.16$$

Therefore by substituting Equations 3.11 and 3.13 into the corresponding Lineweaver-Burk plot of Equations 3.15 as described in section 2.8, Equation 3.17 can be written.

$$\frac{1}{D + m_{Fe^{2+}} Y_{Fe^{2+}X}^{\max}} = \frac{1}{\mu^{\max} + m_{Fe^{2+}} Y_{Fe^{2+}X}^{\max}} + \frac{K'_{Fe^{2+}}}{\mu^{\max} + m_{Fe^{2+}} Y_{Fe^{2+}X}^{\max}}\left(\frac{[Fe^{3+}]}{[Fe^{2+}]}\right) \qquad 3.17$$

Similarly, Equation 3.18 below is obtained by combining Equations 3.12 and 3.14 with 3.16 in the same fashion for oxygen based constant:

$$\frac{1}{D + m_{O_2} Y_{O_2X}^{\max}} = \frac{1}{\mu^{\max} + m_{O_2} Y_{O_2X}^{\max}} + \frac{K'_{O_2}}{\mu^{\max} + m_{O_2} Y_{O_2X}^{\max}}\left(\frac{[Fe^{3+}]}{[Fe^{2+}]}\right) \qquad 3.18$$

Therefore by using the values of energetic parameters described above and plotting $1/\left(D + m_{Fe^{2+}} Y_{Fe^{2+}X}^{\max}\right)$ or $1/\left(D + m_{O_2} Y_{O_2X}^{\max}\right)$ versus $[Fe^{3+}]/[Fe^{2+}]$, the maximum specific microbial growth rate can be alternatively determined. In addition to the above method, $\mu^{\max}$ can also be determined using an equation analogous to equations written in terms of specific growth rate, μ (*i.e.* dilution, *D*) as shown in Equation 3.19

$$\mu = \frac{\mu^{\max}}{1 + K\dfrac{[Fe^{3+}]}{[Fe^{2+}]}} \qquad 3.19$$

3.4.5 Determination of $-r_{O_2}$, $-r_{CO_2}$, $-r_{Fe^{2+}}$ and r_X in a continuous stirred tank bioreactor

Given the oxygen and carbon dioxide concentration measurement in the bioreactor off-gas and in the reference feed air, the following equations are applicable for accurate determination of $-r_{O_2}$ and $-r_{CO_2}$ for continuous culture experiments. The rate of oxygen

consumption and the rate of carbon dioxide consumption are calculated from Equations 3.20 and 3.21 respectively:

$$-r_{O_2} = \left(\Phi_{gas,in}[O_2]_{ref} - \Phi_{gas,out}[O_2]_{G,out}\right)/V_{lig} \quad 3.20$$

$$-r_{CO_2} = \left(\Phi_{gas,in}[CO_2]_{ref} - \Phi_{gas,out}[CO_2]_{G,out}\right)/V_{lig} \quad 3.21$$

The amount of both oxygen and carbon dioxide consumed from the gas phase need to be taken into account when $\Phi_{gas,out}$ is to be determined. Assuming that $\Phi_{gas,out}$ equals $\Phi_{gas,in}$ will introduce a systematic error in the analysis. Boon (1996) reported that this will result into an error of about 20% in the calculation of oxygen consumption rate. The flow rate of off-gas can be calculated from nitrogen balance in the gas phase:

$$\Phi_{gas,out} = \Phi_{gas,in}\frac{1-[O_2]_{ref}-[CO_2]_{ref}}{1-[O_2]_{G,out}-[CO_2]_{G,out}} \quad 3.22$$

Both oxygen and carbon dioxide concentrations are dimensionless, measured in volume per volume. The rate of ferrous-iron oxidation, $-r_{Fe^{2+}}$ can be calculated from the degree of reduction balance, Equation 3.5. It can also be determined by performing a ferrous-iron balance over the bioreactor at steady state, as given in Equation 3.23

$$-r_{Fe^{2+}} = D\left([Fe^{2+}]_{inlet} - [Fe^{2+}]_{outlet}\right) \quad 3.23$$

Equations 3.5 and 3.23 are critical to the overall analysis of experimental data. They are used as a check for the validity of the off-gas measurement as discussed in section 3.4.6

The biomass concentration can be determined from the carbon dioxide off-gas analysis. Given that for a continuous culture at steady state, it has been shown earlier that the specific growth rate is equal to the dilution rate (see Equation 2.24) and that since $r_X = -r_{CO_2}$, the biomass concentration in a continuous culture, C_X (C-mole L^{-1}) is given as:

$$C_X = \frac{r_x}{\mu} = -\frac{r_{CO_2}}{D} \qquad 3.24$$

3.4.6 The concept of parity plot

Given that a parameter P can be measured from two independent methods x and y, giving rise to values P_x and P_y respectively, the measured P value should not be dependent on the mode of measurement. Therefore P_x and P_y are essentially the same. The consistency of P_x and P_y values can be verified on a parity plot, this is essentially the plot of P_x versus P_y or vice versa as shown in Figure 3.2, From the figure, the closer the values of P_x and P_y to the plot of line $y = x$, the more consistent and accurate is the mode of measurement, and either P_x or P_y values can be treated as equal for purpose of data analysis.

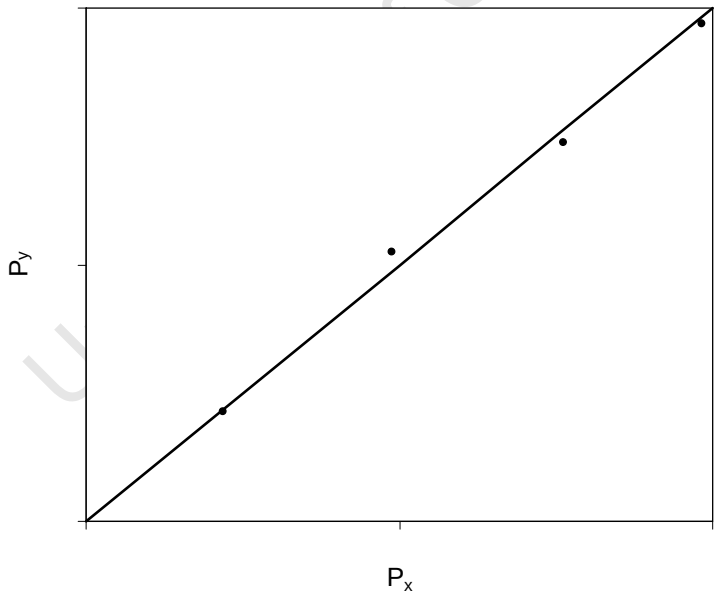

Figure 3.2 Schematic representation of measure data on a parity plot

Chapter 4

The effect of temperature on microbial ferrous-iron oxidation in a continuous culture

4.1 Introduction

As stated in Chapter 2, microbial ferrous-iron oxidation is the key sub-process in bioleaching techniques for the recovery of valuable metals from their sulphide ores. Ferric-iron is the critical reagent for the oxidation of most of these minerals. The mechanisms of ferrous-iron oxidation are well understood, at least for *At. ferrooxidans*, and it is believed that the same holds for other iron oxidising bacteria and archaea. To date a reasonable number of iron- and sulphur- oxidizing bacteria and archaea have been isolated from inorganic mining environment – classified into mesophiles, moderate thermophiles, thermophiles and extreme thermophiles. Until recently, *At. ferrooxidans* was considered to be the primary microbe responsible for bioleaching of sulphide minerals (Brierley, 1982; Lundgren and Silver, 1980), but it was later shown that *L. ferrooxidans* was in fact more dominant than *At. ferrooxidans* (Boon, 1996; Rawlings *et al.*, 1999). Earlier studies on bioleaching and microbial ferrous-iron oxidation with respect to effect of temperature were carried out using these bacteria at temperatures between 30 and 40 ºC, and mostly in batch cultures.

A number of studies have been carried out on the effect of temperature on the kinetics of microbial ferrous-iron oxidation of *At ferrooxidans* (Ahonen and Tuovinen, 1989; Guay *et*

al., 1977; Lacey and Lawson, 1970; MacDonald and Clark, 1970; Nemati and Webb, 1997), and recently of *L. ferrooxidans* (Breed *et al.*, 1999). Most of these studies were carried out in batch cultures except for the work of Breed and co-workers. It is important to note that these studies were limited to narrow range of temperatures within or near the optimum temperature of the bacteria, except for the recent work of Kupka *et al.* (2007) that was conducted at between 5 and 30 ºC and also Franzmann *et al.* (2005), where emphasis was on determining the optimum operating temperatures for most bioleaching organisms. These studies have found applications in tank bioleaching of sulphide minerals, where operating temperature can be controlled for optimum microbial performance.

However, now that bioleaching is increasingly finding application in heap leaching, research efforts have been directed towards improving the efficiency of metal recovery in heap bioleaching (for review, see Ojumu *et al.*, 2006; Petersen and Dixon, 2004; Petersen and Dixon, 2006; Petersen and Dixon, 2007b; Petersen and Dixon, 2007c; Remonselle *et al.*, 2007; Renman *et al.*, 2007; Vilcaez *et al.*, 2007; Zepeda *et al.*, 2007). It is clear that earlier studies on temperature effects may not reflect a real heap scenario. Heap temperature is not uniform and is difficult/impossible to control. Mixing is impossible in bioleach heap; internal zones of heaps may reach higher temperatures (in excess of 60 ºC due to the exothermic sulphide oxidation), also in cold environments such as low and high latitudes and at high altitudes, low temperature of less than 10 ºC can be found. This might become a limiting factor, reducing the rate and extent of microbial ferrous-iron oxidation, and as a result, leaching rates under such conditions may render operations uneconomical. It is important therefore, to study the kinetics of microbial growth and ferrous-iron oxidation under wide range of temperatures found in heap bioleaching. Bioleach heaps normally contain consortia of microorganisms ranging from mesophiles to extreme thermophiles and temperature is a major selective pressure for the dominant organisms that will inhabit different regions in heaps.

Franzmann *et al.* (2005) have recently determined the physiological operating temperature windows in temperature controlled batch systems, for most of the microbial species found in tank and heap bioleaching environments. The authors determined their optimum

temperatures and activation energies using the Ratkowsky and Arrhenius equations respectively. The aim of this work is to investigate in a continuous culture, the effect of changes in temperature on the kinetics of microbial ferrous-iron oxidation of *Leptospirillum ferriphilum* studied within the physiological operating temperature range reported by Franzmann and co-workers. This will provide the understanding of the kinetic contribution of *L. ferriphilum* in the consortium to overall microbial oxidation process.

4.2 Methodology

The kinetic studies were carried out in continuous culture experiments at 18, 20, 25, 30, 36, 42 and 45^{o}C and at a pH of 1.3 with feed substrate containing 12 g L^{-1} total iron concentration. It should be noted that changes in the temperature were made about the base case, 36°C (near reported optimum temperature) to minimize bacterial adaptation. The experimentation is described in detail in Section 3.2.2.

4.3 Results and discussion

During the experiments to investigate the effect of temperatures on ferrous-iron oxidation kinetics, single bioreactors were maintained at corresponding temperatures, and the pH in each of the bioreactors was maintained at pH 1.3. It was technically not possible to cultivate *L. ferriphilum* at 18 and 45°C, the cells washed out from the bioreactor at these temperatures even at 5 days residence time. To demonstrate this, Figure 4.1 shows in addition to $-r_{O_2}, -r_{CO_2}$ the biomass concentration C_x of a chemostat that was maintained 20 hours residence time and at 42^{o}C. The utilisation rate and C_x decreased progressively when the chemostat was perturbed by increasing the temperature to 45^{o}C, indicating a progressive washout of the cells. A similar plot was obtained for the 18 ^{o}C study. However, when the system was converted to a batch operation, it took three weeks to record solution potential of 650 mV (Ag/AgCl) when cultivated at 18°C, and 30 hours at 45°C. This indicates that *L. ferriphilum* is capable of active growth at 45 °C, while the growth is retarded but not ceased at 18°C. Also only a

single data point could be obtained at 20°C when cultivated at 103 hours (~ 4.2 days) below which the cells start to wash out.

Figure 4.2 – Figure 4.4 show the relationship between the measured off-gas data – the rate of oxygen, $-r_{O_2}$, carbon dioxide utilisation, $-r_{CO_2}$ and the rate of rate of ferrous-iron utilisation/oxidation, $-r_{Fe^{2+}}$ with dilution rate, D. The figures show that a linear relationship exists between the respective rates and dilution rate. This therefore suggests a linear relationship between the utilisation rates. On careful observation, Figure 4.4 can be interpreted to be a plot of $-r_{Fe^{2+}}$ versus D in Equation 3.23, the material balance equation.

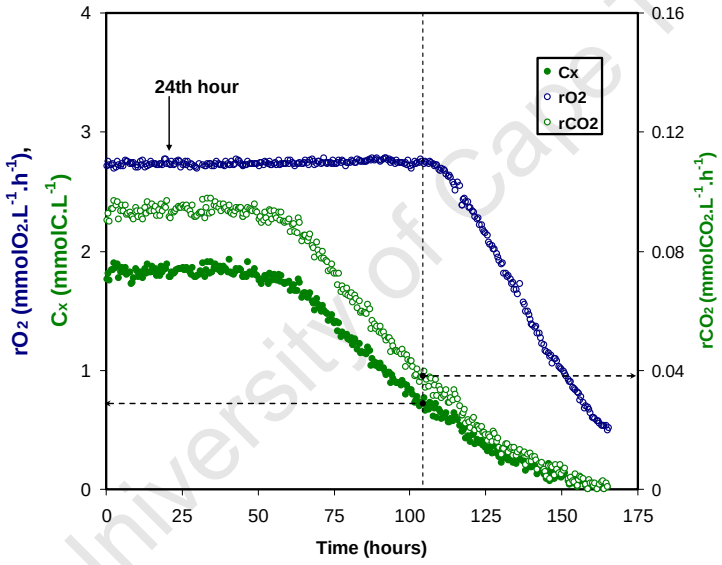

Figure 4.1 Variation of $-r_{O_2}$, $-r_{CO_2}$ and Cx with time for a chemostat running at 42 °C when the temperature increased to 45 °C after 24th hour.

$$-r_{Fe^{2+}} = D\left([Fe^{2+}]_{inlet} - [Fe^{2+}]_{outlet}\right) \qquad 3.23$$

However, it is not expected that the change in ferrous-iron concentration, $([Fe^{2+}]_{inlet} - [Fe^{2+}]_{outlet})$ would be constant over the entire range of dilution rates studied.

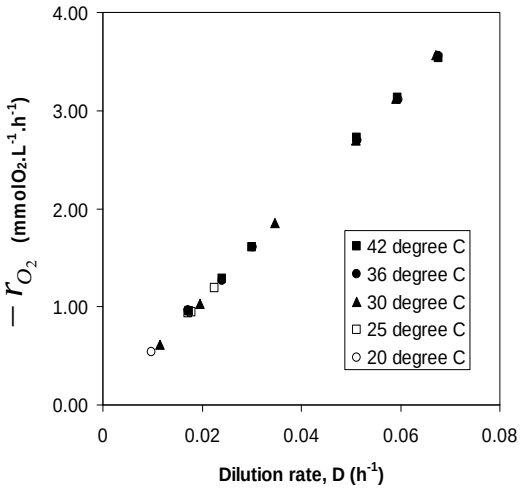

Figure 4.2 Changes in oxygen utilisation rate with the rate of dilution

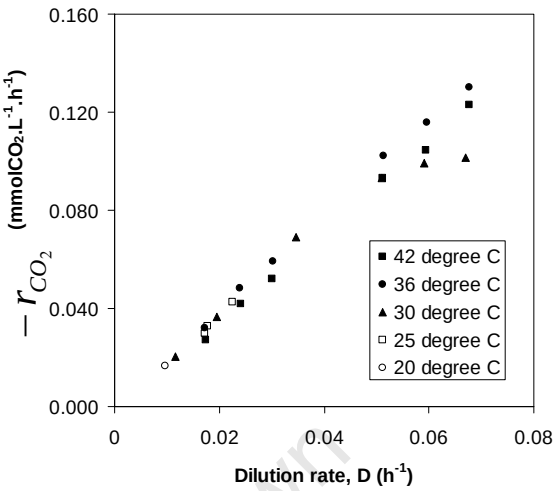

Figure 4.3 Changes in carbon dioxide utilisation rate with the rate of dilution

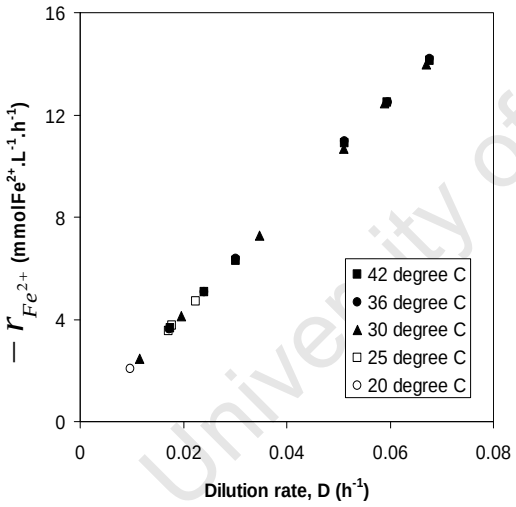

Figure 4.4 Changes in ferrous-iron utilisation rate with dilution rate

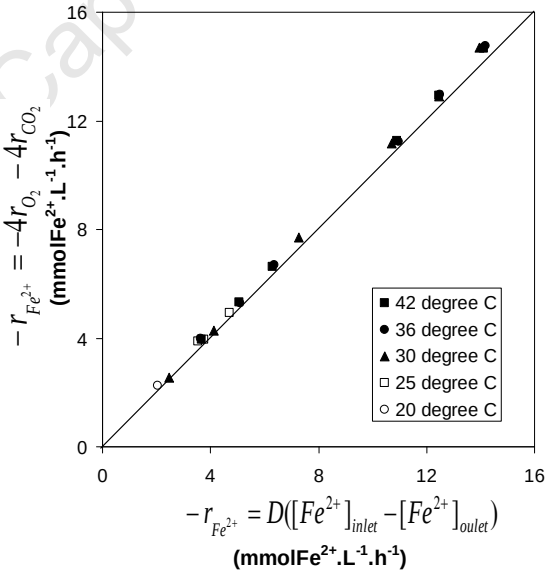

Figure 4.5 Parity plot comparing the predicted (Eq. 3.5) and experimental (Eq. 3.23) $-r_{Fe^{2+}}$ values

The validity of the data was checked by comparing the rate of ferrous-iron oxidation, determined by a simple material balance of the chemostat (Equation 3.23) using the titration method with that obtained through the degree-of-reduction balance using off–gas measurement as shown in Equation 3.5 – this is shown on the parity plot in Figure 4.5.

$$-r_{Fe^{2+}} = -4r_{O_2} - 4.2r_{CO_2} \qquad 3.5$$

The figure suggests a good agreement between the two methods, thus confirming the validity of the off-gas data.

Although the change in ferrous-iron concentration ($[Fe^{2+}]_{inlet} - [Fe^{2+}]_{outlet}$), which represents the slope of Equation 3.23, seemed to be constant with dilution rate (see Figure 4.4), it can be seen that the ferric-to-ferrous iron ratio decreased with increasing dilution as shown in Figure 4.6. This reflected a corresponding increase in the residual ferrous-iron concentration $[Fe^{2+}]_{outlet}$ in the bioreactor as shown in Figure 4.7. However, Figure 4.6 and Figure 4.7 also suggest that increase in temperature within the range studied promotes microbial ferrous iron oxidation as revealed by increase in ferric-to-ferrous ratio and a corresponding decrease in residual ferrous-iron concentration in the bioreactor.

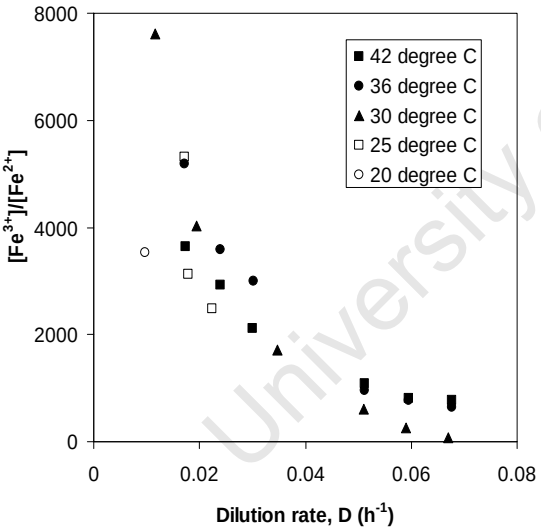

Figure 4.6 Variation in ferric-to-ferrous iron ratio, ([Fe3+]/[Fe2+]) with dilution rate.

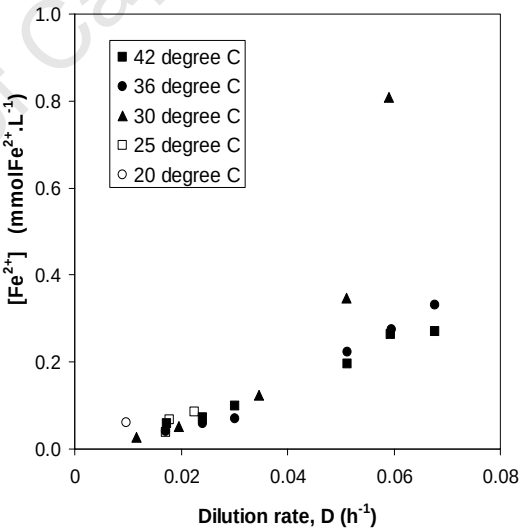

Figure 4.7 Variation in the residual ferrous-iron concentration with dilution rate.

Figure 4.8 shows the variation of the biomass concentration with dilution rate over the range of temperatures (20 to 42 °C) studied. These values were calculated from the rate of carbon dioxide utilisation, $-r_{CO_2}$ according to Equation 3.24.

$$C_X = -r_{CO_2}/\mathrm{D} \qquad 3.24$$

The figure shows that irrespective of solution temperature, the maximum biomass was obtained at about the intermediate dilution rate, around 0.035 h^{-1} and decreased slightly to the either side (see Figure 4.8). This trend is similar to the trend shown by the simulation plot in Figure 2.7 which shows the trend of biomass concentration with dilution rate as predicted by Equation 2.26, given a reasonable guess of the parameters involved. This trend is the same as the trend obtained when the simulation was plotted using the Hanford Equation (Equation 2.33). This observation is also similar to the trend reported in the previous studies (Boon, 1996; Breed *et al.*, 1999; van Scherpenzeel *et al.*, 1998).

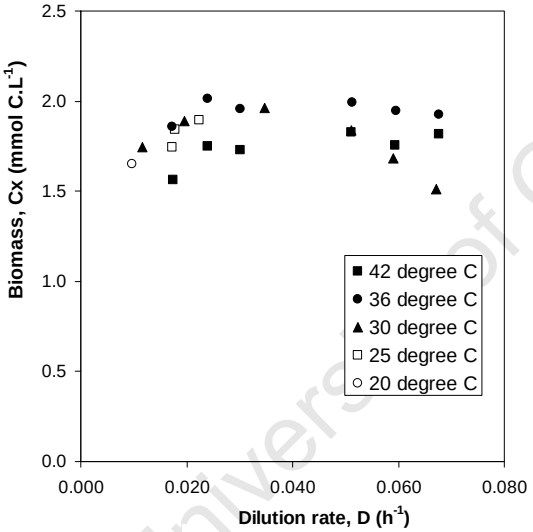

Figure 4.8 Variation of biomass concentration Cx with dilution rate.

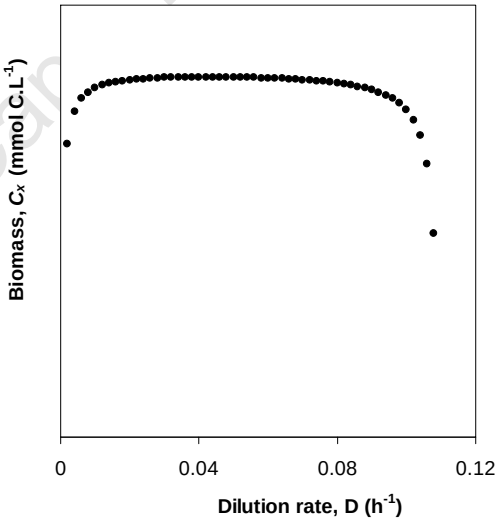

Figure 4.9 Simulation plot of variation of biomass concentration Cx with dilution rate (Eq. 2.24)

The reduced biomass at low dilution rate (*i.e* long residence time) can be attributed to increase in maintenance due to substrate limitation, while according to Breed *et al.* (1999), the reduction at high dilution rates is an indication that the system is approaching a washout region, thus the Pirt's Equation will not be valid in this region. On the contrary, Sundkvist *et al.*(2007) observed a progressive increase in biomass concentration until washout was observed. Although, the authors used fewer data points to arrive at this conclusion and washout is expected at the region suggested by

their data, the contrast might be due to the different methods used for biomass determination.

The trend of C_x with temperature is not very obvious from the plot (Figure 4.8). It appears that lowest biomass concentration is observed at the maximum temperature (42°C) with increasing number as solution gets colder. This phenomenon is thought to be a response to adversity by increasing population density.This is discussed in more detail in Chapter 7.

4.3.1 The energetic parameters

The values of maximum bacterial yield coefficients ($Y^{\max}_{Fe^{2+}X}, Y^{\max}_{O_2X}$) and maintenance coefficients ($m_{Fe^{2+}}, m_{O_2}$) on ferrous-iron and oxygen respectively were determined using Pirt's Equation, Equations 3.8 – 3.12 written in a general form as in Equations 4.1

$$q_S = \frac{D}{Y^{\max}_{SX}} + m_S, \qquad \frac{1}{Y_{SX}} = \frac{1}{Y^{\max}_{sX}} + \frac{m_S}{D} \tag{4.1}$$

where S represents the substrate. The plot of specific ferrous-iron utilisation, $q_{Fe^{2+}}$ versus dilution rate, D yields a straight line with slope $1/Y^{\max}_{Fe^{2+}}$ and an intercept of $m_{Fe^{2+}}$ while the plot of reciprocal of the observed yield versus the reciprocal of the dilution rate should also give a linear plot with a slope of $m_{Fe^{2+}}$ and intercept of $1/Y^{\max}_{Fe^{2+}}$. Similar plot analyses can be performed to obtain the parameters based on oxygen. These are shown in Figure 4.10 (a – d).

The values shown in Table 4.1 are obtained from Figure 4.10 (a and c), giving a good fit of the data compared to the reciprocal plots. As shown in the figures, Pirt's Equation appears to be valid (*i.e.* shows linear correlation between q and D) within the region studied, except for the study at 30°C where it appeared not to be valid beyond residence time of 25 hours ($\tau = 1/D$) at this temperature (Figure 4.10 a and c). This was due to the fact that the system was approaching the washout region, as is evident from decreasing corresponding biomass data at this condition, as shown in Figure 4.8.

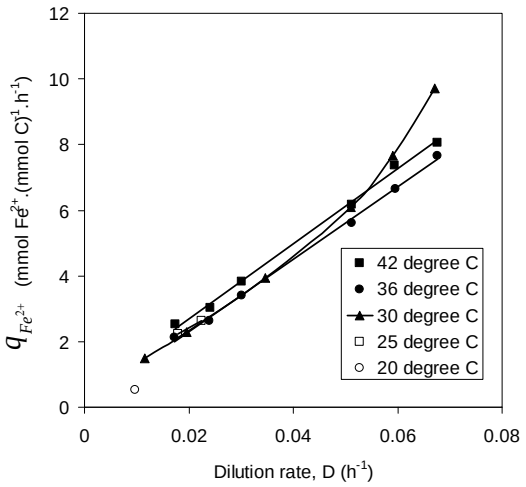

(a) Data used to determine maximum biomass yield and maintenance coefficient on ferrous-iron using Equation 3.11

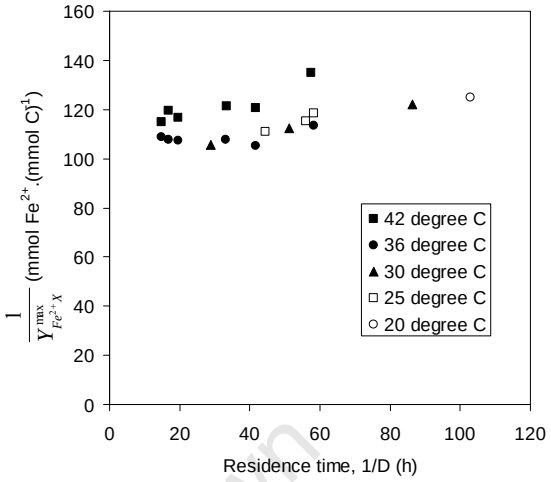

(b) Data used to determine maximum biomass yield and maintenance coefficient on ferrous-iron using Equation 3.9

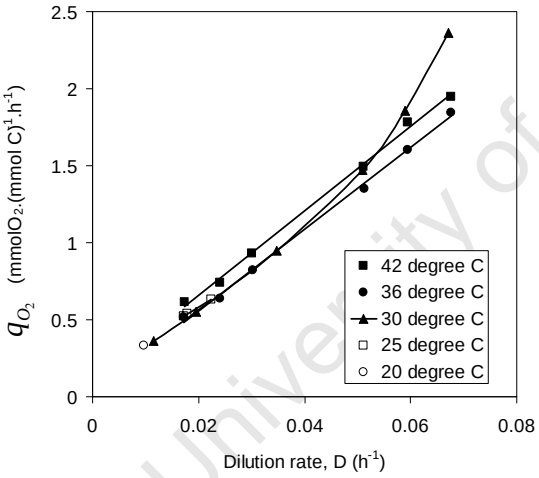

(c) Data used to determine maximum biomass yield and maintenance coefficient on oxygen using Equation 3.12

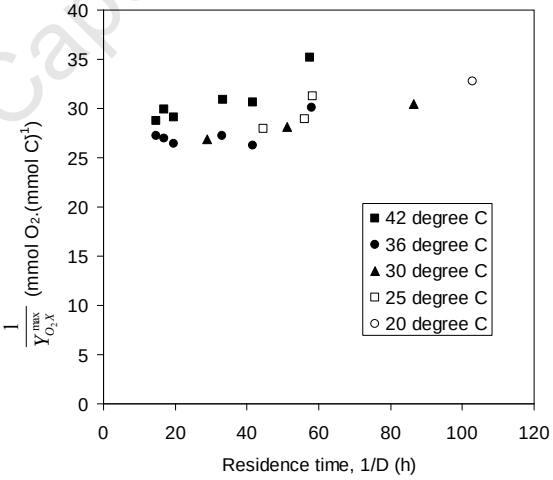

(d) Data used to determine maximum biomass yield and maintenance coefficient on oxygen Equation 3.8

Figure 4.10 Pirt's plot used to determine the energetic parameters; $Y^{max}_{Fe^{2+}X}, Y^{max}_{O_2X}, m_{Fe^{2+}}, m_{O_2}$

The Figures suggest (Figure 4.10) that the specific utilisation rates ($q_{Fe^{2+}}, q_{O_2}$) are strong functions of dilution rate while the biomass yields ($Y_{Fe^{2+}X}, Y_{O_2X}$) are weak functions. This can also be inferred from the fact that the biomass concentration did not vary much

with dilution rate as shown in Figure 4.8. The maximum biomass yields on ferrous-iron and oxygen, $Y^{max}_{Fe^{2+}X}$, $Y^{max}_{O_2X}$ decrease, albeit insignificantly, with increasing temperature between 25 and 42 °C (see Table 4.1) as a linear function (Figure 4.11), while on the other hand, the maintenance coefficients $m_{Fe^{2+}}$, m_{O_2} do not show a linear trend.

The data suggests that the maintenance coefficient values are relatively small and insignificant compared to measured $1/Y^{max}_{Fe^{2+}X}$ values in all cases (<5 %) and thus may be negligible, which points at an actively growing culture. A minimum maintenance requirement occurred at 36 °C (the base case), and the value increases towards either side of the minimum (see Figure 4.12). The highest value of maintenance coefficient occurred at 25 °C followed by 42 °C. This could be explained by the fact that temperature changes were made about the base case temperature to a colder and hotter conditions, and the bacteria tend to divert their energy towards cell maintenance during these situations. The trend of the maintenance coefficient can be represented by a quadratic function of the form:

$$m_{Fe^{2+}} = 0.0054T^2 - 0.376T + 6.64 \qquad 4.2$$

Table 4.1 The values of maximum biomass yields and maintenance coefficients on ferrous-iron and oxygen respectively for a chemostat maintained at pH 1.3 various temperatures.

Temperature	$Y^{max}_{Fe^{2+}X}$	$m_{Fe^{2+}}$	R^2	$Y^{max}_{O_2X}$	m_{O_2}	R^2	m_{O_2} *Calculated*	$Y^{max}_{O_2X}$ *Calculated*
45	*nd*	*nd*	*nd*	*nd*	*nd*	*nd*	*nd*	*nd*
42	0.0088	0.43	0.9976	0.037	0.11	0.9974	0.11	0.036
36	0.0091	0.09	0.9975	0.038	0.03	0.9974	0.02	0.038
30	0.0094	0.24	0.9996	0.039	0.06	0.9996	0.06	0.039
25	0.0115	0.72	1.0000	0.049	0.17	0.9985	0.18	0.049
20	*nd*	*nd*	*nd*	*nd*	*nd*	*nd*	*nd*	*nd*
18	*nd*	*nd*	*nd*	*nd*	*nd*	*nd*	*nd*	*nd*

Units: $Y^{max}_{Fe^{2+}X}$ [molC.(molFe^{2+})$^{-1}$], $m_{Fe^{2+}}$ [molFe^{2+}.(molC)$^{-1}$], $Y^{max}_{O_2X}$ [molC.(molO_2)$^{-1}$], m_{O_2} [molO_2.(molC)$^{-1}$], *nd* not determined

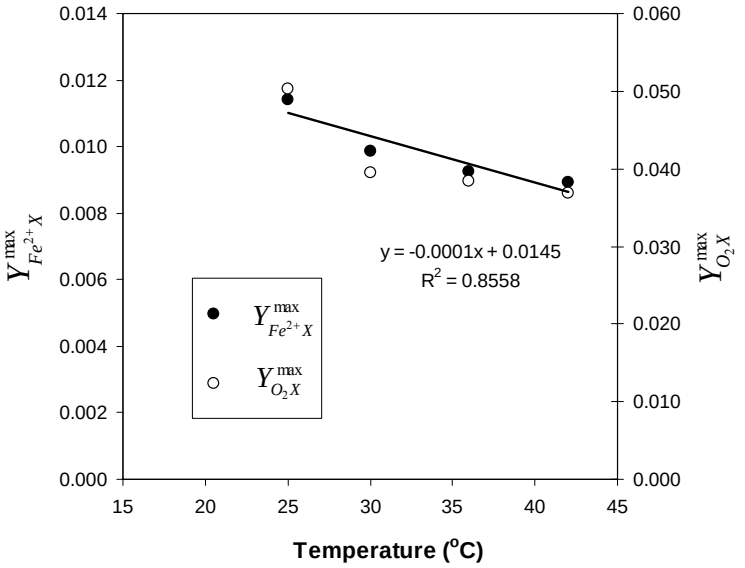

Figure 4.11 Variation of maximum biomass yields ($Y^{max}_{Fe^{2+}X}, Y^{max}_{O_2X}$) with temperature

This experimental approach reflects the effect of temperature fluctuation in a real heap scenario. It should be noted that for the 30 °C study the energetic parameters were determined within the linear range of dilution rates where the Pirt equation can be applied. Table 4.1 also shows that the experimental data were valid and consistent. The validity was checked by comparing the experimentally determined values of Y_{O_2X} and m_{O_2} with the expected values as determined from the Equations in Equation 3.10. This is also shown on a parity plot (Figure 4.13)

$$\frac{1}{Y^{max}_{O_2X}} = \frac{1 - 4.2Y^{max}_{Fe^{2+}X}}{4Y^{max}_{Fe^{2+}X}}, \qquad m_{O_2} = \frac{m_{Fe^{2+}}}{4} \qquad 3.10$$

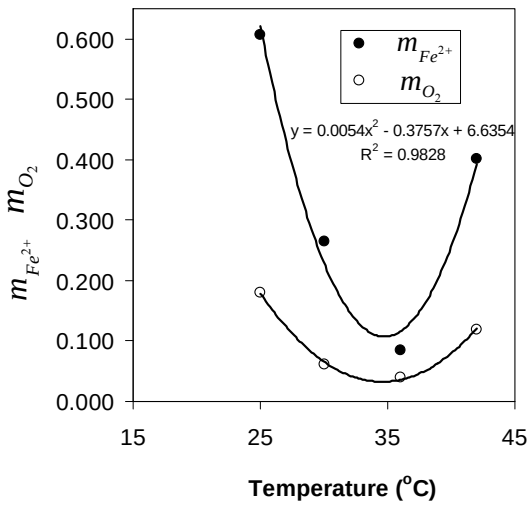

Figure 4.12 Variation of maintenance requirements ($m_{Fe^{2+}}, m_{O_2}$) with temperature

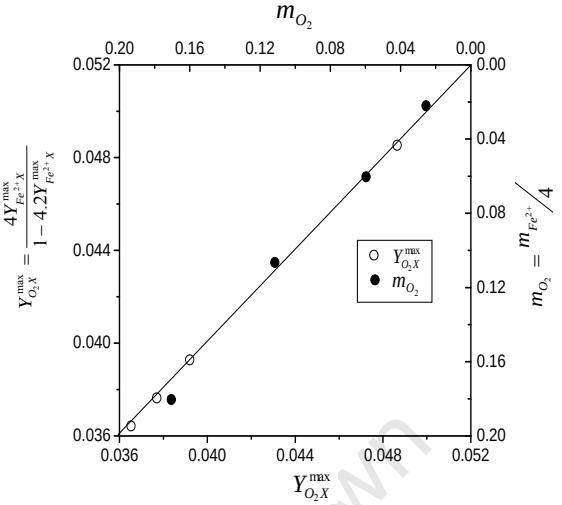

Figure 4.13 Parity plot for comparison between the experimental and the predicted biomass yield and maintenance coefficients for the data shown in Table 4.1

4.3.2 The kinetic parameters

Assuming that the kinetics of microbial ferrous-iron oxidation of *L. ferriphilum* can be described by simplified q based model (Equations 3.15 and 3.16) by Hansford and his co-workers (Boon *et al.*, 1995a), then the values of the kinetic parameters, $q_{Fe^{2+}}^{max}, q_{O_2}^{max}$ and $K'_{Fe^{2+}}, K'_{O_2}$ can be determined using two different analytical approaches:

- the fit of each set of experimental data to Equations 3.15 and 3.16 using the Solver routine in Microsoft Excel©, and by minimizing the sum of the squared errors (SSE) between the experimentally determined values of $q_{Fe^{2+}}$ and q_{O_2}, and the values predicted by the model as given in Equations 4.3 and 4.4, the constants of the Equations can be obtained. This is shown in Figure 4.14 (a) and (b)

$$SSE = \sum_{Eh_i}^{Eh_f} \left[(q_{Fe^{2+}}^{Experimental}) - (q_{Fe^{2+}}^{Theoretical}) \right]^2 \qquad 4.3$$

$$SSE = \sum_{Eh_i}^{Eh_f} \left[(q_{O_2}^{Experimental}) - (q_{O_2}^{Theoretical}) \right]^2 \qquad 4.4$$

- The values of $q_{Fe^{2+}}^{max}, q_{O_2}^{max}$ and $K'_{Fe^{2+}}, K'_{O_2}$ can also be determined using Lineweaver-Burk plot described in section 2.8 Plotting the inverse of the specific rates versus $[Fe^{3+}]/[Fe^{2+}]$ ratio give a linear graph (see Figure 4.14 (c) and (d)) from which $q_{Fe^{2+}}^{max}, q_{O_2}^{max}$ and $K'_{Fe^{2+}}, K'_{O_2}$ were determined from the intercept and slope respectively.

Figure 4.14 (a) and (b) show that there is a good agreement between the experimentally determined $q_{Fe^{2+}}$ and q_{O_2}, and their predicted values. The average values of these parameters are presented in Table 4.2. The values of the maximum specific biomass utilisation rates of ferrous-iron and oxygen, $q_{Fe^{2+}}^{max}, q_{O_2}^{max}$, increase significantly with increasing temperature, and so did the $K'_{Fe^{2+}}, K'_{O_2}$ values.

However, only a minor increase in the $K'_{Fe^{2+}}, K'_{O_2}$ values occurred between the temperatures of 30 and 36^{o}C. Although the observed trend in the plot is similar to the results of other workers using similar systems (Breed *et al.*, 1999; van Scherpenzeel *et al.*, 1998), the $K'_{Fe^{2+}}, K'_{O_2}$ values are significantly lower than published values as shown in Table 4.3. The microbial activity can not be predicted with $K'_{Fe^{2+}}$ values being a lumped parameter (constituting K_s/K_i – affinity constant and inhibition constant).

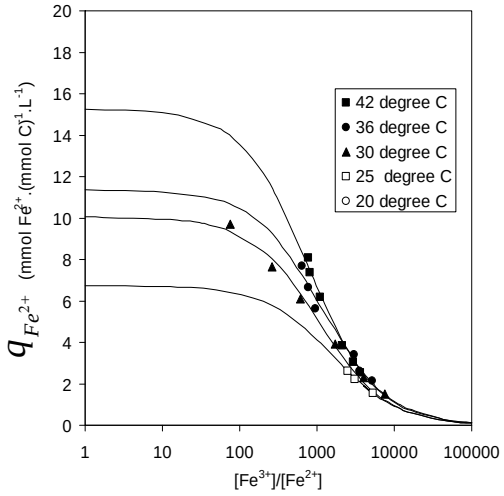

(a) The fit of experimentally determined specific ferrous-iron oxidation rate at different ferric-to-ferrous ratio to Equation 3.15

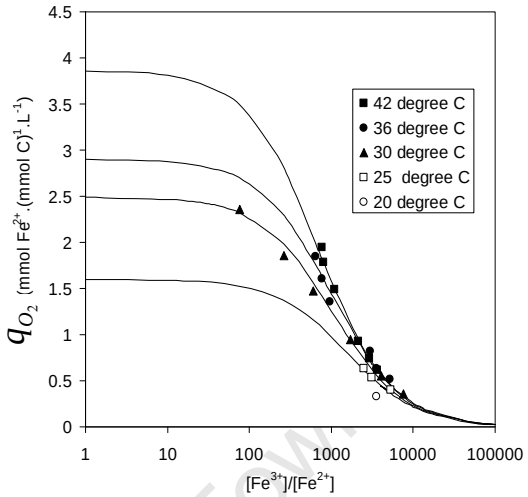

(b) The fit of experimentally determined specific oxygen utilisation rate at different ferric-to-ferrous ratio to Equation 3.16

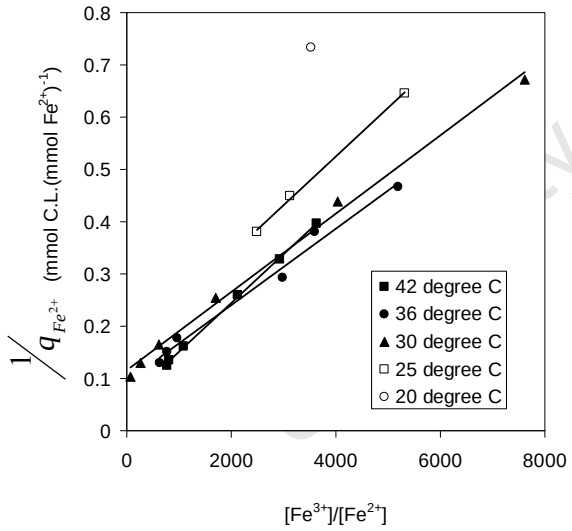

(c) Lineweaver-Burk plot of inverse of specific ferrous-iron oxidation rate versus ferric-to-ferrous ratio

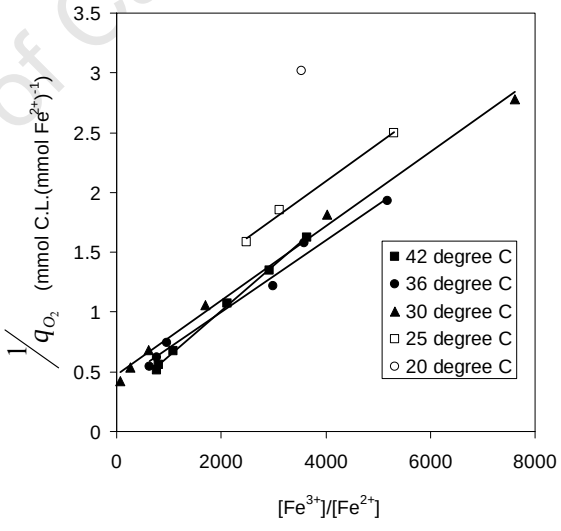

(d) Lineweaver-Burk plot of inverse of specific oxygen utilisation rate versus ferric-to-ferrous ratio

Figure 4.14 Data used for determination of kinetic parameters $q^{max}_{Fe^{2+}}, q^{max}_{O_2}$ and $K'_{Fe^{2+}}, K'_{O_2}$ shown in Table 4.2 [note that only one data point can be obtained at 20 °C in this study]

Table 4.2 Average of maximum specific ferrous-iron oxidation and kinetic constant, determined from Lineweaver Burke method and the fit of simplified ferric-iron inhibition model

	Temp-erature	Lineweaver-Burk method			Simplified ferric inhibition model			Average	
		$q^{max}_{Fe^{2+}}$	$K'_{Fe^{2+}}$	R^2	$q^{max}_{Fe^{2+}}$	$K'_{Fe^{2+}}$	R^2	$q^{max}_{Fe^{2+}}$	$K'_{Fe^{2+}}$
Ferrous-iron based parameters	42	17.21	0.0015	0.999	15.29	0.0018	0.994	16.25	0.0017
	36	10.58	0.0007	0.986	11.37	0.0009	0.978	10.97	0.0008
	30	8.68	0.0006	0.996	10.05	0.0010	0.991	9.36	0.0008
	25	6.48	0.0006	0.999	6.73	0.0006	0.999	6.60	0.0006
		$q^{max}_{O_2}$	K'_{O_2}	R^2	$q^{max}_{O_2}$	K'_{O_2}	R^2	$q^{max}_{O_2}$	K'_{O_2}
Oxygen based parameters	42	4.06	0.0016	0.999	3.87	0.00144	0.994	3.96	0.0015
	36	2.53	0.0008	0.986	2.91	0.00102	0.978	2.72	0.0009
	30	2.10	0.0006	0.995	2.49	0.00098	0.991	2.29	0.0008
	25	1.21	0.0004	0.994	1.60	0.00064	0.991	1.40	0.0005

Units: $q^{max}_{Fe^{2+}X}$ [molFe^{2+}(molC.h)$^{-1}$], $q^{max}_{O_2X}$ [mol O_2(molC.h)$^{-1}$], $K'_{Fe^{2+}}$ & K'_{O_2} are dimensionless

The predicted maximum specific rates $q^{max}_{Fe^{2+}}, q^{max}_{O_2}$ increased with temperature. The values of $q^{max}_{Fe^{2+}}, q^{max}_{O_2}$ can be said to agree reasonably well with literature values (Breed *et al.*, 1999) for oxidation between 30 – 40°C for *Leptospirillum*-like species. The maximum biomass specific ferrous-iron oxidation rate was achieved at 42°C. This temperature is higher than the optimum temperature, 38.6 °C, reported by Franzmann *et al.* (2005) at pH 1.3. However, no comparison can be made as no data were taken at this temperature.

The figures also show that most of the data points occur in the region of high ferric-to-ferrous ratio. This confirms the earlier work of Rawlings *et al.* (1999) that *L. ferriphilum* thrives and is less subjected to ferric inhibition than *At. ferrooxidans*. This is also reported in Breed *et al.* (1999) by calculating the threshold ferrous-iron concentration (*i.e.* a minimum concentration of ferrous-iron beyond which no further growth will occur) to be much less than the reported value for *At. ferrooxidans* (Boon, 1996).

Table 4.3 Values of $q_{Fe^{2+}}^{max}, q_{O_2}^{max}$ and $K_{Fe^{2+}}, K_{O_2}$ at temperatures ranging from 30 to 40 °C and pH ranging from pH1.10 to pH 1.70+

Bacterial culture	Temperature (°C)	pH	$q_{Fe^{2+}}^{max}$ mmol Fe^{2+}. $(mmol\ C)^{-1}h^{-1}$	$K_{Fe^{2+}}$	μ_{max}
Predominantly *L. ferrooxidans*	30	1.70	8.65	0.0018	0.040
	35	1.70	11.01	0.0023	0.063
	40	1.70	13.62	0.0034	0.084
Predominantly *L. ferrooxidans*	40	1.10	15.25	0.0010	0.103
	40	1.30	15.57	0.0022	0.108
	40	1.70	19.02	0.0037	0.124
Leptospirillum –like (van Scherpenzeel *et al.*, 1998)	30	1.5 – 1.6	7.09	0.004	0.069
At. ferrooxidans (Boon, 1996)	30	1.8 – 1.9	9.20	0.05	0.140

+ Soucre: Adapted from Breed, 2000

By modifying Equation 3.15 to account for the ferrous-iron threshold term, $[Fe^{2+}]_{Threshold}$, the constants $q_{Fe^{2+}}^{max}, q_{O_2}^{max}$ and $K'_{Fe^{2+}}, K'_{O_2}$ as determined by minimizing the sum of squares error as previously described, did not show any significant improvement to warrant the inclusion of this parameter into Equation 3.15. The values of $[Fe^{2+}]_{Threshold}$ were much lower than those previously reported for mesophilic systems; 0.054 – 0.268 mM (*L.ferrooxidans*, (Breed *et al.*, 1999)) and 0.5 mM (*At. Ferrooxidans*, (Boon, 1996)). The $[Fe^{2+}]_{Threshold}$ values obtained [~0.004 – 0.01 mM] confirmed that *L. ferriphilum* is less subjected to inhibition by ferric-iron. Therefore Hansford and co-workers' (Boon *et al.*, 1999a; Hansford, 1997) observation that the contribution of the term $K_s/[Fe^{2+}]$ to the ferric inhibition rate equation is negligible, that allowed the simplification of the ferric inhibition equation to Equation 3.15 may not necessarily apply to *L. ferriphilum*. This will be discussed further in Chapter 7.

$$q_{Fe^{2+}} = \frac{q_{Fe^{2+}}^{max}}{1 + K'_{Fe^{2+}} \dfrac{[Fe^{3+}]}{[Fe^{2+}] - [Fe^{2+}]_{Threshold}}} \qquad 3.15$$

4.3.3 The effect of temperature

As previously discussed, the maximum utilization rates increased with the increase in temperature, the relationship between the maximum microbial specific ferrous-iron utilisation rates, $q_{Fe^{2+}}$ and operating temperature can be described using the Arrhenius equation:

$$q_{Fe^{2+}}^{\max} = K_0 \exp\left(-\frac{E_a}{RT}\right) \quad ....a$$
$$\ln q_{Fe^{2+}}^{\max} = -\frac{E_a}{R}\left(\frac{1}{T}\right) + \ln K_0 \quad ....b \qquad 4.5$$

The activation energy E_a and the frequency factor K_o for microbial ferrous-iron oxidation kinetics can be obtained from the plot of $\ln q_{Fe^{2+}}^{\max}$ versus 1/T respectively as shown in Figure 4.15(a). The values of activation energy for microbial ferrous-iron oxidation and oxygen utilization rates were 34.46 and 37.31 kJ.mol^{-1} respectively. These values fall within the range previously reported (33 – 96 kJ.mol^{-1}) (Ahonen and Tuovinen, 1989; Breed *et al.*, 1999; Guay *et al.*, 1977; Lacey and Lawson, 1970; MacDonald and Clark, 1970; Nemati and Webb, 1997). While a similar value of 35.62 kJ.mol^{-1} was reported by Breed *et al.* (1999) for *Leptosprillum*-like organisms, a significantly higher activation energy value (89 kJ.mol^{-1}) was reported for *L. ferriphilum* by Franzmann *et al.* (2005).

The variation in reported values may have resulted from different monitoring approaches. Nemati and Webb (1997) obtained an activation energy of 68.4 kJ mol^{-1} using an initial rate method while the recent study of Franzmann and co-workers was carried out in a temperature-gradient batch type system of 20 mL capacity. The effect of evaporation at elevated temperature, though accounted for, might introduce some uncertainties into Franzmann and co-workers' data. Although differences in microbial strain and experimental conditions may also be responsible for the variation, it is expected that microbial processes will have lower activation energies compared to purely chemical processes.

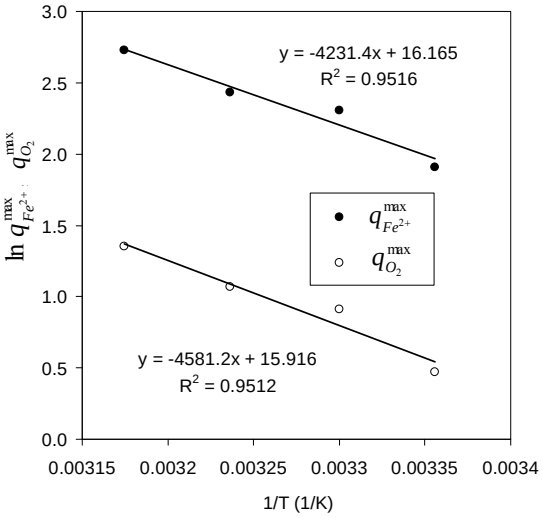

(a) Arrhenius to show the effect of temperature on the specific utilisation rates

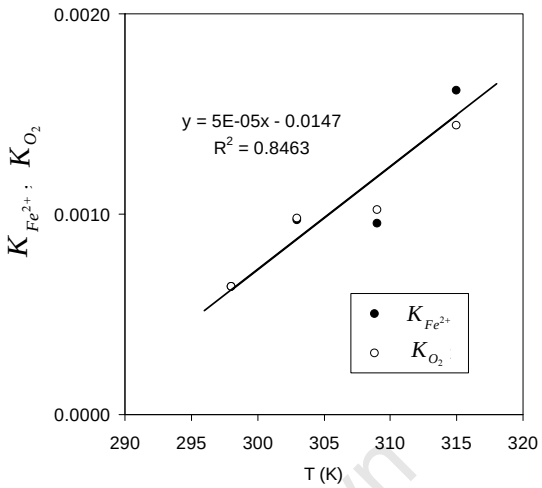

(b) The effect temperature on the kinetic constants $K_{Fe^{2+}}$ and K_{O_2}

Figure 4.15 Variation of the kinetic parameters, $q_{Fe^{2+}}^{max}$ $q_{O_2}^{max}$ and $K_{Fe^{2+}}$ K_{O_2} with temperature

All activation energy values reported for a chemical oxidation fall to the upper limit of the above reported range – (Chmielewski and Charewicz, (1984) obtained 56.9 kJ.mol^{-1} between 40 – 135 °C; Verbaan and Crundwell (1986), 68.6 between 25 – 85 °C) – and recently an E_a value between 61.3 – 69.7 kJ.mol^{-1} were reported by (Kazadi, 2007). The frequency factor K_0 determined from the intercept of the Arrhenius plot (Figure 3.10(a)) was found to be 1.05×10^7 mmol Fe^{2+}.(mmol C)$^{-1}$h^{-1}. The relationship between the kinetic constants, $K'_{Fe^{2+}}$, K'_{O_2} and temperature can be represented linearly, as shown in Figure 4.15. Both can be reasonably described by the expression

$$K_{Fe^{2+}} = 5 \times 10^{-5} T - 0.0147, \qquad R^2 = 0.85$$

By substituting the values of E_a , q_0 and the expression for $K_{Fe^{2+}}$ into the modified Monod equation for competitive inhibition (Equation 3.15), model which predicts $q_{Fe^{2+}}^{max}$ as a function of the ferric/ferrous-iron ratio (redox potential) across a range of temperatures can be obtained as shown in Figure 4.16. The error analysis of the predicted data based on measured and suggests that the model can accurately (to 98 %

accuracy) describe the effect of temperature on microbial ferrous-iron oxidation as shown in Figure 4.16. See Appendix C1.1 & C1.2 for the statistics and error analysis.

$$q_{Fe^{2+}} = \frac{q_0 \exp(-E_a / RT)}{1 + \left(5 \times 10^{-5} T - 0.0147\right)\frac{[Fe^{3+}]}{[Fe^{2+}]}} \qquad 3.25$$

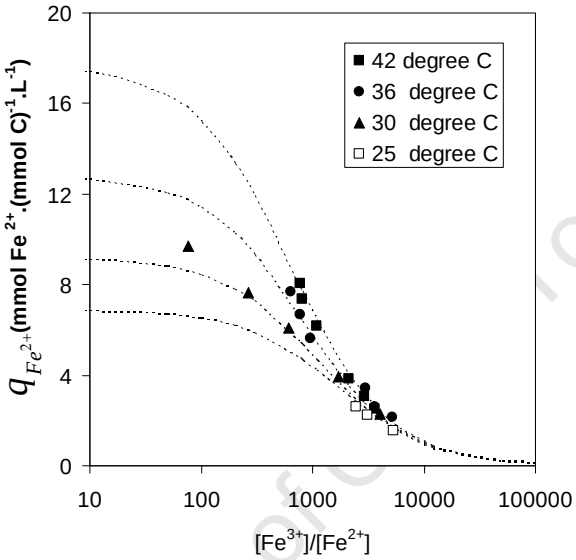

Figure 4.16 The specific microbial ferrous-iron utilization rate as a function of ferric-to-ferrous ratio in continuous culture for 12 g L^{-1} total iron at pH 1.3

4.3.4 Maximum microbial specific growth rate

The values of the maximum specific growth rate, μ_{max} calculated at different temperatures were obtained as average values determined from Equations 3.13 and 3.14 using the respective yield and maintenance parameters from Table 4.1. Since the value of μ_{max} should not be dependent on the substrate type, the ferrous-iron and oxygen based kinetic equations should give the same result. These values are listed in Table 4.4.

The results show that the highest μ_{max} was obtained at 42 °C, this value decreases as the temperature decreased to 25 °C. Although the dilution rate at which washout occurred was not monitored throughout the experiment, the results show that the washout dilution rate at 42 °C was the highest which is consistent with the results presented by Breed *et al.* (1999).

Table 4.4 Calculated values of maximum microbial specific growth rate, determined from parameters extracted from Tables 4.1 and 4.2

Temperatures	Fe^{2+} based parameters				O_2 based parameters				$\mu_{max} \pm SD$
	$q_{Fe^{2+}}^{max}$	$Y_{Fe^{2+}X}^{max}$	$m_{Fe^{2+}}$	μ_{max}	$q_{O_2}^{max}$	$Y_{O_2X}^{max}$	m_{O_2}	μ_{max}	
45		nd	nd	nd		nd	nd	nd	nd
42	16.25	0.009	0.40	0.156	3.96	0.037	0.12	0.15	0.154 ± 0.003
36	10.97	0.009	0.08	0.101	2.72	0.038	0.04	0.10	0.100 ± 0.001
30	9.36	0.010	0.26	0.090	2.29	0.040	0.06	0.09	0.089 ± 0.002
25	6.60	0.011	0.61	0.068	1.40	0.050	0.18	0.05	0.061 ± 0.011
20	nd	nd	nd	nd	nd	nd	nd	nd	nd
18	nd	nd	nd	nd	nd	nd	nd	nd	nd

nd not determined, SD Error expressed as standard deviation from the mean

Units: $Y_{Fe^{2+}X}^{max}$ [molC (mol Fe^{2+})$^{-1}$], $Y_{O_2X}^{max}$ [molC (molO_2)$^{-1}$], μ_{max} [h^{-1}],

$m_{Fe^{2+}}$ [molFe^{2+} (molC.h)$^{-1}$], m_{O_2} [mol O_2 (molC.h)$^{-1}$]

4.4 Conclusion

The microbial ferrous-iron oxidation kinetics of *Leptospirillum ferriphilum* was studied in continuous stirred bioreactors at dilution rates ranging from 0.0095 to 0.07 h^{-1} (*i.e.* 14 to 105 h residence time). The pH of the bioreactors was maintained at pH 1.3 while the temperatures were varied from 15 to 45 ^{o}C in order to capture extreme variation in temperatures that could possibly support mesophilic microbes in a typical bioleach heap as reported in Franzmann *et al.* (2005). Analysis of the data showed that the rate of ferrous-iron oxidation could be measured accurately from the rates of microbial oxygen and carbon dioxide consumption using the degree of reduction balance as shown by Boon *et al.*(1995b).

The biomass concentration did not show a particular trend with temperature, highest biomass concentration occurred at 36 °C while the lowest at 42 °C. This observation differs from the work of Breed et al (2000). However, the lowest maintenance requirement at 36 °C supports why biomass concentration is highest at this temperature. The biomass yield on ferrous-iron and oxygen decreased albeit insignificantly, with

increase in temperature, whereas the maintenance coefficient appeared to be minimum at 36 °C, while it increases as the temperature increases to 42 °C and decreases to 25 °C. However, the maintenance coefficient is small in all cases.

The maximum biomass activity measured as maximum microbial specific ferrous-iron and oxygen utilization rates, and corresponding kinetic constants increased with an increase in temperature. The relationship between the biomass activities and temperature can be described with the Arrhenius Equation, while the 'apparent affinity' constants, $K'_{Fe^{2+}}$ showed a linear dependence on temperature. The calculated maximum growth rate increased with increasing temperature, the highest μ_{max} = 0.154 h^{-1} was obtained at 42 °C and pH 1.30. It was not impossible to cultivate *L. ferriphilum* at temperatures below 20 °C and above 42 °C in a continuous culture as the cells washed out when this study was conducted at these temperatures at residence time of 105 hours. However it took approximately three weeks to obtain solution potential of 650 mV when the bioreactor was converted to batch mode at 18 °C, while it took 48 hours when the bioreactor was operated at 45 °C.

Therefore, increase in temperature increased the microbial specific ferrous-iron oxidation rate of *L. ferriphilum* within the region studied, and biomass yield is a weak function of temperature. The results indicate that *L. ferriphilum* in bioleach heap microbial consortia is likely to perform optimally and control the kinetic of ferrous-iron oxidation within temperature region of 42 °C in heap bioleach operations. However, the microbial oxidizing ability would be taken over by moderate thermophiles, thermophiles and extreme thermophiles as the case might be, as heap temperature increases beyond 45 °C. In cold conditions however, the kinetics is likely to be driven by psychrophilic strain of *At. ferrooxidans* (Kupka *et al.*, 2007). The authors have shown that *At. ferrooxidans* can be cultivated at 5 °C, and this is supported by the reported minimum temperature of growth being much lower than *L. ferriphilum* (Franzmann *et al.*, 2005).

Chapter 5

The effect of solution pH on microbial ferrous-iron oxidation in a continuous culture

5.1 Introduction

As described in Section 2.11.1, solution pH is one of the key factors affecting the microbial ferrous-iron oxidation. A high proton environment is necessary for the biooxidation process (see Equation 5.1), as this facilitates the reverse electron transport within the chemolithotrophic autotrophic bacteria for the cell nutritional purpose, as described by Ingledew (1982).

$$4Fe^{2+} + 4H^{+} + O_2 \xrightarrow{bacteria} 4Fe^{3+} + 2H_2O \qquad 5.1$$

It is also necessary to keep iron in solution (iron cycle) by preventing the precipitation of ferric-iron as hydroxyl and sulphate complexes which reduce the amount of ferric-iron in the leaching medium. Apart from iron conservation, du Plessis *et al* (2007) and van Aswegen *et al.* (2007) reported that a pH greater than 2.0 has a negative effect on microbial population. Ferric-iron precipitates, such as jarosite, represent one of the challenges in bioleach heap operations: it occupies the space on the biomass carrier material (i.e. the ore surface) creating diffusion barriers, and, if dislodged, can cause blockages in pumps and valves or can clog up the heap bed, reducing its permeability. This challenge is managed in tank bioleach reactors by working at pH values around 1.5. However, bioleach heaps are marked by a wide pH gradient. Furthermore, liquid

channeling, which often occurs in bioleach heaps, can also result in an erratic pH variation across the heap, making this challenge difficult to manage.

A number of studies have been carried out on the effects of pH on microbial ferrous-iron oxidation (Breed and Hansford, 1999a; Nemati *et al.*, 1998; Özkaya *et al.*, 2007b). Although a wide optimum pH 1.5 – 3.5 was reported in Nemati *et al.* (1998) for *At. ferrooxidans* (Drobner *et al.*, 1990), recent studies have shown solution pH greater than 2.0 leads to high risk of bacterial deactivation, which can result in the total loss of the microbial culture (Meruane and Vargas, 2003; van Aswegen *et al.*, 2007). Studies on a heap bioleach operation in the South America has shown that, while the fresh feed contained 8 g L^{-1} of concentrated sulphuric acid as free acid, the effluent pH was between 2.2 – 2.4 (Petersen, 2001). However, studies on the effect of pH on microbial ferrous-iron oxidation were carried out under a narrower range of pH values, pH 1.1 – 1.7 (Breed, 2000; Breed and Hansford, 1999a), which is suitable for tank bioleaching where parameters can be controlled to optimum. It was recently shown that microbial ferrous-iron oxidation can be carried out at pH below 1.0 (Kinnunen and Puhakka, 2005; Özkaya *et al.*, 2007a; Özkaya *et al.*, 2007b).

This chapter presents the results of microbial ferrous-iron oxidation studied over a range of pH using *Leptospirillum ferriphilum,* with a view to understanding how the microbial activity and ferrous-iron oxidation change over the range of pHs away from the optimum previously studied. This study will provide the understanding of how a heap bioleach system can be managed optimally and for diagnosing related challenges arising from bioleach heap operation. Studies were carried out at pH range $0.8 < pH < 2.0$. This experiment was carefully designed such that changes in pH were made about the established base case (pH 1.3) in order to minimize possible adaptation of the bacteria.

5.2 Methodology

Studies were carried out using 12 g L^{-1} total iron concentration at 42 °C, and the effect of pH was investigated by maintaining pH 0.8±0.05, 1.00±0.05, 1.30±0.05, 1.60±0.05 and 2.00±0.05 in the bioreactor. Refer to Chapter 3 for the detailed experimental method.

5.3 Results and Discussion

The bioreactors used for the experiments were maintained at 42 °C and steady state conditions were established at dilution rates between 0.018 and 0.075 h^{-1} (~13 – 56 hours residence time). At each steady state, ferrous-iron, oxygen and carbon dioxide utilization rates were determined by the off-gas analysis. The parity plot (Figure 5.1) shows that there is a good agreement between the off-gas data for computing the rate of ferrous-iron oxidation, $-r_{Fe^{2+}}$ (from degree of reduction balance equation, *i.e.* Equation 3.5) and the $-r_{Fe^{2+}}$ values obtained by performing material balance for ferrous-iron over the bioreactor for each dilution rate (*i.e.* Equation 3.23) at steady state[2]. This shows that the off-gas data is reasonably consistent within the limit of experimental errors incurred.

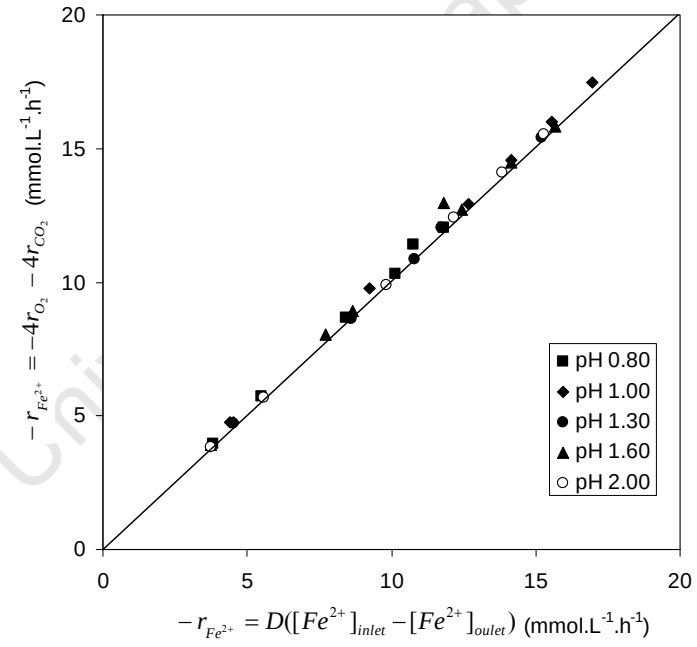

Figure 5.1 Parity plot comparing the off-gas data (Eq. 3.5) with experimental data obtained from (Eq. 3.23) for the effect of solution pH on microbial ferrous-iron oxidation

[2] For the construction of the parity plot, the total iron of the effluent stream at pH 1.6 and 2.0 included the precipitated iron. The data were not used for further analysis.

5.3.1 Iron balance

Figure 5.2(a) shows the iron balance of the bioreactor. This was determined by comparing the total iron concentration (dissolved) in the feed stream with that in the effluent, with the assumption that the difference represents the amount of iron lost due to precipitation. The figure shows that total iron in solution decreased, as the solution pH increases from 0.8 to 2.0. This implies that some of the iron in solution was lost due to precipitation of ferric-iron since most (*i.e.* more than 90%) of the iron was in ferric form. The amount of iron lost due to ferric precipitation increased from 0.3 to 12.6 % due to increase in solution pH from pH 0.8 to 2.0 as shown in Figure 5.2(b). As the solution pH increased beyond 1.3, cleaning of the bioreactor became a 48 hourly routine in order to reduce the interference on the experimental data. Figure 5.3 shows the pictures of ferric precipitate removed from the bioreactor maintained at pH 2.0 when it was shut down for cleaning. From the above discussion it can be inferred that ferric precipitation would have serious implications in a typical bioleach heaps by causing a diffusion barrier on the mineral surfaces.

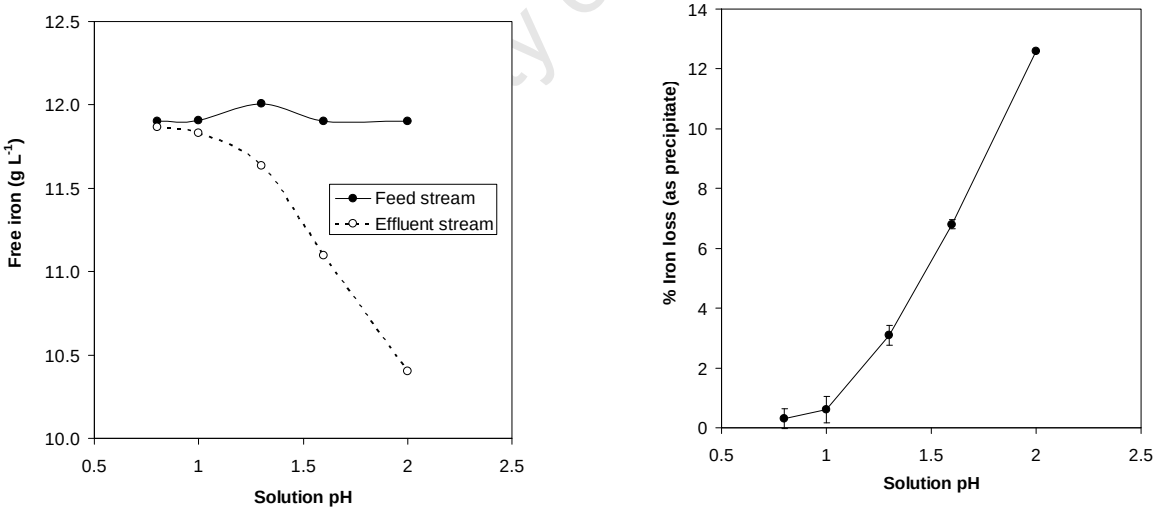

Figure 5.2 (a) Total iron balance (measured as free iron) in feed and effluent stream of the bioreactor, and (b) Percentage iron loss due to ferric precipitation as a function of solution pH at 42°C

Figure 5.3 (a) Ferric precipitate present in bioreactor operated at solution pH 2.0, (b) precipitate on the work bench during cleaning of the bioreactor

5.3.2 Biomass concentration versus pH

The biomass concentration C_x (*expressed in mole carbon per litre*) determined from the steady state value of the rate of carbon dioxide consumption, $-r_{CO_2}$ did not vary significantly over the range of dilution rates investigated (see Figure 5.4). A progressive but not significant increase in biomass was observed up to an intermediate dilution rate, (0.05 – 0.06 h^{-1}), where the highest biomass concentration was obtained. This trend has been previously supported by theory (see Figure 4.8 and Figure 4.9 in Section 4.3).

The intermediate dilution rate at which the highest biomass was observed is independent of the solution pH as the same dilution rate holds over the range of pHs investigated (see Figure 5.4). However, Figure 5.4 also shows that the biomass concentration decreased with a decrease in pH over the range investigated. Although from a previous study, C_X appeared not to be dependent on pH in the range 1.1 – 1.7 (Breed and Hansford, 1999a), a noticeable decrease in C_X with declining pH was observed when the pH of the bioreactor was at much lower values (pH 1.0 to 0.8) as shown in Figure 5.5. The declining C_X as pH tends to 0.80 is indicative of higher proton inhibition at this condition. Although pH gradient drives cell metabolism, higher gradient beyond optimum could impose stress on the microbial cell thus increasing homeostasis

maintenance since the microbial cytoplasm must be maintained closed to neutrality (Ingledew, 1982). This might explain the observed relatively higher maintenance coeffient (See Figure 5.7)

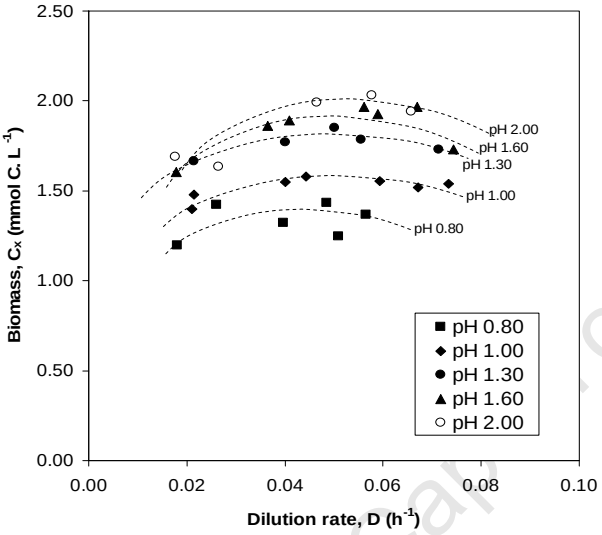

Figure 5.4 Variation of biomass concentration C_X with dilution rate for studies showing the effect of solution pH on microbial ferrous-iron oxidation. [the dotted lines indicate the trends of biomass with pH]

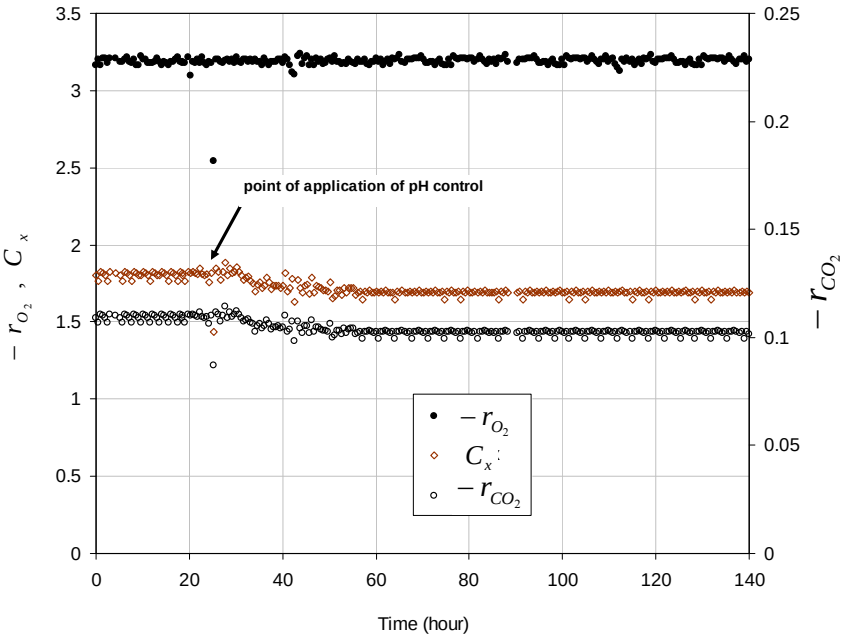

Figure 5.5 The effect of controlling solution pH of a chemostat previously at pH 1.00 to pH 0.80 at the same residence time, 16 hour, for studies on the effect of solution pH on microbial ferrous-iron oxidation.

5.3.3 Energetic parameters – *yield and maintenance coefficients*

Assuming that the energy derived from ferrous-iron oxidation is channelled to microbial growth and cell maintenance as described by the Pirt's Equation, the biomass yield, $Y_{SX}^{\max}$ and maintenance, m_S coefficient can be determined from the Pirt plots of Equation 4.1 as shown in Figure 5.6(a) and (b)

$$q_S = \frac{D}{Y_{SX}^{\max}} + m_S \qquad 4.1$$

The energetic parameters derived from Figures 5.6 show that the maintenance coefficient was minimum at pH 1.3, and it increased as the solution pH moves away from pH 1.3 as illustrated in Figure 5.7. However, the maximum biomass yields decreased with decreasing solution pH within the pH range investigated, as shown in Figure 5.7. This observation tends to support the earlier observed decrease in biomass concentration as proton concentration increased. The energetic parameters were shown to be valid and consistent when compared with the predicted value using the degree of reduction balance (Equation 3.10). These values are reported in Table 5.1

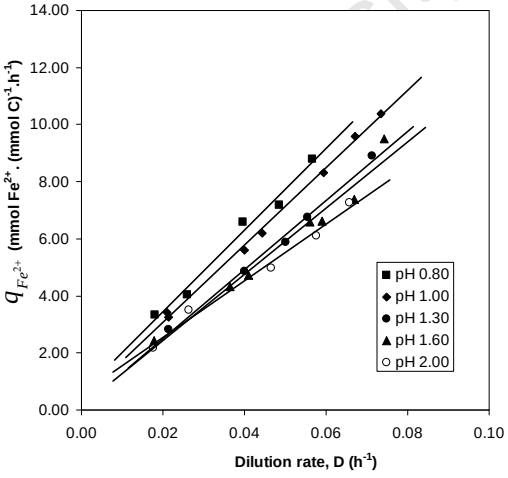

(a) Variation of specific microbial ferrous-iron oxidation rate with dilution rate, determined from the plot of Equation 3.11

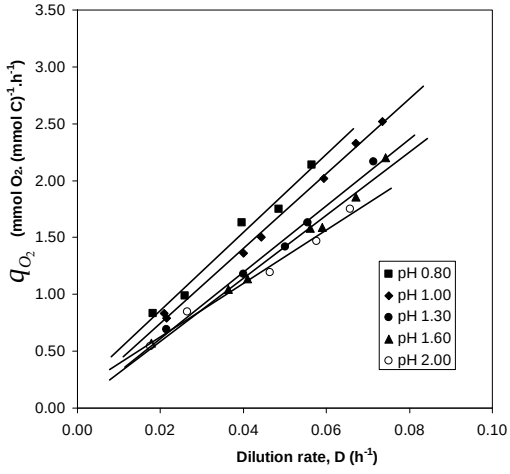

(b) Variation of specific microbial oxygen utilisation rate with dilution rate, determined from the plot of Equation 3.12

Figure 5.6 Variation of biomass activity with dilution rate for studies on the effect of solution pH on microbial ferrous-iron oxidation

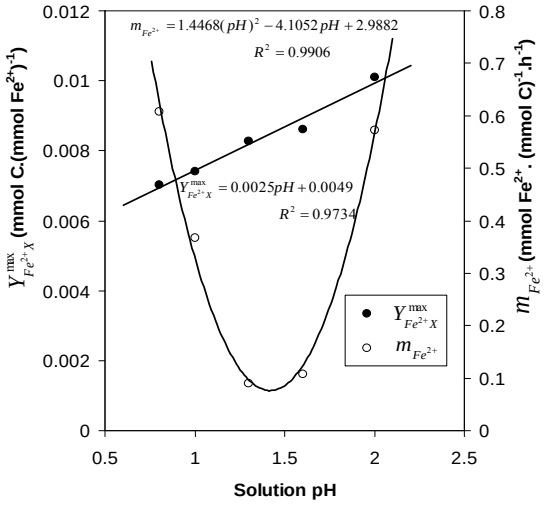

(a) Variation of maximum biomass yield and maintenance on ferrous-iron utilisation with solution pH

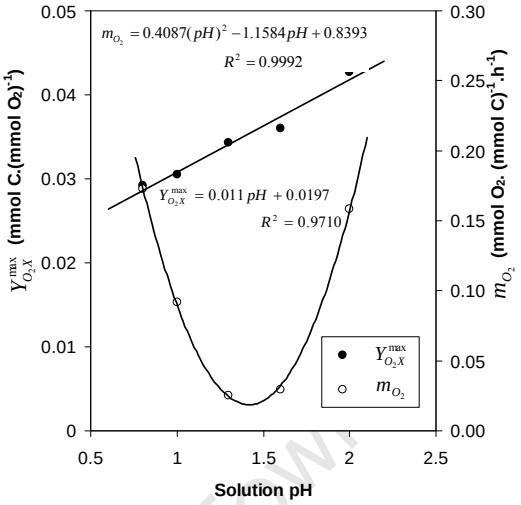

(b) Variation of maximum biomass yield and maintenance on oxygen utilisation with solution pH

Figure 5.7 Variation of biomass yield and maintenance coefficients with solution pH for studies on the effect of solution pH on microbial ferrous-iron oxidation

Table 5.1 The maximum biomass yield and maintenance coefficients, and maximum microbial growth rate at various solution pH investigated.

pH	$Y^{max}_{Fe^{2+}X}$	$m_{Fe^{2+}}$	R^2	$Y^{max}_{O_2X}$	m_{O_2}	R^2	μ^{max}	$Y^{max}_{O_2X}$ *Calculated from Equations 3.10*	m_{O_2} *Calculated from Equations 3.10*
0.8	0.0070	0.61	0.989	0.029	0.173	0.984	0.064	0.0289	0.152
1	0.0075	0.37	0.997	0.031	0.092	0.997	0.090	0.0305	0.092
1.3	0.0080	0.09	0.993	0.034	0.025	0.991	0.123	0.0343	0.023
1.6	0.0086	0.11	0.968	0.036	0.030	0.988	0.093	0.0357	0.027
2	0.0100	0.57	0.986	0.043	0.158	0.986	0.092	0.0422	0.143

Units: $Y^{max}_{Fe^{2+}X}$ [mol C (molFe^{2+})$^{-1}$], $m_{Fe^{2+}}$ [molFe^{2+} (molC h)$^{-1}$],
$Y^{max}_{O_2X}$ [mol C (molO$_2$)$^{-1}$], m_{O_2} [mol O$_2$ (molC h)$^{-1}$]

5.3.4 The Kinetic Parameters

The simplified ferric inhibition model is assumed to describe reasonably well the microbial ferrous-iron oxidation by *L. ferriphilum*. The maximum specific ferrous-iron, $q_{Fe^{2+}}^{max}$ and oxygen, $q_{O_2}^{max}$ utilization rates, and the corresponding apparent affinity constants, $K'_{Fe^{2+}}$ and K'_{O_2} were obtained from Lineweaver-Burk plot of Equations 3.15 and 3.16 as shown in Figure 5.8 (a) & (b). The parameters can also be determined from the fit of the experimental data using the Solver routine in Microsoft Excel, minimizing the sum of the squared errors (SSE) between the measured and predicted values of $q_{Fe^{2+}}$ (see Figure 5.9 a and b), as previously described in Section 4.3.2. The average values are shown in Table 5.2

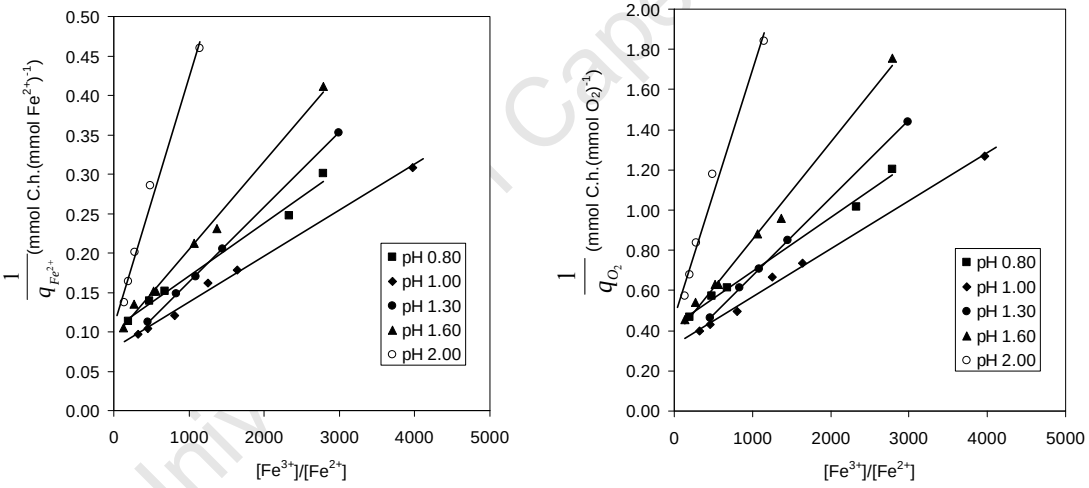

(a) Lineweaver-Burk plot for ferrous-iron oxidation at various solution pH investigated

(b) Lineweaver-Burk plot for oxygen utilisation at various solution pH investigated

Figure 5.8 Lineweaver-Burk plot of reciprocal of specific substrate utilisation versus ferric to ferrous irons for studies on the effect of solution pH on microbial ferrous-iron oxidation

The maximum specific utilization rate of ferrous-iron, $q_{Fe^{2+}}^{max}$, and oxygen, $q_{O_2}^{max}$, show an increasing trend as solution pH increase from pH 0.8 to 1.3, where it is maximum and further increase in pH resulted in a declining activity, this form of dependency can be fitted with a quadratic as shown in Figure 5.10 (a). The decreased rates at lower pH indicated that the cell was faced with the challenge of maintaining neutrality of the

cytoplasmic pH, while the reduction at increasing pH (from 1.3) could be explained by the lack of protons, which are essential component of the oxidation process. Solution pH around 1.3 seemed to be a comfortable zone for the cell where cell maintenance was minimum. On the other hand, the constants, $K'_{Fe^{2+}}$ and K'_{O_2} in the simplified product inhibition model show an increasing trend with an increase in solution pH, as shown in Figure 5.10 (b). The dependence of the apparent affinity constants $K_{Fe^{2+}}, K_{O_2}$ with solution pH can be represented by a linear function as illustrated in Figure 5.10.

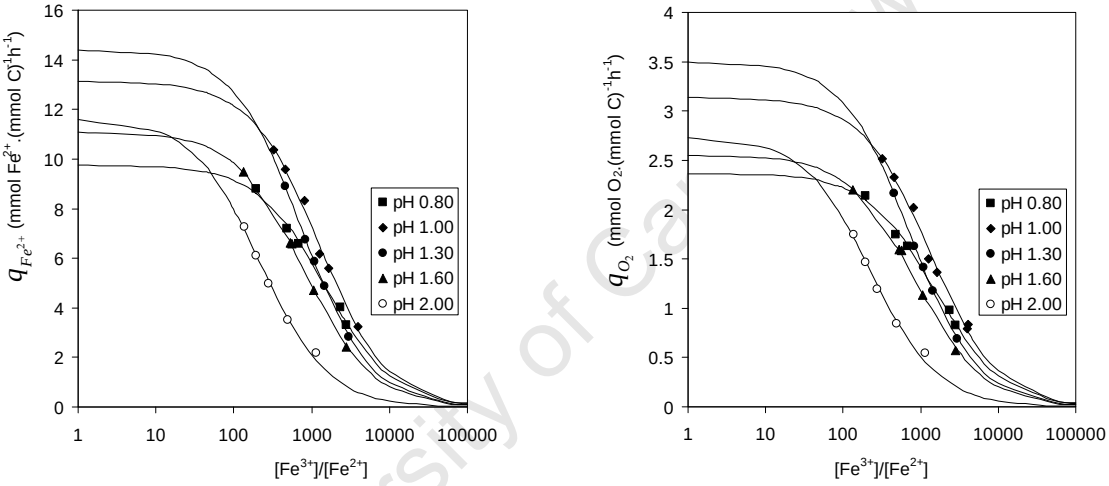

(a) Data used for determination of maximum microbial specific ferrous-iron oxidation rate, $q^{max}_{Fe^{2+}}$ and kinetic constants, $K_{Fe^{2+}}$

(b) Data used for determination of maximum microbial specific oxygen utilisation rate, $q^{max}_{O_2}$ and kinetic constants, K_{O_2}

Figure 5.9 The fit of experimentally determined specific ferrous-iron oxidation rate at different ferric-to-ferrous ratio to Equation 2.14 for determination of kinetic parameters

Although Breed and Hansford (1999a) reported that only the affinity constants are linearly dependent on pH while maximum biomass utilization rate remains constant and independent of pH. The authors investigation was carried out over a narrow pH range (pH 1.1 to 1.7). However, if the data point at pH 1.6 is ignored as shown in Figure 5.10a, it can be seen that maximum biomass activity changes by a small amount over the region investigated by Breed and Hansford (1999a).

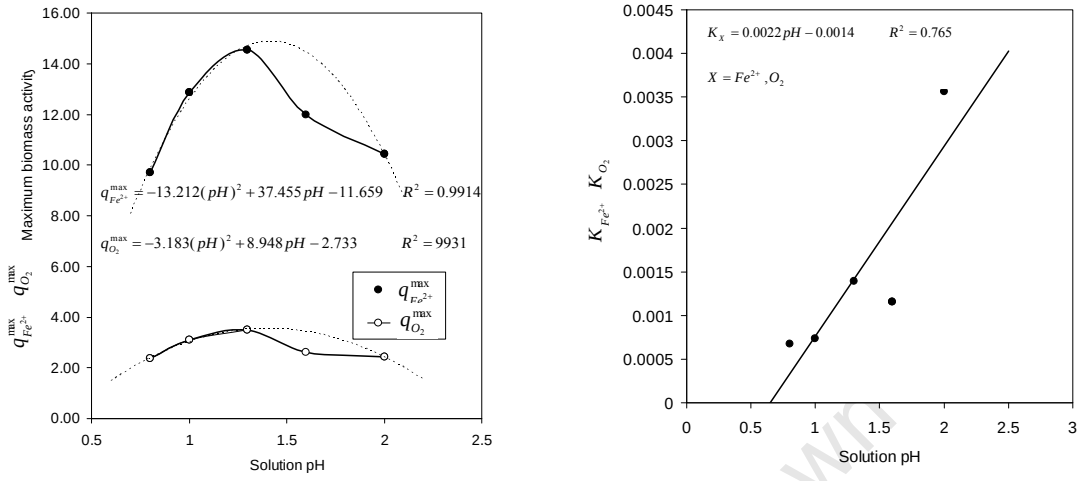

Figure 5.10 (a) Variation of maximum microbial activity and (b) kinetic constant with solution pH

The maximum specific growth rates at various pH studies were calculated from Equations 3.13 and 3.14 for both ferrous-iron and oxygen based parameters respectively. The average value is shown in Table 5.1. It should be noted that the maximum microbial growth rate is independent of the substrate, thus an average value was considered. The highest maximum growth rate was obtained at solution pH 1.3, this is similar to the result presented by Breed (2000) for *L. ferrooxidans* under similar conditions. Although, the washout was not monitored in this study, it was observed that the residence time beyond which washout was expected decreased with increasing solution pH, this observation is similar to the trend of the calculated maximum specific growth rate shown in Table 5.1. In theory, at washout dilution rate, the rate of cell growth is less than (*i.e.* cannot cope with) the feed dilution rate. This can be shown to be lesss than the maximum growth rate (Doran, 1995); Therefore, the cell would get to washout earlier than predicted by Equations 3.13 and 3.14.

Table 5.2 Ferrous-iron and oxygen based kinetic parameters at various solution pH investigated.

pH	Lineweaver-Burk method			Simplified ferric inhibition model			$q^{max}_{Fe^{2+}}$	$K'_{Fe^{2+}}$
	$q^{max}_{Fe^{2+}}$	$K'_{Fe^{2+}}$	R^2	$q^{max}_{Fe^{2+}}$	$K'_{Fe^{2+}}$	R^2	average	
0.80	9.66	0.00068	0.989	9.75	0.00067	0.993	9.71	0.00067
1.00	12.59	0.00076	0.986	13.14	0.00081	0.993	12.87	0.00078
1.30	14.66	0.00147	0.996	14.42	0.00135	1.000	14.54	0.00141
1.60	11.86	0.00109	1.000	11.14	0.00113	0.999	12.00	0.00111
2.00	9.20	0.00276	0.987	11.64	0.00457	0.992	10.42	0.00367
	$q^{max}_{O_2}$	K'_{O_2}	R^2	$q^{max}_{O_2}$	K'_{O_2}	R^2	$q^{max}_{O_2}$	K'_{O_2}
0.80	2.35	0.00070	0.993	2.37	0.0007	0.994	2.36	0.00068
1.00	3.05	0.00061	0.995	3.14	0.0008	0.989	3.09	0.00069
1.30	3.47	0.00139	1.000	3.51	0.0014	1.000	3.49	0.00137
1.60	2.69	0.00135	0.992	2.55	0.0011	0.997	2.62	0.00121
2.00	2.13	0.00255	0.982	2.74	0.0044	0.988	2.44	0.00346

Units: $q^{max}_{Fe^{2+}X}$ [molC.(molFe^{2+}.h)$^{-1}$], $q^{max}_{O_2X}$ [molC.(molO$_2$.h)$^{-1}$], $K'_{Fe^{2+}}$ & K'_{O_2} are dimensionless

5.4 Conclusion

The effect of pH on microbial ferrous-iron oxidation kinetics of *Leptospirillum ferriphilum* was studied in continuous stirred tank bioreactors at dilution rates ranging from 0.018 to 0.075 h^{-1} (*i.e.* 13 to 60 hour residence time). The temperature was maintained at 42 °C in all the experiments while the effect of solution pH was studied at pH 0.8, 1.0, 1.3, 1.6 and 2.0. The parity plot Figure 5.1 showed that the rate of ferrous-iron concentration can be determined accurately from the rates of microbial oxygen and carbon dioxide consumption using the degree of reduction balance.

Increase in solution pH resulted in an increase in iron loss due to ferric-iron precipitation. It was negligible at pH 0.8 while over 12% of iron was lost at pH 2.0, this condition is undesirable in a typical bioleach heap operation, as the usual marginal iron concentration needs to be kept in solution in order to sustain the leaching process. The microbial cell concentration increased with increasing solution pH. This is contrary to the previous result obtained by Breed *et al.*, (1999a) where no significant relationship

was observed between solution pH and biomass. The maximum biomass yield also showed the same trend as the biomass concentration. However, a minimum maintenance coefficient ($m_{Fe^{2+}}$ = 0.09) was observed at pH 1.3, this value is so small relative to $q^{max}_{Fe^{2+}X}$ that can be neglected, indicating and actively growing culture. It increased with both increase and decrease in pH from this reference. The maintenance requirement on ferrous-iron can be said to be equal at pH 0.8 and 2.0 within the limit of experimental error ($m_{Fe^{2+}}$ =0.6).

The maximum microbial specific substrate utilisation rate (based on both ferrous-iron and oxygen) and the corresponding kinetic constants are both dependent on pH, the biomass activity increased with increasing solution pH up to a maximum at pH 1.3, followed by a decreasing trend. This showed that the optimum microbial activity occurred at an approximate pH of 1.3, which also corresponds to a maximum specific microbial growth rate. The relationship between the biomass activities and solution pH can be described by a polynomial of order 2 with an optimum pH calculated to be at pH 1.4. The kinetic constants also showed a positive quadratic dependency on pH.

This result has implications on the operation of bioleach heaps; operating a bioleach heaps within pH 0.8 and 1.3 would conserve the low iron concentration associated with typical bioleach heaps. This challenge could be managed if the solution pH of below 1.00 could be used at start-up. Although, lower microbial activity on ferrous-iron was observed at pH below 1.30 (for example 9.20 mmol Fe^{2+}.(mmol C)$^{-1}$ h^{-1} at pH 0.8), it was only about 70% of the maximum activity achievable at pH 1.30. However, lowering the pH would have to be done with some caution, as this would also increase the reactivity of gangue minerals, resulting in their increased dissolution. This would increase the concentration of total dissolved salts in solution, which may result in detrimental solution ionic strength effects on microbial activity (Blight and Ralph, 2004; Shiers *et al.*, 2005). Therefore, periodic purging of the PLS would be necessary to remove undesired salts (cations and anions) once they reach a level where they may be toxic to the microbial community. The knowledge of the microbial tolerance limit of these salts is essential in this regard.

Chapter 6

The effect of dissolved cations on microbial ferrous-iron oxidation in a continuous culture

6.1 Introduction

High concentrations of dissolved salts from acid-leached gangue minerals is one of the key factors affecting microbial ferrous-iron oxidation (Blight and Ralph, 2004; Shiers *et al.*, 2005), which may affect the performance of bioleach heaps(Ojumu *et al.*, 2007). The salts create potentially adverse conditions for the microbial population and interfere with the microbial ferrous-iron oxidation. The principal mechanisms and dynamics of bioleaching are well understood (Rawlings, 2002), and have been discussed in Chapter 2. Nonetheless, in many heap bioleach operations to this day, rate and extent of metal recovery remains below what could be achieved in theory, and it is postulated that adverse solution conditions affect the microbial growth and activity with respect to ferrous-iron oxidation.

The reported composition of the pregnant leach solution (PLS) from a Chilean copper heap operation indicates very high concentrations, especially of Al and Mg (12.2 and 10.1 g/L respectively), predominantly as sulphates (Ojumu *et al.*, 2006; Petersen and Dixon, 2004). This condition is far from what would be considered an optimum in a typical tank bioleach system. Inhibitory concentrations of dissolved metals, especially heavy metals, on microbial growth and ferrous oxidation have been occasionally reported (Bruins *et al.*, 2000; Garcia and Silva, 1991; Nies, 1999; Nies and Silver, 1995; Tuovinen *et al.*, 1971;

Wang *et al.*, 2004), but emphasis had been mostly on arsenic with respect to its effect on microbial ferrous-iron oxidation kinetics (Harvey and Crundwell, 1997). The effect of high concentrations of Na sulphate on *Acidithiobacillus ferrooxidans* has been investigated (Blight and Ralph, 2004; Shiers *et al.*, 2005), indicating an immediate, five-fold decline in growth rate in a 40g/L Na_2SO_4 solution, and a 50% permanent retardation of growth rate at this concentration of Na_2SO_4. An adverse effect of Al concentrations exceeding 10 g/L on the growth of an unspecified ferrous iron oxidizer has been reported (Tuovinen *et al.*, 1971). Comparative testing of the column leaching of a chalcocite ore using a laboratory culture and a native culture in high salinity solution indicated severe retardation of leaching in the latter case (Petersen and Dixon, 2007c).

This present study investigates the effects of dissolved Al and Mg sulphates on microbial ferrous-iron oxidation kinetics of *Leptospirillum ferriphilum* in a continuous tank bioreactor with a view to providing understanding on how these effects could be effectively managed.

6.2 Methodology

These experiments were carried out in two sets, in identical reactors and running under identical operating condition (42 ºC and pH 1.3). The ferrous-iron substrate media were formulated as described in Table 3.1 in Section 3.2.5, to investigate the effects of dissolved Al and Mg on microbial ferrous-iron oxidation kinetics. The first set of experiments (run 1 to run 4, Table 3.1) studied the effects of individual cations and the second set, the composite cations (run 5 to run 10, Table 3.1). Ferrous-iron concentration of the bioreactor feed was determined by titration using potassium dichromate solution (see Appendix D for details of the procedure). Both the feed and reactor effluent samples were prepared with concentrated hydrochloric acid (to stabilise the ions) before sending for analysis of Al and Mg concentrations using AAS.

6.3 Result and Discussion

Off-gas data

The validity of the off-gas data was checked by comparing the rate of microbial ferrous-iron oxidation obtained via the degree-of-reduction balance (*i.e.* Equation 3.5) with that determined by performing a ferrous-iron mass balance on the chemostat (*i.e.* Equation 3.23). These were compared on a parity plot, Figure 6.1. The data show that there is at least good agreement between the two methods the lower rates, the noticeable outliers from the parity line could be attributed to the systematic error due to the equipment (gas analyzer), the data obtained seemed to be the best that could be obtained during this experiment. However, the data obtained using Equation 3.23 was used for further analysis with $-r_{Fe^{2+}}$.

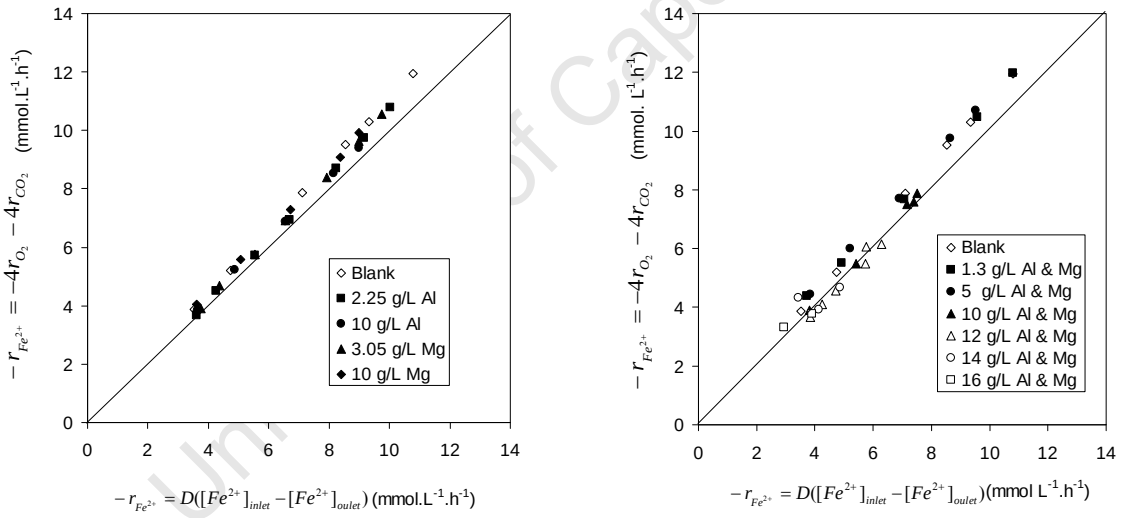

Figure 6.1 Comparison between $-r_{Fe^{2+}}$ determined via degree-of-reduction balance and from ferrous mass balance, (Equations 3.5 and 3.23) for study on effect of dissolved Al and Mg on microbial ferrous-iron oxidation at 42 ºC, pH 1.3 and at 5 g L^{-1} total iron concentration

6.3.1 Analysed Data – Reproducibility of data

Single experiments were repeated under identical conditions to the previous study in order to verify the reproducibility and consistency of the data. This was done only at 24 hours residence time for the study with the feed containing at 5 g L^{-1} Al and 5 g L^{-1} Mg (run 6 in Table 3.1), and 10 g L^{-1} Al and 10 g L^{-1} Mg (run 7 in Table 3.1).

The experiment was repeated about five months after the previous investigation. Figure 6.2 shows the data reproducibility obtained under the two identical conditions performed at different times. The data obtained at different times were reasonably the same within the limit of experimental error incurred as shown in Figure 6.2. This confirms that there was no variation or change in the microbial culture used for this study and that the experimental procedure is reliable, generating reproducible results.

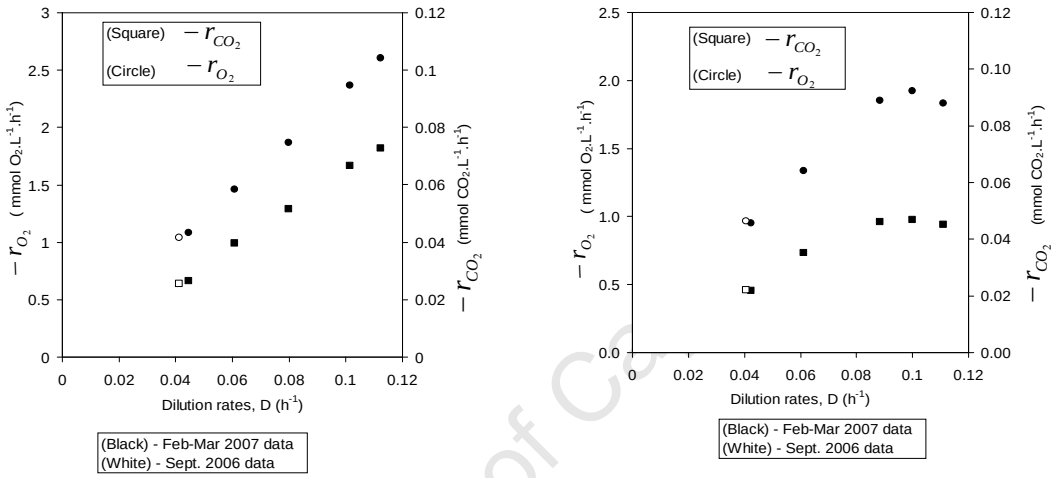

Figure 6.2 Data reproducibility plot for identical studies at different times for variation of $-r_{O_2}$ and $-r_{CO_2}$ with dilution rate (a) for feed containing 5 g. L^{-1} Al and 5 g. L^{-1} Mg, (b) for feed containing 10 g. L^{-1} Al and 10 g. L^{-1} Mg. (c) variation of $-r_{Fe^{2+}}$ with dilution rate for feed containing 5 g. L^{-1} Al and 5 g. L^{-1} Mg, and 10 g L-1 Al and 10 g. L^{-1} Mg for study on effect of dissolved Al and Mg on microbial ferrous-iron oxidation at 42 ºC, pH 1.3 and at 5 g. L^{-1} total iron concentration

6.3.2 The rate of microbial ferrous-iron oxidation, $-r_{Fe^{2+}}$

The rates of microbial ferrous-iron oxidation obtained from both sets of experiments are plotted against dilution rates as shown in Figure 6.3. The value of $-r_{Fe^{2+}}$ is the same when compared with blank solution, over the entire region of dilution rates investigated (Figure 6.3a) for the individual cation concentrations. However, these rates were obtained at decreasing ferric-to-ferrous ratios (or solution redox potentials) when compared with the blank experiment as shown in Figure 6.3b. This was due to the increased inhibition of the oxidation process due to added Al and Mg. Similarly for runs

with both Al and Mg concentration, the data show a decreasing trend in $-r_{Fe^{2+}}$ with increasing composite concentration of Al and Mg beyond 10 g L^{-1} (Figure 6.3 c & d), corresponding also to a d ecrease in the ferric-to-ferrous ratio in the bioreactor. The above results indicate a progressive increase in inhibition due to added salts (*i.e.* either or both Al & Mg), resulting to an increase in residual ferrous-iron concentration in the reactor as shown in Figure 6.4.

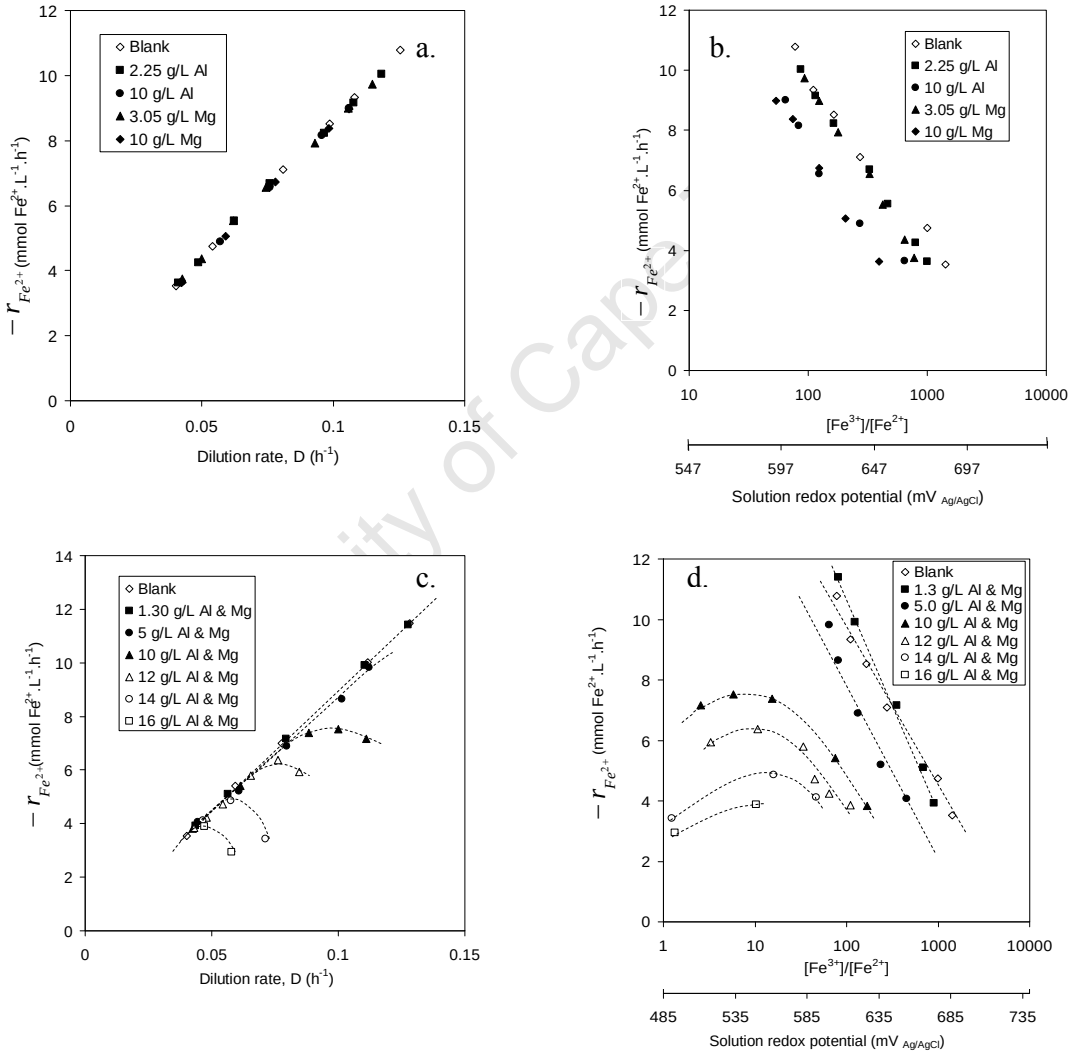

Figure 6.3 Variation of rate of microbial ferrous-iron oxidation $-r_{Fe^{2+}}$ with (a,c) dilution rate, (b,d) ferric-to-ferrous ratio/solution redox potential for study on effect of dissolved Al and Mg on microbial ferrous-iron oxidation at 42 ºC, pH 1.3 and at 5 g L^{-1} total iron concentration

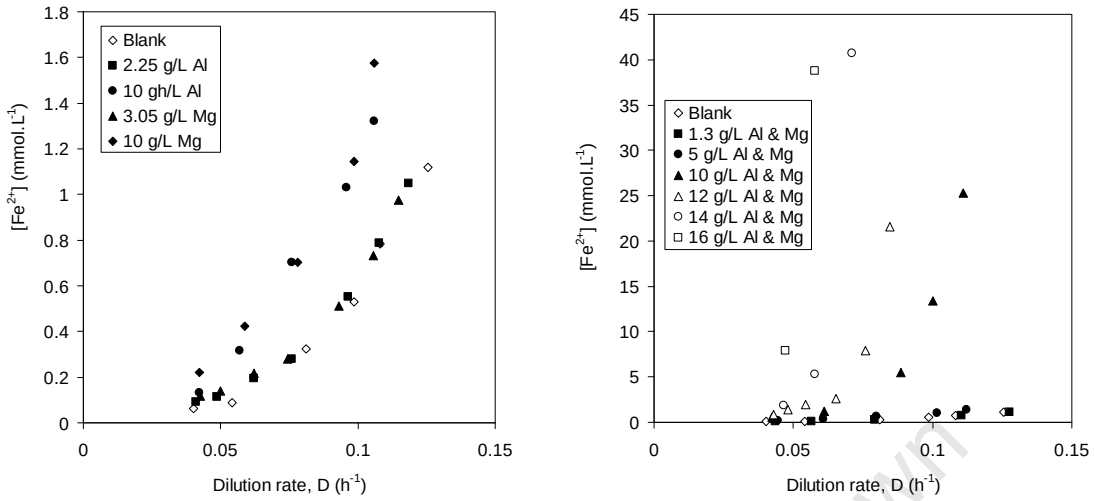

Figure 6.4 Variation of residual ferrous-iron oxidation [Fe^{2+}] with dilution rate (a) individual cation concentration (b) composite concentration, for study on effect of dissolved Al and Mg on microbial ferrous-iron oxidation at 42 ºC, pH 1.3 and at 5 g L^{-1} total total iron concentration

However, in all experiments with dissolved cation concentration of greater than 5 gL^{-1}, a crystalline precipitate was observed at upper part of the bioreactor as shown in Figure 6.5. It can be deduced from the analysis of the precipitate that the crystalline solid is possibly an individual complex of Al, Mg and Fe and not a ferric-iron complex of these cations as shown by the irregular distribution of iron in all the samples. In addition to the fact that Al and Mg are not suitable cation for jarosite formation, it can also be deduced from the results that iron loss due to ferric precipitation could only be through formation of K-jarosites and H-jarosite. The iron balance obtained was similar (between 0.5 – 3.5% iron loss due to precipitation) to what was observed in Chapter 5 at pH 1.3 when there were no added salts (see Appendix D, Table D1.1).

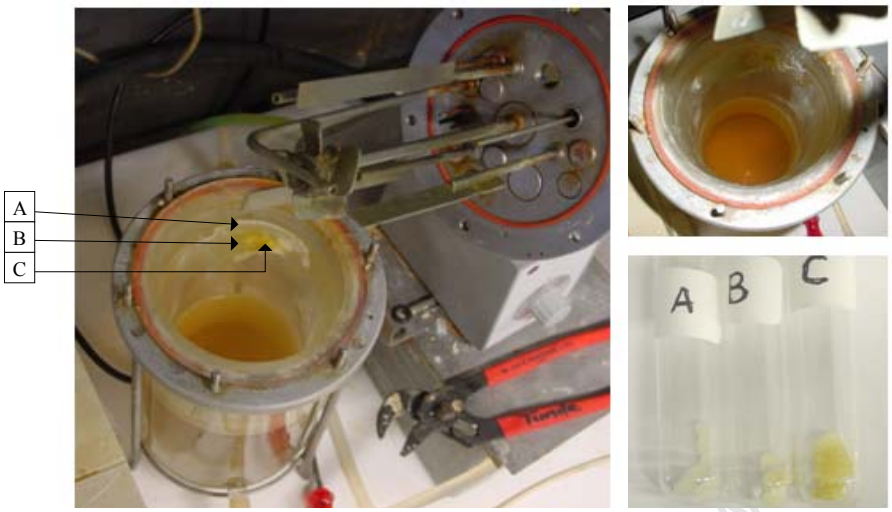

	Mass		
	A	B	C
Fe	0.54	0.91	1.38
Mg	0.35	1.42	2.08
Al	7.63	5.9	5.01
Total	8.52	8.23	8.47

Figure 6.5 Figure showing crystalline solid on the upper part of the bioreactor with the elemental analysis of sample taken at positions A, B & C (on dry weight basis) *i.e.* from different parts of the precipitate based on the intensity of the yellow colour imparted due to presence of ferric-iron.

6.3.3 Cell concentration

The steady state biomass concentration, C_X, measured in millimoles carbon assimilated per litre was determined from the rate of carbon dioxide utilisation as shown in Equation 3.24. In the runs with Mg and Al in individual concentrations, moderate concentrations of Mg tend to promote biomass growth as the biomass concentrations at 3.05 and 10 g/L were greater than in blank ferrous-iron solution as shown in Figure 6.6. On the other hand, Al is shown to be pernicious at all concentrations, leading to a decrease in the cell concentrations. However, biomass concentration decreased dramatically with increasing cation concentration above 10 g/L, thereby confirming the observed decrease in $-r_{Fe^{2+}}$ (see Figure 6.3) and the corresponding increase in the residual ferrous-iron concentration shown in Figure 6.4.

The observed increase in biomass concentration due to moderate increase in dissolved Mg (Figure 6.6a) can be explained with the fact that magnesium is one of the essential metals for physiological function of the cell, it is needed for stabilizing various enzymes and DNA through electrostatic forces, like zinc (Bruins *et al.*, 2000; Nies, 1999; Nies and Silver, 1995). On the other hand, Al belongs to the non-essential metals of no biological importance, its toxicity is through displacement of essential metals from active protein sites. Non-essential metals are known to form stronger bonds with protein than the essentials, thus are easily displaced (Bruins *et al.*, 2000). However, it can be inferred from Figure 6.6, that Mg seemed to cushioning the inhibitory effect of Al at concentration below 10 g L^{-1} when both cations were combined (Figure 6.6b).

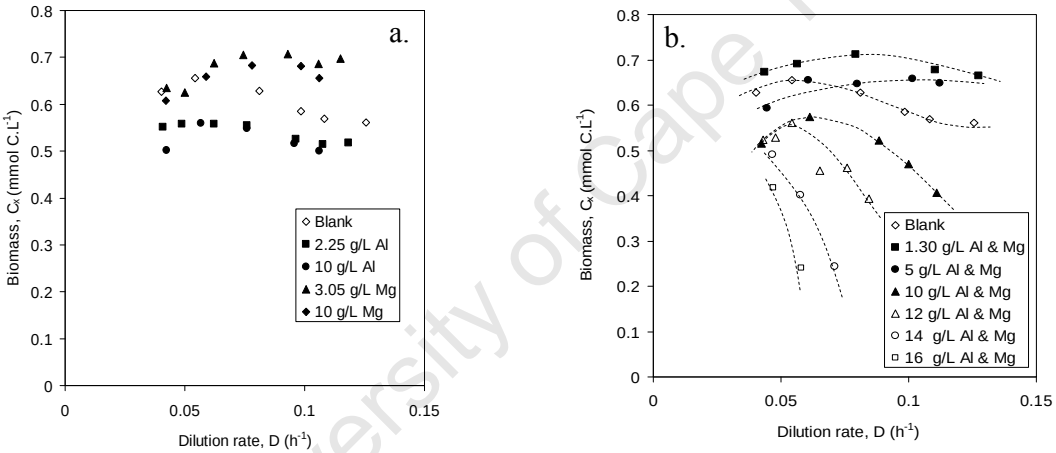

Figure 6.6 Variation of biomass concentration with dilution rate (a) individual cation concentration (b) composite concentration, for study on effect of dissolved Al and Mg on microbial ferrous-iron oxidation at 42 ºC, pH 1.3 and at 5 g L^{-1} total iron concentration

6.3.4 Specific substrate utilisation rates

Using the simplified ferric inhibition model (Equation 3.15 and 3.16) to describe the effect of dissolved cations on microbial ferrous-iron oxidation by *L. ferriphilum*. The kinetic parameters viz: the maximum specific substrate utilisation rates, $q_{Fe^{2+}}^{\max}$ and $q_{O_2}^{\max}$, and the corresponding kinetic constant, $K'_{Fe^{2+}}$ and K'_{O_2} were obtained from (1) the least squared error calculation, using the Solver routine in Microsoft Excel, minimizing the sum of the squared errors (SSE) between the measured and predicted values of $q_{Fe^{2+}}$ and q_{O_2} as shown in Figure 6.7 and Figure 6.8 for both sets of experiments, and (2) the

Lineweaver-Burk plot of Equations 3.15 and 3.16 (see Figure 6.9 and Figure 6.10) as described previously.

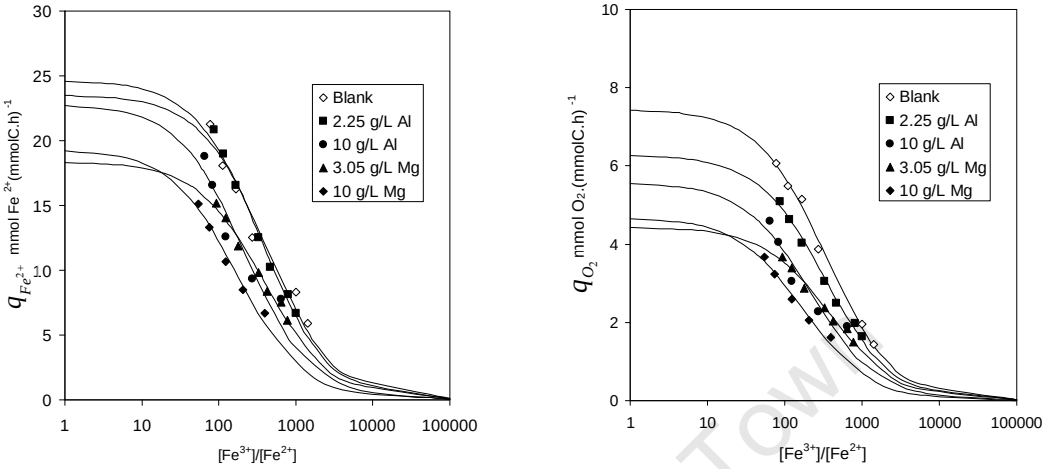

Figure 6.7 Variation of specific substrate utilisation rate with ferric-to-ferrous ratio and the fit of Equations to the corresponding data by minimising the sum of square errors between the predicted and measure values for study on effect of individual ions of individual ions of Al and Mg on microbial ferrous-iron oxidation at 42 ºC, pH 1.3 and at 5 g L^{-1} total iron concentration

The error in Lineweaver-Burk is larger due to the scattered plot and the fewer data obtained at higher dissolved ions, the kinetic parameters obtained from the fit to the corresponding Equations are shown in Table 6.1. The lines in Figure 6.7 and Figure 6.8 represent the plot of Equations 3.15 and 3.16 fitted with these parameters.

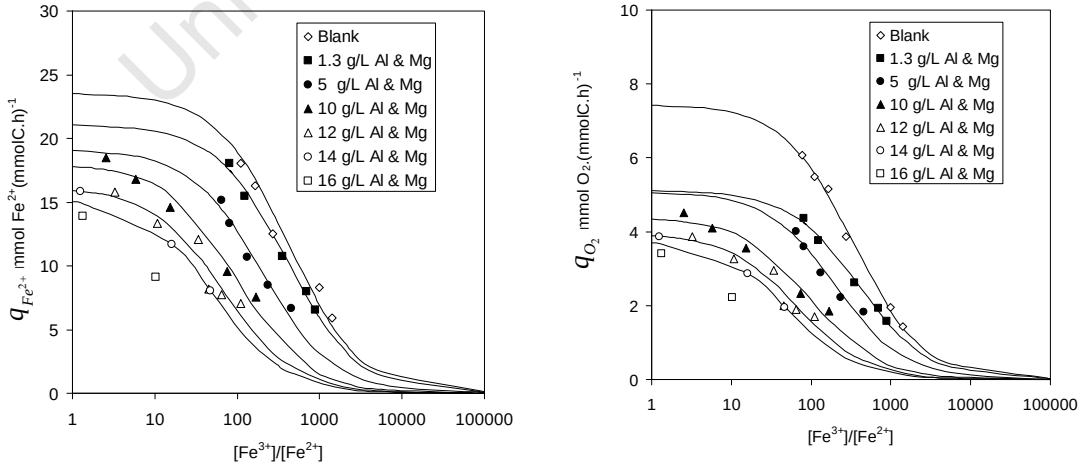

Figure 6.8 Variation of specific substrate utilisation rate with ferric-to-ferrous ratio and the fit of Equations to the corresponding data by minimising the sum of square errors between the predicted

and measure values for study on effect of dissolved mixture of Al and Mg on microbial ferrous-iron oxidation at 42 ºC, pH 1.3 and at 5 g L-1 total iron concentrati

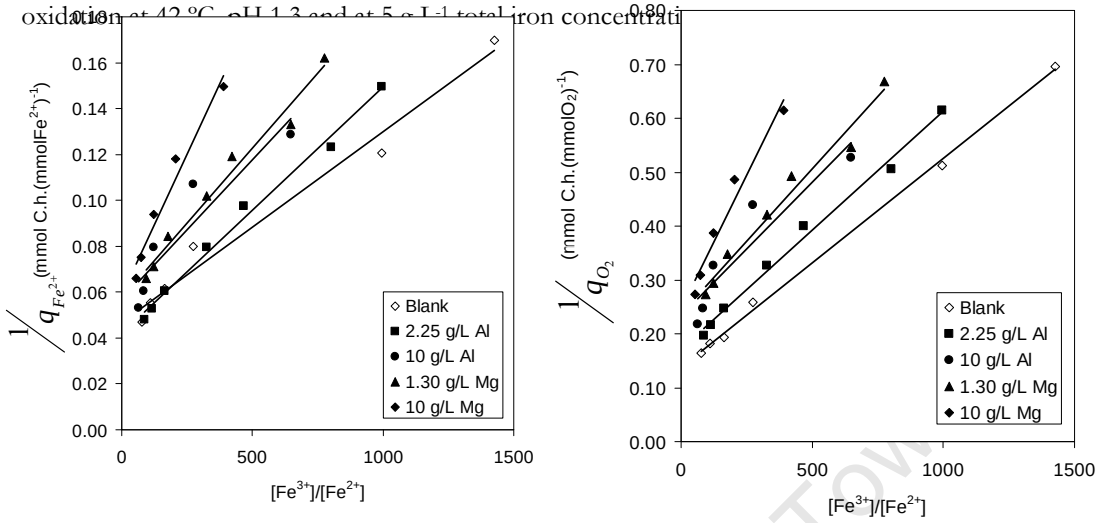

Figure 6.9 Lineweaver-Burk plot of (a) Equation 3.15 and (b) Equation 3.16 using the data obtained from the study of effect of individual ions of dissolved Al and Mg microbial ferrous-iron oxidation at 42 ºC, pH 1.3 and at 5 g L^{-1} total iron concentration

From the data in Figures 6.7 and 6.8, the increase in concentration of either Mg or Al or both ions not only depresses the specific rate of ferrous-iron oxidation, it also shifts the curve increasingly to the left, i.e. the range of ferric to ferrous iron ratios in which oxidation proceeds at reasonable rates becomes lower and lower.

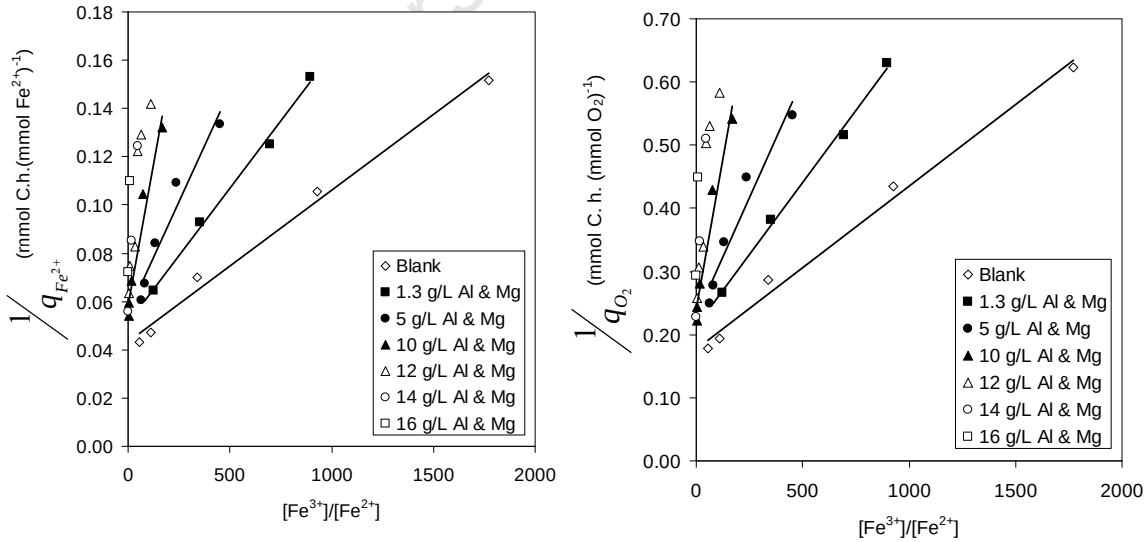

Figure 6.10 Lineweaver-Burk plots of (a) Equation 2.14 and (b) Equation 2.15 using the data obtained from the study of effect of dissolved Al and Mg mixture on microbial ferrous-iron oxidation at 42 ºC, pH 1.3 and at 5 g L-1 total iron concentration

The same trend was observed for $-r_{Fe^{2+}}$ as discussed previously in section 6.3.2. The results also show an increasing trend in the value of $K'_{Fe^{2+}}$ with increase in the concentration of the dissolved ions. These effects can be explained primarily by the effect increasing ionic strength (0 – 1.3 mol/L) due to the dissolved ions in the feed solution. The ionic strength tends to impose an energy load on microbial cell due to the osmotic gradient that exists between the interior and exterior of the cell (Blight and Ralph, 2004), it could also have an effect on iron speciation in solution as is analyzed in Section 8.2.3. The ionic strength of the bioreactor feed shown in Table 6.1 was calculated using Visual MINTEQ at an average room temperature of 25°C in the computation. It appears that the maximum specific ferrous-iron oxidation rate decreased linearly with increase in ionic strength while the $K'_{Fe^{2+}}$ values (*i.e.* the affinity constant) increased exponentially with increasing ionic strength as shown in Figure 6.11

Table 6.1 Kinetic parameters based on ferrous-iron and oxygen, obtained by fitting experimental data to Equation 3.15 and 3.16

Experiment	Ferrous-iron based substrate			Oxygen based substrate			Ionic strength	μ^{max}
	$q^{max}_{Fe^{2+}}$	$K'_{Fe^{2+}}$	R^2	$q^{max}_{O_2}$	K_{O_2}	R^2		
Blank	23.55	0.0024	0.959	7.44	0.0030	0.995	0.22	0.13
2.25 g/L Al	24.68	0.0028	0.990	6.28	0.0031	0.998	0.34	0.139
10 g/L Al	22.82	0.0046	0.896	5.57	0.0046	0.894	0.42	0.15
3.05 g/L Mg	18.35	0.0026	0.982	4.43	0.0026	0.999	0.77	0.13
10 g/L Mg	19.35	0.0058	0.975	4.68	0.0058	0.974	0.71	0.14
1.3 g/L Al & Mg	21.11	0.0026	0.991	5.12	0.0026	0.991	0.36	0.15
5.0 g/L Al & Mg	19.14	0.0050	0.961	5.08	0.0049	0.961	0.67	0.143
10 g/L Al & Mg	17.98	0.0104	0.966	4.38	0.0104	0.965	0.99	0.11
12 g/L Al & Mg	16.16	0.0149	0.908	3.96	0.0151	0.907	1.10	0.08
14 g/L Al & Mg	15.35	0.0194	1.000	3.77	0.0198	1.000	1.21	0.07
16 g/L Al & Mg*	15.03	0.0630	1.000	3.70	0.0639	1.000	1.32	0.05

Units: $q^{max}_{Fe^{2+}X}$ [mol Fe^{2+} (mol C h)$^{-1}$], $q^{max}_{O_2X}$ [mol O_2 (molC h)$^{-1}$], $K_{Fe^{2+}}$ & K_{O_2} are dimensionless

* Subject to huge error due to insufficient data

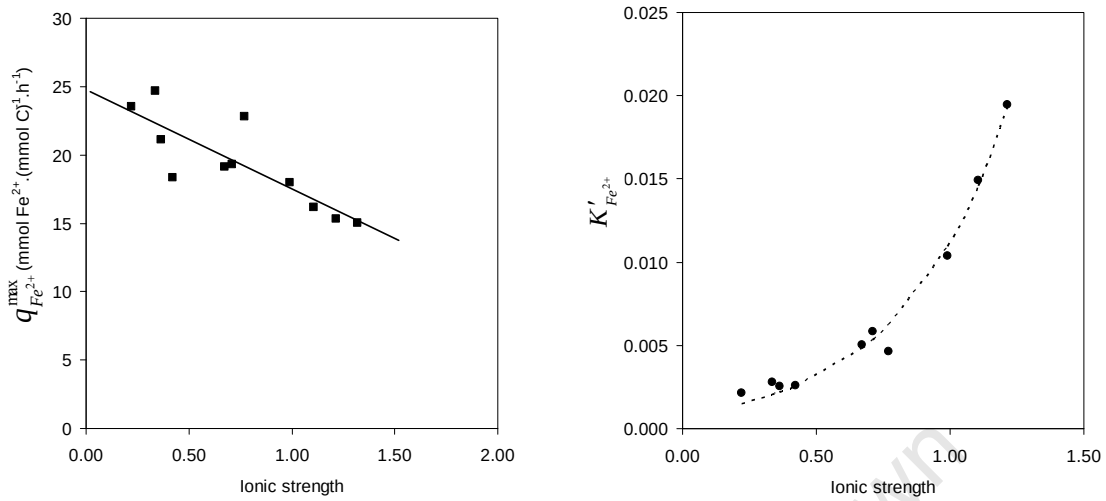

Figure 6.11 Variation of (a) maximum specific ferrous-iron oxidation rate, (b) the kinetic constant, $K'_{Fe^{2+}}$ with solution ionic strength for the study of effect of dissolved Al and Mg mixture on microbial ferrous-iron oxidation at 42 ºC, pH 1.3 and at 5 g L^{-1} total iron concentration

6.3.5 Energetic parameters

The maximum yield on substrates, $Y^{max}_{Fe^{2+}X}$ and $Y^{max}_{O_2X}$, and the corresponding maintenance coefficients, $m_{Fe^{2+}}$ and m_{O_2},were determined from the Pirt's Equation, which is based on the assumption that the energy derived from ferrous-iron oxidation is channeled to microbial growth and cell maintenance as described previously in Chapter 3. From the Pirt plots (Figure 6.12 and Figure 6.13), Mg ion at moderate concentration increased the maximum microbial yield when compared with blank ferrous solution which supported the increased cell mass observed in Figure 6.5a while for the case of Al at moderate concentrations, the observed yield did not differ from the blank experiment (*i.e.* without added salt). This may suggest that the observed decrease in cell concentration may not be significant. The values of the parameters obtained from the figures are presented in Table 6.2.

However, in general, it can be seen that $Y^{max}_{Fe^{2+}X}$ decreased significantly at increasing concentrations of the Al and/or Mg (commensurate with increasing ionic strength), especially above an ionic strength around 1 M as shown in Table 6.2 and Figure 6.14. The solution ionic strength was calculated using Visual MINTEQ™ at 25°C. Sufficient data could not be obtained at higher concentrations (especially 16 g L^{-1} Al and Mg) due to

severe impairment of oxidation because of inhibition, and this put an uncertainty in the confidence of result obtained at these conditions. It has been shown in preceding chapters (4 & 5) that the maintenance coefficient of *L. ferriphilum* is small under normal operating conditions, and difficult to determine with any degree of accuracy. The runs at very high cation concentrations suggest large negative values for $m_{Fe^{2+}}$ (Table 6.2), which makes no sense. However, considering that these runs also showed a levelling-off of reaction rates at higher dilution rates (Figure 6.3b), it is reasonable to assume that for these runs the behaviour of $q_{Fe^{2+}}$ does not follow a linear trend over the entire range of dilution rates and that therefore Pirt equation no longer holds.

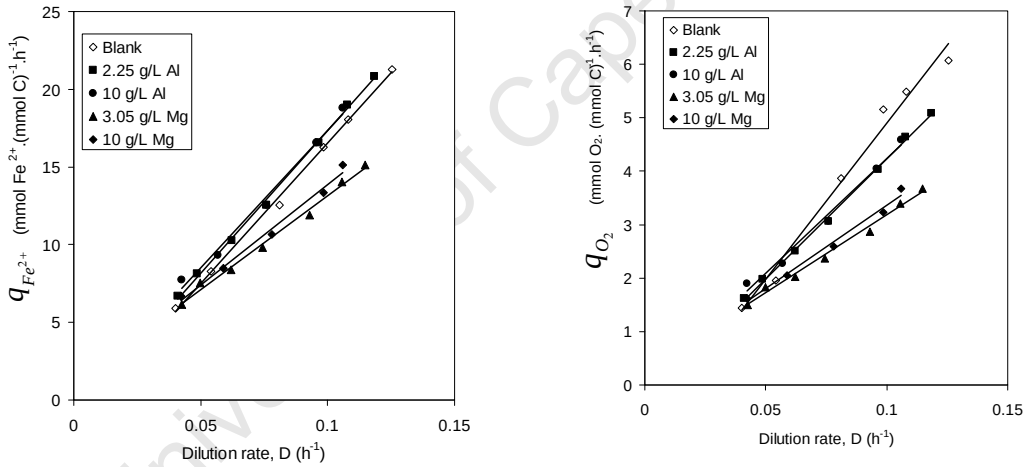

Figure 6.12 Lineweaver-Burk plots of (a) Equation 3.15 and (b) Equation 3.16 using the data obtained from the study of effect of dissolved Al and Mg mixture on microbial ferrous-iron oxidation at 42 ºC, pH 1.3 and at 5 g L^{-1} total iron concentration

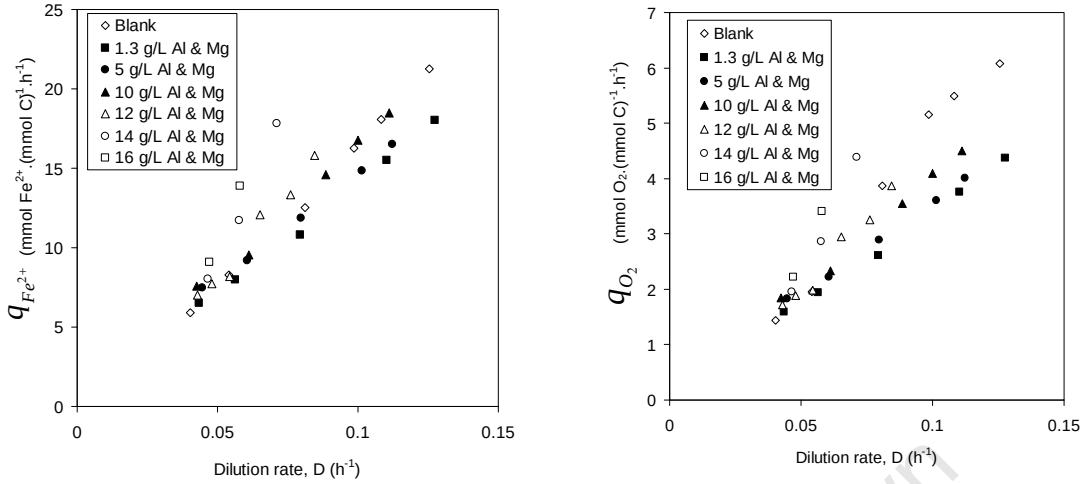

Figure 6.13 Lineweaver-Burk plots of (a) Equation 3.15 and (b) Equation 3.16 using the data obtained from the study of effect of dissolved Al and Mg mixture on microbial ferrous-iron oxidation at 42 ºC, pH 1.3 and at 5 g L^{-1} total iron concentration

Table 6.2 Maximum yield and maintenance parameters based on ferrous-iron and oxygen, obtained by from Pirt's plot (Figure 6.12 and Figure 6.13)

	$Y^{max}_{Fe^{2+}X}$	$m_{Fe^{2+}}$	R^2	Ionic strength	$Y^{max}_{O_2X}$	m_{O_2}	R^2
Blank	0.0055	-1.58	0.998	0.22	0.017	-0.96	0.984
2.25 Al	0.0055	-0.99	0.998	0.34	0.022	-0.25	0.998
10 Al	0.0057	-0.27	0.990	0.77	0.023	-0.07	0.989
3.05 Mg	0.0083	1.06	0.992	0.42	0.034	0.27	0.992
10 Mg	0.0078	1.00	0.989	0.71	0.032	0.25	0.988
1.3 g/L Al & Mg	0.0072	0.25	0.997	0.36	0.030	0.06	0.997
5 g/L Al & Mg	0.0074	1.26	0.997	0.67	0.031	0.31	0.997
10 g/L Al & Mg	0.0061	1.12	0.992	0.99	0.025	0.28	0.992
12 g/L Al & Mg	0.0047	-2.60	0.974	1.10	0.019	-0.66	0.973
14 g/L Al & Mg	0.0025	-10.88	0.993	1.21	0.010	-2.72	0.993
16 g/L Al & Mg	0.0023	-11.59	1.000	1.32	0.009	-2.90	1.000

Units: $Y^{max}_{Fe^{2+}X}$ [mol C (mol Fe^{2+})$^{-1}$], $m_{Fe^{2+}}$ [mol Fe^{2+} (molC h)$^{-1}$],
$Y^{max}_{O_2X}$ [mol C (mol O_2)$^{-1}$], m_{O_2} [molO_2 (mol C h)$^{-1}$]

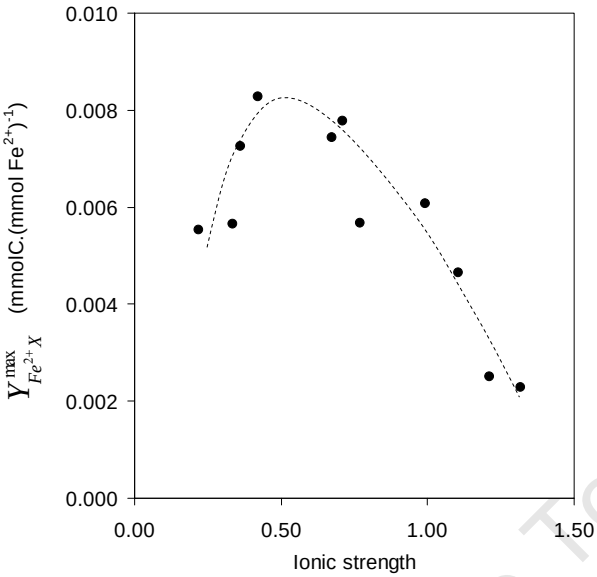

Figure 6.14 The effect of solution ionic strength on maximum yield on ferrous-iron from the study of effect of dissolved Al and Mg mixture on microbial ferrous-iron oxidation at 42 ºC, pH 1.3 and at 5 g L^{-1} total iron concentration

6.3.6 Specific microbial growth rate

The values of the maximum specific growth rate, μ_{max} cannot be determined accurately from Equation 3.13 due to the fact that maintenance coefficient is small and cannot be obtained with confidence. However, μ_{max} were determined from a μ-based form of Equation 3.15, by regression, minimising the sum of squares between the predicted and experimental values.

$$\mu = \mu^{max} \frac{1}{1 + K\frac{[Fe^{3+}]}{[Fe^{2+}]}} \qquad 6.1$$

The values of μ_{max} obtained (see Table 6.1) suggest that the oxidation is competitively inhibited: the μ_{max} is constant for the effect of the individual cations, and for the mixture up to 10 g L^{-1} of composite ions, and the decrease at higher concentration might be attributed to complete inhibition.

Although the dilution rate at which washout occurred was not monitored throughout the experiment, the data suggests that washout will occur at dilution rates less than 0.14 h^{-1}, which was the average for most of the experiments. However, at higher concentrations

of dissolved ions, the washouts are expected to occur at lower values. This might be due to the fact that the cells were severely inhibited at these concentrations, precluding acquisition of data within the dilution rate region that are technically feasible in the laboratory.

6.4 Summary

The effect of dissolved cations (*i.e.* Al^{3+} and Mg^{2+}) on microbial ferrous-iron oxidation was investigated in a continuous tank bioreactor. Total iron concentration of 5 g L^{-1} was used in the growth medium while the oxidation kinetics was monitored at dilution rates ranging between 0.04 and 0.13 h^{-1} (*i.e.* 7.5 to 25 hour residence time). The operating conditions were maintained at 42 °C and pH 1.3 for all the experiments. The rate of microbial ferrous-iron oxidation was accurately measured from the rates of oxygen and carbon dioxide consumption via the degree of reduction balance.

While aluminium ion at all concentrations decreased the biomass concentration, magnesium, at moderate concentration promoted biomass accumulation over and above blank growth medium (*i.e.* without any ion). This contrast trend is explained with the fact that Mg^{2+} is essential for some physiological functions in bacterial cells. Al^{3+} has no biological functions, it is a non-essential metal known to be toxic. However, at higher concentration both cations resulted in a significant reduction in cell concentration, as the cells are severely inhibited and washed out, leaving only the fewer resilient cells.

Although the overall rate of microbial ferrous-iron oxidation with dilution rate remained unaffected by dissolution of moderate concentrations of either or both Al^{3+} and Mg^{2+} up to 10 g L^{-1}, the corresponding solution redox potential (a proxy measure of ferric-to-ferrous ratio) decreased significantly with increasing concentration of either or both ions. The rates progressively decreased with higher ion concentrations, with a corresponding decrease in the ferric-to-ferrous ratio. The resulting ionic strength increased from 0.22 M (for blank solution) to 1.3 M (due to added salts). The results showed that ionic strength has a strong negative effect on microbial ferrous-iron oxidation as previously shown by Blight and Ralph (2004).

Not only is the specific ferrous-iron oxidation rate (*i.e.* rate of oxidation per cell) depressed by increasing in the solution ionic strength due to added salts, the rate also occurred at lower solution redox potential. However, the maximum specific growth rate appeared to be reasonably constant 0.13 to 0.15 h^{-1} (except at 12, 14 and 16 g L^{-1} of added Al^{3+} and Mg^{2+}) while the affinity constant in the simplified inhibition model $K'_{Fe^{2+}}$ indicated a competitive inhibitory effect within this window, other authors have reported a non-competitive inhibition for the effect of dissolved heavy metals (Cabrera *et al.*, 2005b).

The maximum biomass yield followed the same trend as the cell concentration, dissolved Mg promoting the yield at moderate concentration, while significant decrease occur with increasing dissolved ions. Unfortunately the maintenance coefficient, cannot be determined with any accuracy, it is increasingly negative which is not meaningful and might suggest that Pirt equation no longer holds. The foregoing analysis shows that salts liberated from gangue dissolution in heap bioleaching and accumulated in the re-circulated solution have an increasingly adverse effect on ferrous iron bio-oxidation kinetics as concentrations increase. Therefore *Leptospirillum ferriphilum* is likely to under-perform in a heap environment which contains high concentrations of dissolved gangue minerals, as does occur in some operations. Although at least some bacterial growth could be maintained even in solutions with an ionic strength as high as 1.3 M, growth rates are severely reduced. This would likely result in much retarded colonisation of heaps. The reduced yield would suggest increased ferrous iron utilisation at high ionic strengths, but this is offset by the much lower growth rate, resulting overall in lower oxidation rates and hence bioleaching activity.

Chapter 7

The effect of total iron concentration on microbial ferrous-iron oxidation in a continuous culture

7.1 Introduction

The kinetics of microbial ferrous-iron oxidation has been widely studied for the past three decades, mostly in tank systems, and mostly focused on *Acidithiobacillus ferrooxidans* bacteria (Boon *et al.*, 1999a; Boon *et al.*, 1999b; Jones and Kelly, 1983; Kupka *et al.*, 2007; Lacey and Lawson, 1970), and more recently on *Leptospirillum* species (Breed *et al.*, 1999; Breed and Hansford, 1999a; Özkaya *et al.*, 2007b; Sundkvist *et al.*, 2007). Several authors have used different experimental systems (ranging from continuous cultures, batch cultures, initial rate and electrochemical measurements), and various rate equations describing the microbial ferrous-iron oxidation kinetics have been proposed (for review see Ojumu *et al.*, 2006; Searby, 2006).

The effects of ferrous-iron and ferric-iron concentration on the microbial oxidation rates have been widely studied. While some authors studied these effects by direct measurement of the iron species (Özkaya *et al.*, 2007b) especially in the case of *At. ferrooxidans* (Cabrera *et al.*, 2005b; Jones and Kelly, 1983; Kupka *et al.*, 2007; Lacey and Lawson, 1970; MacDonald and Clark, 1970), others have used redox potential as a proxy measure for these species, especially for *Leptospirillum* cultures where the ferrous-iron concentration is usually too small to be measured directly (Boon *et al.*, 1999a; Boon *et al.*, 1999b; Breed *et al.*, 1999; Breed and Hansford, 1999a; Meruane *et al.*, 2002).

However, in all of the above work, studies were mostly carried out at a fixed total iron concentration (Boon *et al.*, 1999a; Breed *et al.*, 1999; Breed and Hansford, 1999a; Sundkvist *et al.*, 2007), and when varied, usually in the excess of 10 g L^{-1}. Elevated levels of total iron concentration are relevant to tank bioleaching (usually resulting from the dissolution of pyrite ore, to sustain the leaching process). Now that bioleaching has been extended to heap leaching, primarily due to its applicability to marginal ore at considerably lower cost when compared to tank processes, research interest has turned to conditions relevant here. In bioleach heaps, solution conditions are substantially different from those commonly found in tank bioleaching, with total iron concentration usually less than 5 g L^{-1}. It is yet unexplored whether the kinetics of microbial ferrous-iron oxidation obtained under these conditions can be directly applied to heap situation characterised by considerable lower total iron.

There are few studies on the effect of iron concentration on microbial ferrous-iron oxidation. In Boon *et al.* (1999a) the effect total iron concentration was not clearly reported, the authors measured maximum specific oxygen utilisation rate, $q_{O_2}^{\max}$ using the Biological Oxygen Monitor (BOM), and reported that the rate was dependent on dilution rate. Sundkvist (2007) only very recently reported that kinetics and the yield parameter would change with solution composition. In the thermophilic ferrous-iron oxidation study by Searby (2006), the author reported a decrease in both cell biomass concentration and the rate of microbial ferrous-iron oxidation with decreasing total iron concentration. Further, the author reported a decreasing specific rate and increasing biomass yield with decreasing total iron. However, thermophilic culture may behave different from a mesophile. The aim of this study is to investigate the kinetics of microbial growth and ferrous-iron oxidation of *Leptospirillum ferriphilum,* at feed total iron concentrations ranging from 2 to 12 g L^{-1}, typical of both tank and heap environments. The study is intended to provide further understanding, in addition to the total iron effect, on the inhibitory effect (if any) of ferric or ferrous-iron, as previously reported in Ojumu *et al.*(2006) on microbial growth kinetics and ferrous-iron oxidation, and an insight into the development of a suitable rate equation under such conditions.

7.2 Methodology

Experiments were carried out in four identical reactors. Each bioreactor was run at 42 ºC and pH 1.3. Microbial oxidation kinetics of ferrous-iron were carried out by varying the concentration of total iron concentration (measured as total iron in corresponding g L^{-1} of $FeSO_4.7H_2O$), and bioreactors were operated at 2 ± 0.08, 3 ± 0.01, 5 ± 0.10, 8 ± 0.14 and 12 ± 0.09 g L^{-1} total iron concentration (error expressed as standard deviation of the mean). The total iron concentration of the bioreactor feed was determined by titration using potassium dichromate solution (see Appendix D1.2 & D1.3 for details of the procedure). The details of the experimental description have discussed in Section 3.2.4. It should be noted that even though the kinetic studies were investigated at dilution rates between 0.015 and 0.17 h^{-1}, the range of dilution rates for each experiment increases with lower total iron concentrations.

7.3 Results and Discussion

7.3.1 Raw Data – *Steady state oxygen and carbon dioxide utilisation rates*.

Figure 7.1 shows the plots of oxygen and carbon dioxide utilisation rates versus the dilution rates. As described previously, these rates were calculated from the difference between the inlet and outlet gas concentrations, and these measurements were used to monitor the microbial growth and substrate utilisation reaction kinetics.

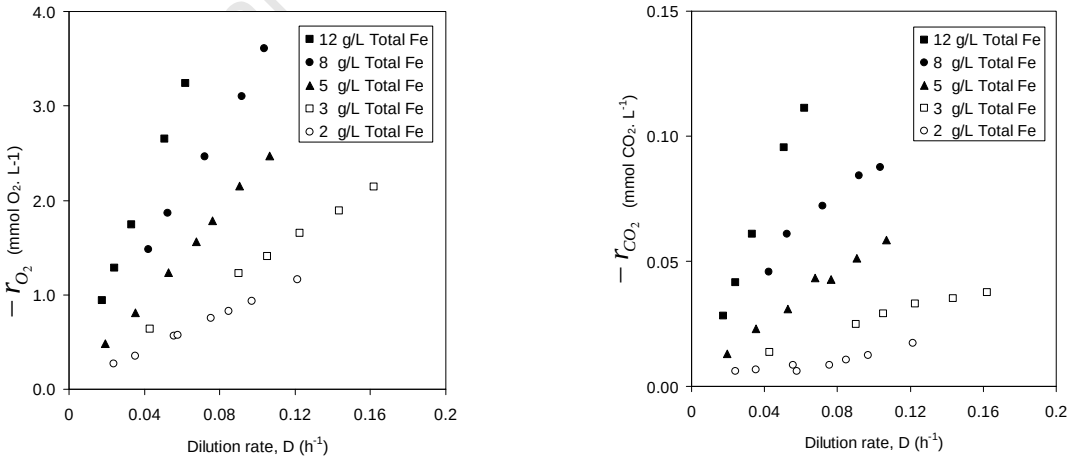

Figure 7.1 Oxygen and carbon dioxide utilisation rates determined for continuous microbial ferrous-iron oxidation at 42 ºC, pH 1.3 and at 2,3,5,8 and 12 g L^{-1} total iron feed concentration.

Both the oxygen and carbon dioxide utilisation rates follow the same trend, all increasing with dilution rates within the region investigated. The low rates observed at low dilution rates are an indication that the influent substrate concentration is low under these conditions, and the increase in rate, as the dilution rate increases, corresponds to the increased availability of substrates. This characteristic is expected and can be described by simple Monod kinetics. Figure 7.1 also shows increased rates with increase in total iron concentration at the same dilution rate. This can be explained in a similar fashion as above, indicative of the fact that the influent ferrous-iron concentration at the same dilution rate increased with increasing total iron concentration. The similarity in the pattern of carbon dioxide utilisation rates to that of oxygen may suggest, however, that cell maintenance was not at the expense of microbial growth, since the trend suggested that the cultures were actively growing within the region of dilution rates investigated.

7.3.2 Total iron and ferrous-iron concentration

Figure 7.2 shows the total iron concentration (determined by titration) of the inlet and effluent stream of the bioreactor over the entire dilution rates investigated. The data show that the steady state total iron concentration in the bioreactor is similar to that in the inlet feed, indicating that iron loss, usually to ferric precipitation, is can be assumed to be negligible (max value of 2.92%) at the operating condition (42 ºC and pH 1.3) for the entire investigation as shown in Table D1.3. The steady state ferrous-iron concentration in the effluent stream, on the other hand, was close to the detection limit of the titrimetric method. This was determined by the combination of ferric-to-ferrous ratios (calculated from the measured solution redox potential using redox probe and calibrated parameters) and total iron concentration measured at steady state (Boon, 1996; Boon *et al.*, 1995b), with the assumption that total iron concentration is the summation of ferric and ferrous iron concentrations. The calculation is described in the Appendix D1.5.

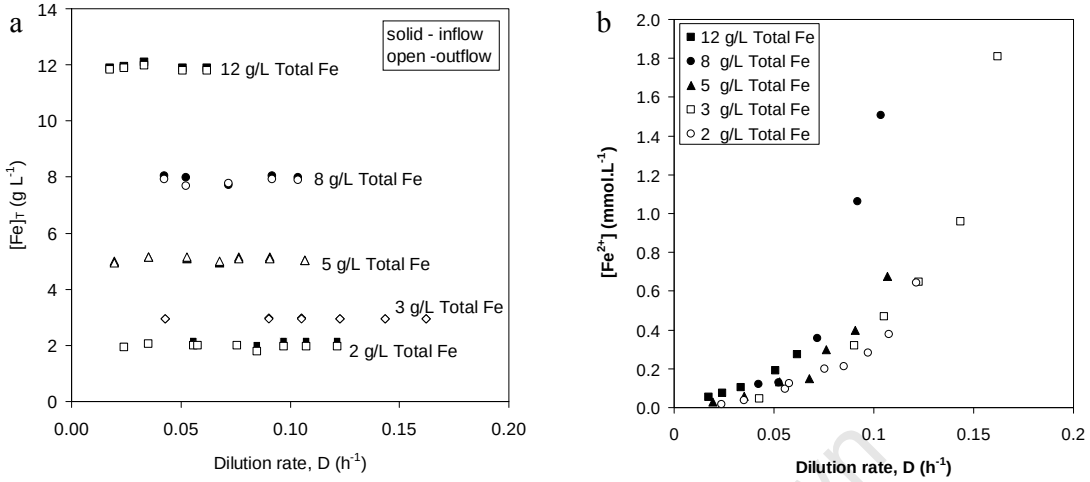

Figure 7.2 (a) Total iron and (b) ferrous-iron concentration measured at varying dilution rates for continuous microbial ferrous-iron oxidation at 42 ºC, pH 1.3 and at 2,3,5,8 and 12 g L^{-1} total iron concentration

The residual ferrous-iron concentration at the same dilution rate increased with total iron concentration. The ferrous-iron concentration was low at low dilution rates for all experiments, and increased as the dilution rate increased. This is consistent with Monod theory for continuous culture. The increase in ferrous-iron concentration with increasing dilution rate was consistent with the corresponding decrease in ferric-to-ferrous ratio (or drop in measured solution redox potential) as shown in Figure 7.3. This figure also indicates that the measured redox potential as a function of dilution rate is independent on total iron concentration. This is consistent with the observation of Boon *et al.* (1999a).

At very low dilution rate (*i.e.* long residence time), the observed low ferrous-iron concentration suggests that the microbial oxidation reaction was almost completed. The microbial culture might be subjected to substrate limitation under this condition. The bioreactors were converted to batch mode in order to determine minimum ferrous-iron concentration via the measurement of redox potential (Appendix D, Table D1.2). The maximum measured potential for all experiments was 775 ± 8 (error expressed as standard deviation). This corresponds to threshold ferrous-iron concentration, which increased from 0.0012 to 0.006 mmol L^{-1} for measurements taken at 2 and 12 g L^{-1} total

iron respectively respectively. The value obtained at 12 g L^{-1} is comparable to the 0.005 mmol L^{-1} reported for *Leptospirillum*-like bacteria (van Scherpenzeel *et al.*, 1998) but less than 0.5 mmol L^{-1} reported for *At. ferrooxidans* (Boon, 1996) which is expected. Also the higher values (0.0862 – 0.268 mmol L^{-1}) reported for *L. ferrooxidans* (Breed *et al.*, 1999) might be due to the difference in the method used to determine the threshold values.

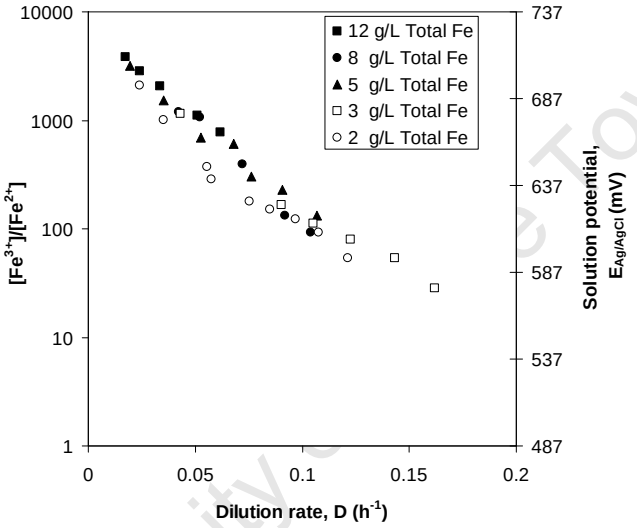

Figure 7.3 Ferric-to-ferrous ratio and corresponding solution redox potential measured in the bioreactor at varying dilution rates for continuous microbial ferrous-iron oxidation at 42 ºC, pH 1.3 and at 2,3,5,8 and 12 g L^{-1} total iron concentration

7.3.3 Analysed Data: Reproducibility of data

Figure 7.4 shows the reproducibility of data obtained under identical conditions performed at two different times. The Figure shows that the data were reasonably similar within the limit of experimental error. This confirms that the experimental procedure is reliable, generating reproducible results; it also confirms there was no variation or change in the microbial culture used for this study. The two data sets were treated as a single data set for subsequent analysis.

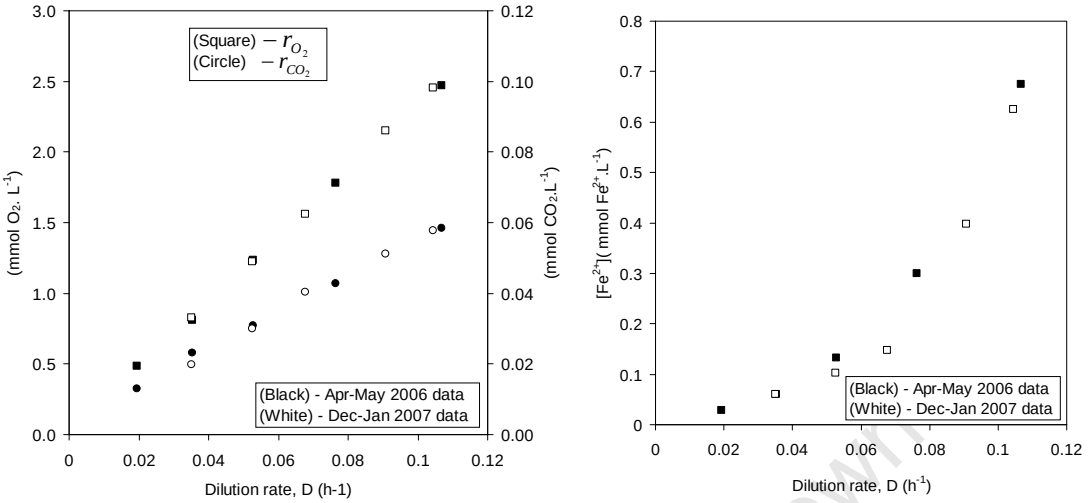

Figure 7.4 Comparison of data obtained under identical condition (but at different times) at varying dilution rates for continuous microbial ferrous-iron oxidation at 42 ºC, pH 1.3 and at 5 g L^{-1} total iron concentration

7.3.4 Consistency of data: *Off – gas data*

As described in Sction 3.4.1, the microbial ferrous-iron oxidation rate was calculated from the rates of oxygen and carbon dioxide utilisation using the degree-of-reduction balance, as shown in Equation 3.5. This rate was compared on a parity plot, Figure 7.5, with that determined by performing an iron mass balance over the bioreactor at steady state, using Equation 3.23

$$-r_{Fe^{2+}} = -4r_{O_2} - 4.2r_{CO_2} \qquad 3.5$$

$$-r_{Fe^{2+}} = D.\left([Fe^{2+}]_{inlet} - [Fe^{2+}]_{outlet}\right) \qquad 3.23$$

The plot shows that both methods agree reasonably and that the off–gas result is consistent and valid.

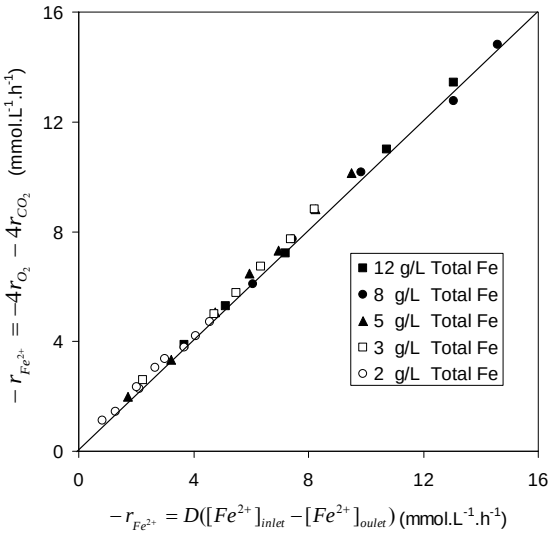

Figure 7.5 Comparison of data obtained under identical condition (but at different times) at varying dilution rates for continuous microbial ferrous-iron oxidation at 42 °C, pH 1.3 and at 5 g L^{-1} total iron concentration

7.3.5 Cell concentration

As described previously in Chapter 3, the microbial biomass concentration, C_X was determined from the rate of carbon dioxide utilisation. This method is based on the assumption that all CO_2 consumed is converted into viable cell biomass, that no wall growth occurs, and that death rate is negligible. Thus, at steady state, the specific microbial growth rate is equal to the dilution rate, and Equation 3.24 is used to determine the steady state biomass concentration:

$$C_X = \frac{r_x}{\mu} = \frac{-r_{CO_2}}{D} \qquad 3.24$$

The steady state biomass concentrations obtained over the dilution rate investigated is shown in Figure 7.6**.**

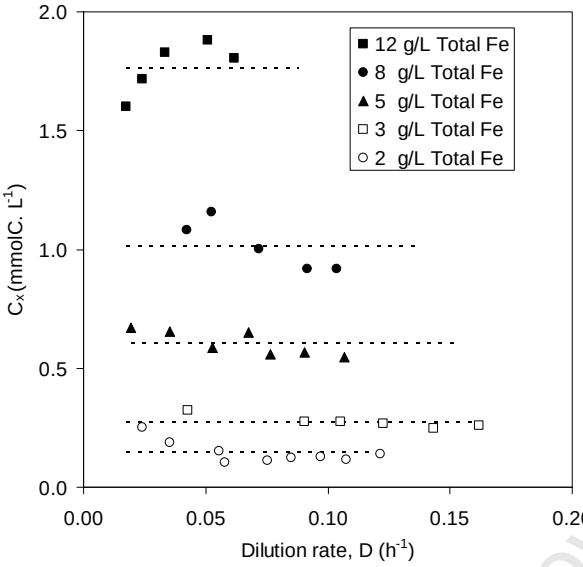

Figure 7.6 Microbial biomass concentration at varying dilution rates for continuous microbial ferrous-iron oxidation at 42 ºC, pH 1.3 and at 2,3,5,8 and 12 g L^{-1} total iron concentration. [Dotted lines represent the plotted average values of biomass concentration]

Although, the biomass concentration appears to be scattered around a distinct level reasonably constant over the range of dilution rates investigated, it varies about this average between 2.5 – 26 % for most of the experiments, except for the study at 2 g L^{-1}, where variation greater than 100% was observed. However, the effect of total iron concentration on the cell concentration is indeed quite dramatic, a six-fold increase in total iron concentration resulted in a twelve-fold increase in average cell concentration while about fifteen-fold increase was observed from the cell count analysis (Figure 7.7). A similar result was obtained when the biomass was measured as protein concentration (Sundkvist *et al.*, 2007) – a two-fold increase in total iron concentration resulted to 2.5 increase in biomas concentration. It appears that this effect cannot be explained simply in terms of the lower total iron concentration – this will be discussed further in Section 7.4

The method used for biomass concentration measurement is an indirect one, as it allows for online monitoring of the biomass growth without affecting the steady state operation of the bioreactor. However, the limitation of this method lies in the fact that, not all the carbon dioxide assimilated is necessarily converted to cell growth. It has been shown that other forms of carbon-containing compound like extracellular polymeric substance (EPS) are formed (Gehrke *et al.*, 1998; Harneit *et al.*, 2006; Kinzler *et al.*, 2003),

although this is more pronounced in attached microbes than planktonic. Therefore, the observed biomass concentrations probably include carbon used for producing other carbon compounds other than cell mass.

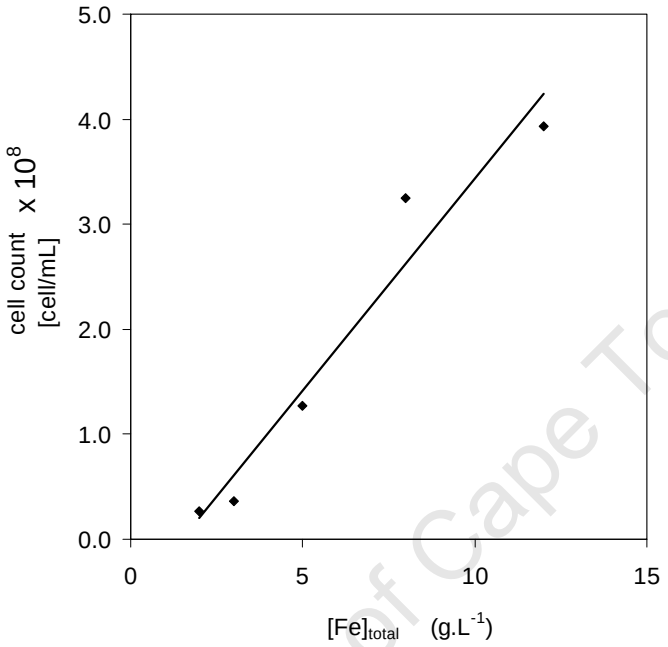

Figure 7.7 Variation of biomass (determined from cell count method) with total iron concentration

7.3.6 Specific substrate utilisation rates

The specific ferrous-iron utilisation rate were determined from Equation 7.1.

$$q_{Fe^{2+}} = -\frac{r_{Fe^{2+}}}{C_X} \qquad 7.1$$

The plots of $q_{Fe^{2+}}$ and q_{O_2} as function of $[Fe^{3+}]/[Fe^{2+}]$ ratio, determined in a similar fashion to previous chapters, show a reverse sigmoidal curve with a steady increase in the rate with decrease in $[Fe^{3+}]/[Fe^{2+}]$ ratio (Figure 7.8 a & b). This is characteristic of Michaelis-Menten kinetics. The rates drop from a $[Fe^{3+}]/[Fe^{2+}]$ ratio of about 100, corresponding to a solution potential of 600 mV (Ag/AgCl), which is similar to Breed *et al.*(1999) results, for *Leptospirillum* species. This corresponds to a region of high redox potential in bioleach system. In the case of *At. ferrooxidans*, the rate dropped from $[Fe^{3+}]/[Fe^{2+}]$=10 (Boon, 1996), which corresponds to much lower redox potential (~400 mV). The ability to maintain a higher redox potential while rapidly oxidizing ferrous-

iron than *At. ferrooxidans* may explain why *Leptospirillum* was found to be dominant over *At. ferrooxidans* in a bioleaching plant (BIOX) operating at high redox potential (Rawlings *et al.*, 1999).

$$q_{Fe^{2+}} = \frac{q_{Fe^{2+}}^{\max}}{1 + K'_{Fe^{2+}} \dfrac{[Fe^{3+}]}{[Fe^{2+}]}} \qquad 3.15$$

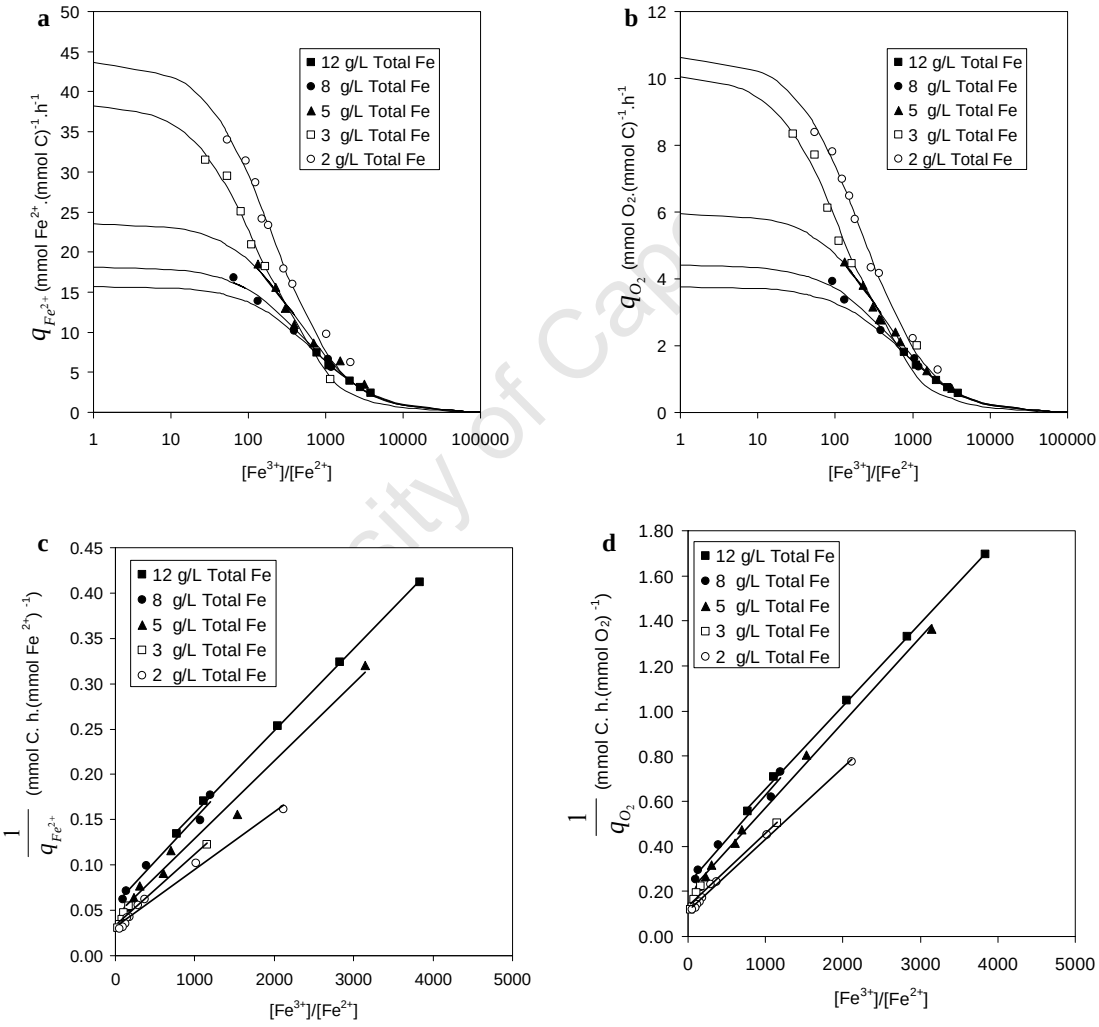

Figure 7.8 (a & b) The plots of specific utilisation rates as a function of ferric-to-ferrous ratio, and (c & d) the Lineweaver-Burk plot of Equation 3.15 & 3.16 for continuous microbial ferrous-iron oxidation at 42 ºC, pH 1.3 and at 2,3,5,8 and 12 g L^{-1} total iron concentration. Used to determine the kinetic parameters in Table 7.1

The $q_{Fe^{2+}}^{max}$ and $K'_{Fe^{2+}}$ values were obtained by fitting the observed data to Equation 3.15, using regression to minimise the sum of square errors between observed and predicted values of the experimental data as discussed in Section. 4.3.2

A similar equation can be written for oxygen based substrate to determine $q_{O_2}^{max}$ and K_{O_2}. These parameters were also determined from Lineweaver-Burk plot of Equation 3.15, as also shown in Figure 7.8.

A dramatic increase in maximum specific substrate utilisation rates, $q_{Fe^{2+}}^{max}$ and $q_{O_2}^{max}$ at low total iron concentration was noted. This trend was not expected: $q_{Fe^{2+}}^{max}$ should be fairly constant or vary only slightly. The relative energy required to fix carbon to produce new cells should not be a function of total iron concentration if the culture is not under substrate limitation. In a similar study, an increase from 9 to 18 g L^{-1} total iron resulted in a 25 % increase in $q_{Fe^{2+}}^{max}$ (Sundkvist *et al.*, 2007). In contrast, Boon (1999a) reported similar $q_{O_2}^{max}$ values, measured using Biological Oxygen Monitor for similar experiments carried out at 6, 9, 12 and 15 g L^{-1} total iron which varied with dilution rate. However, this effect can be linked to the decreasing trend of biomass concentration and the cell yield with decrease in total iron concentration (Figure 7.6). The decreased maximum rates at high total iron concentration must be attributed to microbial inhibition either by substrate, $[Fe^{2+}]$, or due to product formed, $[Fe^{3+}]$. The converse increase in biomass concentration at high total iron could as well be a result of either of the iron species, possibly acting as a stimulus, promoting biomass increase. An attempt to explain this phenomenon is discussed in Section 7.4.

Table 7.1 shows the values of kinetic parameters obtained from Figure 7.8 and their averages. Although the mean square errors of the regression method are very small, and negligible in the case of Lineweaver-Burk method, the two methods have inherent experimental errors. While the error in Lineweaver-Burk method is significant at high $[Fe^{3+}]/[Fe^{2+}]$ ratios, the error in the fit to Equation 2.14 is significant at low $[Fe^{3+}]/[Fe^{2+}]$. Therefore, the average values of the kinetic parameters were used in subsequent analysis. These values were determined from Equation 3.15 and plotted against the experimental data as shown in Figure 7.9

Table 7.1 Kinetic parameters obtained from Figure 5.6 for continuous microbial ferrous-iron oxidation at 42 ºC, pH 1.3 and at 2,3,5,8 and 12 g L-1 total iron concentration

Fe	Lineweaver Burke			Fit to Equation 2.14			Average values			
($g.L^{-1}$)	$q^{max}_{Fe^{2+}}$	$K'_{Fe^{2+}}$	R^2	$q^{max}_{Fe^{2+}}$	$K'_{Fe^{2+}}$	SSE	$q^{max}_{Fe^{2+}}$	Error*	$K'_{Fe^{2+}}$	Error*
12	14.73	0.0013	1.000	15.75	0.0015	0.029	15.24	0.72	0.0014	0.0001
8	17.45	0.0017	0.984	18.14	0.0019	1.259	17.80	0.49	0.0018	0.0001
5	22.37	0.0019	0.988	23.59	0.0024	4.742	22.98	0.86	0.0022	0.0004
3	29.07	0.0023	0.977	38.48	0.0068	3.461	33.77	6.65	0.0046	0.0032
2	31.75	0.0020	0.985	43.89	0.0048	5.120	37.82	8.59	0.0034	0.0020
	$q^{max}_{O_2}$	K'_{O_2}	R^2	$q^{max}_{O_2}$	K'_{O_2}	SSE	$q^{max}_{O_2}$	Error	K'_{O_2}	Error
12	3.48	0.0013	0.999	3.76	0.0014	0.002	3.62	0.19	0.0014	0.0001
8	4.26	0.0017	0.984	4.41	0.0019	0.080	4.33	0.11	0.0018	0.0001
5	5.18	0.0020	0.997	5.97	0.0026	0.061	5.58	0.56	0.0023	0.0004
3	7.30	0.0023	0.971	10.13	0.0074	1.339	8.71	2.00	0.0049	0.0036
2	8.85	0.0028	0.996	10.68	0.0045	0.279	9.76	1.30	0.0037	0.0012

* Error expressed as standard deviation of the mean

Units: $q^{max}_{Fe^{2+}}$ [mol Fe^{2+} (molC h)$^{-1}$], $q^{max}_{O_2}$ [mol O_2 (mol C h)$^{-1}$], K'_{O_2} & $K'_{Fe^{2+}}$ are dimensionless

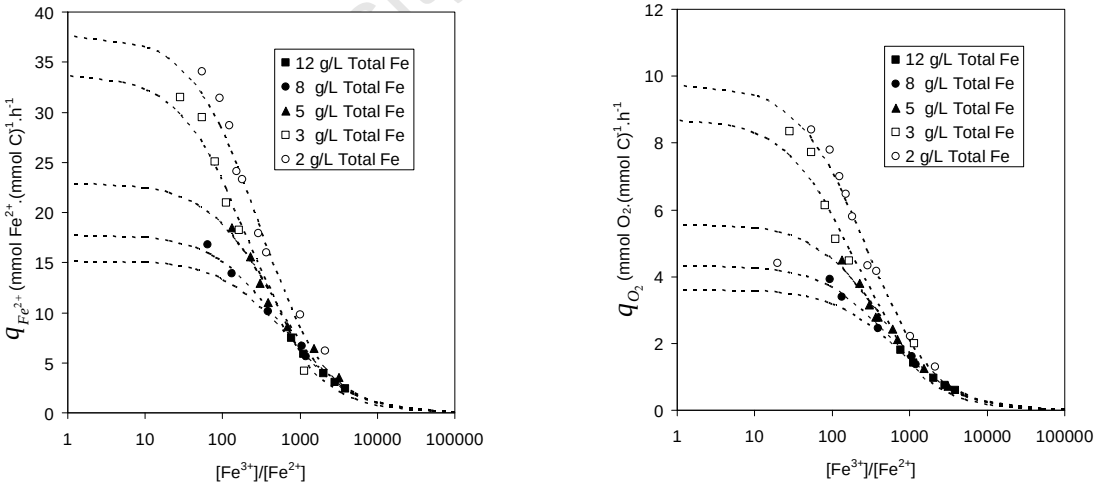

Figure 7.9 The plots of specific substrate utilisation rates as a function of ferric-to-ferrous ratio for continuous microbial ferrous-iron oxidation at 42 ºC, pH 1.3 and at 2,3,5,8 and 12 g L^{-1} total iron concentration. [dotted lines represent plot of Eq. 3.15 and 3.16 using data from Table 7.1]

7.3.7 Yield and maintenance parameters

As described in Section 2.3, assuming that the microbial growth kinetics are coupled to the iron oxidation kinetics via cell yield and maintenance:

$$-r_{Fe^{2+}} = \frac{r_x}{Y^{\max}_{Fe^{2+}X}} + m_{Fe^{2+}}$$

i.e. the energy derived from ferrous-iron oxidation is channeled to microbial growth and cell maintenance as described by the Pirt Equation for constant maintenance. This can be written in the form of Equation 3.9 and 3.11 (since $r_x = \mu C_X$) to determine the energetic parameters.

$$\frac{1}{Y_{Fe^{2+}X}} = \frac{1}{Y^{\max}_{Fe^{2+}X}} + \frac{m_{Fe^{2+}}}{D} \qquad 3.9$$

$$q_{Fe^{2+}} = \frac{D}{Y^{\max}_{Fe^{2+}X}} + m_{Fe^{2+}} \qquad 3.11$$

It can be seen from Equations 3.9 and 3.11 that the plot of specific ferrous-iron utilisation rate, $q_{Fe^{2+}}$ versus the dilution rate, D gives a linear curve with slope of $1/Y^{\max}_{Fe^{2+}X}$ and an intercept of $m_{Fe^{2+}}$, while the plot of reciprocal of the yield, $1/Y_{Fe^{2+}X}$ versus the residence time (inverse of dilution rate) should also give a linear curve with a slope of $m_{Fe^{2+}}$ and intercept of $1/Y^{\max}_{Fe^{2+}X}$.

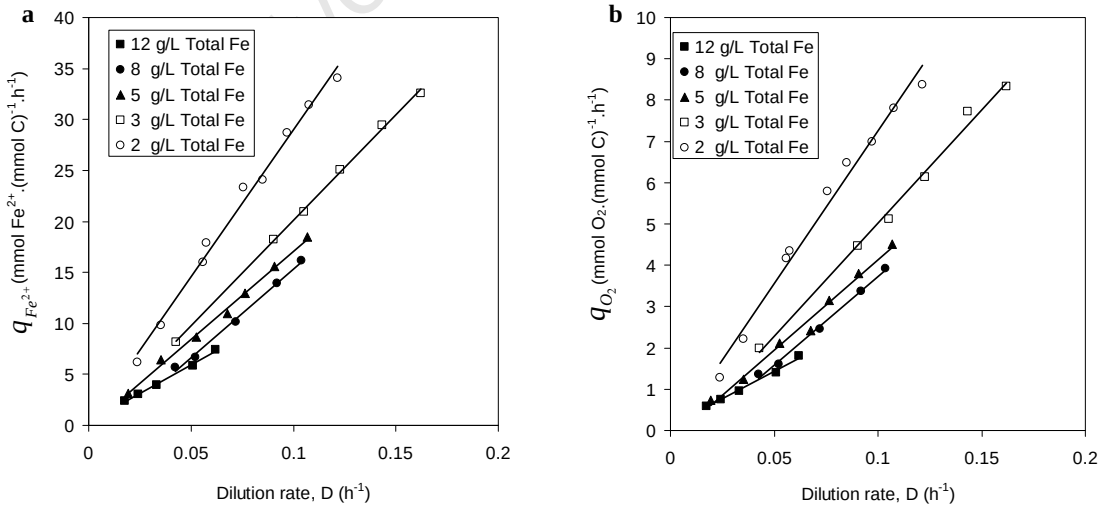

Figure 7.10 Microbial specific ferrous-iron and oxygen utilisation rates at varying dilution rates for continuous microbial ferrous-iron oxidation at 42 ºC, pH 1.3 and at 2,3,5,8 and 12 g L^{-1} total iron concentration

These were plotted as shown in Figure 7.10 for both ferrous and oxygen based substrates, the values obtained for these parameters are shown in Table 7.2. The slopes of the data sets in Figure 7.10 (a) and (b) show that both $Y_{Fe^{2+}X}^{max}$ and $Y_{O_2X}^{max}$ increased with increase in total iron concentration from 2 to 12 g L^{-1} as shown in Figure 7.11. This observation is supported by a similar report, an increase from 9 to 18 g L^{-1} total iron concentration doubled $Y_{Fe^{2+}X}^{max}$ (Sundkvist *et al.*, 2007). However, the maintenance coefficient cannot be accurately determined. This is due to fact that it is small compared to the reciprocal of the yield, $1/Y_{SX}^{max}$ (*i.e.* $m_s Y_{SX}^{max}$ is very small) (as determined in previous Chapters, 4 and 5), the corresponding maintenance coefficients for iron concentration less than 12 g L^{-1} can not be determined with any confidence. It sometimes results in a negative value of maintenance (Table 7.2), which makes no physical sense.

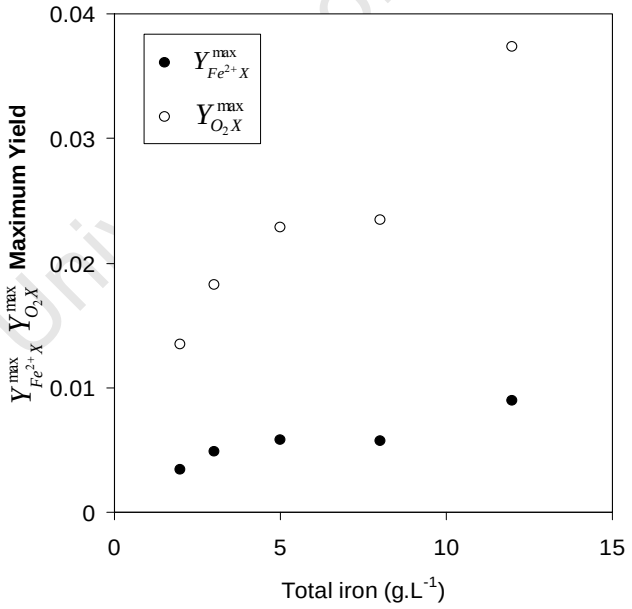

Figure 7.11 Plot of maximum biomass yield versus total iron concentration

Table 7.2 Bioenergetic parameters obtained from Figure 7.9 and Equation 7.2 for continuous microbial ferrous-iron oxidation at 42 ºC, pH 1.3 and at 2,3,5,8 and 12 g L^{-1} total iron concentration.

	Obtained from Figure 7.10			Obtained from Equation 7.2		
Total Fe (g L^{-1})	$Y^{max}_{Fe^{2+}X}$	$m_{Fe^{2+}}$	R^2	$Y^{max}_{Fe^{2+}X}$	$m_{Fe^{2+}}$	R^2
12	0.0089	0.37	0.99	0.0089	0.37	0.99
8	0.0057	-2.17	0.99	0.0055	-2.59	0.99
5	0.0058	-0.19	0.99	0.0056	-0.39	0.98
3	0.0048	-0.64	0.99	0.0047	-2.00	0.99
2	0.0035	0.07	0.99	0.0035	-0.47	0.98

Units: $Y^{max}_{Fe^{2+}X}$ [molC.(molFe^{2+})$^{-1}$], $m_{Fe^{2+}}$ [molFe^{2+}.(molC.h)$^{-1}$],

The values of $Y^{max}_{Fe^{2+}X}$ = 0.009 and $m_{Fe^{2+}}$ = 0.37 are similar to 0.01 and 0.24 obtained in a similar work conducted by van Scherpenzeel (1998) at 12 g L^{-1} total iron concentration. However, an attempt was made to determine the maintenance parameters using another method. By substituting Equation 3.15 into Equation 3.11, Equation 7.2 can be written

$$\mu = D = Y^{max}_{Fe^{2+}X}\left(\frac{q^{max}_{Fe^{2+}}}{1+K'_{Fe^{2+}}\dfrac{[Fe^{3+}]}{[Fe^{2+}]}} - m_{Fe^{2+}}\right) \qquad 7.2$$

The kinetic constants given in Table 7.1 were substituted into Equation 7.2. Therefore by fitting Equation 7.2 to the specific growth rate (= dilution rate) and the corresponding ferric-to-ferrous ratio data using the Solver routine in Excel, that minimises the sum of square error between measured and the predicted μ, $Y^{max}_{Fe^{2+}X}$ and $m_{Fe^{2+}}$ can be calculated. This did not yield any improved result for maintenance coefficients (see Table 7.2), confirming that below 12 g L^{-1} maintenance coefficient is so small that can not be measured accurately. However, Sundkvist *et al.* (2007) reported that maintanance activities constitute about 90% of $q^{max}_{Fe^{2+}}$ which is in contrast to this study, although it was noted that all their experiment were carried out a dilution rates near wash-out.

The variable maintenance equation, Equation 2.18, as decribed by Dempers (2003) was also applied to the experimental data. The results in Table D1.3 (Appendix D) suggest

that the biokinetics cannot be described by variable maintenance function due to the fact that both the constant and growth dependent maintenance terms are very small, often resulting in negative values, especially at total iron concentrations less than 12 g L^{-1}. The biomass yield obtained from the variable maintenance equation is the same as the values obtained from the Pirt equation, where a constant maintenance term is assumed. The small value of maintenance coefficients determined for all the experiments suggests that the culture is actively growing. This is expected for a continuous system where the bacterial growth rate is limited solely by the energy source (ferrous-iron). The variable maintenance requirement decreases to zero, allowing the Pirt equation to be applicable (Dempers *et al.*, 2003).

7.4 Modelling the microbial ferrous-iron oxidation – *Effect of total-iron*

7.4.1 Biomass concentration

The critical analysis of the biomass concentration (12 fold over the 2 to 12 g/L interval of total iron) shows that the increasing trend was as a result of ferric-iron concentration. The iron species in the bioreactor are mostly ferric, as ferric-iron concentration in all the experiment was in excess of 97%, irrespective of the dilution rate. The effect of ferric-iron on biomass concentration is shown in Figure 7.12 (plotted by taking the average of biomass concentration and ferric-iron over the entire dilution rate investigated). The same trend was observed for cell count measurement (see Figure 7.12 *insert*) indicating that the presence of ferric-iron actually stimulates microbial growth rather than inhibiting it. However, it was found that neither the residual ferrous-iron concentration, nor the rate of ferrous-iron oxidation have any significant effect on biomass concentration, since no relationship was found with either parameter as shown in Figure 7.13

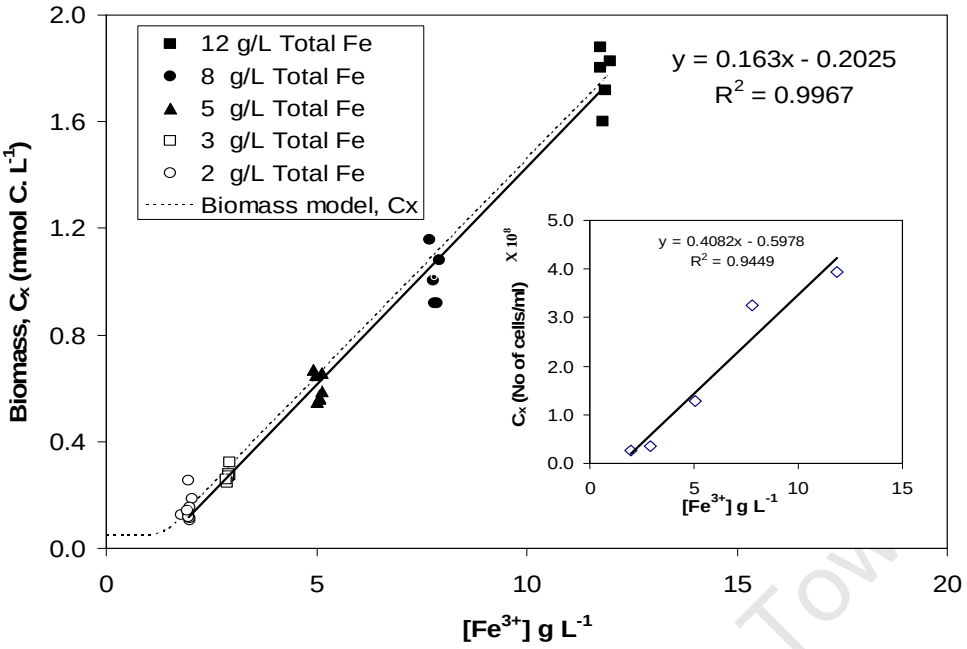

Figure 7.12 Microbial biomass concentrations at varying ferric-iron concentrations (in g.L^{-1}) for continuous microbial ferrous-iron oxidation at 42 ºC, pH 1.3 and at 2,3,5,8 and 12 g.L^{-1} total iron concentration [***insert***: biomass concentration were determined by cell count in Cells.ml^{-1}]

It is necessary to establish a correlation between the microbial biomass concentration, C_X and ferric-iron, as the linear fit of the available data, (Figure 7.12) does not account for the trend below 1.96 g L^{-1} ferric iron concentration (for 2 g L^{-1} total iron).

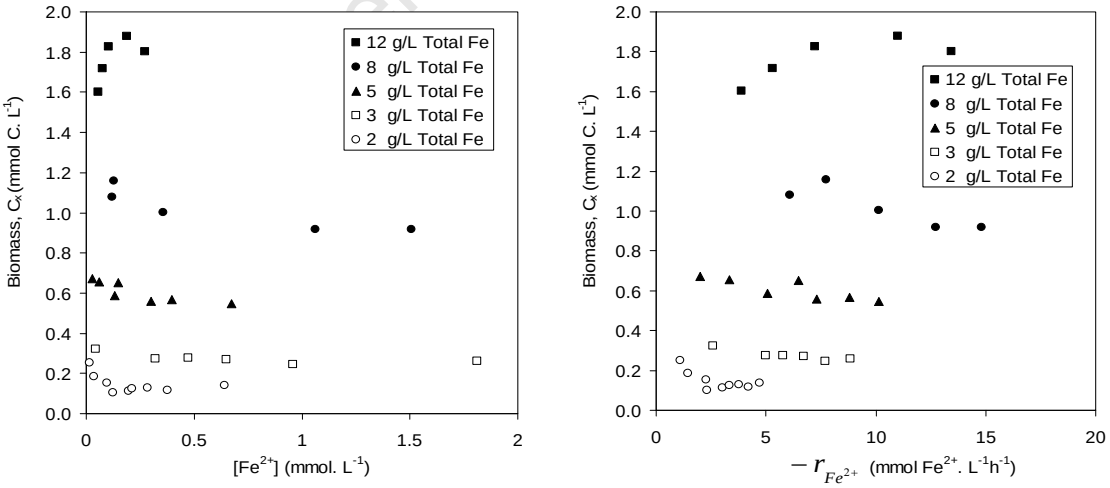

Figure 7.13 Microbial biomass concentrations at varying ferrous-iron concentrations and ferrous-iron oxidation rates for continuous microbial ferrous-iron oxidation at 42 ºC, pH 1.3 and at 2,3,5,8 and 12 g L^{-1} total iron concentration

In order to establish this correlation, it was initially assumed that there is a certain constant minimum microbial biomass concentration, $C_{x,min}$, at ferric-iron concentrations below a certain threshold, $[Fe^{3+}]_{min}$. The validity of this assumption requires more data from an investigation of the microbial oxidation at total iron concentrations below $2gL^{-1}$. This is technically challenging in the current experimental system due to the detection limit of the off-gas analyzer. Thus, the biomass concentration was tentatively correlated with ferric-iron concentration using Equation 7.3

$$C_X = C_{X,\min} + b\left([Fe^{3+}] - [Fe^{3+}]_{\min}\right) \qquad 7.3$$

where $C_{x,min}$ = 0.05 mmol $C.L^{-1}$, b = 0.163 mmol C/g Fe^{3+} (or 0.0091 mmol C/mmol Fe^{3+}) and $[Fe^{3+}]_{min}$ = 1.36 g/L (or 24.42 mmol/L). Both $C_{x,min}$ and $[Fe^{3+}]_{min}$ were estimated based on the above assumption, whereas the parameter b was determined from linear regression of the data shown in Figure 7.12 . The biomass model is plotted against the experimental data as shown by the dotted lines in Figure 7.12.

7.4.2 Maximum specific ferrous-iron utilisation rate

Since the microbial specific ferrous-iron utilisation rate is a function of the overall rate of ferrous-iron oxidation, $-r_{Fe^{2+}}$, and biomass concentration, C_X, as shown previously with Equation 3.11, the data was re-analysed by plotting the overall microbial ferrous-iron oxidation rate against the residual ferrous-iron concentration in the bioreactor (see Figure 7.14)

$$q_{Fe^{2+}} = -\frac{r_{Fe^{2+}}}{C_X} \qquad 3.11$$

To evaluate this data, a Monod-type relationship between oxidation rate and ferrous iron concentration as given by Equation 7.4 was postulated.

$$r_{Fe} = r_{Fe^{2+}}^{\max} \frac{[Fe^{2+}]}{K_{Fe^{2+}} + [Fe^{2+}]} \qquad 7.4$$

where $K_{Fe^{2+}}$ represents the affinity coefficient of the bacteria on ferrous-iron and $r_{Fe^{2+}}^{\max}$ the maximum rate of ferrous-iron oxidation under no substrate limitations. The values of $r_{Fe^{2+}}^{\max}$ and $K_{Fe^{2+}}$ were determined from a fit of Equation 7.4 (by minimising the sum of square errors using the Excel solver routine). This resulted in excellent fits (see lines shown in

Figure 7.14a), better than the Lineweaver-Burk plot, which gave a poor fit, especially at lower total iron concentrations (Figure 7.14b).

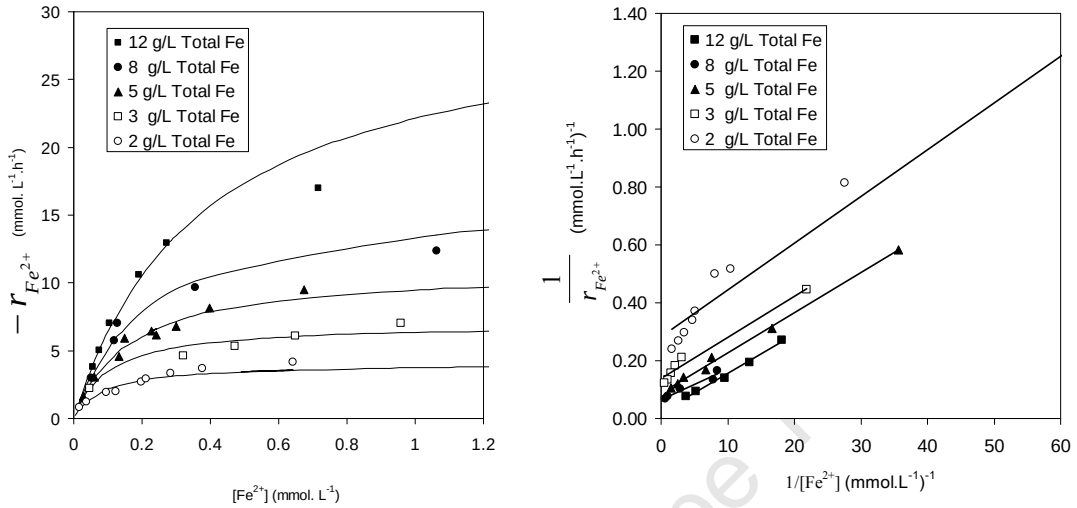

Figure 7.14 The rate of microbial ferrous-iron oxidation at varying residual ferrous-iron concentrations and reciprocal of ferrous-iron oxidation rates versus reciprocal of ferrous-iron concentration for continuous microbial ferrous-iron oxidation at 42 ºC, pH 1.3 and at 2,3,5,8 and 12 g L^{-1} total iron concentration

The data obtained (Table 7.3) indicates a decreasing overall maximum rate of ferrous-iron oxidation with decrease in ferric-iron concentration (see Figure 7.15a), and that a linear relationship exists between the ferrous affinity coefficient $K_{Fe^{2+}}$ and ferric-iron concentration as shown in Figure 7.15b. This essentially corresponds to the Jones and Kelly model (Jones and Kelly, 1983), which represents the ferric inhibition term obtained by expanding the original Monod term in Equation 7.4 as follows:

$$r_{Fe} = r_{Fe^{2+}}^{\max} \frac{[Fe^{2+}]}{K_1 + K_2[Fe^{3+}] + [Fe^{2+}]} \qquad 7.5$$

Therefore, $K_{Fe^{2+}}$ in the Monod Equation can be expanded as shown in Equation 7.6. Dividing the values of $r_{Fe^{2+}}^{\max}$ by the corresponding average biomass concentration (Equation 7.7) yields the calculated value of maximum specific ferrous iron utilisation rates shown in Figure 7.15a. The values of the calculated $q_{Fe^{2+}}^{\max}$ only compared reasonably with the average values determined using the simplified ferric inhibition model, Equation 3.15 at

higher total iron concentrations (see Table 7.1 and Figure 7.15a). The significant difference at lower concentration (especially at 2 and 3 g L^{-1} total iron) can be attributed to the average biomass value used in the calculation.

$$K_{Fe^{2+}} = 0.0177 + 0.0016[Fe^{3+}] \equiv K_1 + K_2[Fe^{3+}] \quad 7.6$$

$$q^{\max}_{Fe^{2+}} = \frac{r^{\max}_{Fe^{2+}}}{C_X} \quad 7.7$$

Table 7.3 Maximum overall ferrous-iron oxidation and microbial affinity constant obtained from continuous microbial ferrous-iron oxidation at 42 ºC, pH 1.3 and at 2,3,5,8 and 12 g L-1 total iron concentration

Total Fe	$[Fe^{3+}]$ mmol L^{-1}	Lineweaver-Burk		Regression fit		Calculated from Hansford model (from Table 7.1)	Calculated from Equation 7.7
		$r^{\max}_{Fe^{2+}}$	$K_{Fe^{2+}}$	$r^{\max}_{Fe^{2+}}$	$K_{Fe^{2+}}$	$q^{\max}_{Fe^{2+}}$	$q^{\max}_{Fe^{2+}}$
12	212	47.62	0.638	30.49	0.378	15.24	17.27
8	140	15.18	0.159	16.26	0.215	17.80	16.01
5	90	11.29	0.157	10.97	0.159	22.98	18.11
3	52	7.29	0.104	7.00	0.102	33.77	25.46
2	35	3.53	0.057	4.08	0.089	37.82	27.81

Units: $r^{\max}_{Fe^{2+}}$ [mol Fe^{2+} L^{-1} h^{-1}], $q^{\max}_{Fe^{2+}}$ [mol Fe^{2+} (molC h)$^{-1}$], $K_{Fe^{2+}}$ [mol Fe^{2+} L^{-1}]

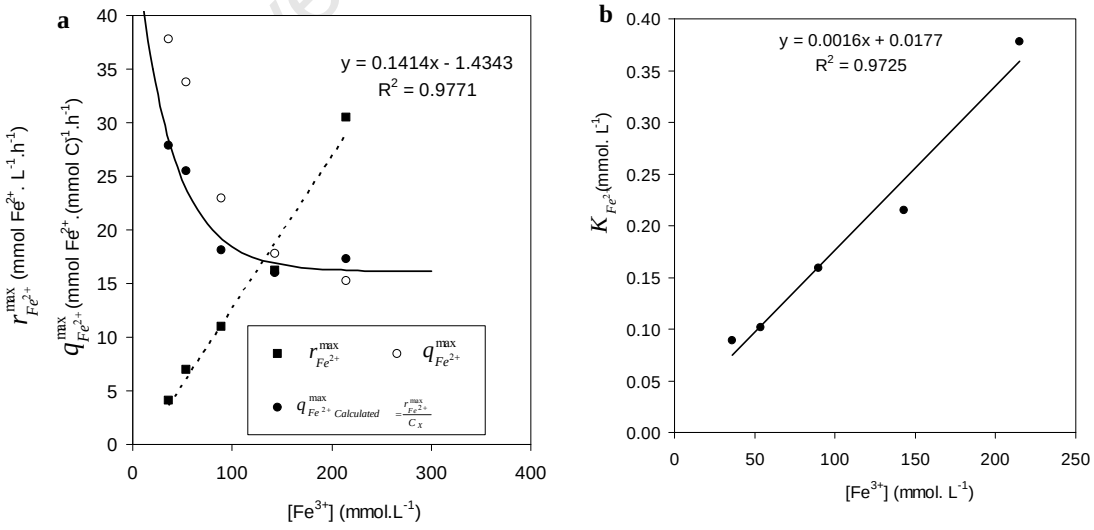

Figure 7.15 (a.)Maximum ferrous iron oxidation rate and maximum specific ferrous iron oxidation rate, (b.) Microbial ferrous-iron affinity constant vs. ferric iron for continuous microbial ferrous-iron oxidation at 42 ºC, pH 1.3 and at 2,3,5,8 and 12 g L^{-1} total iron concentration

As can be seen in Figure 7.15a, the data indicates an exponential decay of $q_{Fe^{2+}}^{max}$ with increasing ferric iron concentration asymptoting to a constant value. It was therefore attempted to model $q_{Fe^{2+}}^{max}$ with Equation 7.8.

$$q_{Fe^{2+}}^{max} = q_{Fe^{2+}}^{min} + q_{Fe^{2+}}^{excess} \exp\left(-a.[Fe^{3+}]\right) \quad 7.8$$

The model is based on the following hypothesis: that there is minimum energy needed for each cell to remain viable and reproductive, and that at high ferric-iron concentration each microbial cell tends to reduce its energy demand due to the fact that some metabolic functions require energy that can be shared within the microbial population, reducing the burden on the individual cell. Microorganisms are know to communicate by the quorum sensing theory (Bauer and Robinson, 2002; Chopp *et al.*, 2003), which has also been reported in bioleaching organisms (Valenzuela *et al.*, 2007). This might be mode of communication when energy sharing is necessary, however, this hypothesis cannot be proven at this stage.

Thus, the $q_{Fe^{2+}}^{min}$ represents the minimum specific rate needed for each cell to remain viable and reproductive, and $q_{Fe^{2+}}^{excess}$ the excess specific rate for additional metabolic functions, which can be shared out between cells depending on the prevailing ferric-iron stress. The calculated values of $q_{Fe^{2+}}^{max}$ from Equation 7.8 accurately predict the values determined from experimental data (shown by the solid line in Figure 7.15a) with the following parameters:

$q_{Fe^{2+}}^{min}$ = 16.132 mmol Fe^{2+} (mmol C)$^{-1}$ h^{-1}
$q_{Fe^{2+}}^{exess}$ = 31.879 mmol Fe^{2+} (mmol C)$^{-1}$ h^{-1}
a = 0.0262 L (mmol Fe^{2+})$^{-1}$

7.4.3 Maximum specific microbial growth rate

The maximum specific growth rate was determined and modelled by a further detailed analysis of the data. The plot of $-r_{Fe^{2+}}$ against the dilution rate, D results in an almost perfect linear fit for all the data sets with $R^2 \sim 1$ in all cases (see Figure 7.16 a)

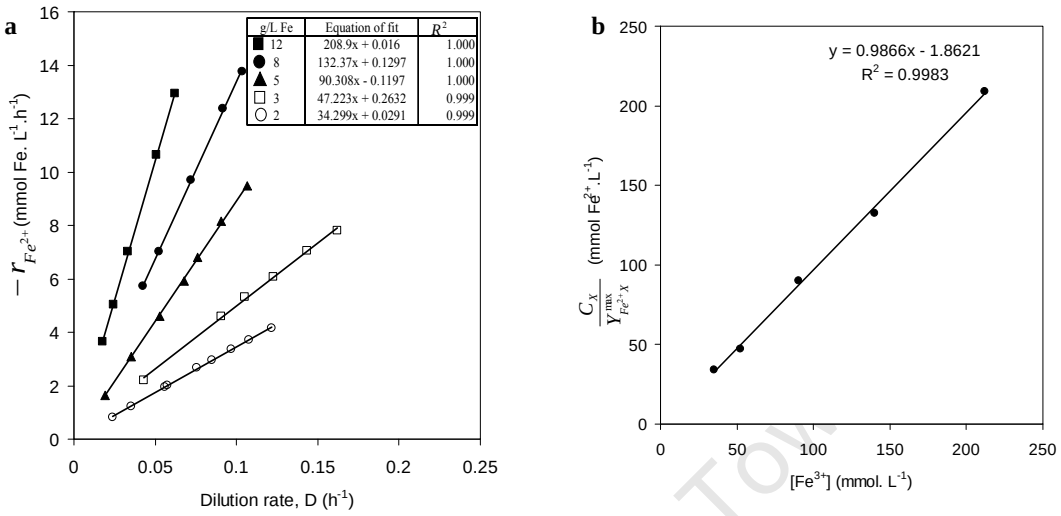

Figure 7.16 a.) Rate of microbial ferrous-iron oxidation versus growth rate (=dilution rate), (b.) Variation of $C_X/Y^{max}_{Fe^{2+}X}$ with ferric-iron concentration for continuous microbial ferrous-iron oxidation at 42 ºC, pH 1.3 and at 2,3,5,8 and 12 g L^{-1} total iron concentration

A careful analysis of the data suggests that the equation representing the best fit is of the form:

$$-r_{Fe^{2+}} = \Theta\mu + m_s \qquad 7.9$$

where Θ is the slope and m_s, the intercept which is negligible in all cases. Equation 7.9 is a modified form of Equation 2.12 and can be interpreted as per Equation 7.10.

$$-r_{Fe^{2+}} = \frac{C_X}{Y^{max}_{Fe^{2+}X}}\mu \qquad 7.10$$

The term $C_X/Y^{max}_{Fe^{2+}X}$ represents the corresponding slope Θ, of the different experiments. The slopes vary linearly with ferric-iron concentration with a negligible offset as shown in Figure 7.16b. A linear regression of the resulting line suggests

$$\frac{C_X}{Y^{max}_{Fe^{2+}X}} = a[Fe^{3+}] \qquad 7.11$$

where the value of a = 0.987 represent the slope of Figure 7.16b. Now, μ^{max} can be determined by re-writing Equation 7.10 to the forms shown by Equation 7.12. It should be noted here that μ^{max} values were determined using three approaches compared together in Table 7.4.

$$q_{Fe^{2+}}^{max} = \frac{r_{Fe^{2+}}^{max}}{C_X} = \frac{1}{Y_{Fe^{2+}X}^{max}}.\mu^{max} \quad \text{a}$$

$$\mu^{max} = q_{Fe^{2+}}^{max}.\frac{Y_{Fe^{2+}X}^{max}}{C_X}.C_X \quad \text{b} \qquad 7.12$$

$$\mu^{max} = r_{Fe^{2+}}^{max}.\frac{Y_{Fe^{2+}X}^{max}}{C_X} \quad \text{c}$$

By using Equation 7.12b and c such that the fractional term represent the inverse of the corresponding slope of Figure 7.16a (*i.e.* $1/\Theta$), $q_{Fe^{2+}}^{max}$ values derived from Equation 7.8 and $r_{Fe^{2+}}^{max}$ values from Table 7.3, and by fitting the experimental data to Equation 6.1. The values are listed in Table 7.4**.** The values can be said to be reasonably consistent in all the investigation, varying between 0.131 to 0.143 h^{-1} on the average. The maximum microbial growth rate should not be a function of substrate concentration, provided the culture is not under substrate limitation.

Table 7.4 Maximum specific growth rates obtained from data and model Equations for continuous microbial ferrous-iron oxidation at 42 ºC, pH 1.3 and at 2,3,5,8 and 12 g L-1 total iron concentration.

Total g/L Fe	Experimental data					Calculated from		
	$[Fe^{3+}]$		C_X (Average)	$-r_{Fe^{2+}}^{max}$	$C_X / Y_{Fe^{2+}X}^{max}$	Equation 7.12b	Equation 7.12c	Equation 6.1
	g L^{-1}	mmol L^{-1}	mmolC L^{-1}	mmol h^{-1}	mmolC L^{-1}	μ^{max} (h^{-1})	μ^{max} (h^{-1})	μ^{max} (h^{-1})
12	11.84	212.06	1.77	30.49	208.9	0.137	0.146	0.148
8	7.81	139.88	1.02	16.26	132.37	0.129	0.123	0.130
5	5.05	90.41	0.61	10.97	90.308	0.129	0.121	0.129
3	2.91	52.13	0.27	7.00	47.223	0.139	0.148	0.160
2	1.96	35.01	0.15	4.08	34.299	0.122	0.119	0.146

By combining Equation 7.3 for biomass, C_X and Equation 7.8 for the $q_{Fe^{2+}}^{max}$ model into Equation 7.12b (given that the fractional term represent the inverse of the slope $1/\Theta$ derived from Figure 7.16b), a simulation of μ^{max} model can be obtained. This is plotted against the values determined from experimental data as shown in Figure 7.17 a.

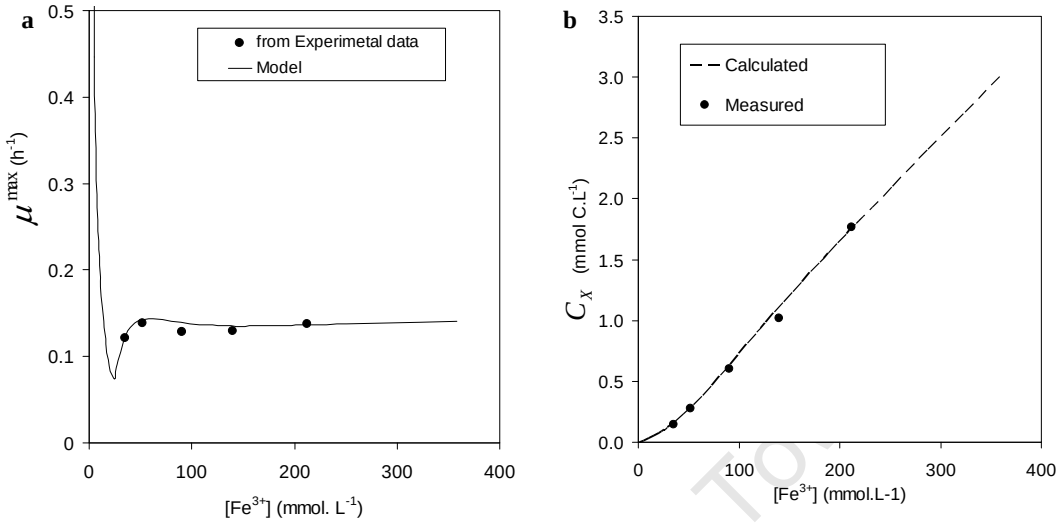

Figure 7.17 Comparison between (a) the μ^{max} model with calculated values from Equation 7.12b, (b) the biomass model with experimental values for continuous microbial ferrous-iron oxidation at 42 ºC, pH 1.3 and at 2,3,5,8 and 12 g L^{-1} total iron concentration

The simulation fitted the data as shown reasonably to suggest that the maximum microbial specific growth rate, μ^{max} is actually a constant, since the modelled curve settled around a constant value. An average value of 0.137 ± 0.004 h^{-1} (error expressed as standard deviation of the mean) was taken as μ^{max}, which is comparable to the data shown in Table 7.4 above. However, the model tends to infinity at very low ferric concentration (below 30 mmol L^{-1}). This is possibly because reasonable biomass data cannot be obtained below 2 g L^{-1} total iron concentration making Equation 7.3 not to be valid at low ferric-iron concentration. Therefore, by manipulating Equation 7.12b a new biomass model can be written as:

$$C_X = \mu^{\max}\left(\frac{C_X}{Y^{\max}_{Fe^{2+}X}}\right)\frac{1}{q^{\max}_{Fe^{2+}}} \qquad 7.13$$

$$C_X = 0.137 \times 0.987 \times [Fe^{3+}] \times \frac{1}{q^{\min}_{Fe^{2+}} + q^{exess}_{Fe^{2+}} \exp\left(-a \times [Fe^{3+}]\right)} \qquad 7.14$$

The plot of Equation 7.14 accurately predicts biomass concentration as shown in Figure 7.17b. Therefore, following from the determined values μ^{max} for *L. ferriphilum* and by combining Equation 7.4, 7.8 and 7.14, given that the maintenance term is sufficiently small and can be neglected such that Equation 7.10 is valid, a new ferrous iron oxidation rate model for continuous culture can be formulated as shown in Equation 7.15

$$r_{Fe} = 0.137 \times 0.9866 \times [Fe^{3+}] \times \frac{[Fe^{2+}]}{K_1 + [Fe^{2+}] + K_2[Fe^{3+}]} \qquad 7.15$$

where K_1 = 0.0177 mmol L^{-1} and K_2 = 0.0016 L $mmol^{-1}$. The model describing the rate of microbial ferrous-iron oxidation, Equation 7.15, predicts fairly accurately the experimental data as shown by the dotted lines in Figure 7.18a. The assumption made in the modelling of $q_{Fe^{2+}}^{max}$, especially due to large variation of C_X, explains the slight deviation from the data at higher dilution rates. Therefore Equation 7.15 can be used to describe the microbial ferrous-iron oxidation rate of *L. ferriphilum* within the range of conditions studied.

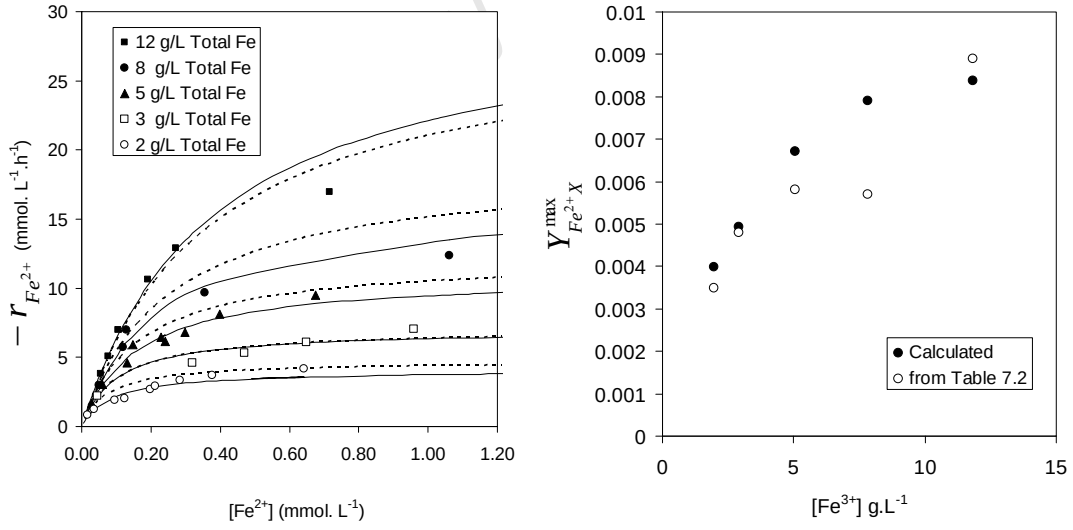

Figure 7.18 Comparison between (a) the new rate model and the experimental data (b) $Y^{max}_{Fe^{2+}X}$ calculated by neglecting maintenance and from Table 7.2 , for continuous microbial ferrous-iron oxidation at 42 ºC, pH 1.3 and at 2,3,5,8 and 12 g L^{-1} total iron concentration [dotted lines represent the Equation 7.15 and solid lines represent Equation 7.5]

7.5 Concluding Analysis

This study investigated the effect of total iron concentration (from 2 to 12 g L^{-1}) on microbial ferrous-iron oxidation kinetics of *L. ferriphilum* in continuous stirred tank bioreactors at dilution rates ranging between 0.017 and 0.165 h^{-1} (*i.e.* 6 to 60 hour residence time). The operating conditions were maintained at 42 °C and pH 1.3 for all the experiments. The rate of microbial ferrous-iron oxidation was accurately measured from the rates of oxygen and carbon dioxide consumption via the degree of reduction balance and found to be reliable and repeatable.

The trend of biomass concentration with total iron concentration was dramatic; a significantly lower cell concentration ensues at low total iron concentrations. A 6-fold increase in total iron resulted to a 12-fold increase in cell mass. However, the trend was reversed in terms of specific substrate utilisation rate. This means that the energy requirement per cell decreased, as the total iron concentration increased (though the overall demand would increase with increasing total iron concentration). The foregoing analysis revealed that high total iron concentration leads to increased cell mass due to the presence of ferric-iron.

This is conceptually explained as follows: In the first instance, a high ferric-iron concentration inhibits desorption of Fe^{3+} from the bacterial surface. The desorption reaction in a sense becomes rate-limiting in the electron transfer chain (Figure 2.4). It is therefore postulated that as a response, bacteria need to increase their total surface area. However, if the load per bacterial remainded unchanged, then q would be the same irrespective of the total iron concentration, this do not support the data. Therefore, it is further postulated that some sort of load sharing is achieved under the high ferric stress condition. This suggests that some functions (requiring energy) can be shared so that the individual bacterium becomes more energy efficient – thus energy demand (q-) declines at higher ferric-iron concentration. How and what is exactly shared is not clear at this stage and is beyond the scope of this study. However, quorum sensing is a communication tool amongst microorganisms and could be seen as the way bacteria 'tell' each other that they need to embark on this load sharing.

The observed decrease in maximum biomass yields on ferrous-iron, $Y_{Fe^{2+}X}^{\max}$ with decreasing total iron concentration (Table 7.2) with a corresponding decreasing maintenance (though negligible in all cases) can also be explained as above – a corresponding reduction in inhibitory stress as a result of decrease in ferric-iron concentration, thereby increasing the tendency of each cell to be fully functional and independent and thus decreasing their population density, or the decrease in maximum biomass yields could possibly be due to substrate limitation. It is impossible to determine the maintenance requirement with confidence at total iron concentration less than 12 g L^{-1} due to the fact that the coefficients are very small compared to the corresponding reciprocal of the yield in the Pirt's equation, and therefore, they may possibly equal to zero as the bacterial are unlikely to be in maintenance mode.

7.6 Conclusion

The foregoing analysis has given an indication that in continuous culture the biomass concentration of *Leptospirillum ferriphilum* is strongly determined by the concentration of ferric iron in the reactor. Higher concentrations of ferric iron clearly stimulate growth and thus also ferrous iron oxidation which supplies the energy needed for growth. The per-cell energy requirement declines, however, indicating that at high ferric iron concentrations individual cells might not fulfil all metabolic functions that require energy, but instead might share some of these between a number of cells. This postulation requires further investigation. A new model is formulated which shows the dependency of both the biomass concentration and maximum specific ferrous-iron utilisation rate on ferric-iron concentration. The model has been shown to be capable of predicting the entire sets of results with a reasonable accuracy.

Chapter 8

Effects of solution conditions on microbial ferrous-iron oxidation kinetics – *A general discussion*

The review of the relevant literatures in Chapter 2 showed the importance of microbial ferrous-iron oxidation, as the main *driver* of bioleaching of sulfide minerals. It also showed that a lot of effort has been directed towards the study of microbial ferrous-iron oxidation over the past three decades, and that most of the studies were carried out under conditions within a narrow operating window near the optimum condition of desired microbial culture. The application of bioleaching to heap leaching has opened another chapter in this study, as the results of previous kinetic studies are only suitable for tank bioleaching, and cannot be translated directly into heap bioleach scenarios – where operating/solution conditions have limited controllability.

This chapter gives an overall discussion of the series of studies carried out in this research work as discussed in Chapters 4, 5, 6 and 7. The basis for the choice of the simplified ferric inhibition equation 'Hansford model' over others has been discussed in chapter 2. It was shown that the model can be made to fit experimental data equally well like others (Ojumu *et al.*, 2006), and at the same time offers simplicity. The modeling study discussed in Chapter 7 has shown that the inclusion of ferric inhibition term was in fact very important to describe microbial ferrous-iron oxidation kinetics. In this section, the Hansford model is re-examined and compared with the product inhibition model by a theoretical analysis.

This is followed by a brief review of the effects of various factors affecting microbial ferrous-iron oxidation in the context of bioleach heaps. An attempt was made to proffer some explanations using the commercially available speciation softwares: Visual Minteq and HSC Chemistry to develop the fundamental understanding for a comprehensive rate equation governing microbial ferrous-iron oxidation under various solution conditions that may be relevant to bioleach heaps.

8.1 The product inhibition type model for microbial ferrous-iron oxidation kinetics

The ferric inhibition type model obtained for this study was discussed exhaustively in Section 7.4. The model can be written in the q-based form as shown in Equation 8.1 by combining Equation 7.14 and 7.15

$$q_{Fe^{2+}} = \frac{r_{Fe^{2+}}}{C_X} = \frac{q_{Fe^{2+}}^{\max}}{1 + \frac{K_1}{[Fe^{2+}]} + K_2 \frac{[Fe^{3+}]}{[Fe^{2+}]}} \qquad 8.1$$

K_1 and K_2 are essentially the microbial affinity constant ($K_{Fe^{2+}}$) for ferrous-iron, and the ratio of $K_{Fe^{2+}}$ to ferric inhibition constant, $K_{Fe^{3+}}$ (*i.e.* $K_{Fe^{2+}} / K_{Fe^{3+}}$) respectively, when compared to the Jones and Kelly (1983) equation for competitive ferric inhibition. However, following from Equation 2.30 (see Section 2.10), microbial ferrous-iron oxidation is a special case of linear mixed inhibition, in which the rate depends on the concentrations *S*, of substrate, and *I*, of product, according to Equation 8.2

$$f_R = \frac{V.S}{K_S\left(1 + \frac{I}{K_C}\right) + S.\left(1 + \frac{I}{K_U}\right)} \qquad 8.2$$

where f_R is a rate function, *V* is the maximum rate (i.e. maximum value of f_R), K_S is the Michaelis-Menten constant, K_C is the competitive inhibition constant and K_U is the

uncompetitive inhibition constant. For a pure non-competitive inhibition, the two constants are equal (i.e. $K_C = K_U = K_I$) and Equation 8.2 takes the form:

$$f_R = \frac{S}{K_S + S} \cdot \frac{K_I}{K_I + I} \tag{8.3}$$

where K_I represent the non-competitive inhibition constant. Therefore, for the non-competitive ferric inhibition for microbial ferrous-iron oxidation, Equation 8.3 can be written as Equation 8.4 which is a product of Monod Equation and inhibition function due to ferric-iron.

$$f_R = \frac{[Fe^{2+}]}{K_{Fe} + [Fe^{2+}]} \cdot \frac{K_p}{K_p + [Fe^{3+}]} \tag{8.4}$$

Equation 8.4 can be re-arranged to give Equation 8.5.

$$f_{prod.inhibition} = \frac{1}{1 + \left(\frac{K_{Fe}}{K_p} + \frac{[Fe^{2+}]}{K_p} + \frac{K_{Fe}}{[Fe^{3+}]} \right) \frac{[Fe^{3+}]}{[Fe^{2+}]}} \tag{8.5}$$

It should be noted that Equations 8.3 to 8.5 are treated as normalized functions of Equation 8.2 with the maximum rate V taken to be unity. Similarly, the normalised functions of Equations 8.1 and 3.15 (the simplified ferric inhibition model) can be written as $f_{q-model}$ and $f_{Simplified}$ respectively

$$f_{q-model} = \frac{1}{1 + \frac{K_1}{[Fe^{2+}]} + K_2 \frac{[Fe^{3+}]}{[Fe^{2+}]}} \tag{8.6}$$

$$f_{Simplified} = \frac{1}{1 + K'_{Fe^{2+}} \frac{[Fe^{3+}]}{[Fe^{2+}]}} \tag{8.7}$$

Therefore, by comparison, $K'_{Fe^{2+}}$ in the simplified model, Equation 8.7, is equal to the trems in parenthesis of of the ferric inhibition model (Equation 8.5). Similarly, Equation 8.5 can be re-written in the form of Equation 8.8, such that it can also be compared to the proposed q-model (*i.e.* Equation 8.6)

$$f_{prod.inhibition} = \frac{1}{1+\left(K_{Fe}+\frac{[Fe^{3+}][Fe^{2+}]}{K_p}\right)\frac{1}{[Fe^{2+}]}+\frac{K_{Fe}}{K_p}\frac{[Fe^{3+}]}{[Fe^{2+}]}} \qquad 8.8$$

where K_1 (i.e $K_{Fe^{2+}}$) in Equation 8.6 is equal to the terms in the parenthesis of Equation 8.8.

Therefore, by calibrating the ferric inhibition model (i.e. Equation 8.5 or 8.8) theoretically, while monitoring the K expression in Equations 8.6 ($K'_{Fe^{2+}}$) and Equation 8.7 (K_1), gave some interesting insight about the trend of K values over the region of applicability of the rate equations as shown in Figure 8.1. This calibration was done at 5 g L^{-1} of total iron over a range of ferric-to-ferrous ratio applicable in bioleaching.

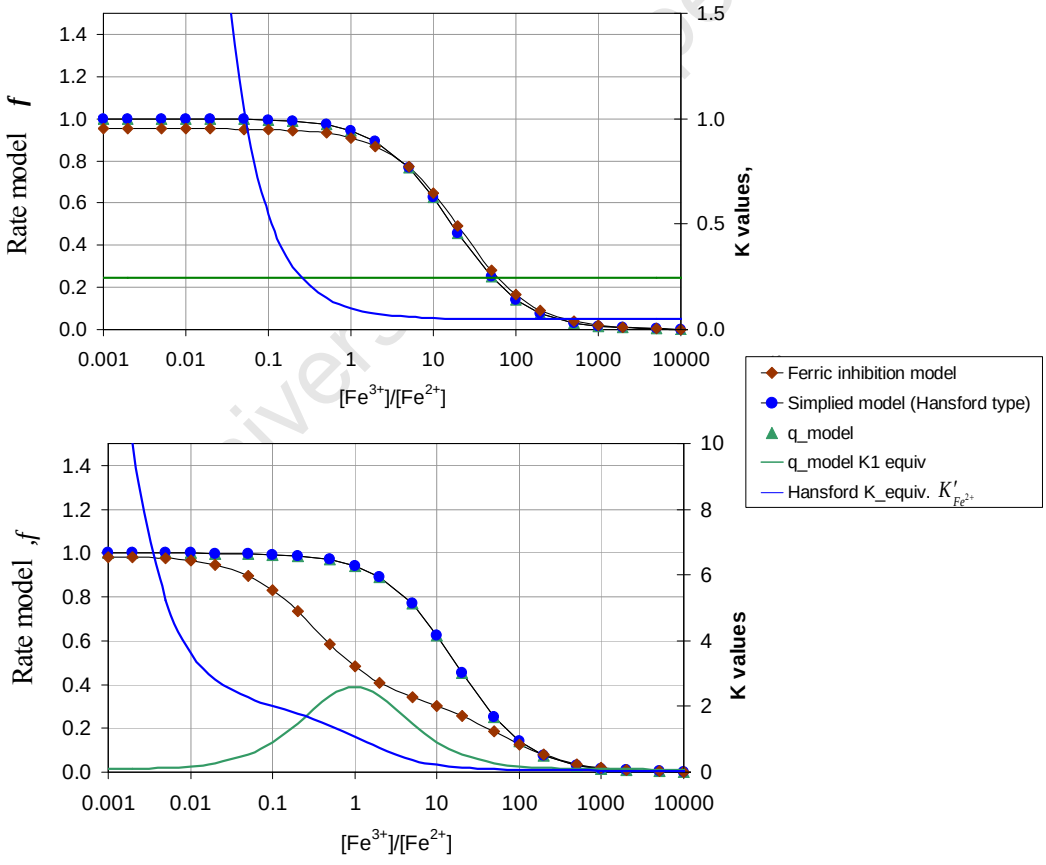

Figure 8.1 Comparison of the ferric-iron inhibition model, (Equation 8.5), q-model (Equation 8.6) and the simplified ferric inhibition form (Equation 8.7)
[K_1=4.8x10^{-5}, K_2= 0.06, $K'_{Fe^{2+}}$=0.06, (a) $K_{Fe^{2+}}$=0.25, K_p = 2.95 x 10^3 (b) $K_{Fe^{2+}}$ = 0.08, K_p=2.5]

Some deductions can be drawn from Figure 8.1: The three models can be made equivalent, thereby predicting experimental data to the same accuracy (see Figure 8.1a), this is suppoted by the previous work (Ojumu *et al.*, 2006), that some of the exisisting rate equations can be made to fit any data. The implication for Equation 8.5 is that the inhibitory contribution of both ferric-iron is removed, *i.e.* the contribution of the second and third terms in the parenthesis of Equation 8.5 are the same and insignificant to affect the value of the first term up to ratio of 10. However, the implication of this analysis on the K values of simplied model (*i.e* $K'_{Fe^{2+}}$) and the proposed q-model (K_1) is such that, while the $K'_{Fe^{2+}}$ trend varied widely at ratios less than 10, K_1 ($K_{Fe^{2+}}$) is faily constant as shown in Figure 8.1a. This analysis suggests strongly that, at ratio less than 10 (where Fe^{2+} concentration is becoming prevalent), the value of $K'_{Fe^{2+}}$ increased significantly, taken on different values due to the removal of ferric-iron inhibition.

This is shown in another calibration, Figure 8.1b, in which Equation 8.5 a shows a hump at ferric-to-ferrous ratio of less than 10. The figure shows clearly the region where both substrate and product effects are dominant. At higher ferric-to-ferrous ratios, the inhibitory effect of ferric is dominant, while the hump at ratios of less than 10 represents the onset of the removal of ferric inhibiton effect. This may be used to explain the decrease in rate observed by Searby (2006) at low redox potential (low ratio, less than 10) for a thermophilic culture. The trend of the parameter $K'_{Fe^{2+}}$ increased significantly similar to Figure 8.1a, it takes on an increasing values below ferric-to-ferrous ratios less than 10. However, it is at much larger scale, as revealed by the scale on the secondary y-axes of Figure 8.1b.

This observation was confirmed by a preliminary study by Kazadi (2007) carried out between ferric-to-ferrous ratio from 0.17 to 1.65 in a controlled potential device, Redostat^{TM}. The author reported $K'_{Fe^{2+}}$ value which was 2-fold larger than the value obtained in this study and similar studies (Breed *et al.*, 1999; Breed and Hansford, 1999a) at higher ratios (> 100). However, in the case of the parameter K_1 of Equation 8.6, K_1 takes opposite values as shown by the parabola, which is obvious in Figure 8.1b.

This analysis further revealed that substrate effect (*i.e* removal ferric inhibition) and product (ferric-iron) inhibition take place at different ferric-to-ferrous ratios.

Although it was shown that both Equation 8.6 and 8.7 can be made equivalent when used to model the same experimental data (see Figure 8.1), Equation 8.6 allows for the determination of the substrate affinity and product inhibition constants, which are lumped together as apparent affinity constant ($K'_{Fe^{2+}}$) in Equation 8.7 . This theoretical analysis revealed that *At. ferrooxidans* shows overlap of substrate and product inhibition whereas in *L. ferriphilum* cultures these parameters are separated, product inhibition is always prevalent at ferric to ferrous-iron ratio of greater than 10 and at very low potential (*i.e.* <10), the effect becomes insignificant.

8.2 The kinetics of microbial ferrous-iron oxidation: *proposed model*

Given that microbial ferrous-iron oxidation can be modelled reasonably well by the proposed equation (Equation 8.9), as discussed in Section 8.1, and the kinetic parameters of the other investigations (i.e. temperature, pH and salts effects) were re-determined in order to find and interpret the variation of the affinity and inhibitory constants (*i.e.* via K_1 and K_2 of Equation 8.9). It should be noted that K_1 and K_2 in Equation 8.9 are $K_{Fe^{2+}}$ and $K_{Fe^{2+}}/K_{Fe^{3+}}$ when compared to the Jones and Kelly equation, thus the ferric inhibition constant can be determined from K_1 and K_2.

$$q_{Fe^{2+}} = \frac{q^{\max}_{Fe^{2+}}}{1 + \frac{K_1}{[Fe^{2+}]} + K_2 \frac{[Fe^{3+}]}{[Fe^{2+}]}} \qquad 8.9$$

8.2.1 Effect of Temperature

Figure 8.2 shows the re-analysed kinetic data previously discussed in Chapter 4. The $q^{\max}_{Fe^{2+}}$ values obtained were more or less the same as the values obtained with the simplified model, with the average percentage error of ± 2% as shown in Table 8.1. However, the ferrous affinity constant, K_1 (*i.e.* $K_{Fe^{2+}}$) appeared to remain constant with

an increase in temperature. The apparent affinity constant, $K'_{Fe^{2+}}$ in the simplified model has been reported to increase linearly with temperature (Breed *et al.*, 1999) for *Leptospirillum.* It should be recalled, however, that $K'_{Fe^{2+}}$ is a lumped parameter and cannot be used to discribe/ interprete the microbial affinity/activity with respect to the substrate. The data suggests that the cell maintains increasing tolerance to ferric inhibition as temperature increases. A linear increase in K_2 (corresponding to decrease in $K_{Fe^{3+}}$) values with increasing temperature should lead to a decrease in $q_{Fe^{2+}}$.

Table 8.1 Comparison of kinetic parameters of Hansford model and the proposed q-model for the study on the effect of temperature.

Temperature	q-model model				Simplied ferric inhibition model		
(°C)	$q^{max}_{Fe^{2+}}$	K_1	K_2	R^2	$q^{max}_{Fe^{2+}}$	$K'_{Fe^{2+}}$	R^2
42	16.59	0.0104	0.00160	0.96	15.29	0.0013	0.99
36	11.41	0.0101	0.00101	0.94	11.37	0.0009	0.98
30	10.05	0.0117	0.00091	0.99	10.05	0.0010	0.99
25	6.67	0.0084	0.00059	1.00	6.73	0.0006	1.00

Units: $q^{max}_{Fe^{2+}}$ [mol Fe^{2+} (molC h)$^{-1}$], K_2 & $K'_{Fe^{2+}}$ are dimensionless, K_1 [mol Fe^{2+} L^{-1}]

However, this effect is outweighed by corresponding increase in $q^{max}_{Fe^{2+}}$ with increase in temperature as shown in Table 8.1. The usual predominance of *L. ferriphilum* over *At ferrooxidans* in bioleach operation can be explained by the fact that at high redox potential where all the data were obtained, the activity of *At ferrooxidans* is inhibited (Rawlings *et al.*, 1999). The linear increasing trend of K_2 with temperature is represented by Equation 8.10 and shown in Figure 8.2(c)

$$K_2 = 5.53 \times 10^{-5} T - 0.015897 \qquad 8.10$$

The activation energy and the frequency factor of the system were similar to previously determined values, 38 kJ mol^{-1} and 4.7 × 10^7 respectively. Therefore, the effect of temperature can be incorporated into Equation 8.9 as shown in Equation 8.11. The

Equation predicts experimental data to an accuracy of 92 % on the average as shown by the dotted lines in Figure 8.2(a)

$$f_{\text{q-model}} = \frac{4.67\times10^{7}\exp\left(-\frac{3810}{RT}\right)}{1+\frac{0.01014}{[Fe^{2+}]}+(5.53\times10^{-5}T-0.015897)\frac{[Fe^{3+}]}{[Fe^{2+}]}} \qquad 8.11$$

where T is in Kelvin scale.

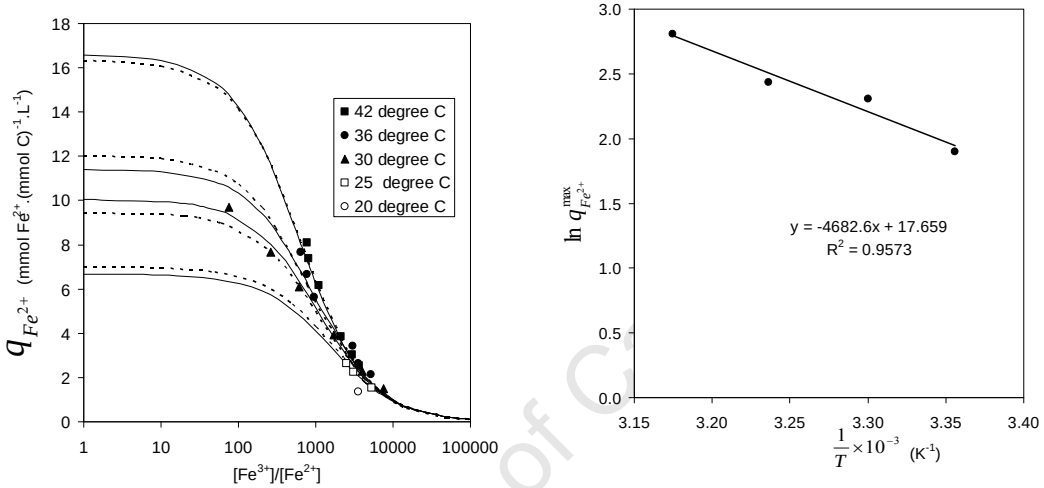

(a) $q_{Fe^{2+}}$ versus ferric-to-ferrous ratio

(b) $q^{max}_{Fe^{2+}}$ versus 1/T

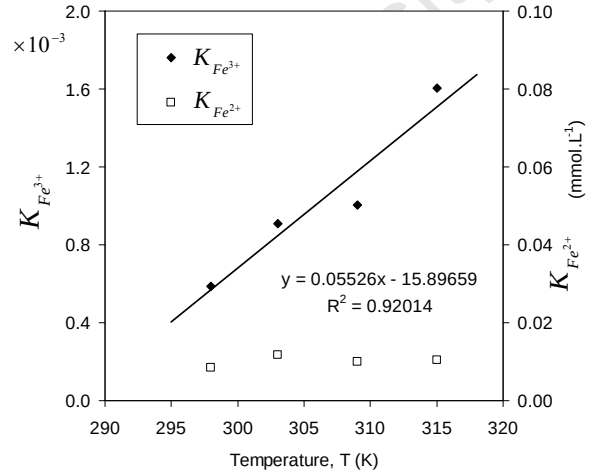

(c) $K_1(=K_{Fe^{2+}})$ and $K_2(=K_{Fe^{3+}})$ versus temperature

Figure 8.2 Kinetic parameters re-determined for the effect of temperature using the proposed q-model: Solid lines in (a) represents fits to Equation 8.9 using the kinetic constants in Table 8.1, and the dotted lines represent the fit of Equation 8.11

Chemical modelling was attempted using Visual MINTEQ by calculating the ionic activities, species distribution and saturation index from the measured redox potential (ferric-to-ferrous ratio) and solution pH. The species distribution table (Table 8.2) shows that the percentage of free substrate increases while free ferric iron decreased with increasing temperature. It can be inferred that these species may not be the only contributors to the measured solution potential and that the microbial cells are capable of oxidizing not only free the ferrous-iron but also other ferrous-iron species, due to the huge difference in the measured redox potential and the calculated if only free ions were considered. The decrease in the free ferric-iron concentration with increasing temperature (see Table 8.2) could be used to explain the corresponding increase in $q_{Fe^{2+}}^{\max}$ possibly due to decrease in resulting ferric inhibition which is contrary to what K_2 suggests. This contradiction cannot be explained.

The chemical modelling also showed that the ferric-iron would precipitate as goethite, hematite, K-jarosite even at 18°C with H-jarosite precipitating from 42°C as shown by their saturation indices (see Table 8.2), goethite and hematite are not expected to be formed as their formation is kinetically slow. It should be noted that chemical modelling performed using computer codes only provides an indication of the tendency for a reaction to occur, it does not prove the presence or absence of such reaction or phase.

The modelling also showed that about 18% of the total iron precipitated as ferric-iron, which accounted for almost all the potassium ion in the growth medium. However, a maximum of about 3% iron was lost due to precipitation in this study. The modelling made use of thermodynamic data in the calculation. The possibility of such a huge precipitate might occur, if the experiment were left to run for several months.

The insignificant increase in ferrous-iron concentration (8%) as a result of temperature increase from 18 to 45°C (see Table 8.2) might be used to explain why the substrate affinity constant, K_1 remained almost constant as the temperature increases. On the other hand, the speciation does not suggest any significant effects that would explain the variation of ferric inhibition constant (associated with K_2) with temperature.

Table 8.2 Effect of temperature on distribution of selected aqueous species and saturation indices for *L. ferriphilum* culture at ferric-to-ferrous ratio of 1000, calculated using Visual MINTEQ

Component*	Species name / Temperature	% of total component concentration					
		18	20	30	36	42	45
K^+	K^+	93.10	93.05	92.90	92.92	93.02	93.10
(0.498)	KSO_4^-	6.90	6.95	7.10	7.08	6.98	6.90
Fe^{2+}	Fe^{2+}	57.98	58.18	59.63	60.86	62.35	63.18
(0.012)	$FeSO_{4\ (aq)}$	42.02	41.82	40.37	39.14	37.66	36.82
Fe^{3+}	Fe^{3+}	5.77	5.61	5.00	4.76	4.60	4.55
(11.99)	$FeOH^{2+}$	0.18	0.19	0.23	0.27	0.31	0.33
	$Fe_2(OH)_2^{4+}$	0.02	0.03	0.04	0.06	0.08	0.10
	$FeSO_4^+$	80.42	81.05	83.94	85.43	86.75	87.34
	$Fe(SO)_4^{2-}$	13.61	13.12	10.79	9.48	8.26	7.68
SO_4^{2-}	SO_4^{2-}	11.94	11.65	10.19	9.31	8.44	8.02
(32.87)	HSO_4^-	19.08	19.61	22.34	24.01	25.67	26.50
	$FeSO_{4\ (aq)}$	0.03	0.03	0.03	0.03	0.02	0.02
	$FeSO_4^+$	50.44	50.84	52.65	53.59	54.42	54.79
	$Fe(SO)_4^{2-}$	17.08	16.46	13.54	11.90	10.36	9.64
	KSO_4^-	0.26	0.26	0.26	0.26	0.26	0.26
	$NH_4SO_4^-$	1.18	1.15	1.00	0.91	0.82	0.78
NH_4^+	NH_4^+	88.73	89.00	90.41	91.26	92.10	92.51
(0.64)	$NH_4SO_4^-$	11.28	11.00	9.59	8.74	7.90	7.49
*Saturation indices for solid phases***							
$Fe(OH)_2$		-30.45	-30.34	-29.79	-29.48	-29.17	-29.03
$Fe_3(SO_4)_3$		-9.30	-9.07	-7.98	-7.37	-6.79	-6.51
$Fe_3(OH)_8$		-20.50	-20.53	-20.66	-20.72	-20.77	-20.79
Ferrihydrite	$Fe_5O_3(OH)_9$	-5.17	-4.95	-3.91	-3.31	-2.71	-2.43
Goethite	$FeOOH$	0.04	0.10	0.39	0.56	0.72	0.81
Hematite	Fe_2O_3	2.44	2.57	3.19	3.56	3.92	4.10
H-Jarosite	$HFe_3(SO_4)_2(OH)_6$	-2.25	-2.05	-1.07	-0.51	0.03	0.29
K-Jarosite	$KFe_3(SO_4)_2(OH)_6$	3.11	3.17	3.43	3.58	3.73	3.80
Lepidocrocite	$\gamma - Fe^{3+}O(OH)$	-0.59	-0.60	-0.67	-0.70	-0.73	-0.74
Maghemite	Fe_2O_3	-4.82	-4.85	-4.98	-5.05	-5.10	-5.13
Magnetite	$Fe^{2+}Fe_2^{3+}O_4$	-4.56	-4.33	-3.24	-2.60	-1.98	-1.68
Melanterite	$FeSO_4.7H_2O$	-4.07	-4.11	-4.29	-4.40	-4.51	-4.57

* Figures in the bracket represent actual concentration in $g.L^{-1}$

**Positive and negative values indicate over saturation and undersaturation respectively while SI =0 represents apparent equilibrium

8.2.2 Effect of solution pH

It can be seen from the re-analysed kinetic parameters shown in Figure 8.3 that the predicted specific ferrous-iron utilisation rate ($q_{Fe^{2+}}^{max}$) values by the proposed model are approximately equal to the values previously determined in Chapter 5, using the simplified ferric inhibition model (Equation 3.15). This is also shown in Table 8.3. However, the affinity constant (=K_1) increases with solution pH, this implies a decreasing cell affinity for the substrate as the solution pH increases – corroborating the fact that microbial activity of bioleaching microorganisms decreases with increasing pH (du Plessis *et al.*, 2007; van Aswegen *et al.*, 2007)

Table 8.3 Comparison of kinetic parameters of Hansford model and the proposed q-model for the study on the effect of solution pH

pH	q-model				Simplified ferric inhibition model		
	$q_{Fe^{2+}}^{max}$	K_1	K_2	R^2	$q_{Fe^{2+}}^{max}$	$K'_{Fe^{2+}}$	R^2
0.80	9.76	0.091	0.00025	0.99	9.75	0.00067	0.99
1.00	13.15	0.097	0.00036	0.99	13.14	0.00081	0.99
1.30	14.41	0.116	0.00081	1.00	14.42	0.00135	1.00
1.60	11.10	0.050	0.0010	1.00	10.48	0.00113	1.00
2.00	11.65	0.126	0.0040	0.99	11.64	0.00457	0.99

Units: $q_{Fe^{2+}}^{max}$ [mol Fe^{2+} (molC h)$^{-1}$], K_2 & $K'_{Fe^{2+}}$ are dimensionless, K_1 [mmol Fe^{2+} L^{-1}]

The data point at pH 1.6 has to be treated with caution. It was taken as an outlier as it only introduced an error of 9%, when manipulated to fit as shown in Figure 8.3c (see error analysis in Appendix E, Table E1.4), or it possibly indicated an effect which cannot be explained in this analysis. Also accepting $q_{Fe^{2+}}^{max}$ at pH 1.6 as an outlier could explain the assumed constant value of $q_{Fe^{2+}}^{max}$ (also plotted on Figure 8.3b) reported by Breed *et al.*(1999a) when similar experiment was carried out within a narrow pH range of 1.1 – 1.7. The analysis also showed that constant K_2 increases exponentially with increasing pH as shown in Figure 8.3d (This corresponds to decrease in inhibition constant $K_{Fe^{3+}}$ with increasing pH).

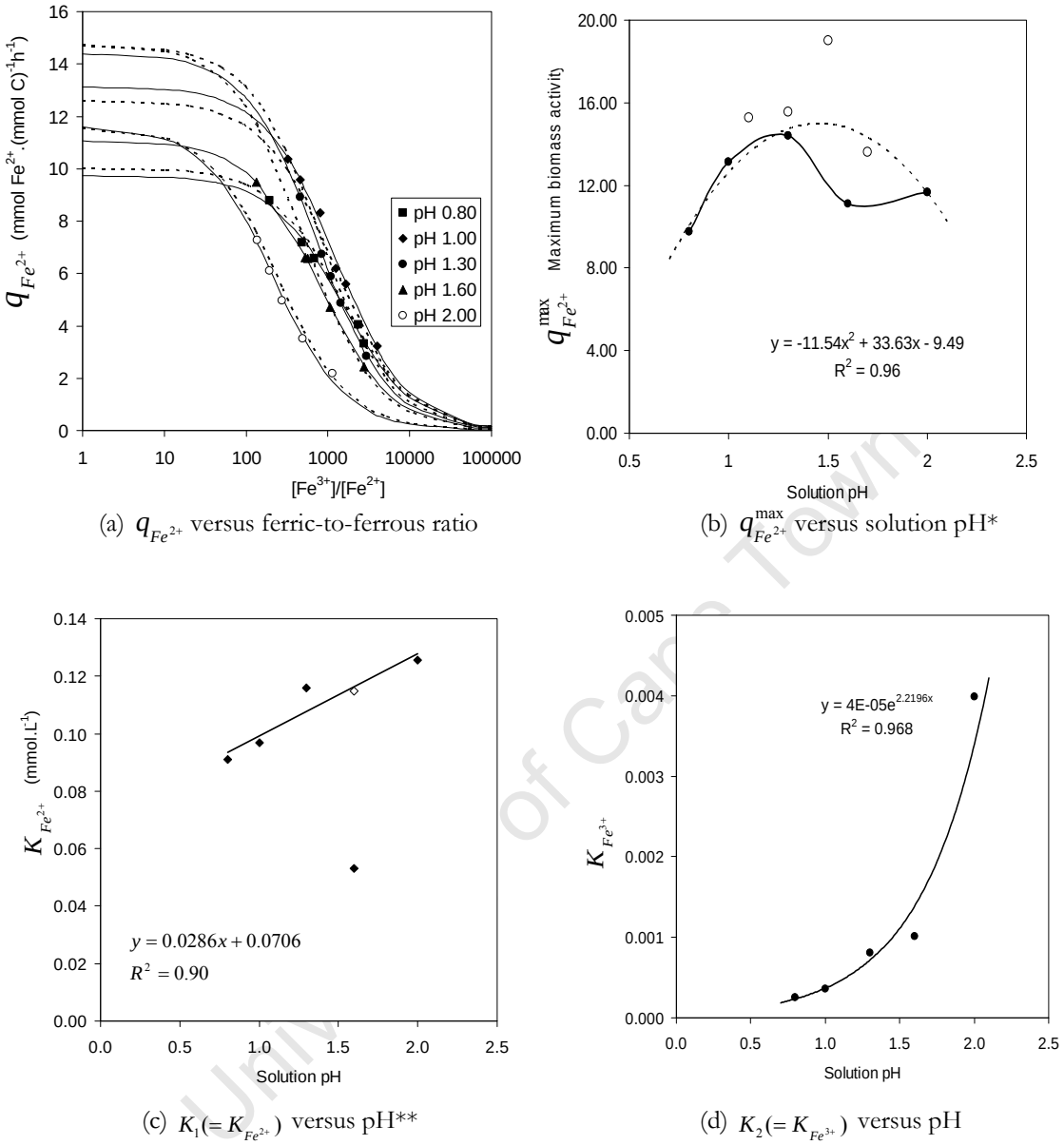

(a) $q_{Fe^{2+}}$ versus ferric-to-ferrous ratio

(b) $q^{max}_{Fe^{2+}}$ versus solution pH*

(c) $K_1(=K_{Fe^{2+}})$ versus pH**

(d) $K_2(=K_{Fe^{3+}})$ versus pH

Figure 8.3 Kinetic parameters re-determined for the effect of temperature using the proposed q-model: Solid lines in (a) represents fits to Equation 8.9 using the kinetic constants in Table 8.3, and the dotted lines represent the fit of Equation 8.12
* open circle in (b) represents Breed et al. (1999a) data
** open diamond in (c)represents manipulated data

Therefore, the effect of solution pH can be incorporated into Equation 8.9 as shown in Equation 8.12. The Equation predicts experimental data to an accuracy of less than 8% average error, as shown by the dotted lines in Figure 8.3. Although the $q^{max}_{Fe^{2+}}$ is

overestimated by the q-model due to the assumption of an outlier data point, the model predicted the experimental data with an average percentage error of 10.92%.

$$f_{\text{q-model}} = \frac{33.63\,pH - 11.54(pH)^2 - 9.49}{1 + \dfrac{0.0286\,pH + 0.0706}{[Fe^{2+}]} + 4\times10^{-5}e^{2.22\,pH}\dfrac{[Fe^{3+}]}{[Fe^{2+}]}} \qquad 8.12$$

The chemical modelling revealed a significant, decreasing trend in the percentage of free Fe^{2+} and Fe^{3+} species with increase in pH from 0.8 to 2.0, with a consequent increase in the sulphate species, $Fe(SO)_4^{2-}$, responsible for jarosite formation (see Table 8.4). The significant decrease in $[Fe^{2+}]/[FeSO_4]$ ratio with increasing pH could serve as a possible explanation for the decreasing affinity of the microbial cell for ferrous-iron as revealed by increasing K_1 value as pH increases. The calculated saturation indices revealed that the oversaturation of the solution with respect to goethite, hematite, H-jarosite and K-jarosite increase with increasing solution pH, however, goethite and hematite are not expected to be predominant components of the precipitate, as they are only significant at higher pHs (Shum and Lavkulich, 1999).

The modelling shows the tendency for about 15% of iron lost through K-jarosite formation at pH 0.8, which increased to about 87.3% of at pH 2.0 (see Table 8.5) accounting for all the potassium present in the feed medium. However, the actual experiment showed that ferric precipitation is negligible at pH 0.8 and that only about 14% of total iron was lost due to jarosite formation at pH 2.0 (see Chapter 5), the simulation was based on thermodynamic data as previously stated, it does not explain the kinetic feasibility of the process. However, at higher solution pH, large scale precipitation could be possible in actual heap bioleach operations since the operation could last for several months.

Table 8.4 Effect of solution pH on distribution of selected aqueous species and saturation indices for L. ferriphilum culture at ferric-to-ferrous ratio of 1000, calculated using Visual MINTEQ

Component*	Species name	Percentage of total component concentration				
		pH0.8	pH1.0	pH1.3	pH1.6	pH2.0
NH_4^+	NH_4^+	96.05	94.44	91.32	84.79	75.52
(0.64)	$NH_4SO_4^-$	3.95	5.56	8.68	15.21	24.48
Fe^{2+}	Fe^{2+}	78.08	70.86	59.49	43.15	30.20
(0.012)	$FeSO_{4\ (aq)}$	21.92	29.14	40.51	56.85	69.80
Fe^{3+}	Fe^{3+}	9.78	6.80	4.05	1.95	1.00
(11.99)	$FeOH^{2+}$	0.20	0.22	0.27	0.26	0.33
	$Fe_2(OH)_2^{4+}$	0.03	0.04	0.05	0.03	0.01
	$FeSO_4^+$	86.06	87.24	86.51	81.53	72.55
	$Fe(SO)_4^{2-}$	3.93	5.70	9.13	16.23	26.10
SO_4^{2-}	SO_4^{2-}	4.38	6.28	9.99	22.53	49.84
(32.87)	HSO_4^-	41.70	38.00	30.64	35.10	30.43
	$FeSO_{4\ (aq)}$	0.02	0.02	0.03	0.05	0.07
	$FeSO_4^+$	48.97	48.70	48.19	28.78	9.09
	$Fe(SO)_4^{2-}$	4.47	6.37	10.17	11.46	6.54
	KSO_4^-	0.02	0.00	0.00	0.00	
	$NH_4SO_4^-$	0.44	0.63	0.98	2.09	4.02
K^+	K^+	96.52	95.10	92.32	86.44	77.91
(0.498)	KSO_4^-	3.48	4.90	7.68	13.56	22.09
*Saturation indices for solid phases***						
$Fe(OH)_2$		-30.98	-30.25	-29.17	-28.11	-26.66
$Fe_3(SO_4)_3$		-7.14	-6.98	-6.79	-6.65	-6.54
$Fe_3(OH)_8$		-24.00	-22.72	-20.77	-18.78	-15.98
Ferrihydrite	$Fe_5O_3(OH)_9$	-5.05	-4.11	-2.71	-1.25	0.814
Goethite	$FeOOH$	-0.44	0.02	0.72	1.45	2.49
Hematite	Fe_2O_3	1.59	2.51	3.92	5.38	7.45
H-Jarosite	$HFe_3(SO_4)_2(OH)_6$	-2.15	-1.27	0.03	1.34	3.14
K-Jarosite	$KFe_3(SO_4)_2(OH)_6$	1.06	2.13	3.73	5.33	7.50
Lepidocrocite	$\gamma - Fe^{3+}O(OH)$	-1.90	-1.43	-0.73	0	1.03
Maghemite	$\gamma - Fe_2O_3$	-7.43	-6.51	-5.10	-3.643	-1.58
Magnetite	$Fe^{2+}Fe_2^{3+}O_4$	-5.21	-3.93	-1.98	0.01	2.81
Melanterite	$FeSO_4.7H_2O$	-4.76	-4.65	-4.51	-4.42	-4.35

* Figures in the bracket represent actual concentration in $g.L^{-1}$

**Positive and negative values indicate over saturation and undersaturation respectively while SI =0 represents apparent equilibrium

Table 8.5 Amount (Percentage) of iron predicted to be lost at various pH due to ferric precipitation as jarosite using the visual MINTEQ

Component	Percentage precipitated at indicated pH				
	pH 0.8	pH 1.0	pH 1.3	pH 1.6	pH 2.0
Fe^{2+}	0	0	0	0	0
Fe^{3+}	14.98	17.53	17.79	57.18	87.31
H^{+}	0	0	0	0	0
K^{+}	84.13	98.49	99.96	99.989	99.995
NH_4^{+}	0	0	0	0	0
SO_4^{-}	6.26	7.33	7.44	23.91	36.51

8.2.3 Effect of dissolved cations

The re-analysed kinetic parameters using the q-model (Equation 8.9) predicted the $q_{Fe^{2+}}^{max}$ values similarly like the Hansford model (Equation 3.15) as shown in Figure 8.4 and Table 8.6. The results revealed decreasing microbial affinity for the substrate as the ionic strength due to dissolved cation increases, this is shown by an exponential increase in affinity constant K_1 (see Figure 8.4d). This effect has been explained in chapter 6. The decreasing substrate affinity with increase in ionic strength could also be interpreted to mean the decreasing ferrous-iron concentration shown in the chemical modelling result (see Table 8.8). The constant K_2 decreased with increasing dissolved cation (corresponding to increasing ionic strength, IS), which implied that the microbial ability to withstand ferric inhibition increases or that the inhibitory effect of ferric decreases as shown by the increase in the corresponding ferric inhibition constant, $K_{Fe^{3+}}$ with increasing ionic strength.

The reduction in K_2 could also be explained by the decreasing ferric-iron concentration with increase IS as shown in Table 8.8. However the decreasing substrate affinity constant is comparable to the expected decrease in reaction rate (rate constant *k*) with increasing ionic strength from basic chemical reaction stand point using Debye-Huckel principle (Atkins and Paula, 2002; Laidler and Meiser, 1982) in a typical catalysed chemical reaction (see Section 2.12.2)

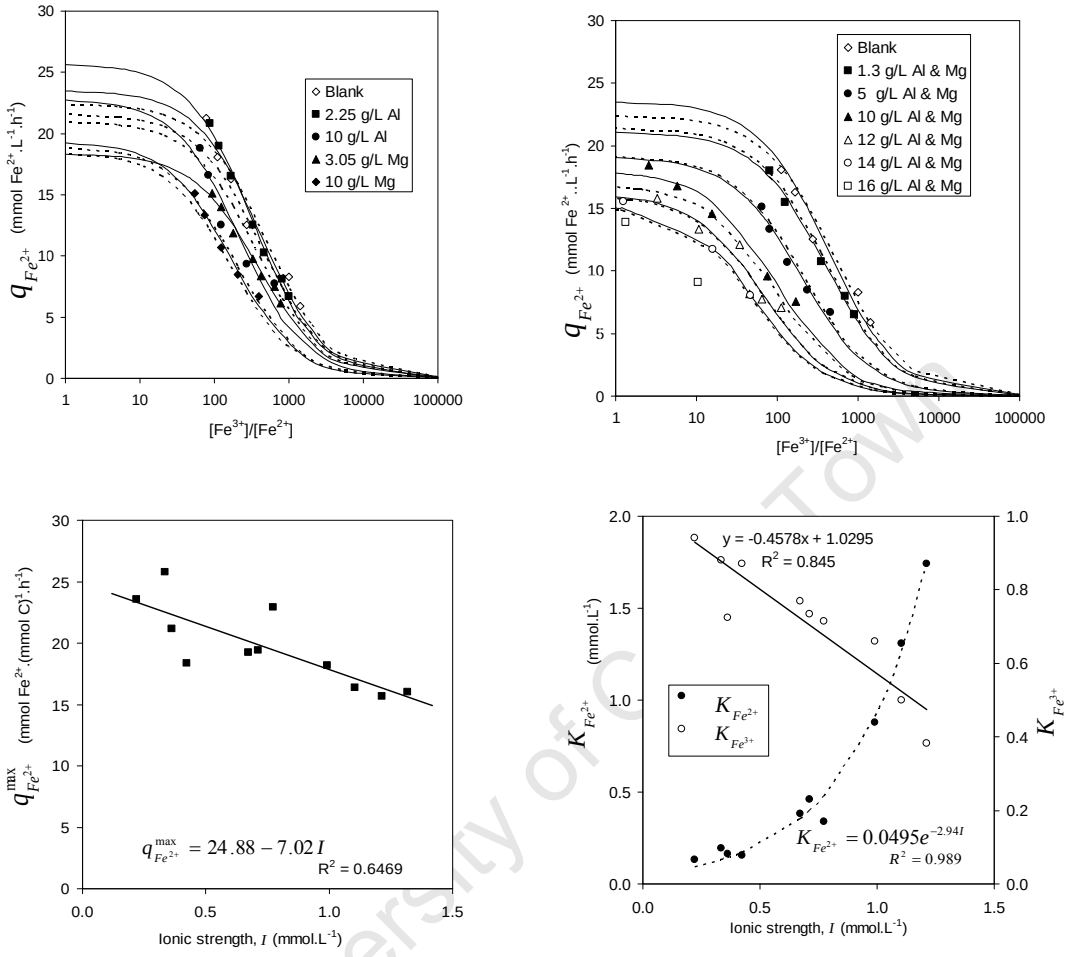

(c) $(q^{max}_{Fe^{2+}})$ versus ionic strength

(d) $K_1 (= K_{Fe^{2+}})$ and $K_2 (= K_{Fe^{3+}})$ versus strength

Figure 8.4 Kinetic parameters re-determined for the effect of dissolved cations using the proposed q-model: Solid lines in (a) represents fits to Equation 8.9 using the kinetic constants in Table 8.6, and the dotted lines represent the fit of Equation 8.13

Although the redox potential also decreased as discussed previously (implying that ferric concentration decreases), the increased IS caused by dissolved (Al and Mg) inhibited the cell rather than removing iron by forming precipitate. This can be inferred from result obtained from the chemical modelling that the saturation indices of all possible Al and Mg complexes other than goethite, hematite and K-jarosite to be negative (see Table 8.8) at ferric-to-ferrous-iron ratio of 500 indicating that even if formed, are soluble.

The modelling results also show that while iron was lost due to K-jarosite formation (Table 8.8), the percentage loss decreased with increasing IS. This may indicate increased inability of the cell to oxidise the substrate thus reducing ferric-iron available for jarosite formation. This supports the fact that the decreased redox potential due to increasing TDS was due to decreasing oxidising ability of the microbe rather than removal of iron due to precipitation as discussed earlier in Chapter 6.

Therefore, by substituting the expression for K_1 and K_2 in Equation 8.9, the specific ferous-iron oxidation rate can be predicted with respect to the resulting ionic strength due to dissolved Al and Mg according to Equation 8.13

$$f_{\text{q-model}} = \frac{24.88 - 7.02I}{1 + \frac{0.0494e^{-2.94I}}{[Fe^{2+}]} + (1.03 - 0.458)\times 10^{-3} I \frac{[Fe^{3+}]}{[Fe^{2+}]}} \qquad 8.13$$

Table 8.6 Comparison of kinetic parameters of Hansford model and the proposed q-model for the study on the effect of ionic strength due to added Al and/or Mg sulphates

Ionic strength	TDS	q-model				Simplified ferric inhibition model		
		$q_{Fe^{2+}}^{max}$	K_1	K_2 (x10^{-3})	R^2	$q_{Fe^{2+}}^{max}$	$K'_{Fe^{2+}}$	R^2
0.2197	Blank	23.58	0.133	0.94	0.959	23.55	0.0024	0.995
0.3355	2.25 g/L Al	25.76	0.195	0.88	0.993	24.68	0.0028	0.990
0.3631	1.3 g/l Al & Mg	21.15	0.165	0.73	0.991	21.11	0.0026	0.991
0.4223	3.05 g/L Mg	18.38	0.157	0.87	0.982	18.35	0.0026	0.982
0.6723	5 g/l Al & Mg	19.22	0.385	0.77	0.961	19.14	0.0050	0.961
0.7111	10 g/L Mg	19.44	0.460	0.73	0.975	19.35	0.0058	0.975
0.7715	10 g/L Al	22.91	0.340	0.72	0.894	22.82	0.0046	0.896
0.991	10 g/l Al & Mg	18.16	0.880	0.66	0.966	17.98	0.0104	0.965
1.1044	12 g/l Al & Mg	16.39	1.310	0.50	0.908	16.16	0.0149	0.907
1.2128	14 g/l Al & Mg	15.65	1.741	0.38	0.987	15.35	0.0194	1.000
1.3174	16 g/l Al & Mg	16.03	5.976	0.50	1.000	15.03	0.0630	1.000

Units: $q_{Fe^{2+}}^{max}$ [mol Fe^{2+} (molC h)$^{-1}$], K_2 & $K'_{Fe^{2+}}$ are dimensionless, K_1 [mol Fe^{2+}.L^{-1}]

Table 8.7 Amount (percentage) of iron predicted to be lost due to ferric precipitation as jarosite at various ionic strength using the visual MINTEQ

Component		Al^{3+}	Fe^{2+}	Fe^{3+}	H^+	K^+	Mg^{2+}	NH_4^+	SO_4^{2-}
Blank	0.22	0	0	42.43	0	99.23		0	16.38
1.3 g/l Al & Mg	0.36	0	0	42.132	0	98.53	0	0	8.96
5 g/l Al & Mg	0.67	0	0	41.6	0	97.29	0	0	3.89
10 g/l Al & Mg	0.99	0	0	41.216	0	96.39	0	0	2.19
12 g/l Al & Mg	1.10	0	0	41.12	0	96.17	0	0	1.86
14 g/l Al & Mg	1.21	0	0	41.05	0	96.00	0	0	1.62
16 g/l Al & Mg	1.32	0	0	40.996	0	95.87	0	0	1.44

Table 8.8 Effect of dissolved Al and Mg on distribution of selected aqueous species and saturation indices for L. ferriphilum culture at ferric-to-ferrous ratio of 500, calculated using Visual MINTEQ

Component*	Species name	Percentage of total component concentration						
		Blank	1.3[a]	5[a]	10[a]	12[a]	14[a]	16[a]
NH_4^+	NH_4^+	95.27	92.56	88.06	84.75	83.86	83.14	82.56
(0.64)	$NH_4SO_4^-$	4.73	7.44	11.94	15.25	16.14	16.86	17.44
Al^{3+}	Al^{3+}	0.00	12.14	5.24	2.38	1.85	1.48	1.20
	$AlSO_4^+$	0.00	51.13	42.85	37.43	36.10	35.05	34.22
	$Al(SO_4)_2^-$	0.00	36.73	51.91	60.19	62.06	63.48	64.58
Fe^{2+}	Fe^{2+}	71.60	64.24	51.55	41.50	38.61	36.15	34.01
(0.00998)	$FeSO_4$ (aq)	28.40	35.76	48.45	58.50	61.39	63.86	65.99
Fe^{3+}	Fe^{3+}	6.64	5.01	2.51	1.27	1.01	0.83	0.69
(4.99)	$FeOH^{2+}$	0.50	0.33	0.18	0.11	0.10	0.09	0.08
	$Fe_2(OH)_2^{+4}$	0.08	0.04	0.01	0.00	0.00	0.00	0.00
	$FeSO_4^+$	87.94	86.88	84.57	82.20	81.48	80.88	80.39
	$Fe(SO_4)^{2-}$	4.85	7.75	12.73	16.42	17.40	18.20	18.85
Mg^{2+}	Mg^{2+}	0.00	71.77	60.09	50.09	47.09	44.48	42.17
	$MgSO_4$ (aq)	0.00	28.24	39.91	49.91	52.91	55.52	57.83
SO_4^{2-}	SO_4^-	9.84	9.75	6.73	4.22	3.58	3.06	2.63
	HSO_4^-	32.17	29.47	21.45	15.46	13.84	12.48	11.33
	$AlSO_4^+$	0.00	8.80	12.45	12.38	12.22	12.06	11.93
	$Al(SO_4)^{2-}$	0.00	12.64	30.18	39.81	42.01	43.70	45.04
	$FeSO_4$ (aq)	0.03	0.02	0.01	0.00	0.00	0.00	0.00
	$FeSO_4^+$	50.91	27.72	11.85	6.55	5.54	4.79	4.22
	$Fe(SO_4)^{2-}$	5.61	4.95	3.57	2.62	2.37	2.16	1.98
	$MgSO_4$ (aq)	0.00	5.39	12.87	18.32	19.87	21.21	22.38
	KSO_4^-	0.34	0.30	0.21	0.16	0.14	0.13	0.12
	$NH_4SO_4^-$	1.10	0.95	0.67	0.49	0.44	0.40	0.37
K^+	K^+	95.84	93.43	89.40	86.40	85.59	84.94	84.40
(0.498)	KSO_4^-	4.16	6.57	10.61	13.60	14.41	15.06	15.60

* Figures in the bracket represent actual concentration in g L^{-1}

Table 8.8 (Contd.) Effect of dissolved Al and Mg on distribution of selected aqueous species and saturation indices for L. ferriphilum culture at ferric-to-ferrous ratio of 500, calculated using Visual MINTEQ

*Saturation indices for solid phases***		Blank	1.3[a]	5[a]	10[a]	12[a]	14[a]	16[a]
$Al(OH)_3$ (am)			-9.35	-9.06	-8.92	-8.88	-8.84	-8.80
$Al(OH)_3$ (Soil)			-6.89	-6.60	-6.46	-6.42	-6.38	-6.35
Al2O3			-16.40	-15.82	-15.54	-15.46	-15.38	-15.30
Al4(OH)10SO4			-25.81	-24.42	-23.74	-23.54	-23.36	-23.20
AlOHSO4			-1.09	-0.57	-0.31	-0.24	-0.18	-0.12
Alunite			-5.62	-4.31	-3.64	-3.45	-3.28	-3.13
Boehmite			-7.06	-6.77	-6.63	-6.59	-6.55	-6.51
Brucite	$Mg(OH)_2$		-15.40	-14.86	-14.56	-14.47	-14.40	-14.34
Diaspore	$AlO(OH)$		-5.49	-5.21	-5.07	-5.02	-4.98	-4.95
Epsomite	$MgSO_4.7H_2O$		-2.08	-1.32	-0.89	-0.78	-0.68	-0.60
$Fe(OH)_2$		-29.13	-29.32	-29.45	-29.47	-29.47	-29.47	-29.46
$Fe_2(SO4)_3$		-7.75	-7.58	-7.36	-7.22	-7.18	-7.15	-7.12
$Fe_3(OH)_8$		-21.00	-21.55	-22.07	-22.32	-22.37	-22.40	-22.42
Ferrihydrite	$Fe_5O_3(OH)_9$	-2.97	-3.41	-3.87	-4.11	-4.15	-4.19	-4.23
Gibbsite (c)	$Al(OH)_3$		-6.34	-6.05	-5.91	-5.87	-5.83	-5.80
Goethite	$FeOOH$	0.60	0.37	0.14	0.02	0.00	-0.02	-0.03
Hematite	Fe_2O_3	3.67	3.21	2.75	2.52	2.47	2.44	2.41
Hercynite	$Fe^{2+}Al_2O_4$		-21.02	-20.51	-20.24	-20.15	-20.07	-19.99
H-Jarosite	$HFe_3(SO_4)_2(OH)_6$	-0.83	-1.09	-1.32	-1.42	-1.44	-1.45	-1.45
K-Alum	$KAl(SO_4)_2.12H_2O$		-4.93	-4.19	-3.80	-3.70	-3.61	-3.53
K-Jarosite	$KFe_3(SO_4)_2(OH)_6$	2.89	2.61	2.36	2.27	2.26	2.25	2.25
Lepidocrocite	$\gamma - Fe^{3+}O(OH)$	-0.86	-1.08	-1.31	-1.43	-1.45	-1.47	-1.49
Maghemite	$\gamma - Fe_2O_3$	-5.36	-5.81	-6.27	-6.50	-6.55	-6.59	-6.61
Magnesioferrite	$MgFe^{3+}_2O_4$		-13.02	-12.95	-12.88	-12.84	-12.80	-12.76
Magnetite	$Fe^{2+}Fe^{3+}_2O_4$	-2.21	-2.76	-3.28	-3.53	-3.58	-3.61	-3.63
Melanterite	$FeSO_4.7H_2O$	-4.73	-4.61	-4.45	-4.34	-4.31	-4.28	-4.26
$Mg(OH)_2$ (active)			-18.17	-17.63	-17.33	-17.25	-17.17	-17.11
Periclase	MgO		-19.53	-18.99	-18.69	-18.61	-18.53	-18.47
Spinel	$MgAl_2O_4$		-31.75	-30.63	-30.05	-29.88	-29.73	-29.59

[a] equal $g.L^{-1}$ of Al and Mg

**Positive and negative values indicate over saturation and undersaturation respectively while SI =0 represents apparent equilibrium

Equation 8.13 predicted the experimental data fairly accurately except for the effect due to individual cations. The higher rates at individual concentrations of Al can be attributed to the significant reduction of biomass under this condition while the lower rate at individual Mg concentration can be attributed to increased biomass. In both cases,

the rate of ferrous-iron oxidation did not change significantly. The predicted data and regression coefficients are shown in Appendix E, Table E1.5

8.2.4 Effect of total iron concentration

In addition to the modelling studies on the effect of total iron concentration discussed in Chapter 7, the fit of Equation 8.14 (derived by combining Equations 7.14 and 7.15) to the experimental q-data is shown in Figure 8.5 a. The equation did not fit the data particularly well ($0.85 < R^2 < 0.96$). The reason for this is due to the inherent error in the formulation of maximum specific ferrous-iron utilisation rate, $q_{Fe^{2+}}^{\max}$, which is represented by the numerator of Equation 8.14 as discussed in Section 7.4:

$$q_{Fe^{2+}} = \frac{q_{Fe^{2+}}^{\min} + q_{Fe^{2+}}^{excess} \exp\left(-a.[Fe^{3+}]\right)}{1 + \frac{K_1}{[Fe^{2+}]} + K_2 \frac{[Fe^{3+}]}{[Fe^{2+}]}} \qquad 8.14$$

This is not surprising as it can be seen from the significant difference between specific rates shown in Figure 7.15a. The steady state biomass concentrations at (especially at lower total iron) were significantly lower than the average values used for $q_{Fe^{2+}}^{\max}$ (calculated) as shown by their percentage variations.

A careful examination of the numerator (*i.e.* Equation 7.8) and Figure 7.15a shows that the model is sensitive to $q_{Fe^{2+}}^{excess}$ and a. However, any value of $q_{Fe^{2+}}^{\max}$ between the calculated value (using the average biomass concentration) and that value determined the simplified model is considered acceptable. The values choosen is shown by solid line in Figure 8.5a. Thus, $q_{Fe^{2+}}^{excess}$ and a values changed significantly while the minimum energy need for the cell to remain viable, $q_{Fe^{2+}}^{\min}$, remained unchanged, which would expected. Thus the new set of $q_{Fe^{2+}}^{\max}$ model parameters are:

$q_{Fe^{2+}}^{\min}$ = 16.15 mmol Fe^{2+} (mmol C)$^{-1}$ h^{-1}
$q_{Fe^{2+}}^{exess}$ = 49.43 mmol Fe^{2+} (mmol C)$^{-1}$ h^{-1}
a = 0.025 L (mmol Fe^{2+})$^{-1}$

The plot of Equation 8.14 using the above parameters is shown in Figure 8.5b. The regression analysis of the predicted values shows that Equation 8.14 predicts the

experimental data fairly well, at least within the limit of experimental error (See Table E 1.10). Figure 8.5b clearly confirmed the theoretical analysis discussed in Section 8.2, showing the two regions where substrate effect and ferric inhibition are predominant. The Figure suggests that $q_{Fe^{2+}}^{\max}$ is the same irrespective of the total-iron concentration, this is expected ideally, especially since the culture is not under any substrate limitation and ferric-iron inhibition is removed in this region.

However, there is need for further studies in the region of low redox potential in order to complement this study. This is beyond the scope of work

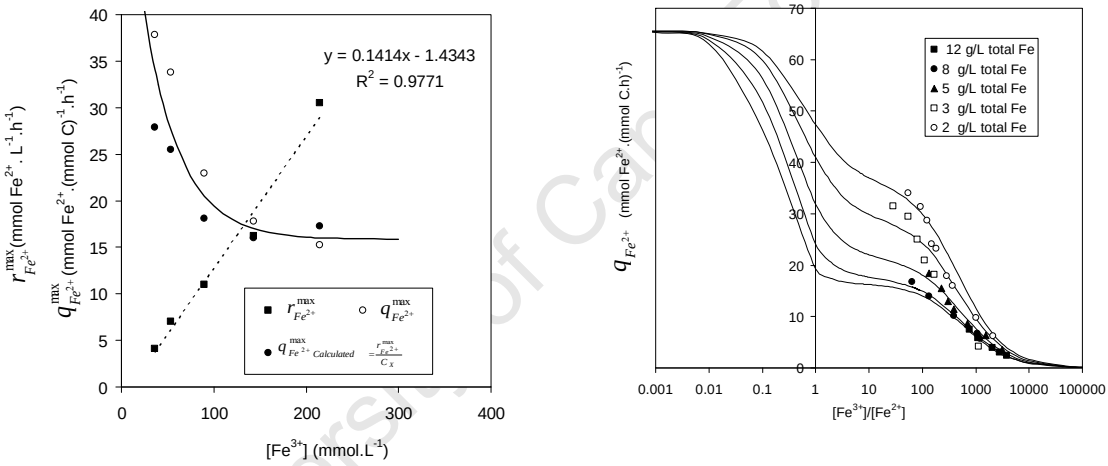

Figure 8.5: (a) the plot of maximum rate and maximum specific rate with ferric-iron concentration (b) Plot of $q_{Fe^{2+}}$ versus ferric-to-ferrous ratio [the solid line represent the plot of (a) Equation 7.8 and (b) Equation 8.14 with [Fe^{3+}] and ferric-to-ferrous ratio respectively; dotted line represent the fit of maximum ferrous oxidation rate]

8.3 Discussion of analysis

A number of factors affect the microbial ferrous-iron oxidation in a typical bioleach system. The overall effect of the combination of these factors on microbial ferrous-iron oxidation is rather complex to resolve. From the foregoing studies, the thermodynamics analyis of the simulation studies has shown that these effects (*i.e.* pH, temperature, ionic strength) influence the iron speciation. Although the chemical modelling could explain the fairly constant substrate affinity constant, K_1 with increasing temperature, the speciation cannot be used to explain the variation of ferric inhibition parameter. The

chemical modeling also revealed decrease of free [Fe^{2+}] ions as pH and ionic strength (due to added salts) increase (see Table 8.4 and Table 8.8). In these cases, the microbial substrate affinity decreased. Also, the inhibition due to ferric-iron decreased as the pH and IS increase as shown by the corresponding decrease in the available free [Fe^{3+}] ions. However, the observed decrease in biomass activities` as determined by $q_{Fe^{2+}}^{max}$ were due to the the inhibitory effects of the added salt (Al– and Mg– salts) (Bruins *et al.*, 2000; Nies and Silver, 1995; Shiers *et al.*, 2005) and the decreasing acidity of the environment (van Aswegen *et al.*, 2007).

Increasing temperature increased the maximum specific ferrous-iron oxidation rate. Although $q_{Fe^{2+}}^{max}$ increseases with temperature within the region studied, the result showed that at higher temperatures (*i.e.* greater than 42°C) microbial activity measured by $q_{Fe^{2+}}^{max}$ was significantly retarded as the culture cannot be cultivated under a countinuous mode. The same was observed at lower (less than 20 °C) temperatures. At temperatures outside the "normal physiological" range, be it higher or lower temperature, the effect is such that it denatures the enzyme/protein system of the bacteria (De los Rios and Caldarell, 2000; Privalov, 1990). The mode of denaturation is through unfolding of proteins within the bacteria, which causes hydrophobic hydration of the non-polar components in the proteins. This results in conformational changes in the enzyme structure that expose hydrophobic amino acid groups to the surrounding water molecules (Ratkowsky *et al.*, 1982; Ratkowsky *et al.*, 2005).

Although the pH study revealed that lowest $q_{Fe^{2+}}^{max}$ was observed at pH 0.8, the value, 9.79 mmolFe^{2+}(mmolC.h)$^{-1}$ is greater than the reported values for *At. ferrooxidans* and *Leptospirilum-like* bacterial by Boon (1996) and van Scherpenzeel *et al.* (1998) respectively. Although a high acid environment is necessary for the bacteria respiratory process as a trans-membrane pH gradient is required to produce the protons needed to reduce CO_2 to cell mass. Acidophiles have mechanism to cope with pH fluctuations which is based on the cell wall/cytoplasmic membrane composition – the cell constituents within the membrane function by increasing the cell rigidity and decreasing cell membrane permeability and vice versa, thus the cell is able to maintain neutrality

with the cytoplasm. However, at very low pH (pH < 0.8), cell lysis may occur due to membrane instability.

Microbial activity was affected significantly by solution ionic strength due to added Al and Mg sulphate concentration. The fact that metals like Mg stabilise various enzymes and DNA may be responsible for the observed increase in biomass concentration at moderate concentrations of this cation. However, at higher concentrations, ionic strength imposes energy load on the microorganism to control influx of these metals due to the resultant higher osmotic gradient existing between the cell cytoplasm and the environments(Blight and Ralph, 2004; Bruins *et al.*, 2000). The toxicity action of these metals is through the displacement of essential metals from their native binding sites or through ligand interaction, which often results into distruption of cellular functions and damage of DNA structure (Bruins *et al.*, 2000).

The overall effect of wide changes in solution conditions investigated constitutes an adverse condition. The increased biomass concentration observed at low temperatures (less than 42°C) and at higher pHs (greater than pH 1.3) is similar to the effect of increasing ferric-iron concentration on cell concentration observed in Chapter 7. This can also be used to support the conceptual 'sharing' mechanism of metabolic function postulated in Chapter 7. That is, the tendency of microorganisms to increase their cell numbers in order to cope with adverse conditions and the concomitant decrease in $q_{Fe^{2+}}^{\max}$.

This study has revealed that maximum microbial activity measured by the maximum specific microbial substrate utilisation rate is dependent on all the factors investigated (temperature, pH, salt and total iron concentration). The parameter K_1, the substrate affinity, in Equation 8.9 is function dependent on solution pH ionic strength while K_2 is dependent on temperature in addition to solution pH and ionic strength. The overall rate equation of the form of Equation 8.15 is proposed from Equations 8.11, 8.12, 8.13 and 8.14

$$f_{\text{q-model}} = \frac{q_{Fe^{2+}}^{\max}(T, pH, [Fe^{3+}], I)}{1 + \frac{K_1(pH, I)}{[Fe^{2+}]} + K_2(T, pH, I)\frac{[Fe^{3+}]}{[Fe^{2+}]}} \qquad 8.15$$

The exact functionality of each of these parameters cannot be determined at this stage, and need to be considered further. However, this study only considered the effect of individual factors, it does not consider the simultaneous effect of all the factors investigated.

Chapter 9

Conclusions and Recommendations

9.1 Conclusions

The objective of this work was to investigate and describe the kinetics of microbial ferrous-iron oxidation by *L. ferriphilum*, over a wide range of operating conditions, relevant to heap bioleach operations. This was achieved in the first instance by using a simplified equation, developed to describe the kinetics of *At. ferrooxidans,* but which has also been used for *Leptospirillum*–like mesophiles. The equation was applied to the data obtained from experimental investigations of the effects of temperature, solution pH, dissolved cations and total iron concentration on microbial ferrous-iron oxidation kinetics of *L. ferriphilum* in a continuous culture, with the view to developing an integrated model to describe the kinetics over wider ranges of these conditions than was previously done.

The microbial ferrous-iron oxidation was studied in a well-mixed and well-aerated continuous stirred tank bioreactor. The oxidation kinetics was monitored by measuring the redox potential and analysing the off-gas from the biorectors for oxygen and carbon dioxide. The ferrous-iron oxidation rate was determined from the gas consumption rates via the degree-of-reduction balance. A good agreement was found between the rate and that determined from the ferrous-iron balance over the bioreactor, which confirmed the validity of this methodology.

In all investigations, the observed kinetics could be described reasonably well by the simplified ferric inhibition equation describing the specific ferrous-iron utilisation rate as a function of ferric-to-ferrous ratio in the bioreactor (a proxy measure of redox potential), and coupled to biomas yield expression in terms of a maximum yield and maintenance coefficient as proposed by Pirt (1965). However, the study on the effect of total iron concentration on the microbial ferrous-iron oxidation kinetics showed that the kinetics could be better described by an equation of the form of Equation 8.1; which is similar to that proposed by Jones and Kelly (1983):

$$q_{Fe^{2+}} = \frac{q_{Fe^{2+}}^{\max}}{1 + \frac{K_1}{[Fe^{2+}]} + K_2 \frac{[Fe^{3+}]}{[Fe^{2+}]}} \qquad 8.1$$

Although both models predicted the experimental data accurately to the same degree of accuracy (shown by the correlation coefficients), the assumption made for the simplified model is not valid for *L. ferriphilum*, as the ratio $K_1/[Fe^{2+}]$ would be significant at the higher potentials *i.e.* low $[Fe^{2+}]$, thus contributing significantly to the denominator of Equation 8.1. Therefore, the values of K_1 and K_2 can be used as indicators of substrate affinity and product inhibition respectively, rather than the K-term in the simplified model, which, being a lumped parameter, cannot be used to predict microbial activity.

The effect of change in temperature on the system showed that, the oxidation can be described by a simple function of the kinetic constants in Equation 8.1, determined for each data set. The maximum specific ferrous-iron utilisation rate, $q_{Fe^{2+}}^{\max}$, increased exponentially with temperature as expressed by the Arrhenius Equation (Equation 4.5*a*) as described in Chapter 4. The maintenance coefficient, on the other hand can be described with a quadratic function, but is insignificant, as it is never more than 8% (mostly < 3%) of $q_{Fe^{2+}}^{\max}$ in all the experiments. Such low values are characteristic of an actively growing culture. The maximum biomass yield on ferrous, $Y_{Fe^{2+}X}^{\max}$, decreased, but insignificantly with increasing temperature. The substrate affinity constant K_1 remained constant with increasing temperature, while the inhibition function due to ferric-iron, K_2, increased and can be represented by a linear function as discussed in Section 8.2.1. Therefore, Equation 8.1 can be written as:

$$q_{Fe^{2+}} = \frac{k_0 \exp\left(-\frac{E_a}{RT}\right)}{1 + \frac{K_1}{[Fe^{2+}]} + (mT - d)\frac{[Fe^{3+}]}{[Fe^{2+}]}} \qquad 9.1$$

Where k_0 = 4.67 x 10^7 mol Fe^{2+} mol C^{-1} h^{-1} m = 5.53 x$10^{-5}K^{-1}$
E_a = 38.1 kJ mol^{-1} K_1 = 0.01014 mol Fe^{2+} L^{-1}
d = 0.0159

producing a rate equation capable of predicting the effect of change in temperature between 25 to 42°C on microbial ferrous-iron oxidation kinetics.

The study on the effect of solution pH showed that the maximum specific ferrous-iron utilisation rate, $q_{Fe^{2+}}^{\max}$, followed an inverse parabolic trend with solution pH, approaching a maximum at pH 1.3 within the range (0.8<pH<2.0) investigated. This pH also corresponds to the minimum maintenance coefficient. The maintenance coefficient can also be represented by a quadratic function of pH. The maximum microbial biomass yield increases linearly with increasing solution pH. The microbial affinity constant for ferrous-iron showed a decreasing trend with increase in pH and can be represented by a linear function of pH. The ferric inhibition constant however, increased exponentially, indicating that decrease in microbial activity beyond pH 1.6. The study also showed about 14% of the total iron were lost due to jarosite precipitation beyond pH 1.6, but this percentage could be much more as shown by the simulation result obtained using Visual Minteq. Thus, by substituting the expression for the constants in Equation 8.10, an expression of the form (Equation 9.3) can be written, which is capable of predicting the effect of change in solution pH on the ferrous-iron oxidation kinetics to a reasonable accuracy.

$$q_{Fe^{2+}} = \frac{q_{Fe^{2+}0}^{\max}\left(a_0 pH - (pH)^2 - a_1\right)}{1 + \frac{b_0 pH + b_1}{[Fe^{2+}]} + c_o e^{c_1 pH}\frac{[Fe^{3+}]}{[Fe^{2+}]}} \qquad 9.3$$

where $q_{Fe^{2+}0}^{\max}$ = 11.54, b_0 = 0.0286 mol Fe^{2+} mol C^{-1} h^{-1},
c_0 = 4x10^{-5} b_1 = 0.0706 mol Fe^{2+} mol C^{-1} h^{-1},
c_1 = 2.22, a_1 = 0.822
a_0 = 2.91,

The maximum specific ferrous-iron utilisation rate, $q^{max}_{Fe^{2+}}$, also show a decreasing trend with increasing solution ionic strength (IS) due to dissolved Al and Mg, represented by a linear expression of $q^{max}_{Fe^{2+}}$ in Equation 8.10. The inhibition due to increasing IS is reflected by the reduce microbial affinity for the substrate as shown by an exponential increase of the affinity constant (K_1). However, the result showed a decreasing trend in ferric-iron inhibition with increasing IS due to impaired oxidation as reflected by decreasing redox potential in the bioreactor. Although at low concentrations Mg appears to actually promote biomass growth, while Al is pernicious at all concentrations, the result indicated that Mg exhibited a cushioning for the Al effect, when both salts were combined. At extremely high salt concentrations (> 1 M ionic strength), microbial ferrous-iron oxidation appeared to be severely impaired. The maximum biomass yield, like the biomass concentration, decreased significantly with increasing IS. This can be expressed as a linear function of IS, while cell maintanance, though increased, cannot be expressed as a reasonable function due to the scattered plot. Equation 8.13 can be expressed in the form (Equation 9.4) to describe the effect of IS due to dissolved Al and Mg on the microbial ferrous-iron oxidation accurately.

$$q^{max}_{Fe^{2+}} = \frac{q^{max}_{Fe^{2+}TDS}(1-d_0 I)}{1+\frac{K_{10}e^{d_1 I}}{[Fe^{2+}]}+K_{20}(1-K_{21}I)\frac{[Fe^{3+}]}{[Fe^{2+}]}} \qquad 9.4$$

where $q^{max}_{Fe^{2+}TDS}$ = 24.00 molFe^{2+} mol C^{-1} h^{-1}, d_0 = 0.029 M^{-1},
K_{21} = 0.445 M^{-1}, K_{10} = 0.0494 mol Fe^{2+}mol C^{-1} h^{-1},
d_1 = 2.94 M^{-1}, K_{20} = 1.03

The study on the effect of total iron concentration has revealed that the biomass concentration of *L. ferriphilum* is strongly determined by the concentration of ferric iron in the bioreactor. Increased ferric-iron concentration due to increased total iron clearly stimulates cell growth and likewise the microbial ferrous-iron oxidation, which supplies the energy. However, the maximum specific ferrous-iron utilisation rate, $q^{max}_{Fe^{2+}}$, decreased with increasing ferric and total iron concentrations – this indicates that the energy requirement/demand per cell decreases. It follows that, at high ferric iron concentrations, individual cells might not fulfill all metabolic functions that require

energy, but might share some of these between a numbers of cells, although this requires further substantiation. A comprehensive Jones and Kelly-type rate Equation has been developed to describe the overall rate of microbial ferrous-iron oxidation in continuous culture in terms of ferric and ferrous iron concentrations. An expression, which predicts the average biomass concentration in a countinuous culture as a function of ferric-iron, was also developed. This predicts the experimental data accurately within the range of total iron concentration investigated.

The conceptual sharing mechanism can also be supported by increased biomass and the corresponding decline in maximum specific rates observed at low and high temperatures and pH respectively. The functionality of a comprehensive rate equation has been proposed to be of the form of Equation 8.15 to describe the rate of microbial ferrous iron oxidation in continuous culture of *L. ferriphilum*, entirely in terms of ferric and ferrous iron concentrations.

The implication of this study for heap is that the low level of iron in most heaps is sufficient to support high biomass activity and *Leptospirillum ferriphilum* is likely to be the dominant mesophile conrolling the ferrous-iron oxidation kinetics at 42 – 45°C. The solution pH of heap bioleach liquor can be kept low in order to conserve the magnial iron level. However, the concentration of dissolved cations (of Al and Mg) resulting from the dissolution of gangue minerals must be kept low by purging, as *L. ferriphilum* culture may under-perform in a heap environment which contains high concentrations of dissolved gangue minerals.

9.2 Recommendation for further studies

This study attempted to simulate solution and operating conditions (with parameters carefully chosen to extend beyond the narrow ranges where similar studies have been carried out) relevant to heap bioleach operation, and investigate their effects on microbial ferrous-iron oxidation kinetics. However, the work was limited in scope to a completely mixed and well-aerated continuous system. The complexities in a heap bioleach setup were not considered. Since the experiments were carried out in a well-aerated stirred tank bioreactor, the microbial oxidation kinetics were not affected by the concentration of oxygen and carbon dioxide. In heap bioleach scale, gas-liquid mass

transfer can be rate controlling. Therefore the study of the effect of oxygen and carbon dioxide concentrations on the kinetics needs to be investigated with respect to mass transfer limitations.

The bioreactor pH was controlled by adjusting the pH of the feed stream which was quite challenging as the set point also depended on the current biorector residence time. However, experiments performed at pH 1.6 and 2.0 required frequent downtimes for cleaning and removal of jarosite, which may affect the steady state data with respected to biomass concentration. Solution pH is an important parameter in microbial oxidation of ferrous-iron. However, while *L. ferriphilum* could be cultured continuously at pH below 1.00, this study did not investigate the effect on cell morphology vis-à-vis cell membrane stability. The cell maintains its cytoplasmic pH close to neutrality by controlling proton gradient – a function performed by the cell membrane. Further molecular study on the effect of solution pH on the stability of cell membrane would be essential.

Generally, for continuous culture operation, the dilution rate (or residence time) is the only manipulated parameter for controlling the solution redox potential (a proxy measure of ferric-to-ferrous ratio) in the bioreactor. The rate increases with increasing dilution rate, and it is not possible to obtain any data in the region low redox potential (where cell washout is likely to occur). A theoretical analysis (Section 8.1), supported with preliminary experimental investigation, has revealed that the product inhibition is insignificant in this region (*i.e.* low ferric-to-ferrous ratio). Further investigation of microbial ferrous-iron oxidation at low ferric-to-ferrous ratio (*i.e.* $[Fe^{3+}]/[Fe^{2+}]$) is necessary to complement existing knowledge.

In this study, the effects of different conditions (pH, temperature, dissolved cations and total iron) were investigated independently of one another, and the proposed equation was calibrated with data obtained from individual effect. However, in a real industrial scale bioleach heap situation, most of the effects are not separable. Therefore, further investigation into the study of how all these effects could be incorporated into a single rate equation is necessary. The form of a comprehensive rate equation that incorporates simultaneously all the effects investigated was proposed. The functional relationship between the parameters of the equation and these effects requires a further design of experiments in order to generate more data to complement the existing database provided by this study.

Chapter 10

Chapter 10 References

Acevedo, F., (2000). The use of reactors in biomining processes, *Electronic Journal of Biotechnology*, pp. 184-194.

Acevedo, F., (2002). Present and future of bioleaching in developing countries, *Electronic Journal of Biotechnology*, pp. 197-199.

Ahonen, L. and Tuovinen, O.H., (1989). Microbiological oxidation of ferrous-iron at low temperatures. *Appl Environ Microbiol.*, 55(2): 312 - 316.

Akcil, A., (2004). Potential bioleaching developments towards commercial reality: Turkish metal mining's future. *Minerals Engineering*, 17: 477 - 480.

Archer, K.H.L., (1997). Potential of thermophilic bioleaching, effect of temperature on the process performance, M.Sc. Thesis, University of Cape Town, Cape Town, 134 pp.

Atkins, P. and Paula, J.d., (2002). Atkins' Physical Chemistry. Oxford University Press, 35 pp.

Barrett, J., Hughes, M.N., Karavaiko, G.I. and Spencer, P.A., (1993). Metal Extraction by Bacterial Oxidation of Minerals. Ellis Horwood series in Inorganic Chemistry. Ellis Horwood Limited, England.

Bauer, W.D. and Robinson, J.B., (2002). Disruption of bacterial quorum sensing by other organisms. *Current Opinion in Biotechnology*, 13: 234 - 237.

Beck, J.V., (1960). *J. Bacteriol.*, 79: 502 - 509.

Blight, K.R. and Ralph, D.E., (2004). Effect of ionic strength on iron oxidation with batch cultures of chemolithptrophic bacterial. *Hydrometallurgy*, 73: 325 - 334.

Bockris, J.O.M. and Reddy, A.K.N., (1970). Modern Electrochemistry, 1. Macdonald & Co. Ltd, London, 175-266 pp.

Boon, M., (1996). Theoretical and Experimental Methods in the Modelling of Bio-oxidation Kinetics of Sulphide Minerals, PhD Thesis, Technical University, Delft, Netherlands, 453 pp.

Boon, M., (2001). The mechanism of 'direct' and 'indirect' bacterial oxidation of sulphide minerals. *Hydrometallurgy*, 62: 67 - 70.

Boon, M., Hansford, G.S. and Heijnen, J.J., (1995a). Recent developments in modelling bio-oxidation kinetics. Part II: Kinetic modelling of the bio-oxidation of sulphide minerals in terms of critical sub-processes involved. In: D.S. Holmes and R.W. Smith (Editors), Proceedings of Engineering Foundation Conference, July 1994. Minerals Bioprocessing II. The Minerals Metals and Materials Society, Salt Lake City, Warrendale, Pennsylvania, pp. 63 – 8.

Boon, M., Heijnen, J.J. and Hansford, G.S., (1995b). Recent developments in modelling bio-oxidation kinetics. Part I. Measurement methods. In: D.S. Holmes and R.W. Smith (Editors), Proceedings of Engineering Foundation Conference, July 1994. Minerals Bioprocessing II. The Minerals Metals and Materials Society, Salt Lake City, Warrendale, Pennsylvania, pp. 41 - 61.

Boon, M., Meeder, T.A., Thöne, C., Ras, C. and Heijnen, J.J., (1999a). The kinetic modelling of ferrous iron oxidation kinetics with Thiobacillus ferrooxidans in continuous cultures. *Appl. Microbiol. Biotechnol.*, 51: 820 - 826.

Boon, M., Ras, C. and Heijnen, J.J., (1999b). The ferrous iron oxidation kinetics of Thiobacillus ferrooxidans in batch cultures. *Appl. Microbiol. Biotechnol.*, 51: 813 – 819.

Braddock, J., Luong, H.V. and Brown, E.J., (1984). *Applied Environmental Microbiology*, 48: 48 – 55.

Brandl, H., (2001). Microbial leaching of metals. In: H.-J. Rehm (Editor), Biotechnology. Wiley-VCH, Weinheim, pp. 191-224.

Breed, A.W., (2000). Studies on the mechanism and kinetics of bioleaching with special reference to the bioleaching of refractory gold-bearing arsenopyrite/pyrite concentrates, PhD Thesis. University of Cape Town, Cape Town.

Breed, A.W., Dempers, C.J.N., Searby, G.E., Gardner, M.N., Rawlings, D.E. and Hansford, G.S., (1999). The effect of temperature on the continuous ferrous-iron oxidation kinetics of a predominantly *Leptospirillum ferrooxidans* culture. *Biotechnology and Bioengineering*, 65: 44 – 53.

Breed, A.W. and Hansford, G.S., (1999a). Effect of pH on ferrous-iron oxidation kinetics of a predominantly *Leptospirillum ferrooxidans* culture. *Biochemical Engineering Journal*, 3: 193–201.

Breed, A.W. and Hansford, G.S., (1999b). Modeling Continuous Bioleach Reactors. *Biotechnology and Bioengineering*, 64: 761 - 677.

Brierley, C.L., (2005). Bioleaching. AccessScience@McGraw-Hill, http://www.accessscience.com, DOI 10.1036/1097-8542.082525, last modified: September 19, 2005. Visited on 13th May, 2007.

Brierley, C.L., (1982). Microbiological Mining. *Scientific American*, August: 44 - 54.

Brierley, J.A. and Brierley, C.L., (2001). Present and future commercial applications in biohydrometallurgy. *Hydrometallurgy*, 59: 233 – 240.

Bruins, M.R., Kapil, S. and Oehme, F.W., (2000). Microbial Resistance to Metals in the Environment. *Ecotoxicology and Environmental Safety (Environmental Research, Section B)*, 45: 198 - 207.

Bryner, L.C. and Anderson, R., (1957). Microorganisms in Leaching Sulfide Minerals. *Ind. Eng. Chem.*, 39: 1721.

Bryner, L.C., Beck, J.V., Davis, D.B. and Wilson, D.G., (1954). Microorganisms in Leaching Sulfide Minerals. *Ind. Eng. Chem.*, 36: 2587.

Bryson, A. and Nicol, M., (1996). "Thermodynamics of Aqueous Solutions", Continuing Engineering Education Course. University of Witwatersrand, South Africa.

Cabrera, G., Gomez, J.M. and Cantero, D., (2005a). Influence of heavy metals on growth and ferrous sulphate oxidation by *Acidithiobacillus ferrooxidans* in pure and mixed cultures. *Process Biochemistry*, 40: 2683 - 2687.

Cabrera, G., Gomez, J.M. and Cantero, D., (2005b). Kinetic study of ferrous sulphate oxidation of *Acidithiobacillus ferrooxidans* in the presence of heavy metal ions. *Enzyme and Microbial Technology*, 36: 301 - 306.

Casas, J.M., Martinez, J., Moreno, L. and Vargas, T., (1998). Bioleaching model of a coppersulphide ore bed in heap and dump configurations. *Metallurgical and Materials Transactions B*, 29: 899–909.

Cavazza, C., Giudici-Orticoni, M.T., Appia, N.W., Bonnefoy, V. and Bruschi, M., (1996). Characterisation of a soluble cytochrome c4 isolated from Thiobacillus ferrooxidans. *Eur. J. Biochem.*, 242(2): 308 - 314.

Cavazza, C., Guigliarelli, B., Bertrand, P., Bonnefoy, V. and Bruschi, M., (1995). Biochemical and EPR characterization of a high potential iron-sulfur protein in Thiobacillus ferrooxidans. *FEMS Microbiology Letters*, 130(2 - 3): 193 - 199.

Chmielewski, T. and Charewicz, W.A., (1984). The Oxidation of Fe(II) In Aqueous Sulphuric Acid Under Oxygen Pressure. *Hydrometallurgy*, 12.

Chopp, D.L., Kirisits, M.J., Moran, B. and Parsek, M.R., (2003). The Dependence of Quorum Sensing on the Depth of a Growing Biofilm. *Bulletin of Mathematical Biology*, 65: 1053 - 1079.

Clark, D.A. and Norris, P.R., (1996). Oxidation of mineral sulfide by thermophilic microorganisms. *Minerals Engineering*, 9(11): 1119 - 1125.

Colmer, A.R. and Hinkle, M.E., (1947). The role of microorganisms in acid mine drainage; a preliminary report. *Science*, 106: 253-256.

Coram, N.J. and Rawlings, D.E., (2002). Molecular Relationship between two groups of the genus *Leptospirillum* and the finding that *Leptospirillum ferriphilum* sp. nov. dominates South African commercialbiooxidation tanks that operate at 40°C. *Appl. Environ. Microbiol.*, 68: 838 – 845.

Cortes, A., Cascante, M., Cardenas, M.L. and Cornish-Bowden, A., (2001). Relationships between inhibition constants, inhibitor concentrations for 50% inhibition and types of inhibition : new ways of analysing data. *Biochem. J.*, 357: 263 - 268.

Criss, C.M. and Cobble, J.W., (1964a). The thermodynamic properties of high temperature aqueous solution V: The calculations of ionic heat capacities up to 200°C. Entropies and heat capacities above 200°C. *J Am Chem Soc*, 86: 5390 - 5393.

Criss, C.M. and Cobble, J.W., (1964b). The thermodynamic properties of high temperature aqueous solutions IV: Entropies of ions up to 200 °C and the correspondence principle. *J Am Chem Soc*, 86: 5390 - 5393.

Crundwell, F.K., (1997). The kinetics of the chemiosmotic proton circuit of the iron-oxidizing bacterium *Thiobacillus ferrooxidans*. *Bioelectrcchemistry and Bioenergetics*, 43: 115 – 122.

De los Rios, R. and Caldarell, G., (2000). Putting proteins back into water. Phys. Rev, E62: 8449 8452.

Dempers, C.J.N., (2001). An investigation into the use of batch experiments in the determination of the kinetics of ferrous-iron oxidation by *Leptospirillum ferrooxidans.*, M.Sc. Thesis, University of Cape Town, Cape Town.

Dempers, C.J.N., Breed, A.W. and Hansford, G.S., (2003). The kinetics of ferrous-iron oxidation by *Acidithiobacillus ferrooxidans* and *Leptospirillum ferrooxidans*: effect of cell maintenance. *Biochemical Engineering Journal*, 16: 337 - 346.

DeRosa, M., Trincone, A., Nicolaus, B. and Gambacorta, A., (1991). Archaebacteria: lipids, membrane structures, and adaptation to environmental stress. In: G. Prisco (Editor), Life under extreme conditions. Springer, Berlin, pp. 61 - 87.

Devasia, P., Natarajan, K.A., Sathyanarayana, D.N. and Rao, G.R., (1993). Surface chemistry of Thiobacillus ferrooxidans relevant to adhesion on mineral surfaces. *Appl Environ Microbiol.*, 59: 4051 - 4055.

Dixon, D.G., (2000). Analysis of heat conservation during copper sulphide heap leaching. *Hydrometallurgy*, 58: :27–41.

Dixon, D.G. and Petersen, J., (2003). Dixon, D.G., Petersen, J., in: (Eds.), . In: P.A. Riveros, D.G. Dixon, D.B. Dreisinger and J. Menacho (Editors), Copper 2003. Hydrometallurgy of Copper. CIM, Montreal, Canada, pp. 493-516.

Domic, E.M., (2007). A review of the Development and Current Status of Copper Bioleaching Operation in Chile: 25 Years of Successful Commercial Implementation. In: D.E. Rawlings and D.B. Johnson (Editors), Biomining. Springer, Berlin, pp. 81 - 95.

Dopson, M., Baker-Austin, C., Hind, A., Bowman, J.P. and Bond, P.L., (2004). Characteristic of *Ferroplasma* isolates and *Ferroplasma acidarmanus* sp. nov., extreme acidophiles from acid mine drainage and industrial bioleaching environments. *Appl Environ Microbiol.*, 70(4): 2079 - 2088.

Dopson, M., Halinen, A.K., Rahunen, N., Özkaya, B., Sahinkaya, E., Kaksonen, A.H., Lindström, E.B. and Puhakka, J.A., (2007). Mineral and iron oxidation at low temperatures by pure and mixed cultures of acidophilic microorganisms. *Biotechnol Bioeng*, 97(5): 1205-1215.

Doran, P.M., (1995). Bioprocess engineering principles. Academic Press, Harcourt Brace & Company.

Drobner, E., Huber, H. and Stetter, K.O., (1990). *Thiobacillus ferrooxidans* a facultative hydrogen oxidizer. *Appl. Environ. Microbiol.*, 56(9): 2922 - 2923.

Dry, M.J., (1984). Kinetics of Leaching of a Low Grade Matte in Ferric Sulphate Solution, PhD Thesis, University of Witwatersrand, South Africa.

Dry, M.J. and Bryson, A.W., (1988). Prediction of redox potential in concentrated iron sulphate solutions. *Hydrometallurgy*, 21: 59 - 72.

du Plessis, C.A., Batty, J.D. and Dew, D.W., (2007). Commercial Application of Thermophile Bioleaching. In: D.E. Rawlings and D.B. Johnson (Editors), Biomining. Springer, Berlin, pp. 57 - 80.

Duncan, D.W., (1967). Microbiological Leaching of Sulfide Minerals, Aust. Min.

Edwards, K.J., Bond, P.L., Gihring, T.M. and Banfield, J.F., (2000). An Archaeal iron-oxidizing extreme acidophile important in acid mine drainage. *Science*, 287(5459): 1796 - 1799.

Eneroth, E.B. and Koch, C., (2004). Fe-hydroxysulphates from bacterial Fe^{2+} oxidation. *Hyperfine Interact*, 156/157(1 - 4): 423 - 429.

Franzmann, P.D., Haddad, C.M., Hawkes, R.B., Robertson, W.J. and Plumb, J.J., (2005). Effects of temperature on the rates of iron and sulfur oxidation by selected bioleaching Bacteria and Archaea: Application of the Ratkowsky equation. *Minerals Engineering*, 18: 1304 - 1314.

Garcia, O. and Silva, L.L., (1991). Differences in growth and iron oxidation among *Thiobacillus ferrooxidans* cultures in the presence of some toxic metals. *Biotechnology Letters*, 13: 567 - 570.

Gehrke, T., Telegdi, J., Thierry, D. and Sand, W., (1998). Importance of extracellular polymeric substances from Thiobacillus ferrooxidans for bioleaching. *Appl Environ Microbiol.* , 64: 2743-2747.

Goebel, B.M. and Stackebrandt, E., (1994). Cultural and phylogenetic analysis of mixed microbial populations found in natural and commercial bioleaching environments. *Appl. Environ. Microbiol.* , 60: 1614 - 1621.

Golyshina, O.V., Pivovarova, T.A., Karavaiko, G.I., Kondrat'eva, T.F., Moore, E.R.B., Abraham, W.R., Lunsdorf, H., Timmis, K.N., Yakimov, M.M. and Golyshin, P.N., (2000). Ferroplasma acidiphilum gen. nov., sp. nov., an acidophilic, autotrophic, ferrous-iron-oxidizing, cell-wall-lacking, mesophilic member of the Ferroplasmaceae fam. nov., comprising a distinct lineage of the Archaea. *International Journal of Systematic and Evolutionary Microbiology*, 50: 997 - 1006.

Gomez, J.M. and Cantero, D., (1998). Modelling of Ferrous Sulphate Oxidation by *Thiobacillus ferrooxidans* in Discontinuous Culture: Influence of Temperature, pH and agitation Rate *Journal of Fermentation and Bioengineering*, 86: 79 - 83.

Gomez, J.M., Caro, I. and Cantero, D., (1996). Kinetic equation for growth of *Thiobacillus ferrooxidans* in submerged culture over aqueous ferrous sulphate solutions. *J. Biotechnol.*, 48(1,2): 147 - 152.

Guay, R., Silver, M. and Torma, A.E., (1977). Ferrous iron oxidation and uranium extraction by Thiobacillus ferrooxidans. *Biotechnol Bioeng*, 19: 727 - 740.

Hallberg, K.B. and Johnson, D.B., (2001). Biodiversity of acidophilic prokaryotes. *Adv. Appl. Microbiol.*, 49: 37 - 84.

Hansford, G.S., (1997). Recent development in modelling the kinetics of bioleaching. In: D.E. Rawlings (Editor), Biomining: Theory, Microbes and Industrial Processes. Springer, Berlin and Landes Bioscience, Austin, TX, pp. 24.

Hansford, G.S. and Vargas, T., (2001). Chemical and electrochemical basis of bioleaching processes. *Hydrometallurgy*, 59: 135 – 145.

Harneit, K., Göksel, A., Kock, D., Klock, J.-H., Gehrke, T. and Sand, W., (2006). Adhesion to metal sulfide surfaces by cells of *Acidithiobacillus ferrooxidans, Acidithiobacillus thiooxidans* and *Leptospirillum ferrooxidans*. *Hydrometallurgy*, 83(1 - 4): 245 254.

Harneit, K. and Sand, W., (2007). Influence of growth substrate and attachment substratum on EPS and biofilm formation by *Acidithiobacillus ferrooxidans A2*. *Advance Materials Research*, 20 - 21(385 - 385).

Harvey, P.I. and Crundwell, F.K., (1997). Growth of Thiobacillus ferrooxidans: A novel experimental design for batch growth and bacterial leaching studies. *Applied Environmental Microbiology*, 63: 2586 - 2592.

Hawkes, R.B., Franzmann, P.D. and Plumb, J.J., (2006). Moderate thermophiles including "Ferroplasma cupricumulans" sp nov. dominate an industrial-scale chalcocite heap bioleaching operation. *Hydrometallurgy*, 83(1-4): 229 - 236.

Heijnen, J.J. and van Dijken, J.P., (1992). In the search of thermodynamic description of biomass yields for the chemotrophic growth of microorganisms. *Biotechnol Bioeng*, 39(8): 833 - 858.

Herbert, D., Elsworth, R. and Telling, R.C., (1956). The continouous culture of bacteria: a theoretical and experimental study. *J Gen. Microbiol.*, 14(3): 601 - 622.

Hinshelwood, C.N., (1946). Influence of temperature on the growth of bacteria. In: C.N. Hinshelwood (Editor), The chemical kinetics of the bacterial cell. Clarendon Press, Oxford, pp. 4.

Hiroyoshi, N., Kuroiwa, S., Miki, H., Tsunekawa, M. and Hirajima, T., (2004). Synergistic effect of cupric and ferrous ions on active-passive behavior in anodic dissolution of chalcopyrite in sulfuric acid solutions. Hydrometallurgy, 74: 103 - 116.

Hofstee, B.H.J., Ddcon, M. and Webb, E.C., (1959). Non-inverted versus inverted plots in enzyme kinetics. *Nature*, 184: 1296 - 1298.

Holmes, P.R. and Crundwell, F.K., (2000). Geochim. Cosmochim. Acta, 64: 263-274.

Huberts, R., (1994). Modelling of ferrous sulphate oxidation by iron oxidizing bacteria - *a chemiosmotic and electrochemical approach* PhD Thesis, University of Witwatersrand, Johannesburg, 222 pp.

Ingledew, W.J., (1982). The bioenergetics of acidophilic chemolithotroph. *Biochim. Biophys. Acta*, 683: 89–117.

Johnson, D.B., (1995). Selective solid media for isolating and enumerating acidophilic bacteria. *J. Microbiol. Methods*, 23: 205 - 18.

Johnson, D.B., (2006). Biohydrometallurgy and the environment: Intimate and important interplay. *Hydrometallurgy*, 83: 153 - 166.

Johnson, D.B. and McGinness, (1991). An efficient and universal solid medium for growing mesophilic and moderately thermophilic, iron-oxidizing, acidophilic bacteria. *J. Microbiol. Methods*, 13: 113 - 322.

Jones, C.A. and Kelly, D.P., (1983). Growth of *Thiobacillus ferrooxidans* on ferrous iron in chemostat culture: influence of product and substrate inhibition. *Journal of Chemical Technology and Biotechnology*, 33B: 241 - 261.

Kazadi, T.K., (2007). Evaluation of the Redostat™ device for the study of ferrous iron biological oxidation kinetics, M.Sc. Thesis, University of Cape Town, Cape town, 110 pp.

Kazadi, T.K. and Petersen, J., (2007). Kinetic measurement of biological oxidation of ferrous iron at low ferric to ferrous ratios in a controlled potential batch reactor. *Advance Materials Research*, 20 - 21: 160 - 163.

Kelly, D.P. and Jones, C.A., (1978). Factors affecting metabolism and ferrous iron oxidation in suspensions and batch cultures of *Thiobacillus ferrooxidans*: relevance to ferric leach regeneration. In: L.E. Murr, A.E. Torna and J.A. Brierley (Editors), Metallurgical Applications of bacterial leaching and related microbiological phenomena. Academic Press, pp. 19 - 44.

Kinnunen, P., (2004). High-rate ferric sulfate generation and chalcopyrite concentrate leaching by Acidophilic microorganisms, PhD Thesis, Tampere University of Technology 56 pp.

Kinnunen, P.H.-M. and Puhakka, J.A., (2004). High-rate ferric sulfate generation by a Leptospirillum ferriphilum-dominated biofilm and the role of jarosite in biomass retainment in fluidized-bed reactor. *Biotechnology and Bioengineering*, 85: 697-705.

Kinnunen, P.H.-M. and Puhakka, J.A., (2005). High-rate iron oxidation at below pH 1 and at elevated iron and copper concentrations by a Leptospirillum ferriphilum dominated biofilm. *Process Biochemistry*, 40: 3536 - 3541.

Kinzler, K., Gehrke, T., Telegdi, J. and Sand, W., (2003). Bioleaching—a result of interfacial processes caused by extracellular polymeric substances (EPS). *Hydrometallurgy*, 71(1 - 2): 83 - 88.

Konig, H., (1988). Archaeobacterial cell envelopes. *Canadian Journal of Microbiology*, 34: 395 - 406.

Konishi, Y., Yoshida, S. and Asai, S., (1995). Bioleaching of pyrite by acidophilic thermophile *Acidianus brierleyi*. Biotechnol Bioeng, 48: 592 - 600.

Kupka, D., Rzhepishevska, O.I., Dopson, M., Lindström, E.B., Karnachuk, O.V. and Tuovinen, O.H., (2007). Bacterial oxidation of Ferrous Iron at Low Temperatures. *Biofuel and Environmental Biotechnology*, 97: 1470 - 1478.

Lacey, D.T. and Lawson, F., (1970). Kinetics of the liquide-phse oxidation of acid ferrous sulfate by the bacterium *Thiobacillus ferrooxidans*. *Biotechnology and Bioengineering*, 12: 29 - 50.

Laidler, K.J. and Meiser, J.H., (1982). Physical Chemistry. The Benjamin/Cummings Publishing Company. Inc., California, 920 pp.

Lehninger, A.L., (1975). Biochemistry The molecular basis of cell structure and function. Worth Publisher, Inc.

Lineweaver, H. and Burk, D., (1934). The determination of enzyme dissociation constants. *J Am Chem Soc*, 56: 658 - 666.

Liu, M.S., Branion, R.M.R. and Duncan, D.W., (1988). The effect of ferrous iron, dissolved oxygen and inert solid solids concentrations on the growth of Thiobacillus ferrooxidans. *Canadian Journal of Chemical Engineering*, 66: 445 - 451.

Lizama, H.M. and Suzuki, I., (1989). Synergistic competitive inhibition of ferrous iron oxidation by *Thiobacillus ferrooxidans by increasing concentrations of ferric iron and cells*. *Appl. Environ. Microbiol.*, 55: 2588 - 2591.

Lundgren, D. and Silver, M., (1980). Ore leaching by bacteria. *Annu. Rev. Microbiol*, 34: 263 - 283.

MacDonald, D.G. and Clark, R.H., (1970). The oxidation of aqueous ferrous sulfate by *Thiobacillus ferrooxidans*. *Canadian Journal of Chemical Engineering*, 48(Dec.): 669 - 676.

Maciag, W.J. and Lundgren, D.G., (1964). *Biochem. Biophys. Res. Commun.*, 17(603 - 607).

Mafanya, K.Z., Rohwerder, T. and Sand, W., (2007). Study of the Attachment Behaviour of Different Strains of *Acidithiobacillus spp*. to Pyrite. *Advance Materials Research*, 20 - 21(386 - 386).

Marais, H., (1990). Bacterial oxidation of arseno-pyrite refractory gold ore, . In: Innovation in metallurgical plant. South African Institute of Mining and Metallurgy, Johannesburg, pp. 125–129.

Meruane, G., Salhe, C., Wiertz, J. and Vargas, T., (2002). Novel electro-chemical model which quantifies the effect of the solution Eh on the kinetics of ferrous iron oxidation with *Acidothiobacillus ferrooxidans*. *Biotechnology and Bioengineering*, 80: 280 - 288.

Meruane, G. and Vargas, T., (2003). Bacterial oxidation of ferrous iron by *Acidithiobacillus ferrooxidans* in the pH range 2.5–7.0

Hydrometallurgy, 71(1 - 2): 149 - 158.

Mitchell, P., (1966). Chemiosmotic coupling in oxidative and photosynthetic phosphorylation. *Biol. Rev. Cambridge Phil. Soc.*, 41(3): 445 - 502.

Monod, J., (1949). The growth of bacterial cultures. *Annual Review of Microbiology*, 3: 371 - 394.

Montealegre, R., Bustos, S., Rojas, J., Neuburg, H., Araya, C., Yanez, H., Tapia, R. and Rauld, J., (1993). Application of Bacterial Thin Layer leaching Process to

Quebrada Blanca Ores. In: A.E. Torma, J.E. Wey and V.L. Lakshamanan (Editors). The Minerals, Metals and Materials Society, Wyoming, USA, pp. 769.

Murr, L.E. and Brierley, J.A., (1978). The use of large-scale test facilities in studies of the rolw of microorganisms in commercial leaching operations. In: L.E. Murr, A.E. Torma and J.A. Brierley (Editors), Metallurgical Applications of bacterial leaching and related microbiological phenomena. Academic Press, New York, pp. 526.

Neijssel, O.M. and Tempest, D.W., (1976). Bioenergetics aspects of aerobic growth of *Klebsiella aerogenes* NCTC 418 in carbon-sufficient chemostat culture. *Arch. Microbiol.*, 107(2): 215 - 221.

Nemati, M., Harrison, S.T.L., Hansford, G.S. and Webb, C., (1998). Biological oxidation of ferrous sulphate by *Thiobacillus ferrooxidans*: a review of kinetic aspects. . *Biochem. Eng. J.* , 1: 171- 190.

Nemati, M. and Webb, C., (1997). A Kinetic Model for Biological Oxidation of Ferrous Iron by *Thiobacillus ferrooxidans*. *Biotechnology and Bioengineering*, 53: 478 - 486.

Nicol, M.J., (1993). In: J.B. Hiskey and G.W. Warren (Editors), Hydrometallurgy Fundamentals, Technology and Innovations, Proceedings of the Milton E. Wadsworth 4th International Symposium on Hydrometallurgy. SME, Littleton, CO, pp. 43-62.

Nicol, M.J., Needes, C.R.S. and Finkelstein, N.P., (1975). Electrochemical model for the leaching of uranium dioxide. 1. Acid media., Leaching and Reduction Hydrometallurgy. Instn. Min. Metall., London, UK, pp. 1 - 11.

Nies, D.H., (1999). Microbial heavy-metal resistance. *Appl Microbiol Biotechnol*, 51: 730 - 750.

Nies, D.H. and Silver, S., (1995). Ion efflux systems involved in bacterial metal resistances. *J. Indust. Microbiol*, 14: 186 - 199.

Norris, P.R., (2007). Acidophile Diversity in minearal Sulfide Oxidation. In: D.E. Rawlings and D.B. Johnson (Editors), Biomining. Springer-Verlag, Berlin, pp. 199 - 216.

Norris, P.R., Barr, D.W. and Hinson, D., (1988). Iron and mineral oxidation by acidophilic bacteria: affinities for iron and attachment to pyrite. In: P.R. Norris and D.P. Kelly (Editors), Biohydrometallurgy; Proceedings of Internatinal symposium 1987, Warwick, pp. 43 - 59.

Norris, P.R., Burton, N.P. and Foulis, N.A.M., (2000). Acidophiles in bioreator mineral processing. *Extremophiles*, 4(2): 71 - 76.

Norris, P.R. and Owen, J.P., (1993). Mineral sulfide oxidation by enrichment cultures of novel thermoacidophilic bacteria. *FEMS Microbiological Review*, 11(1-3): 51 - 56.

Nunzi, F., Woudstra, M., Campese, D., Bonicel, J., Morin, D. and Bruschi, M., (1993). Amino-acid sequence of rusticyanin from Thiobacillus ferrooxidans and its comparison with other blue copper proteins. *Biochimica et Biophysica Acta (BBA)* - Protein Structure and Molecular Enzymology, 1162(1-2): 28 - 34.

Ojumu, T.V., Petersen, J. and Hansford, G.S., (2007). The effect of aluminium and magnesium sulphate on the rate of ferrous iron oxidation by *Leptospirillum ferriphilum* in continuous culture. *Advanced Materials Research*, 20 - 21: 156 - 159.

Ojumu, T.V., Petersen, J., Searby, G.E. and Hansford, G.S., (2006). A review of rate equations proposed for microbial ferrous-iron oxidation with a view to application to heap bioleaching. *Hydrometallurgy*, 83: 21 - 28.

Okereke, A. and Stevens, S.E., (1991). Kinetics of Iron oxidation by *Thiobacillus ferrooxidans*. *Appl. Environ. Microbiol.*, 57(4): 1052 -1056.

Olson, G.J., Brierley, J.A. and Brierley, C.L., (2003). Progress in bioleaching: applications of microbial processes by the minerals industries. . . *Appl. Microbiol. Biotechnol.*, 63: 249 - 257.

Özkaya, B., Nurmi, P., Sahinkaya, E., Kaksonen, A.H. and Puhakka, J.A., (2007a). Temperature effects on the iron oxidation kinetics of a *Leptospirillum ferriphilum* dominated culture at pH below one. *Advance Materials Research*, 20 - 21: 465 - 468.

Özkaya, B., Sahinkaya, E., Nurmi, P., Kaksonen, A.H. and Puhakka, J.A., (2007b). Kinetics of iron oxidation by *Leptospirillum ferriphilum* dominated culture at pH below one. *Biotechnology and Bioengineering*: DOI 10.1002/bit.21313.

Pesic, B., (1993). Redox potential technique to study the factors of importance during reactions of *T. ferrooxidans* with Fe^{2+}. In: A.E. Torma, J.E. Wey and V.L. Lakshmanan (Editors), Biohysrometallurgical Technologies. The Minerals, Metals and Materials Society, Jackson Hill, Wyoming, pp. 545 - 560.

Petersen, J., (2001). Understanding the Dynamics of Copper Sulphide Bioheap Leaching at Zaldivar.

Petersen, J., (2007). A mathematical comparison between Ratkowsky and Arrhenius models to correlate temperature dependency of microbial oxidation rates, P768 A: Improving Heap Bioleaching (Confidential report). AMIRA international Limited Melbourne.

Petersen, J. and Dixon, D.G., (2004). Bacterial growth and propagation in chalcocite heap bioleach scenarios. In: M. Tsezos, A. Hatzikioseyian and E. Remoundaki (Editors), Biohydrometallurgy - *a sustainable technology in evolution*, IBS 2003, National Technical University of Athens, pp. 65 - 74.

Petersen, J. and Dixon, D.G., (2006). Modeling and Optimisation of Heap Bioleach Processes. In: D.E. Rawlings and D.B. Johnson (Editors), Biomining. Springer Verlag, Berlin. pp. 153 - 176. .

Petersen, J. and Dixon, D.G., (2007a). Competitive bioleaching of pyrite and chalcopyrite. Hydrometallurgy, 83: 40 - 49.

Petersen, J. and Dixon, D.G., (2007b). Modelling zinc heap bioleaching. *Hydrometallurgy*, 85: 127 - 143.

Petersen, J. and Dixon, D.G., (2007c). Principles, Mechanisms and Dynamics of Chalcocite Heap Bioleaching. In: E. Donati and W. Sand (Editors), Microbial Processing of Metal Sulfides. Springer Verlag, Berlin, pp. 193 - 218.

Phelps Dodge Mining Company, (2003). Morenci Overview.

Pirt, S.J., (1965). The maintenance energy of bacteria in growing cultures, In: Proceedings of the Royal Society of London. Biological Sciences, pp. 224 - 231.

Pizarro, J., Jedlicki, E., Orellana, O., Romero, J. and Espejo, R.T., (1996). Bacterial populations in samples of bioleached copper ore as revealed by analysis of DNA obtained before and after cultivation. *Appl. Environ. Microbiol.*, 62: 1323 - 1328.

Plumb, J.J., Gibbs, B., Stott, M.B., Robertson, W.J., Gibson, J.E.A., Nichols, P.D., Watling, H.R. and Franzmann, P.D., (2000). Enrichment and characterization of thermophilic acidophiles for bioleaching of mineral sulfides. *Minerals Engineering*, 15(11): 787 - 794.

Plumb, J.J., Hawkes, R.B. and Franzmann, P.D., (2007a). The Microbiology of Moderately Thermophilic and Transient Thermophilic Ore Heaps. In: D.E. Rawlings and D.B. Johnson (Editors), Biomining. Springer-Verlag, pp. 217 - 235.

Plumb, J.J., Mcsweeney, N., Haddad, C., Muddle, R. and Franzmann, P.D., (2007b). Effects of Temperature on Fe^{2+} and S^0 Oxidations Kinetics of Selected Strains, P768 A: Improving Heap Bioleaching (Confidential report). AMIRA international Limited Melbourne.

Pogliani, C. and Donati, E., (1999). The role of exopolymers in the bioleaching of a non-ferrous metal sulphide. . *Journal of Industrial Microbiology & Biotechnology*, 22: 88 - 92.

Privalov, P.L., (1990). Cold denaturation of proteins. . Crit. Rev. Biochem. Mol. Biol. , 25: 281 - 305.

Raja, S.B., (2005). The effect of particulate-induced hydrodynamic stress on the bioleaching of chalcopyrite by a *Sulfolobus*-like culture, PhD Thesis, University of Cape Town, South Africa.

Ratkowsky, D.A., Lowry, R.K., McMeekin, T.A., Stokes, A.N. and Chandler, R.E., (1983). Model for bacterial culture growthrate throughout the entire biokinetic temperature range. *J. Bacteriol.*, 154: 1222-1226.

Ratkowsky, D.A., Olley, J., McMeekin, T. and BALL, A., (1982). Relationship Between Temperature and Growth Rate of Bacterial Cultures. *J. Bacteriol.*, 49(1): 1 - 5.

Ratkowsky, D.A., Olley, J. and Ross, T., (2005). Unifying temperature effects on the growth rate of bacteria and the stability of globular proteins. *Journal of Theoretical Biology*, 233: 351–362.

Rawlings, D.E., (1997). In: D.E. Rawlings (Editor), Biomining: Theory, Microbes and Industrial Processes. Springer, Berlin and Landes Bioscience, Austin, TX.

Rawlings, D.E., (2002). Heavy metal mining using microbes. *Annual Review of Microbiology*, 56: 65 - 91.

Rawlings, D.E., (2005). Characteristics and adaptability of iron- and sulfur-oxidizing microorganisms used for the recovery of metals from minerals and their concentrates, *Microbial Cell Factories* doi:10.1186/1475-2859-4-13.

Rawlings, D.E., (2007). Relevance of Cell Physiology and Genetic Adaptability of Biomining Microorganisms to Inductrial Processes. In: D.E. Rawlings and D.B. Johnson (Editors), Biomining. Springer-Verlag, Berlin, pp. 177 - 198.

Rawlings, D.E., Dew, D. and Plessis, C., (2003). Biomineralization of metal-containing. *Trends in Biotechnology*, 21: 38 - 44.

Rawlings, D.E., Tributsch, H. and Hansford, G.S., (1999). Reasons why 'Leptospirillum'-like species rather than Thiobacillus ferrooxidans are the dominant iron-oxidizing bacteria in many commercial processes for the biooxidation of pyrite and related ores. *Microbiology*, 145: 5 -13.

Remonselle, F., Galleguillos, F., vanRensburg, S.J., Rautenbach, G.F., Galleguillos, P., Castillo, D. and Demergasso, C., (2007). Monitoring the microbial community inhabiting a low-grade copper sulphide ore by Quantitative Real-Time PCR analysis of 16S rRNA genes. *Advance Materials Research*, 20 - 21: 539 - 542.

Renman, R., Guiying, Z., Biao, W. and Jiankang, W., (2007). Study on Selective Depression of Pyrite during Copper Bioleaching. *Advance Materials Research*, 20 - 21: 172 - 173.

Roels, J.A. and Kossen, N.W.F., (1978). On the Modelling of Microbial Metabolism. *Progr. Ind. Microbiol.*, 14: 95 - 203.

Rohwerder, T., Gehrke, T., Kinzle, K. and Sand, W., (2003). Bioleaching review part A: Progress in bioleaching: fundamentals and mechanisms of bacterial metal sulfide oxidation. *Appl Microbiol Biotechnol.*, 63: 239 - 248.

Rohwerder, T. and Sand, W., (2007). Mechansims and biochemical fundamentals of bacterial metal sulfide oxidation. In: E.R. Donati and W. Sand (Editors), Microbial Processing of Metal Sulfides. Springer, The Netherlands, pp. 35 - 58.

Rossi, G., (1990). Biohydrometallurgy. McGraw-Hill, New York. .

Sand, W., Gehrke, T., Hallmann, R. and Schippers, A., (1995). Sulfur chemistry, biofilm and the indirect attack mechanism—a critical evaluation of bacterial leaching. *Appl. Microbiol. Biotechnol.*, 43: 961–966.

Sand, W., Gehrke, T., Jozsa, P.-G. and Schippers, A., (2001). (Bio)chemistry of bacterial leaching — direct vs. indirect process. *Hydrometallurgy*, 59: 159 - 75.

Sandler, S.I., (1999). Chemical and Engineering Thermodynamics. Third Edition. John Wiley & Son, Inc.

Schippers, A. and Sand, W., (1999). Bacterial leaching of metal sulfides proceeds by two direct mechanisms via thiosulfate or via polysulfides and sulfur. *Appl Environ Microbiol.*, 65(1): 319 - 321.

Schnell, H.A., (1997). Bioleaching of copper. In: D.E. Rawlings (Editor), Biomining: Theory, Microbes and Industrial Processes. Springer, pp. 21 - 43.

Schoolfield, R.M., Sharpe, P.J.H. and Magnuson, C.E., (1981). Nonlinear regression of biological temperature-dependent rate models based on absolute reaction-rate theory. *Journal of Theoretical Biology*, 88(4): 719 - 731.

Searby, G.E., (2006). An investigation of Kinetics of thermophilic microbial ferrous-iron oxidation in continuous culture, PhD Thesis, University of Cape Town, Cape Town.

Searby, G.E. and Hansford, G.S., (2003). The Kinetics of Thermophilic Ferrous-Iron Oxidation, International Biohydrometallurgy Symposium, Athens.

Shiers, D.W., Blight, K.R. and Ralph, D.R., (2005). Sodium sulphate and sodium chloride effects on batch culture of iron oxidising bacteria. *Hydrometallurgy*, 80: 75 - 82.

Shum, M. and Lavkulich, L., (1999). Speciation and solubility relationships of Al, Cu and Fe in solutions associated with sulfuric acid leached mine waste rock. *Environmental Geology*, 38(1): 59 - 68.

Sidborn, M., Casas, J.M., Martinez, J. and Moreno, L., (2003). Two dimensional dynamic model of a copper sulphide ore heap. . *Hydrometallurgy*, 71: 67–74.

Silverman, M.P. and Ehrlich, H.L., (1964). Microbial formation and degradation of minerals. *Adv. Appl. Microbiol.*, 6: 153- 206.

Stumm, W. and Morgan, J.J., (1996). Aquatic Chemistry: Chemical Equilibria and Rates in natural Water. John Willey & Sons, New York, 88 - 147 pp.

Sundkvist, J.E., Gahan, C.S. and Sandström, Å., (2007). Modeling of microbial ferrous iron oxidation by *Leptospirillum ferrooxidans* in a continuous bioreactor. *Biotechnol Bioeng*, 99(2): 378 - 389.

Talvivaara, (2008). Overview. http://www.talvivaara.com/index.phtml?page_id=1088&navi_id=1088, pp. Accessed on 31st January, 2008.

Tijhuis, L., Loosdrecht, M.C.M.v. and Heijnen, J.J., (1993). A thermodynamically based correlation for maintenance Gibbs energy requirements in aerobic and anaerobic chemotrophic growth. *Biotechnol Bioeng*, 42(4): 509 519.

Tributsch, H., (2001). Direct versus indirect bioleaching. Hydrometallurgy. *Hydrometallurgy*, 59: 177 - 185.

Tuovinen, O.H. and Kelly, D.P., (1972). *Z. Allg. Mikrobiol.*, 12: 311 - 346.

Tuovinen, O.H., Niemela, S.I. and Gyllenberg, H.G., (1971). Tolerance of Thiobacillus ferrooxidans to some metals. *Antonie van Leeuwenhoek*, 37: 489 - 496.

Valenzuela, S., Banderas, A., Jerez, C.A. and Guiliani, N., (2007). Cell-Cell Communication In Bacteria: A promising new approach to improve bioleaching efficiency? In: E.R. Donati and W. Sand (Editors), Microbial Processing of Metal Sulfides. Springer Netherlands, Berlin.

van Aswegen, P.C., van Niekerk, J. and Olivier, W., (2007). The BIOX^{TM} process for the Treatment of Refractory Gold Concentrates. In: D.E. Rawlings and D.B. Johnson (Editors), Biomining. Springer, Berlin, pp. 2 - 33.

van Scherpenzeel, D.A., Boon, M., Ras, C., Hansford, G.S. and Heijnen, J.J., (1998). Kinetics of ferrous iron oxidation by Leptospirillum bacteria in continuous cultures. *Biotechnology Progress*, 14: 425 - 433.

Verbaan, B. and Crundwell, F.K., (1986). An electrochemical Model for the Leaching of Sphalerite Concentrate. *Hydrometallurgy*, 16: 345 - 359.

Verger, R. and DeHaas, G.H., (1976). Interfacial Enzyme Kinetics of Lipolysis. *Annual Review of Biophysics and Bioengineering*, 5: 77 - 117.

Vilcaez, J., Suto, K. and Inoue, C., (2007). Modeling the Auto-Thermal Performance of a Thermophilic Chalcopyrite Bioleaching Heap Employing Mesophilic and Thermophilic Microbes. *Advance Materials Research*, 20 - 21: 70 - 74.

Vishniac, W. and Santer, V., (1957). The Thiobacilli. *Bacteriol. Rev*, 21: 195 - 213.

Vogel, A.I., (1987). Vogel's Textbook of Quantitative Inorganic Analysis.

Wang, M., Zhang, Y., Deng, T. and Wang, K., (2004). Kinetic modeling for the bacterial leaching of chalcopyrite catalyzed by silver ions. . *Minerals Engineering*, 17: 943 - 947.

Watling, H.R., (2006). The bioleaching of sulphide minerals with emphasis on copper sulphides – A review. *Hydrometallurgy*, 84: 81-108.

Yarzabal, A., Brasseur, G., Ratouchniak, J., Lund, K., Lemesle-Meunier, D., DeMoss, J.A. and Bonnefoy, V., (2002). The high-molecular-weight cytochrome c Cyc2 of *Acidothiobacillus ferrooxidans* is an outer membrane protein. *J. Bacteriol.*, 184(1): 313 - 317.

Zemaitis, J.F., Clark, D.M., Rafal, M. and Scrivner, N., (1986). Handbook of Aqueous Electrolyte Thermodynamics. American Institute of Chemical Engineers, New York, 3 - 43 pp.

Zeng, A.P. and Deckwer, W.D., (1995). A kinetic model for substrate and energy consumption of microbial growth under substrate-sufficient conditions. *Biotechnology Progress*, 11: 71 - 79.

Zepeda, V., Galleguillos, F., Castillo, D., Lastra, M. and Demergasso, C., (2007). Bacterial Activity at Low Temperature in Cultures Derived from a Low-Grade Copper Sulphide Bioleaching Heap at the Escondida Mine, Chile. *Advance Materials Research*, 20 - 21: 543 - 546.

Zwietering, M.H., deKoos, J.T., Hasenack, B.E., deWit, J.C. and van'tRiet, K., (1991). Modeling of bacterial growth as a function temperature. *Applied and Environmental Microbiology*, 57: 1094 - 1101.

APPENDICES

Appendix A

A1.1 A theoretical formulation of microbial oxidation of Fe^{2+}

In order to determine kinetic and yield parameters for a Fe^{2+} oxidizing culture the overall biomass- and substrate mass balances have to be established for a chemostat at different residence times. The following general assumptions apply:

1. The reaction is carried out in a well-mixed reactor with uniform temperature and concentration
2. There is no accumulation of biomass in the reactor by attachment to the walls etc.
3. There is no formation of iron precipitate such as jarosite;
4. The feed and discharge flow rates are equal and the reactor volume is constant
5. The culture is substrate-limited with respect to Fe^{2+}
6. The feed solution is sterile and no growth inhibition factors are present (or are constant).

The overall biomass balance for active cell in the reactor over time will be given by the following Equation:

$$V\frac{dC_X}{dt} = FC_{X0} - FC_X + \mu C_X V - k_d C_X V \qquad \text{A1.1}$$

where V is the reactor volume; F , the flow rate; C_X biomass concentration; μ specific growth rate, k_d specific death rate. Assuming that the feed is sterile ($C_X = 0$) and that the bioreactor is operated at relative short residence time, then the death rate is negligible ($k_d = 0$). It can be shown as in Equation 1.15 that for a bioreactor operated at steady state, the specific growth rate, μ is equal to the dilution rate, D:

$$\mu = \frac{F}{V} = D = \frac{1}{\tau} \quad \text{A1.2}$$

where τ is the residence time

However, for the overall substrate balance, the amount of Fe^{2+} in the bioreactor at a given time can be written as given in Equation A1.3

$$V\frac{d[Fe^{2+}]}{dt} = F[Fe^{2+}]_0 - F[Fe^{2+}] - \frac{\mu C_X}{Y_{FeX}^{\max}}V - m_{Fe^{2+}}C_X V \quad \text{A1.3}$$

where

$\frac{\mu C_X}{Y_{FeX}^{\max}}$ is the fraction rate used for growth

$m_{Fe^{2+}}C_X$ is the fraction rate used for cell maintenance

At steady-state conditions the change in the rate of ferrous-iron concentration is zero. It can be shown for a constant bioreactor volume that the biomass C_X is:

$$C_X = \frac{D\left([Fe^{2+}]_0 - [Fe^{2+}]\right)}{\frac{D}{Y_{FeX}^{\max}} - m_{Fe^{2+}}} \quad \text{A1.4}$$

The instantaneous biomass yield can be obtained by differentiating Equation A1.4 with respect to $[Fe^{2+}]$ which can be obtained as follows:

$$Y_{Fe^{2+}X} = \frac{dC_X}{dt}\Big/\frac{-d[Fe^{2+}]}{dt} = \frac{-dC_X}{d[Fe^{2+}]} = D\Big/\left(\frac{D}{Y_{FeX}^{\max}} - m_{Fe^{2+}}\right) \quad \text{A1.5}$$

Equation A1.4 can be further simplified by substituting for $Y_{Fe^{2+}X}$ to give:

$$C_X = Y_{Fe^{2+}X}\left([Fe^{2+}]_0 - [Fe^{2+}]\right) \quad \text{A1.6}$$

Equation A1.4 can be also be re-arranged to directly associate to Pirt's Equations;

$$C_X = \left([Fe^{2+}]_0 - [Fe^{2+}]\right)\Big/\left(\frac{1}{Y_{FeX}^{\max}} - \frac{m_{Fe^{2+}}}{D}\right) \quad \text{A1.7}$$

Ferrous-iron concentration, $[Fe^{2+}]$ can also be determined from Monod Equation 2.10, such that μ can be replaced with D for a continuous system as:

$$[Fe^{2+}] = \frac{D.K_{Fe^{2+}}}{\mu_{\max} - D} \quad \text{A1.8}$$

By substituting Equation A1.8 into A1.7, biomass concentration, C_X can be expressed only as a function of dilution rate, other parameters being constants.

$$C_X = \left([Fe^{2+}]_0 - \frac{D.K_{Fe^{2+}}}{\mu_{max} - D} \right) \Big/ \frac{1}{Y_{FeX}^{max}} - \frac{m_{Fe^{2+}}}{D} \qquad \text{A1.9}$$

For feed solution containing predominantly ferrous-iron, it can be assumed that, the total iron concentration is equal to initial substrate concentration. Therefore it is safe to assume that Equation A1.10 is valid

$$[Fe^{2+}]_0 = [Fe^{3+}] + [Fe^{2+}] \qquad \text{A1.10}$$

Therefore ferric iron concentration can be expressed as:

$$[Fe^{3+}] = [Fe^{2+}]_0 - \frac{D.K_{Fe^{2+}}}{\mu_{max} - D} \qquad \text{A1.11}$$

Taking the natural logarithm of the ratio of Equation A1.8 and A1.11, it can be shown that:

$$\ln \frac{[Fe^{3+}]}{[Fe^{2+}]} = \ln \left(\frac{[Fe^{2+}]}{\frac{D.K_{Fe^{2+}}}{\mu_{max} - D}} - 1 \right) \qquad \text{A1.12}$$

The rate of ferrous-iron oxidation can be obtained by performing a substrate balance around the bioreactor as in Equation A1.13

$$-r_{Fe^{2+}} = \frac{F}{V}([Fe^{2+}]_0 - [Fe^{2+}]) = D([Fe^{2+}]_0 - [Fe^{2+}]) \qquad \text{A1.13}$$

By dividing Equation A1.13 by Equation A1.7, an expression for specific ferrous-iron oxidation rate can be written as function of dilution rate as in Equation A1.14. This is a variant form of the Pirt's Equation described Section 2.7 (Equation 2.13)

$$q_{Fe^{2+}} = -\frac{r_{Fe^{2+}}}{C_X} = \frac{D}{Y_{Fe^{2+}X}^{max}} + m_{Fe^{2+}} \qquad \text{A1.14}$$

This equation is particularly useful because $\mu = D$ (at steady state) and therefore need not be determined, and the constant parameters, μ_{max}, $K_{Fe^{2+}}$, $Y_{Fe^{2+}X}^{max}$ and $m_{Fe^{2+}}$ characterize the steady-state conditions of microbial ferrous-iron oxidation under a continuous mode. These values can be calculated if the steady state substrate, Fe^{2+} and biomass, C_X concentrations are known for different dilution rates. The kinetic parameters

(μ_{max}, $K_{Fe^{2+}}$) can be determined graphically by using appropriate linearization method (For example, Lineweaver-Burk, Eadie-Hofstee, and Langmuir plots).

A1.2 Debye-Huckel Activity Coefficient model

The major feature of geochemical solutions is that they are dominated by ionic interactions. Chemical species occur as charged ions and bear little resemblance of their analytical concentration. The Debye-Huckel proposed an important model, an activity coefficient model which enables the conversion of analytical concentrations to activities according to Equation A1.15

$$a_i = \gamma_i C_i \qquad \text{A1.15}$$

The model takes into account the columbic interactions existing between ionic species in the estimation of activity coefficient. Thus allowing effect of ionic charges to be investigated (for review, see Atkins and Paula, 2002; Bockris and Reddy, 1970; Stumm and Morgan, 1996). Hydrometallurgical solution, like electrolytes are non-ideal, there are substantial electrostatic interactions between the ions. These interactions increase with increasing concentration, resulting in an ordered type of distribution. The activity coefficient $\boldsymbol{\gamma_i}$ is expressed as given in Equation A1.16:

$$-\log_{10}\gamma_i = \frac{Az_i^2\sqrt{I}}{1 + d_i B\sqrt{I}} \qquad \text{A1.16}$$

where A and B represent the Debye-Huckel constants at specified temperature and pressure, $\boldsymbol{z_i}$ represents the ionic charge of the specie, d_i the effective ionic diameter and I is the ionic strength of the electrolyte solution (mol/l). The ionic strength is given by

$$I = \tfrac{1}{2}\sum m_i z_i^2$$
$$I \approx \tfrac{1}{2}\sum C_i z_i^2 \qquad \text{A1.17}$$

where m_i = molality of species i , C_i = concentration of species i, z_i = charge of species
The Debye-Huckel Equation is theoretically valid for dilute solution with ionic strength of less than 0.1 molal due to simplifications and assumptions made in considering the ionic atmosphere (Zemaitis et al., 1986). Although the model was derived for dilute

solution (Ionic strength less than 0.1), some success has been reported in applying it at higher concentration (Dry and Bryson, 1988). The Debye-Huckel constants A and B are expressed as shown in Equation A1.18

$$A = \frac{1}{2.3026}\left(\frac{e}{\sqrt{k.\varepsilon.T}}\right)^3\sqrt{\frac{2\pi.N_A.\rho_s}{1000}}$$

A1.18

$$B = \sqrt{\frac{8\pi.N_A.e^2.\rho_s}{1000.k.\varepsilon.T}}$$

where T = absolute temperature (Kelvin)
NA = Avogadro's number 6.022×10^{23} (mol^{-1})
e = Electronic charge 1.6022×10^{23} (C)
k = Boltzman constant, R/NA = 1.380×10^{-23} (J/K)
ε = Dielectric constant

The Deby-Huckel constants can be determined at different temperatures by using the polynomial shown in Equation A1.19 as developed by Dry (1984) and (crudwell 1988).

$$A = 0.4919 + 7.143\times10^{-4}(\Psi) + 2.113\times10^{-6}(\Psi)^2 + 1.173\times10^{-8}(\Psi)^3$$

A1.19

$$B = 0.3249 + 2.099\times10^{-4}(\Psi) + 2.582\times10^{-8}(\Psi)^2 + 2.589\times10^{-12}(\Psi)^3$$

where Ψ = t – 298.15 (adjusted absolute temperature in Kelvin), and t = temperature in °C

Appendix B

B1.1 Calculation of dilution rate by weight decrease of feed vessels

The dilution rate ((or residence time)$^{-1}$) was calculated by weight decrease of feed vessel using the Equation B1.1 below:

$$D = \frac{1}{\tau} = \frac{m_{initial} - m_{final}}{V_{bioreactor} \cdot \rho_{feed} \cdot (t_{initial} - t_{final})} \quad \text{B1.1}$$

where D is the dilution rate (h-1)
τ is the residence time (h)
$m_{initial} - m_{final}$ is weight decrease of the feed vessel
$t_{initial} - t_{final}$ is the time interval for the weight decrease (h)
$V_{bioreactor}$ is the working volume of the bioreactor (litre)
ρ_{feed} is the density of the feed solution (g L-1)

B1.2 The theoretical aspect of the calibration using Nernst Equation

The relationship between the redox potential Eh, the standard redox potential, Eh^o, and the ratio of ferric to ferrous-iron concentrations, $[Fe^{3+}]/[Fe^{2+}]$ in solution is governed by the Nernst Equation (Equation B1.2)

$$Eh = Eh^o + \frac{RT}{nF} \ln \frac{a_{Fe^{3+}}}{a_{Fe^{2+}}} \quad \text{B1.2}$$

For a redox couple of the half cell reaction $Fe^{2+} \rightarrow Fe^{3+} + e$, the standard redox potential E_h^o is 770 mV; this is obtained from thermodynamic data and it refers to situation in which the activities of both ferric, $a_{Fe^{3+}}$ and ferrous-iron $a_{Fe^{2+}}$ are equal and its measured with a standard Hydrogen electrode. The activity of a compound i, a_i is equal its concentration only when the ionic strength is zero, for ionic strength greater than zero, $a_i = \gamma_i c_i$, where γ_i is the activity coefficient (see Section 2.12.1). Therefore, the actual value of E_h at equal ferric and ferrous iron concentrations would change at increasing ionic strength due to the influence of other cations and anion. The presence of complexing agents (e.g. SO_4^{2-} OH^-) causes a decrease of free ferrous and ferric ions (Nagpal and Dahlstrom, 1994)[1] Also it has been shown by simulation using Visual Minteq and HSC® Chemistry softwares that stronger complexes are formed with ferric than with ferrous ions. Equation B1.2 can be re-written as

$$E_h = E_h' + \frac{RT}{nF} \ln \frac{[Fe^{3+}]}{[Fe^{2+}]} \qquad \text{B1.3}$$

where $E_h' = E_h^o + \frac{RT}{nF} \ln \frac{\gamma_{Fe^{3+}}}{\gamma_{Fe^{2+}}}$

Thus the term E_h' is defined as the solution potential measured at equal total ferric and ferrous-iron concentrations and accounts for activity coefficient of Fe^{3+} and Fe^{2+}, formation of complexes with Fe^{3+} and Fe^{2+} and the type of electrode. The adapted Nernst Equation relates the measured redox (solution) potential, E_h, the standard redox potential and the ratio between the total concentrations of ferric and ferrous ions. Thus for a specific electrode, E_h' values can be determined from the intercept of the plot of E_h versus $\ln([Fe^{3+}]/[Fe^{2+}])$, while the slope gives RT/nF

[1] Nagpal, S. and Dahlstrom, D., 1994. A mathematical model for the bacterial oxidation of a sulfide ore concentrate. *Biotechnol. Bioeng.*, 43(357 - 364).

Table B1.1 Parameters determined from standard calibration curve for redox probes used in this study

Temperature (°C)	E_h'	R/nF	R^2
42	484.07	0.0883	0.996
36	482.23	0.0881	0.992
30	481.2	0.0881	0.998
25	474.23	0.0883	0.989
20	466.06	0.0877	0.991
42[b]	481.23	0.0896	0.969

[b] used for pH study

B1.3 The stoichiometric Equation and the degree of reduction balance

The stoichiometry of the Equation representing the growth of bacteria on ferrous-iron substrate (Equation 3.2) was derived as follows (Boon et al., 1995): Given that the carbon source is CO_2, the nitrogen source is NH_4^+, oxygen is the electron acceptor and that the proton is essential for the microbial growth and substrate utilization, the balanced Equation for the aerobic microbial growth of biomass on ferrous-iron can be written as:

$$aCO_2 + bNH_4^+ + cO_2 + dFe^{2+} + eH^+ + 1.CH_{1.8}O_{0.5}N_{0.2} + fFe^{3+} + gH_2O = 0 \qquad \text{B1.4}$$

The rate biomass production can be related to the rate of substrate consumption of ferrous-iron.

$$-r_{Fe^{2+}} = d.r_X$$

The elemental and charge (z) balances can be written as follows:

$$\left.\begin{array}{ll} \text{C:} & a + 1 = 0 \\ \text{H:} & 4b + e + 1.8 + 2g = 0 \\ \text{O:} & 2a + 2c + 0.5 + g = 0 \\ \text{N:} & b + 0.2 = 0 \\ \text{Fe:} & d + f = 0 \\ \text{Z:} & +b + 2d + e + 3f = 0 \end{array}\right\} \qquad \text{B1.5}$$

There are six balanced Equations with seven unknown parameters, the values of these parameter is best expressed in term of the coefficient of the limiting substrate (ferrous-iron), *d*.

$$\left.\begin{array}{ll} a = -1 & e = d + 0.2 \\ b = -0.2 & f = -d \\ c = \dfrac{d + 4.2}{4} & g = 0.6 + \dfrac{d}{2} \end{array}\right\} \quad \text{B1.6}$$

d can be determined from the yield of biomass on ferrous-iron.

$$d = \frac{-r_{Fe^{2+}}}{r_X} = -\frac{1}{Y_{Fe^{2+}X}}$$

Therefore the stoichiometry in Equation 3.2 can be obtained by substituting for *d* in Equations B1.6 which yields

$$\left.\begin{array}{ll} a = -1 & e = -\left(\dfrac{1}{Y_{Fe^{2+}X}} - 0.2\right) \\ b = -0.2 & f = \dfrac{1}{Y_{Fe^{2+}X}} \\ c = -\left(\dfrac{1 - 4.2Y_{Fe^{2+}X}}{4Y_{Fe^{2+}X}}\right) & g = -\left(\dfrac{1}{2Y_{Fe^{2+}X}} - 0.6\right) \end{array}\right\} \quad \text{B1.7}$$

Using the stoichiometric parameters, the relative rates of the compounds can be written with respect to biomass production rate, r_X which follows from:

$$\frac{1}{a}\frac{d[CO_2]}{dt} = \frac{d[X]}{dt} \Rightarrow \frac{d[CO_2]}{dt} \Big/ \frac{d[X]}{dt} = a$$

By substituting Equations B1.8 into B1.4, the Equation for the degree of reduction balance for ferrous-iron oxidation can be written as shown in Equation 3.2.

$$CO_2 + 0.2NH_4^+ + \frac{1 - 4.2Y_{Fe^{2+}X}}{4Y_{Fe^{2+}X}}O_2 + \frac{1}{Y_{Fe^{2+}X}}Fe^{2+} + \left(\frac{1}{Y_{Fe^{2+}X}} - 0.2\right)H^+ \rightarrow CH_{1.8}O_{0.5}N_{0.2} + \frac{1}{Y_{Fe^{2+}X}}Fe^{3+} + \left(\frac{1}{2Y_{Fe^{2+}X}} - 0.6\right)H_2O \quad \text{3.2}$$

A simple method to achieve the above is making use of the concept of degree of reduction as described by Roels (1978). The degree-of-reduction, of a C,H,O,N-containing compound, is the number of electrons that are librated in a redox half-reaction where one C-mole of an organic compound or one mole of inorganic compound is converted to; H^+, CO_2, H_2O, N-source, N_2, SO_4^{2-} or Fe^{3+}.

Table B1.2 Calculated stoichiometric parameters of Equation 3.2 and Gibbs energy of formation obtained from thermodynamic reference.

Relative rate	Compound	Stoichiometric constant	Value	ΔG_f^o	B1.8
r_X / r_X	$CH_{1.8}O_{0.5}N_{0.2}$	1	1	–237.18	(i)
r_{CO_2} / r_X	CO_2	a	-1	–394.36	(ii)
r_{NH_4} / r_X	NH_4^+	b	- 0.2	–79.37	(iii)
r_{O_2} / r_X	O_2	c	$-\left(\frac{1-4.2Y_{Fe^{2+}X}}{4Y_{Fe^{2+}X}}\right)$	0	(iv)
$r_{Fe^{2+}} / r_X$	Fe^{2+}	d	$-\frac{1}{Y_{Fe^{2+}X}}$	–78.87	(v)
r_{H^+} / r_X	H^+	e	$-\left(\frac{1}{Y_{Fe^{2+}X}}-0.2\right)$	–39.87	(vi)
$r_{Fe^{3+}} / r_X$	Fe^{3+}	f	$\frac{1}{Y_{Fe^{2+}X}}$	–4.6	(vii)
r_{H_2O} / r_X	H_2O	g	$-\left(\frac{1}{2Y_{Fe^{2+}X}}-0.6\right)$	–237.18	(viii)

It represents the electron content of a compound relative to these species. By definition, degree-of-reduction equals zero ($\gamma = 0$) for H^+, CO_2, H_2O, N-source, N_2, SO_4^{2-} and Fe^{3+}, and the composition formula of the undissociated compound is normally used when calculating degree-of-reduction.

Compound	C	H	O	N	Fe^{2+}	Fe^{3+}	Charge	Degree of reduction
$CH_{1.8}O_{0.5}N_{0.2}$	1	1.8	0.5	0.2				4.2
CO_2	1		2					0
NH_4^+		4		1			1+	0
O_2								-4
Fe^{2+}					1		2+	1
H^+							1+	0
Fe^{3+}						1	3+	0
H_2O		2	1					0

Equation 3.2 can be split into two half reactions:

$$2Fe^{2+} + \tfrac{1}{2}O_2 + 2H^+ \xrightarrow{microorganisms} 2Fe^{3+} + H_2O \qquad 2.2$$

The energy produced from Equation 2.2 is sued autotrophically to form biomass by assimilation CO_2 as carbon source and NH_4^+ as N-source, which is represented by Equation B1.9

$$CO_2\ ,\ H_2O\ ,NH_4^+ \rightarrow CH_{1.8}O_{0.5}N_{0.2} \qquad B1.10$$

The degree-of-reduction is an alternative way of expressing the conservation of electron in the system i.e.

$$\sum_{i=0}^{i} \gamma_i r_i = 0 \qquad B1.11$$

Therefore the balance becomes:

$$-r_{Fe^{2+}} = -4r_{O_2} + 4.2r_X \qquad B1.12$$

$$-r_{Fe^{2+}} = -4r_{O_2} - 4.2r_{CO_2} \qquad B1.13$$

The Gibbs free energy is equal to the energy dissipated per mole of biomass, and for systems with reverse electron transport mechanism; the energy dissipated per mole biomass is equal to 3500 kJ.molC^{-1} (Heijnen and van Dijken, 1992)

$$\Delta G_R = \sum_{i=0}^{i} a_i \Delta G_{if}^o = -\left(\frac{D_S^{01}}{r_x}\right)_{growth} = -3500 \qquad 2.19$$

where

ΔG_R is the Gibbs free energy of reaction

ΔG_{if}^o is the Gibbs free energy of formation of component *i* at standard conditions

a_i the stoichiometric coefficient of component *i*

By solving Equation 2.19 for $Y_{Fe^{2+}X}$ at standard conditions (*i.e.* at 25 °C, liquid concentration of 1.0 M and 1.0 atm gas partial press), yields $Y_{Fe^{2+}X}^{\max} = 0.011$ molC.(molFe^{2+})$^{-1}$

B1.4 Direct microscopic counting method

Cell concentration can be calculated using Equation B1.14

$$C_X = \frac{c \times \frac{N_T}{N_L}}{D \times A} \times \frac{1}{d_r} \times 10^3 \qquad \text{B1.14}$$

where C_X = cell concentration (in cells.ml-1)

NT = total of number of large squarea = 16

NL = number of large squares where cell were counted

c = number of cells counted in the large squares

D = depth of the chamber (0.02 mm)

A = total area of the chamber (1 mm^2)

d_r = dilution ratio

Appendix C

Statistical analysis[2]: Relationship between sum of squares and correlation coefficient

C1.1 Sum of Squares

Consider two quantities: y_i, the measured data and $\hat{y}_i$, the predicted data, which can be represented by regression line $\hat{y} = a + bx$, where a and b are respectively the intercept and slope of the regression line

We define sum of squares due to error (SSE) as the sum of the square of the difference between the observed quantity and the predicted as shown in Equation .

$$SSE = \sum (y_i - \hat{y}_i)^2 = \sum (y_i - a - bx_i)^2 \qquad \text{C1.1}$$

This quantity will be small if the observed values y_i fall close to the regression line $\hat{y} = a + bx$, and will be large if they do not.

The term $y_i - \hat{y}_i$ is called the error or residual for the ith observation. By substituting $a = \bar{y} - b\bar{x}$ into Equation C1.1, SSE can be expressed as follows:

[2] G Keller and B Warrack (1999) Statistics: for Management and Economics. (5th Edition) Duxbury Thomson Learning, USA. Pp. 626-673

$$\begin{aligned} SSE &= \sum \left(y_i - \bar{y} + b\bar{x} - \bar{x}_i\right)^2 = \sum \left((y_i - \bar{y}) - b(\bar{x}_i - \bar{x})\right)^2 \\ &= \sum (y_i - \bar{y})^2 - 2b\sum (y_i - \bar{y})(x_i - \bar{x}) + b^2 \sum (x_i - \bar{x})^2 \\ &= SS_y + 2bSS_{xy} + b^2 SS_x \end{aligned} \qquad \text{C1.2}$$

But $b = SS_{xy} / SS_x$, then SSE can written from Equation C1.2 as

$$SSE = SS_y - bSS_{xy} \qquad \text{C1.3}$$

The first term on the right-hand side of Equation C1.3 is called total sums of squares and denoted by SST, such that $SST = SS_y$

The second term measures how much the total variability is reduced by the regression line $\hat{y} = a + bx$. Thus the term bSS_{xy} is known as the sums of squares due to regression denoted by SSR, such that Equation C1.3 can be written as

$$SSE = SST - SSR \qquad \text{C1.4}$$

Equation C1.4 is important because it shows that SST can be decomposed into a part that is explained by regression, SSR and the error sum of squares, SSE. Equation C1.4 can be written as

$$\frac{SSE}{SST} = 1 - \frac{SSR}{SST} \qquad \text{C1.5}$$

where

$$\frac{SSR}{SST} = \frac{bSS_{xy}}{SS_y} = \frac{SS_{xy}^2}{SS_x SS_y} = R^2 \quad \text{(regression coefficent)}$$

$$SS_x = \sum x^2 - \left(\sum x\right)^2 / n$$
$$SS_y = \sum y^2 - \left(\sum y\right)^2 / n$$
$$SS_{xy} = \sum xy - \left(\sum x\right)\left(\sum y\right) / n$$

Therefore, using Equation C1.5, the error sum of squares, SSE and the coefficient of regression R^2 can be related as shown in Equation C1.6

$$R^2 = 1 - \frac{SSE}{SST} \qquad \text{C1.6}$$

This relationship will be used for error analysis between modelled and measured data obtained in Chapter 4 as shown in section C1.2

C1.2 Error analysis between modelled and measured data

The result regression coefficients obtained below using Equation C1.6 suggest that the model obtained in chapter 4 accurately predicted the measured data as shown by the R^2 values

Table C1.1 Error analysis of temperature data

	Specific microbial ferrous-iron oxidation values $q_{Fe^{2+}}$							
	42 °C		36 °C		30 °C		25 °C	
	measured data	model data	measured data	model data	measured data	model data	measured data	model data
	8.07	7.88	7.67	7.15	9.71	8.60	2.62	2.82
	7.37	7.73	6.66	6.56	7.66	7.45	2.23	2.45
	6.18	6.43	5.62	5.86	6.08	5.97	1.55	1.68
	3.84	4.02	3.41	2.72	3.93	3.67		
	3.04	3.10	2.62	2.35	2.28	2.02		
	2.52	2.59	2.14	1.72	1.49	1.19		
SSE	0.27		1.07		1.52		0.10	
SST	27.67		28.53		44.87		8.71	
R^2	0.99		0.96		0.97		0.99	

Appendix D

Determination of concentration of iron species

D1.1 Reagents preparation

D1.1.1 Spekker acid

The spekker acid solution was prepared by diluting solution containing equal volumes of concentrated sulphuric acid (98%) and phosphoric acid (85%) with water in ratio 3:4 (solution:water) as described below.

- Measured out 600 ml distilled water in a 2 L beaker.
- Carefully add 225 ml of concentrated sulphuric acid (98%) and 225 ml of phosphoric acid (85%) acid such that the acid pour slowly along the wall of the beaker (Caution: heat of mixing usually result to localised boiling on rapid addition of the acids especially conc. H_2SO_4)
- Allow the regent to cool to room temperature before transferring into storage bottle.

D1.1.2 Ferric acid

Ferric acid solution was prepared from spekker acid as follows;

- Measure out 600 ml distilled water in a 2L beaker
- Slowly and carefully add 150 ml solution of spekker acid and then 300 ml of concentrated solution of hydrochloric acid.

- Agitate on magnetic strirrer and allow to cool to room temperature before transferring into storage bottle

D1.1.3 Stannous chloride souliton

- Weigh out 30 g stannous chloride in a 200 ml beaker then
- Add 100 ml concentrated hydrochloric acid (32%) and agitate at 50°C until it completely dissolves.
- Allow to cool to room temperature and dilute with 200 ml distill water.
- Add a small amount of granular tin to retard precipitation

D1.1.4 Mercuric Chloride solution ($HgCl_2$)

- Weigh out 50 g mercuric chloride in a 2 L beaker
- Add 1 L of distilled water and agitate until the solute completely dissolves (about 2 hours)
- The add a spatula tip more of more solute $HgCl_2$ and stir for further 2 hours before storage

D1.1.5 Potassium Dichromate solution ($K_2Cr_2O_7$) – 0.0149 M

- Dry about 10 g of $K_2Cr_2O_7$ (Molar mass 294.20 g/mol) in an oven at 105 – 110 °C for 1 – 2 hours. Cool in a desicator.
- Accurately weigh out 8.78 g of the dried $K_2Cr_2O_7$ in 100 ml beaker.
- Transfer quantitatively into a 2 L beaker using 1.5 L distilled water and agitate until complete dissolution.
- Transfer quatitative into a 2 L standard flask and make up to mark with distilled water.

D1.1.5 Barium Diphenyllamine Sulphonate (BDS) solution ($C_{24}H_{20}BaN_2O_6S_2$)

Weigh out 1.0 g of barium diphenylamine suphonate in 250 ml beaker and add 100 ml of concentrated sulphuric acid (98%). Agitate until the solute completely dissolves

D1.2 Determination of ferrous-iron concentration by titration with potassium dichromate solution[3]

Pipette 5 ml of the required aliquot solution into 125 ml conical flask.

Add 10 ml of spekker acid solution

Add 2 – 3 drops of DBS indicator

Titrate with the potassium dichromate ($K_2Cr_2O_7$) solution until the first permanent colour change from yellow to intense purple is obtained

Ferrous-iron concentration can be calculated from:

$$\left[Fe^{2+}\right] = \frac{\left[K_2Cr_2O_7\right] \times V_T \times (55.84 \times 6)}{V_{solution}} \qquad \text{D1.1}$$

where: $[Fe^{2+}]$ = Ferrous-iron concentration ($g.L^{-1}$)
$[K_2Cr_2O_7]$ = $K_2Cr_2O_7$ Concentration (i.e. 0.0149 M)
V_T = Titration volume (ml) – i.e. amount of $K_2Cr_2O_7$ added
$V_{solution}$ = Solution aliquot volume (ml)

D1.3 Determination of total iron concentration by titration with potassium dichromate solution[4]

1. Filter 5 ml aliquot of sample solution
2. Pipette the required amount of aliquot (i.e. 5ml) into a 125 ml conical flask
3. Add 10ml of spekker acid solution and heat to boil
4. Add stannous ($SnCl_2$) solution dropwise until yellow colour completely disappears. Add one extra drop and record the amount of stannous chloride added (note that it is important that you record this amount, especially if you will be doing duplicate titrations since it gives you an idea of the amount of $SnCl_2$ required for the next duplicate titrations)
5. Allow the solution to cool to room temperature and add 10ml of mercuric chloride ($HgCl_2$) solution. A silky-white precipitate should appear. If no precipitate forms,

[3] Ferrous-iron concentration less than 0.5 $g.L^{-1}$ can not be accurately determined using this method, a combination of solution potential and total iron concentration allow an accurate estimation.

[4] Potassium chromate and mercuric chloride are toxic and care should be taken when analysing samples that may contain arsenic as this may be converted to toxic volatile arsine gas, AsH_3 during stannous chloride reduction in step 4 above.

too little stannous chloride was added in step 4 above. If the precipitate is heavy and grey/black, too much stannous chloride was added. In either case, abort the experiment and repeat.

6. Add 3 – 4 drops of barium diphenylamine indicator solution (BDS) and titrate with the potassium dichromate solution until the first permanent colour change from yellow to intense purple is obtained.

$$[Fe_T] = \frac{[K_2Cr_2O_7] \times V_T \times (55.84 \times 6)}{V_{solution}} \qquad \text{D1.2}$$

where: $[Fe_T]$ = Total iron concentration ($g.L^{-1}$)
$[K_2Cr_2O_7] = K_2Cr_2O_7$ Concentration (i.e. 0.0149 M)
V_T = Titration volume (ml) – i.e. amount of $K_2Cr_2O_7$ added
$V_{solution}$ = Solution aliquot volume (ml)

D1.4 Vishniac Trace metal Solution

Vishniac Trace Metal Solution was prepared according prescription given below by Vishniac and Santer (1957).

Weigh accurately the following reagents and dilute to 500ml volume with distilled

a) Prepare 6 % KOH by weighing 15 g KOH and dilute to 250 ml with dH_2O.
b) Dissolve 25 g EDTA in 100 ml of 6 % KOH on a magnetic stirrer
c) In a separate 250 ml beaker weigh the following and dissolve in 200 ml dH_2O for 30 minutes on magnetic stirrer.

$ZnSO_4.7H_2O$	11 g
$CaCl_4.2H_2O$	4.62 g
$MnCl_2.4H_2O$	2.53 g
$FeSO_4.7H_2O$	2.50 g
$(NH_4)_6Mo_7O_{24}.\ 4H_2O$	0.55 g
$CuSO_4.5H_2O$	0.79 g
$CoCl_2.6H_2O$	0.81 g

Transfer solution (c) quantitatively into (b) and make up to 500 ml with dH_2O by rinsing the 250 ml beaker with 200 ml dH_2O (a deep greenish brown solution results)

Table D1.1 Percentage iron loss in the bioreactor due to ferric precipitation in the study to investigate effect of dissolved Al and Mg on microbial ferrous-iron oxidation

	$[Fe^T]_{in}$ (mM)	$[Fe^T]_{out}$ (mM)	% iron loss
Blank	4.92	4.89	0.62
2.25 g.L-1 Al	5.11	4.93	3.54
10 g.L-1 Al	4.90	4.85	1.02
3.05 g.L-1 Mg	5.11	4.93	3.54
10 g.L-1 Mg	4.85	4.83	0.41
1.3 g.L-1 Al & Mg	5.02	4.92	1.99
5 g.L-1 Al & Mg	4.94	4.88	1.21
10 g.L-1 Al & Mg	5.03	4.96	1.39
12 g.L-1 Al & Mg	5.09	5.04	0.98
14 g.L-1 Al & Mg	5.04	4.93	2.31
16 g.L-1 Al & Mg	5.07	4.92	2.96

Table D1.2 Maximum measured redox potential (Ag/AgCl) and the corresponding threshold ferrous-iron concentration

Total Iron	Potential (Ag/AgCl)	$[Fe^{2+}]$ (mmol.L^{-1})
12	775	0.006054682
8	780	0.003365216
5	784	0.001844458
3	764	0.002246985
2	770	0.001205506
Average	774.6	
Error (Standard deviation)	7.9	

Table D1.3 Percentage iron loss in the bioreactor due to ferric precipitation in the study to investigate effect of total iron concentration on microbial ferrous-iron oxidation

	$[Fe^T]_{in}$ (mM)	$[Fe^T]_{out}$ (mM)	% iron loss[5]
12 g.L^{-1} Fe	11.95	11.85	0.86
8 g.L^{-1} Fe	7.95	7.85	1.30
5 g.L^{-1} Fe	5.04	5.00	0.78
3 g.L^{-1} Fe	2.96	2.95	0.28
2 g.L^{-1} Fe	2.05	1.99	2.92

[5] Longer time was allowed before cleaning of the bioreactor especially when the feed concentration was changed from 12 to 8 and from 3 to 2 g L^{-1}

Table D1.4 The ferrous-iron based bioenergetic parameters determined using the variable maintenance equation equation

	12 g L^{-1}			8 g L^{-1}			5 g L^{-1}			3 g L^{-1}			2 g L^{-1}		
$m^{v}_{Fe^{2+}}$			0.1683			-0.8385			-0.2709			-0.4690			-0.0887
$m_{Fe^{2+}}$			0.1985			-1.3320			0.0248			-0.1745			0.1582
$\mu^{\max}$			0.1254			0.1305			0.1254			0.1235			0.1281
$Y^{\max}_{Fe^{2+}X}$			0.0091			0.0055			0.0058			0.0047			0.0034
SSE			0.0986			0.3820			1.6063			0.4402			6.1739
SST			17.0504			81.4220			167.87			905.23			724.81
R^2			0.9942			0.9953			0.9904			0.9995			0.9915
	D (h^{-1})	$q_{Fe^{2+}}$	$q_{Fe^{2+}cal.}$	D (h^{-1}))	$q_{Fe^{2+}}$	$q_{Fe^{2+}cal.}$	D (h^{-1})	$q_{Fe^{2+}}$	$q_{Fe^{2+}cal.}$	D (h^{-1})	$q_{Fe^{2+}}$	$q_{Fe^{2+}cal.}$	D (h^{-1})	$q_{Fe^{2+}}$	$q_{Fe^{2+}cal.}$
	0.017	2.43	2.32	0.042	5.66	5.25	0.019	3.13	3.06	0.043	8.14	8.25	0.024	6.19	7.00
	0.024	3.09	3.06	0.052	6.68	6.99	0.035	6.40	5.77	0.090	18.23	18.09	0.035	9.80	10.26
	0.033	3.95	4.09	0.072	10.12	10.41	0.053	8.63	8.76	0.105	20.94	21.17	0.056	16.00	16.19
	0.051	5.86	6.04	0.092	13.92	13.89	0.068	11.00	11.33	0.123	25.04	24.80	0.058	17.92	16.77
	0.062	7.45	7.27	0.104	16.15	15.98	0.076	12.94	12.81	0.143	29.46	29.10	0.076	23.30	21.94
							0.091	15.56	15.26	0.162	32.55	32.96	0.085	24.10	24.65
							0.107	18.47	18.00				0.097	28.70	28.15
							0.070	11.44	11.75				0.108	31.40	31.24
							0.073	11.41	12.23				0.122	34.04	35.25

Appendix E

Kinetic constants using competitive ferric inhibition model

As discussed in Section 8.2, the non-competitive ferric inhibition Equation was also used to described all the experimental data.

Table E1.1 Effect of Temperature

Temperature	qmax	K1	K2	R 2
42	15.63	0.28	13426.45	0.99
36	11.57	0.19	12859.43	0.98
30	10.25	0.21	11154.98	0.99
25	6.88	0.14	10541.16	1.00

Table E1.2 Effect of solution pH

pH	qmax	Kfe	K2	R 2
0.8	9.93	0.14	11139.86	0.99
1.0	13.35	0.17	12518.99	0.99
1.3	14.68	0.29	9949.03	1.00
1.6	11.36	0.30	8292.48	0.99
2.0	11.69	0.97	6274.00	0.99

Table E1.3 Effect of dissolved Al and Mg

Ionic strength	TDS	qmax	Kfe	K2 (10^{-3})	R^2
0.22	Blank	23.93	0.22	6381.86	0.96
0.34	2.25 g/L Al	26.15	0.27	6281.86	0.99
0.36	1.3 g/l Al & Mg	21.48	0.23	6005.60	0.99
0.42	3.05 g/L Mg	18.67	0.23	5904.58	0.98
0.67	5 g/l Al & Mg	19.54	0.45	5506.67	0.96
0.71	10 g/L Mg	19.79	0.53	5104.38	0.98
0.77	10 g/L Al	23.34	0.42	4844.81	0.90
0.99	10 g/l Al & Mg	18.41	0.93	5455.38	0.97
1.10	12 g/l Al & Mg	16.64	1.34	4905.61	0.91
1.21	14 g/l Al & Mg	16.47	1.90	3405.61	1.00
1.32	16 g/l Al & Mg	16.29	5.78	2405.61	1.00

As discussed in section 8.2.3, the predicted data using Equation 8.13 is compared with the experimental data in Table E1.1

$$f_{\text{q-model}} = \frac{24.00 - 7.02I}{1 + \frac{0.0494e^{2.94I}}{[Fe^{2+}]} + 1.03 - 0.458I\frac{[Fe^{3+}]}{[Fe^{2+}]}} \qquad 8.1$$

Table E1.4 Error analysis due to manipulation of data at pH 1.6 (i.e. changing 0.053198 to 0.114029)

	qmax	11.09657		11.09657	
	Kfe	0.1147		0.053198	
	K2	0.00101		0.00101	
	Expt. Data	q-model	% Error	q-model	% Error
	2.43	2.09	13.97	2.46	0.22
	4.71	4.18	11.25	4.73	0.14
	6.59	5.92	10.10	6.48	1.04
	6.61	6.12	7.46	6.67	0.84
	9.50	9.21	3.04	9.51	0.41
Average % Error			9.16		0.53

Table E1.5 Predicted data compared with observed data for the effect of ionic strength on microbial ferrous-iron oxidation

	R	data	Predicted		R	data	Predicted
Blank	1427.48	5.89	5.86	10 g/L Mg	391.00	6.68	6.29
$R^2 = 0.95$	996.21	8.29	7.55	$R^2 = 0.96$	204.63	8.48	9.22
	272.87	12.53	14.56		123.67	10.67	11.57
	164.91	16.27	16.91		74.74	13.33	13.67
	111.02	18.08	18.39		54.07	15.13	14.81
	77.48	21.28	19.45				
2.25 g/L Al	996.21	6.68	6.46	10 g/L Al	646.97	7.76	3.80
$R^2 = 0.89$	802.82	8.11	7.48	$R^2 = 0.14$	272.87	9.34	7.03
	468.04	10.27	10.29		123.67	12.57	10.63
	326.64	12.56	12.22		83.26	16.57	12.35
	164.91	16.57	15.57		64.72	18.81	13.33
	115.09	19.01	17.01				
	86.31	20.82	17.97				
1.3 g/l Al & Mg	894.30	6.53	6.68	10 g/l Al & Mg	167.90	7.57	6.06
$R^2 = 0.99$	695.23	7.98	7.89	$R^2 = 0.91$	74.74	9.56	9.41
	351.00	10.78	11.48		15.35	14.58	14.51
	123.67	15.48	16.41		5.81	16.79	15.89
	80.32	18.02	17.88		2.54	18.46	16.43
3.05 g/L Mg	774.45	6.17	6.72	12 g/l Al & Mg	111.02	7.04	6.14
$R^2 = 0.85$	646.97	7.52	7.57	$R^2 = 0.90$	64.72	7.74	8.27
	420.16	8.38	9.76		45.17	8.18	9.68
	326.64	9.80	11.08		33.87	12.09	10.75
	177.21	11.89	14.13		10.71	13.35	13.87
	123.67	14.03	15.68		3.27	15.79	15.30
	92.75	15.15	16.74				
				14 g/l Al & Mg	46.82	8.03	7.93
5 g/l Al & Mg	451.51	6.68	6.17	$R^2 = 0.98$	15.92	11.72	11.58
$R^2 = 0.95$	236.30	8.48	9.11		1.24	15.54	14.83
	132.90	10.67	11.84				
	80.32	13.33	13.95	16 g/l Al & Mg	10.34	9.10	11.31
	64.72	15.13	14.74	$R^2 = 0.96$	1.33	13.87	13.89

Table E1.6 Steady state data collected for effect of temperature a chemostat run at feed concentration, [Fe^{2+}] of 214 in mmol.L-1, pH 1.3 ± 0.05

Temperature	Dilution rate (h^{-1})	$-r_{O_2}$	$-r_{CO_2}$	Eh (mV)	$[Fe^{2+}]_{out}$ (mM)	$[Fe^{T}]_{in}$ (mM)	$[Fe^{T}]_{out}$ (mM)
42 °C							
	0.068	3.54	0.02	669	0.2710	211.0	210.1
	0.059	3.13	0.01	670	0.2625	211.9	211.0
	0.051	2.72	0.02	678.5	0.1959	214.6	213.7
	0.030	1.60	0.01	697	0.0995	211.9	211.0
	0.024	1.29	0.01	706	0.0723	212.8	211.9
	0.017	0.96	0.01	712	0.0580	212.8	211.0
36 °C							
	0.068	3.55	0.01	658	0.3312	211.9	211.9
	0.060	3.12	0.01	663	0.2757	211.9	211.9
	0.051	2.70	0.01	669	0.2221	215.5	212.8
	0.030	1.61	0.01	700	0.0709	212.8	211.9
	0.024	1.27	0.01	705	0.0587	213.7	211.0
30 °C							
	0.067	3.565	0.0116	597	2.7553	212.8	212.8
	0.059	3.119	0.0127	630	0.8085	213.9	212.8
	0.051	2.696	0.0096	652.5	0.3461	211.9	211.0
	0.035	1.853	0.0087	680	0.1237	211.9	211.0
	0.020	1.035	0.0093	703	0.0528	213.7	212.8
	0.012	0.616	0.0076	720	0.0280	215.5	213.7
25 °C							
	0.0172	0.9368	0.006	700	0.0392	208.3	208.3
	0.0178	0.9503	0.0089	686	0.0682	213.9	212.8
	0.0225	1.1880	0.0061	680	0.0849	211.9	211.0
20 °C							
	0.0097	0.5386	0.0101	676	0.0603	213.704	212.810

Table E1.7 Steady state data collected for effect of pH in a chemostat run at feed concentration, [Fe2+] of 214 in mmol.L-1 and 42 ± 0.05 °

Date	Dilution rate (h^{-1})	$-r_{O_2}$	$-r_{CO_2}$	Eh (mV)	$[Fe^{2+}]_{out}$ (mM)	$[Fe^{T}]_{in}$ (mM)	$[Fe^{T}]_{out}$ (mM)
pH 0.8	0.018	0.971	0.022	705.0	0.076	212.8	211.9
	0.026	1.396	0.037	700.0	0.091	213.7	213.3
	0.040	2.119	0.052	665.3	0.314	215.0	214.6
	0.048	2.503	0.069	655.3	0.440	211.9	211.0
	0.051	2.791	0.063	636.0	0.880	213.7	213.3
	0.057	2.925	0.077	630.0	1.076	211.9	211.0
pH 1.00							
	0.021	1.163	0.029	716	0.051	212.8	211.0
	0.021	1.153	0.034	715	0.053	212.8	211.6
	0.040	2.105	0.062	690	0.131	214.3	213.7
	0.044	2.370	0.070	682.5	0.167	211.0	210.1
	0.059	3.136	0.092	670	0.264	215.5	213.3
	0.067	3.538	0.102	654	0.463	212.8	211.9
	0.073	3.877	0.113	644	0.659	213.7	211.9
	0.081	4.257	0.111	620	1.537	212.8	211.9
pH 1.30							
	0.021	1.144	0.036	707	0.070	213.7	208.3
	0.040	2.082	0.071	686.55	0.144	216.7	208.3
	0.050	2.620	0.093	678.5	0.191	216.5	207.5
	0.055	2.911	0.099	671	0.252	213.7	210.1
	0.071	3.290	0.089	654	0.4532	214.6	207.4
pH 1.60							
	0.018	0.943	0.029	705	0.070	212.8	195.8
	0.036	1.937	0.068	685	0.144	213.7	197.6
	0.041	2.146	0.077	678	0.186	213.3	199.4
	0.056	3.115	0.119	660	0.346	212.8	195.8
	0.059	3.061	0.113	658	0.382	213.3	201.2
	0.067	3.648	0.132	639	0.742	212.8	200.3
	0.074	3.809	0.129	619	1.512	213.7	201.2
pH 2.00							
	0.018	0.921	0.030	680	0.162	213.3	186.6
	0.026	1.383	0.043	656	0.379	213.1	186.1
	0.047	2.373	0.093	640	0.668	213.1	186.3
	0.058	2.986	0.117	630	0.950	213.3	186.3
	0.066	3.394	0.127	620	1.353	213.1	186.6
	0.074	3.764	0.119	584	4.752	213.1	186.3

Table E1.8 Steady state data collected for effect of dissolved Al & Mg in a chemostat run at feed concentration, [Fe^{2+}] of 214 in mmol.L-1 and 42 ± 0.05 °C

	Dilution rate (h^{-1})	$-r_{O_2}$	$-r_{CO_2}$	Eh (mV)	$[Fe^{2+}]_{out}$ (mM)	$[Fe^{T}]_{in}$ (mM)	$[Fe^{T}]_{out}$ (mM)
Blank							
	0.040	0.901	0.0252	686	0.061	88.5	86.7
	0.054	1.282	0.0355	676	0.090	88.5	89.4
	0.081	2.432	0.0509	640	0.322	88.5	88.2
	0.099	3.015	0.0577	626	0.520	87.6	86.3
	0.108	3.128	0.0616	615	0.784	87.6	87.8
	0.125	3.406	0.0704	605	1.105	87.6	86.7
2.25g.L^{-1} Al							
	0.041	0.897	0.0226	676	0.090	91.5	89.4
	0.049	1.102	0.0271	670	0.110	91.5	88.5
	0.062	1.398	0.0348	655	0.193	91.5	90.3
	0.076	1.696	0.0420	645	0.273	91.5	89.4
	0.096	2.125	0.0507	626	0.523	91.5	86.7
	0.108	2.384	0.0554	616	0.747	91.5	86.7
	0.118	2.632	0.0613	608	0.993	91.5	86.7
10 g.L^{-1} Al							
	0.042	0.952	0.0213	664	0.134	86.7	86.7
	0.057	1.274	0.0318	640	0.317	88.5	86.7
	0.076	1.678	0.0416	618	0.703	87.6	87.6
	0.096	2.087	0.0495	607	1.029	89.4	86.7
	0.106	2.295	0.0530	600	1.320	86.7	86.7
3.05g.L^{-1} Mg							
	0.042	0.950	0.0270	669	0.115	91.5	89.4
	0.050	1.143	0.0312	664	0.137	91.5	88.5
	0.062	1.398	0.0427	652	0.214	91.5	90.3
	0.074	1.675	0.0525	645	0.273	91.5	89.4
	0.093	2.030	0.0657	628	0.487	91.5	86.7
	0.106	2.331	0.0726	618	0.696	91.5	86.7
	0.115	2.560	0.0802	610	0.925	91.5	86.7
10g.L^{-1} Mg							
	0.042	0.987	0.0256	650	0.221	86.7	86.7
	0.059	1.356	0.0388	632	0.413	88.5	84.9
	0.078	1.768	0.0533	618	0.703	87.6	87.6
	0.098	2.202	0.0671	604	1.145	86.7	86.7
	0.106	2.408	0.0696	595	1.575	88.5	86.7

Table E1.4 Contd. Steady state data collected for effect of dissolved Al & Mg in a chemostat run at feed concentration, $[Fe^{2+}]$ of 214 in mmol.L^{-1} and 42 ± 0.05 °C

	Dilution Rate (h^{-1})	$-r_{O_2}$	$-r_{CO_2}$	Eh (mV)	$[Fe^{2+}]_{out}$ (mM)	$[Fe^{T}]_{in}$ (mM)	$[Fe^{T}]_{out}$ (mM)
1.3 g.L^{-1} Al & Mg							
	0.044	1.069	0.029	673	0.10	86.7	86.7
	0.056	1.339	0.039	666	0.13	91.5	88.5
	0.079	1.862	0.057	647	0.26	88.5	90.3
	0.110	2.545	0.075	618	0.71	91.5	88.5
	0.128	2.905	0.085	606	1.07	91.5	86.7
5.0 g.L^{-1} Al & Mg							
	0.045	1.083	0.026	654	0.19	92.1	86.7
	0.061	1.459	0.040	636	0.37	86.7	86.7
	0.080	1.870	0.052	620	0.65	87.6	87.6
	0.102	2.369	0.067	606	1.07	86.7	86.7
	0.112	2.602	0.073	600	1.36	89.4	89.4
10 g.L^{-1} Al & Mg							
	0.042	0.953	0.022	626.5	0.53	91.2	89.4
	0.061	1.336	0.035	604	1.19	90.3	90.3
	0.088	1.854	0.046	560	5.41	89.4	88.5
	0.100	1.921	0.047	533	12.73	89.4	86.7
	0.111	1.830	0.045	510	25.25	90.3	89.4
12 g.L^{-1} Al & Mg							
	0.043	0.899	0.022	615	0.80	91.2	89.4
	0.048	0.998	0.025	600	1.37	90.3	90.3
	0.054	1.114	0.030	590	1.94	89.4	89.4
	0.065	1.345	0.030	582	2.62	92.1	91.2
	0.076	1.505	0.035	550	7.79	92.1	91.2
	0.085	1.525	0.033	517	21.15	92.1	90.3
14 g.L^{-1} Al & Mg							
	0.047	0.961	0.023	591	1.87	91.2	89.4
	0.058	1.152	0.023	561	5.23	90.3	88.5
	0.071	1.068	0.017	490	38.76	89.4	86.7
16 g.L^{-1} Al & Mg							
	0.047	0.929	0.020	549	7.89	91.2	89.4
	0.058	0.822	0.014	492	37.22	90.3	86.7

Table E1.9 Steady state data collected for effect of total iron in a chemostat run at feed concentration, pH 1.3 ± 0.05 and 42 ± 0.05 °C

	Dilution Rate (h^{-1})	$-r_{O_2}$	$-r_{CO_2}$	Eh (mV)	$[Fe^{2+}]_{out}$ (mM)	$[Fe^{T}]_{in}$ (mM)	$[Fe^{T}]_{out}$ (mM)
214 mmol.L^{-1} Fe							
	0.017	0.942	0.028	714	0.055	213.7	211.9
	0.024	1.282	0.041	705	0.075	213.7	212.8
	0.033	1.742	0.061	696	0.105	216.7	214.6
	0.051	2.651	0.095	679	0.190	212.8	211.0
	0.062	3.236	0.111	669	0.272	213.7	211.0
143 mmol.L^{-1} Fe							
	0.042	1.477	0.046	681	0.119	144.0	142.2
	0.052	1.868	0.061	678	0.129	143.1	137.7
	0.072	2.461	0.072	650	0.356	138.0	139.5
	0.092	3.098	0.084	620	1.062	144.0	142.2
	0.104	3.608	0.088	610	1.507	143.1	141.3
90 mmol.L^{-1} Fe							
	0.019	0.483	0.013	708	0.028	89.4	88.5
	0.035	0.812	0.023	688	0.058	92.1	89.4
	0.053	1.235	0.031	666	0.132	91.2	92.1
	0.068	1.561	0.043	662	0.148	88.5	89.4
	0.076	1.781	0.043	643	0.290	92.1	88.5
	0.091	2.149	0.051	635	0.398	92.1	91.2
	0.107	2.470	0.059	620	0.661	90.3	88.5
54 mmol.L^{-1} Fe							
	0.043	0.635	0.014	680	0.046	52.8	52.8
	0.090	1.226	0.025	626	0.320	53.1	53.1
	0.105	1.410	0.029	615	0.471	53.1	52.8
	0.123	1.649	0.033	606	0.649	52.8	52.8
	0.143	1.893	0.035	595	0.958	52.8	52.8
	0.162	2.140	0.038	577	1.811	53.6	53.1
36 mmol.L^{-1} Fe							
	0.024	0.272	0.006	697	0.016	35.3	34.9
	0.035	0.354	0.007	677	0.036	36.8	36.8
	0.056	0.563	0.009	649	0.096	38.4	35.8
	0.058	0.576	0.006	642	0.124	35.8	35.8
	0.076	0.752	0.008	629	0.197	35.8	35.8
	0.085	0.828	0.011	624	0.211	35.8	32.2
	0.097	0.932	0.012	618	0.283	38.4	35.3

Table E1.10 The regression analysis of plot of Equation 8.14 compared with $q_{Fe^{2+}}$ determined experimentally*

$q^{min}_{Fe^{2+}}$	16.1529		SSE					0.33						1.52
$q^{excess}_{Fe^{2+}}$	49.4275		SST					16.55						77.75
a	0.0254		R^2					0.98						0.98
K_1	0.0177													
K_2	0.0016													
$q_{Fe^{2+}} = \frac{q^{min}_{Fe^{2+}} + q^{excess}_{Fe^{2+}} \exp(-a.[Fe^{3+}])}{1 + \frac{K_1}{[Fe^{2+}]} + K_2 \frac{[Fe^{3+}]}{[Fe^{2+}]}}$			8.14											
						[Fe^{3+}]	[Fe^{2+}]	[Fe^{3+}]/[Fe^{2+}]	$q_{Fe^{2+}}$	$q_{Fe^{2+}}$ model	[Fe^{3+}]	[Fe^{2+}]	[Fe^{3+}]/[Fe^{2+}]	$q_{Fe^{2+}}$	$q_{Fe^{2+}}$ model
						214.81	0.056	3839	2.43	2.19	143.12	0.120	1193	5.66	5.71
						214.79	0.076	2827	3.09	2.84	143.11	0.134	1071	6.68	6.14
						214.76	0.105	2045	3.95	3.68	142.88	0.365	391	10.12	10.43
						214.67	0.193	1110	5.86	5.71	142.17	1.070	133	13.92	14.23
						214.58	0.277	774	7.45	7.11	141.06	2.179	65	16.78	15.77
			SSE	4.88						31.06					65.70
			SST	127.59						161.02					23737.58
			R^2	0.96						0.81					1.00
[Fe^{3+}]	[Fe^{2+}]	[Fe^{3+}]/[Fe^{2+}]	$q_{Fe^{2+}}$	$q_{Fe^{2+}}$ model		[Fe^{3+}]	[Fe^{2+}]	[Fe^{3+}]/[Fe^{2+}]	$q_{Fe^{2+}}$	$q_{Fe^{2+}}$ model	[Fe^{3+}]	[Fe^{2+}]	[Fe^{3+}]/[Fe^{2+}]	$q_{Fe^{2+}}$	$q_{Fe^{2+}}$ model
89.50	0.026	3500	3.13	2.91		53.39	0.324	165	18.23	21.91	35.79	0.017	2120	6.19	6.63
89.50	0.028	3150	3.50	3.19		53.24	0.480	111	20.94	23.83	35.77	0.035	1014	9.80	11.55
89.47	0.058	1534	6.40	5.65		53.05	0.661	80	25.04	25.10	35.71	0.096	372	16.00	20.30
89.40	0.129	695	8.63	9.45		52.74	0.975	54	29.46	26.34	35.69	0.124	288	17.92	22.51
89.30	0.228	391	11.44	12.49		51.88	1.833	28	31.46	27.86	35.61	0.197	180	23.30	26.23
89.23	0.294	304	12.94	13.76							35.58	0.235	151	24.10	27.46
89.13	0.391	228	15.56	15.10							35.52	0.287	124	28.70	28.74
88.86	0.669	133	18.47	17.21							35.43	0.382	93	31.40	30.34
											35.16	0.650	54	34.04	32.67

* SST and R^2 determined as discussed in Section C1.1